THERMAL DIFFUSION ISOTOPIC ENRICHMENT AND RADIOCARBON DATING BEYOND 50 000 YEARS BP

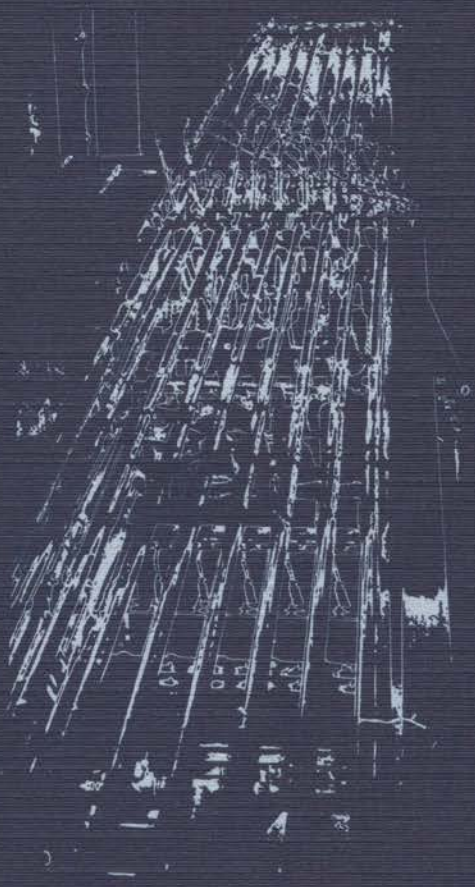

P. M. GROOTES

THERMAL DIFFUSION ISOTOPIC ENRICHMENT AND RADIOCARBON DATING BEYOND 50 000 YEARS BP

RIJKSUNIVERSITEIT TE GRONINGEN

THERMAL DIFFUSION ISOTOPIC ENRICHMENT AND RADIOCARBON DATING BEYOND 50 000 YEARS BP

PROEFSCHRIFT

TER VERKRIJGING VAN HET DOCTORAAT IN DE
WISKUNDE EN NATUURWETENSCHAPPEN
AAN DE RIJKSUNIVERSITEIT TE GRONINGEN
OP GEZAG VAN DE RECTOR MAGNIFICUS DR. M. J. JANSSEN
IN HET OPENBAAR TE VERDEDIGEN OP MAANDAG 25 APRIL 1977
DES NAMIDDAGS TE 2.45 UUR PRECIES

DOOR

PIETER MEIERT GROOTES
geboren te Wieringerwaard

VRB drukkerijen bv - Groningen

PROMOTOR: DR. W. G. MOOK
COREFERENTEN: PROF. DR. H. DE WAARD
DR. W. H. ZAGWIJN

aan Grada
aan mijn moeder

The work described in this thesis was partly supported by the 'Nederlandse Organisatie voor Zuiver-Wetenschappelijk Onderzoek' (Z.W.O.).

CONTENTS

Chapter 1

INTRODUCTION

This thesis deals with the extension of the time range of radiocarbon dating beyond 50 000 years by means of thermal diffusion enrichment of the ^{14}C concentration in the samples to be measured. Actually the relation between thermal diffusion isotopic enrichment and radiocarbon is relatively old. Already in 1947 Anderson et al. (1947a, b) made the first attempt to demonstrate the existence of natural radiocarbon, using methane from the Baltimore sewage plant that had been enriched in the heavy isotopes by thermal diffusion. After Libby's prediction of the presence of ^{14}C in the atmosphere (Libby, 1946) had been more or less confirmed, he developed the radiocarbon dating method. It was successively improved and refined by many workers, of whom Hessel de Vries at Groningen should be mentioned especially, until its range had been extended to about 50 000 years BP. This period covers most of the history of modern man and a substantial part of the Last Glacial. In geological terms, however, it is still short: for instance, the important early part of the Last Glacial, and the middle Palaeolithic fall outside this period.

The time range obtained for a particular counter set-up is determined by the statistical fluctuations in the background contribution to the measured counting rate (sample activities must be more than twice the background uncertainty) and by the counting rate of a sample of age zero measured in that counter. An extension of the range can, therefore, be obtained by reducing the background and/or by increasing the counting rate of a sample (for instance by thermal diffusion enrichment).

Research on isotopic enrichment of ^{14}C using hot wire thermal diffusion columns was started at the F.O.M. Institute for Mass Separation in Amsterdam in 1952, after Kistemaker had visited Libby and coworkers and seen their methane enrichment system, used for the first radiocarbon measurements. The use of CO for the enrichment of ^{14}C and the relation between the simultaneous enrichments of the isobaric molecules $^{14}C^{16}O$ and $^{12}C^{18}O$ were first studied by A. E. de Vries (1956).

In 1956 a joint program of the Amsterdam F.O.M. Institute and the Groningen Radiocarbon Dating Laboratory was started to date samples from the early part of

the Last Glacial. In Amsterdam an apparatus was constructed for the thermal diffusion enrichment of an amount of gas sufficient for filling a proportional CO_2 counter. From 1957 onwards large volumes of gas from low activity samples were regularly enriched in ^{14}C by a factor of about 10 in Amsterdam and subsequently dated in Groningen. In this way dates up to 70 000 years BP were obtained (Haring et al., 1958; Vogel and Zagwijn, 1967).

This activity was temporarily stopped after conflicting results had been obtained in the mid-sixties. It became obvious that some of the samples were seriously contaminated with additional radiocarbon during processing. Changes of scientific interest of the Amsterdam laboratory prompted Kistemaker to suggest a move of the enrichment apparatus to Groningen. In 1970 work was started to bring the enrichment apparatus into operation again.

The enrichment system was set up anew, essentially as it was in operation in Amsterdam (chapter 2). A new combustion system was constructed, while also the reduction system, necessary to convert CO_2 to CO before enrichment, and the oxidation system to oxidize the enriched CO to CO_2 were redesigned (chapter 4).

In order to determine the ^{14}C enrichment of a sample, which in old samples cannot be measured directly, the simultaneous enrichment of the isobaric molecule $^{12}C^{18}O$ is measured with a mass spectrometer (chapter 2). The ^{14}C enrichment follows from the relation between the mass 30 enrichment (mainly $^{12}C^{18}O$) and that of ^{14}C, obtained by making a series of calibration enrichments on recent samples (chapter 2).

An enrichment by a factor 10 can be obtained with the thermal diffusion enrichment set-up in about 30 days. This gives a gain in age range of 18 500 years. It remains to be discussed whether these high ages are still meaningful (chapter 3).

The main problem of ^{14}C dating beyond 50 000 years BP is contamination. Because the residual ^{14}C activity is 10^3 to 10^4 times lower than the recent activity, an admixture of a very small amount of recent carbon will give rise to a serious error in the radiocarbon age.

Therefore we investigated the contamination problem in detail. In order to obtain samples with little or no contamination a careful selection and collection of samples, combined with a rigorous acid-alkali-acid pretreatment, is required. Also during sample handling in the laboratory, contamination may be introduced. Special cleaning procedures and the use of pure reagents are therefore essential (chapter 4).

After a pretreated sample has been enriched, the ^{14}C activity is measured in a proportional CO_2 counter. For old samples the ^{14}C detection limit is set by the statistical fluctuations of the background counting rate. Because this limit is shifted by a reduction in the counter background we investigated the different factors determining this background. For low-activity measurements a gold coated quartz counter was constructed. Counter design, characteristics and operation are reported (chapter 3).

To prove its usefulness the expanded dating range was applied to a specific problem; a series of samples was dated from early glacial deposits in North-west Europe (chapter 5). Until June 1976 we obtained 28 enrichment dates which indicate the existence of three early glacial interstadials. The results of samples enriched before 1967 (Vogel and Zagwijn, 1967; Vogel and Waterbolk, 1972) are compared with our results (appendix).

We have correlated our chronology for the early part of the Last Glacial with the climatic history obtained from δ^{18} measurements on the Camp Century ice core, with the δ^{18} record of deep-sea cores and with the sea level fluctuations as dated on New Guinea. These data were obtained with different techniques (chapter 6).

A few other laboratories have become interested in the use of thermal diffusion enrichment for radiocarbon dating.

In Munich a concentric tube column for the enrichment of ^{14}C in methane was studied by Dickel and coworkers (Malota, 1962; Kretner, 1973). The 10.9 m long enrichment column constructed by Kretner produced 3.7 g of carbon enriched in ^{14}C by a factor 11.4 in 45 days from a sample containing 127 g of carbon (Kretner and Dickel, 1975). This system has not been used for radiocarbon dating.

In Kiel concentric tube columns for the enrichment of methane were constructed by Erlenkeuser (1971a, b, 1976). The apparatus is not yet in routine operation.

In Vienna Felber and Pak constructed a column of the concentric tube type for methane enrichment (Pak, 1970; Felber and Pak, 1972). From a sample containing 90 g of carbon they obtained 2.5 g of carbon enriched in ^{14}C by a factor 23 in 35 days. A system for the production of large methane samples is under construction.

In Seattle Stuiver and coworkers have recently constructed a cascaded hot wire column set-up for the enrichment of ^{14}CO (Stuiver, personal communication). This apparatus has now become operational for radiocarbon dating.

The performance of Kretner's enrichment set-up (discussed above) is comparable to ours, that of Felber and Pak is slightly better. Our system yields 3.2 g of carbon enriched in ^{14}C by a factor 11.4 in 40 days and by a factor 12.8 in 44 days from 130 g of carbon.

Chapter 2

THERMAL DIFFUSION

2.1. Theory

2.1.1. The thermal diffusion column

Thermal diffusion (TD) is the phenomenon that a temperature gradient in a mixture or a solution gives rise to a concentration gradient. Although TD occurs both in the liquid and in the gaseous state, our discussion will be limited to the latter and, more specifically, to isotopic mixtures.

TD (strongly) depends on the nature of the intermolecular forces. Simple dimensional considerations are inadequate to describe the effect. Nevertheless some general statements can be made.

(i) Generally the lighter isotopic species concentrates in the warmer, the heavier in the colder part of the volume. The concentration gradient is maintained by energy transfer from the hot to the cold wall.

(ii) The TD effect increases with increasing exponent ν in an intermolecular repulsion potential of form $r^{-\nu}$; this means that molecules with a short-range repulsion potential (large ν) exhibit a greater effect than those having long-range potentials ('soft' molecules). The limiting case is the molecule which behaves as a rigid elastic sphere ($\nu = \infty$). The actual TD behaviour of a molecule is indicated by R_T, the ratio of the TD constant α as found experimentally, to the value of α which is predicted by the theory for a gas consisting of hard elastic spheres.

(iii) The consequence of (ii) is that also different molecules of equal mass may be subject to TD, since they may have a different momentum transfer: molecules of smaller diameter have a larger mean free path. When applying a temperature gradient, this means that on the average the velocity difference for a collision in which the small molecule comes from the hot wall will be higher. These collisions will dominate the momentum transfer if $\nu > 5$ ($\nu = 5$, Maxwellian gas), resulting in an enrichment of the larger molecules in the colder part.

The existence of TD in gases was first predicted by Enskog (1911a, b) from a rigorous mathematical treatment of the kinetic theory for a mixture of gases. Independently Chapman (1917) predicted the effect and gave an experimental demonstration (Chapman and Dootson, 1917). Although Chapman (1919) suggested a possible application for the separation of isotopes, the separation factor was too small to be of practical use. A break-through occurred by the invention of the thermal diffusion column by Clusius and Dickel (1938).

The *thermal diffusion column* consists of a vertical tube which is cooled on the outside and which has a heated wire along the axis. In a horizontal cross section the gradient effects a small isotope separation. The convection current, going down at the cold wall and up in the warm centre part of the column, results in a net transport of the isotopic molecules. Generally the heavy isotope moves down the column and the light isotope to the top. As a result, a concentration gradient is built up along the tube.

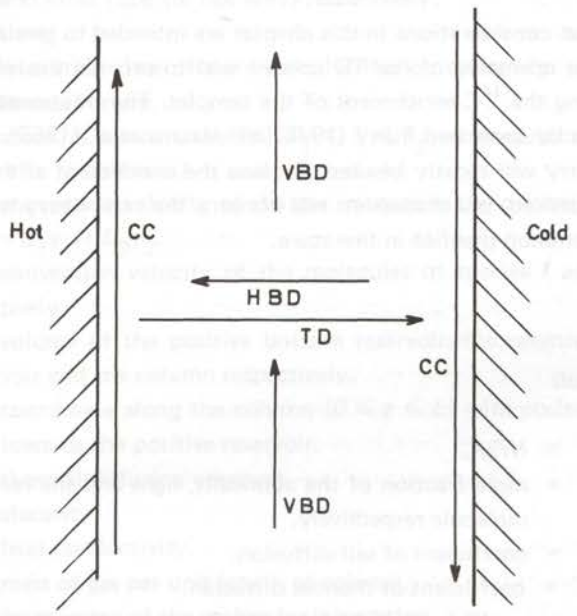

Fig. 2.1. Processes determining the net transport of isotopes in a thermal diffusion column; we consider the transport of the heavy isotopic species.
TD – thermal diffusion isotope separation,
HBD – horizontal back diffusion,
CC – convection current,
VBD – vertical back diffusion.

The net transport of isotopes through the column is determined by four processes (fig. 2.1):

(i) The TD process, which builds up a horizontal concentration gradient;
(ii) A horizontal back diffusion (HBD) due to this concentration gradient;
(iii) A convection current (CC), transporting the isotopically heavy gas downwards along the cold wall and the light gas upwards along the hot wire;
(iv) A vertical back diffusion (VBD) due to the vertical concentration gradient.

The consequence of the vertical concentration gradient in the column is that the convection current replaces the gas in the cold part of a certain cross section by lighter gas from a higher level and vice versa in the warm part. This reduces the horizontal concentration gradient. The processes (i), (ii) and (iii) determine the difference in average isotopic composition between the columns of gas moving up and down. This difference together with the speed of convection determines the transport that separates the isotopic molecules. Because of this the net transport of isotopic molecules will first increase with the speed of convection, but be reduced if it becomes too large.

The theoretical considerations in this chapter are intended to give an understanding of TD and the operation of the TD column and to provide the relations necessary for determining the ^{14}C enrichment of the samples. The treatment is largely based on the reviews by Jones and Furry (1946) and Vasaru et al. (1969). The notation of Jones and Furry will mostly be used. Because the enrichment of the heavy isotopic molecules is desired, our discussion will concern the rare, heavy isotopic species as opposed to common practice in literature.

List of Symbols

A $\equiv H/2K$.
C_1, C_2 = mole fraction of the abundant, light and the rare, heavy isotopic molecule respectively.
D = coefficient of self-diffusion.
D_T = coefficient of thermal diffusion.
$D_{1,2}$ = coefficient of ordinary diffusion.
g = acceleration of gravity.
H = thermal diffusion transport coefficient.
h = thermal diffusion shape factor.
J_1, J_2 = $\rho_1 C_1 v_1$; = $\rho_2 C_2 v_2$; = flux of species 1 and 2 respectively, mass per unit area per unit time.

K = $K_c + K_d + K_p$.

K_c, K_d, K_p = transport coefficients (see eq. 2.3 and 2.4).

$k_c, k_d, k_{d'}, k_t$ = transport coefficient shape factors.

L = length of the column.

m_+, m_- = mass of gas in the positive (enrichment) and the negative (storage) reservoir respectively.

m_+'' = fictitious mass in positive reservoir obtained by correcting m_+ for enrichment in the part of the column adjacent to the positive reservoir and depletion in the part adjacent to the negative one (eq. 2.15).

M = molecular weight.

p = pressure.

q = separation factor.

q' = enrichment.

q_e, q_e' = equilibrium value of the separation factor and enrichment respectively.

r = radial coordinate, $r_2 \leqslant r \leqslant r_1$, where r_1, r_2 are the radii of outer and inner tube (or hot wire) respectively.

t = time.

t_r = relaxation time of the thermal diffusion system for the approach to equilibrium.

T = absolute temperature (K) $T_1 \leqslant T \leqslant T_2$, where subscripts 1 and 2 refer to cold and hot wall respectively.

v = convection velocity of the gas mixture in the columns as a whole $= C_1 v_1 + C_2 v_2$.

v_1, v_2 = convection velocity of the molecules of species 1 and 2 respectively.

V_+, V_-, V_c = volume of the positive bottom reservoir, the negative top reservoir and the column respectively.

z = coordinate along the column ($0 \leqslant z \leqslant L$) with positive direction towards the positive reservoir.

α = thermal diffusion constant.

η = viscosity.

λ = heat conductivity.

μ = mass of gas per unit length of column.

ν = force index of the molecular interaction.

ρ, ρ_1, ρ_2 = density, mass per unit volume; subscripts 1 and 2 refer to densities of gas consisting of the pure light species 1 and the pure heavy species 2 respectively.

τ_1, τ_2 = transport along the column of species 1 and species 2 respectively (in mass per unit time).

The indices $..^{29}$, $..^{30}$ and $..^{14}$ will be used to indicate all molecules of mass 29 (mainly $^{13}C^{16}O$) and 30 (mainly $^{12}C^{18}O$) respectively and all molecules containing the isotope ^{14}C (mainly $^{14}C^{16}O$).

2.1.2. The transport equation

In order to calculate the isotopic enrichment in TD columns, the transport equation has to be solved. The transport equation describes the mass transport of one isotopic species through the column. It can be derived from a consideration of the transport due to (i) thermal diffusion, (ii) concentration diffusion and (iii) movement of the gas as a whole.

Theory predicts that, when applying a temperature gradient to a mixture of gases, two diffusion phenomena occur: the normal concentration diffusion ($C_2(v_2-v) = -D$ grad C_2) and the thermal diffusion which can be represented by $C_2(v_2-v) = -(D_T/T)$ grad T (Jones and Furry, 1946). For definitions see list of symbols (sect. 2.1.1). D_T is directly proportional to the product C_1C_2 of the concentrations. It is therefore useful to introduce the *thermal diffusion constant*

$$\alpha = D_T/D\, C_1 C_2,$$

which only slightly depends on the concentration. The temperature dependence of α is determined by the specific molecular interaction model used. It vanishes for the inverse power repulsion model, but exists for more complicated potential models like the Lennard-Jones 12–6 and the Buckingham exp.–6 model. Experiments have shown that α is temperature dependent.

In a binary gas mixture confined in the annular space between two vertical concentric cylinders the mass flux (J_2) of the heavy isotopic molecule due to the three transport processes is

$$J_2 = \rho_2\, C_2\, v_2 = \rho_2 C_2 v - \rho_2 D(\text{grad } C_2 + \alpha C_1\, C_2 \text{ grad ln } T). \qquad (2.1)$$

It should be noted that in combination with the mole fraction C_2 the density ρ_2 of a gas merely consisting of the heavy isotopic molecules should be used (alternatively the density ρ of the mixture can be combined with the mass fraction, Rutherford (1970)). If we consider a column closed at both ends, there is no net gas flow. The total transport of the heavy isotope down the column (τ_2) is obtained by integrating the z-component of the mass flux J_2 over the column cross section. The positive direction of z is chosen down the column towards the reservoir where the heavy isotope is concentrated.

$$\tau_2 = 2\pi \int_{r_2}^{r_1} J_{2z}\, r\, dr = 2\pi \int_{r_2}^{r_1} \rho_2 C_2 v\, r\, dr - 2\pi \int_{r_2}^{r_1} \rho_2 D\, r \frac{\partial C_2}{\partial z} dr. \qquad (2.2)$$

For the evaluation of eq. 2.2 we assume that the convective flow in the column is laminar and the radial change in composition is so small that it does not influence the transport properties and the density. The value of C_2 is determined not only by convection and concentration diffusion, but also by thermal diffusion in the horizontal temperature gradient. Because of the temperature gradient, ρ_2 as well as v and C_2 depend on the position r in the column.

Macroscopically measurable transport properties of a gas (rate of diffusion D, viscosity η, thermal conductivity λ and TD constant α) are determined by forming averages over all individual collisions in the gas. They can be expressed in terms of the collision integrals.

If we take a realistic potential model like the Lennard-Jones 12–6, the collision integrals, the temperature dependence of the transport properties and thus the integrals of eq. 2.2 can be evaluated (Vasaru et al., 1969),

$$\tau_2 = H\, C_1 C_2 - K_c \frac{\partial C_2}{\partial z} - K_d \frac{\partial C_2}{\partial z} - K_{d'} \frac{\partial^2 C_2}{\partial z^2} + K_t \frac{\partial C_2}{\partial t}. \qquad (2.3)$$

Here H, K_c, K_d, $K_{d'}$ and K_t are the *transport coefficients*.

The first term represents the separation due to thermal diffusion. The second refers to the remixing by convection and the third to the vertical concentration diffusion. The effect of the horizontal concentration diffusion (HBD, fig. 2.1) is incorporated in the other terms. $K_{d'}$ and K_t also represent convection influences. Under practical circumstances, where C_2 changes only slowly, $K_t(\partial C_2/\partial t)$ can be neglected (quasi-stationary assumption). The same applies to $K_{d'}$ $(\partial^2 C_2/\partial z^2)$ which is of the same magnitude as $K_t(\partial C_2/\partial t)$ but of opposite sign.

In practice it turns out, that a term $K_p(\partial C_2/\partial z)$ has to be added, originating from parasitic remixing caused by imperfect geometry in the column and/or an azimuthal temperature gradient.

The constants in eq. 2.3 can be written more explicitely as

$$\begin{aligned} H &= \frac{2\pi}{6!} g \left\{ \frac{\alpha \rho \rho_2}{\eta} \right\}_{T_1} r_1^4\, h; \\ K_c &= \frac{2\pi}{9!} g^2 \left\{ \frac{\rho^2 \rho_2}{\eta^2 D} \right\}_{T_1} r_1^8\, k_c; \\ K_d &= 2\pi \{\rho_2 D\}_{T_1} r_1^2\, k_d; \end{aligned} \qquad (2.4)$$

$$K_{d'} = 2\pi g \left\{ \frac{\rho\rho_2}{\eta} \right\}_{T_1} r_1^6 k_{d'};$$

$$K_t = 2\pi g \left\{ \frac{\rho\rho_2}{\eta D} \right\}_{T_1} r_1^6 k_t.$$

The transport coefficient of parasitic remixing, K_p, cannot be calculated theoretically; g is the acceleration due to gravity and h, k_c, k_d, $k_{d'}$ and k_t are dimensionless quantities called *shape factors*. These depend on the operating conditions (r_1, r_2, T_1, T_2), the kind of gas and the molecular interaction model used. For the models also containing an attraction term (Lennard-Jones) the TD constant α is temperature-dependent.

For a hot-wire column we have an extreme cylindrical geometry where most of the gas is at a temperature close to T_1. Therefore the shape factors and the transport coefficients are commonly expressed in terms of the transport properties of the gas at the temperature of the cold wall T_1.

It should be noted that in eq. 2.4 both ρ and ρ_2 appear. In this formulation eq. 2.3 can be used for either component of the mixture by inserting the corresponding subscripts. Although there is a net mass transport through the column during enrichment, the net particle transport must be zero. If the molecular weights of the isotopic species are M_1 and M_2, $\rho_2 = M_2\rho_1/M_1$. The net particle transport, τ_1/M_1 and τ_2/M_2, is obtained from eq. 2.3. Inserting $\rho_2 = M_2\rho_1/M_1$ we find $\tau_1/M_1 = \tau_2/M_2$ which means a particle transport zero. The factor ρ is introduced by the hydrodynamical equation (Vasaru et al., 1969) used to obtain the total transport by integrating the mass flux over the column cross section.

From experimental values of D, η, ρ and α and from tabulated values of the shape factors for different interaction potentials we can calculate the constants H, K_c and K_d for a binary mixture.

Most natural gases, however, are not simple binary mixtures but contain several isotopic molecules of different mass and symmetry. Theoretical discussions of thermal diffusion in multicomponent mixtures have been given by Hellund (1940), Jones (1941), Laranjeira (1960) and Van der Valk (1963). In a multicomponent isotopic mixture consisting of n components the mass flux of component i due to the interaction between the components i and k is:

$$\tau_i = C_i \sum_{k=1}^{n} H_{ik} C_k - (K_c + K_d) \frac{\partial C_i}{\partial z} - K_{d'} \frac{\partial^2 C_i}{\partial z^2} + K_t \frac{\partial C_i}{\partial t} \qquad (2.5)$$

in complete analogy with a binary mixture. If one isotopic species is dominant while the others are present in sufficiently low concentrations, the interaction between the rare isotopic molecules can be neglected. The multicomponent mixture can then be treated as a system of binary mixtures, a poly-binary mixture (Van der

Valk, 1963). This is true for natural gas samples and for the enrichments normally used.

2.1.3. Isotope separation and enrichment as a function of time

From the transport equation (eq. 2.3)

$$\tau = HC_1C_2 - K\partial C_2/\partial z \quad (K = K_c + K_d\ (+ K_p))$$

the isotope separation and the enrichment can be calculated as a function of time. This is simple in the initial stage of the enrichment and when the final equilibrium has been reached, but complicated in the intermediate stages.

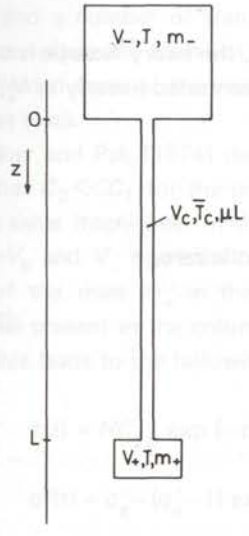

Fig. 2.2. Thermal diffusion column with reservoirs.
V_-, V_+, V_c — volume of storage reservoir, enrichment reservoir and column respectively,
T, $\bar{T}_c$ — temperature in the reservoirs and average temperature in the column,
m_-, m_+, μL — mass of gas in the storage reservoir, the enrichment reservoir and the column of length L, respectively.

The transport equation merely gives the mass transport of the isotopic molecules considered. The isotopic composition of the gas in different parts of the system is determined by the time the transport has lasted and by the amounts of gas in the different volumes. We consider a system represented by fig. 2.2. Since the amount of gas used for the enrichment is finite, an enrichment of one isotope in V_+ necessarily is accompanied by a depletion of this isotope in V_-. It is therefore practical to introduce two quantities:

the separation factor (Jones and Furry, 1946)

$$q \equiv \frac{\text{isotope ratio in enrichment volume } V_+}{\text{isotope ratio in reservoir } V_-}$$

and the enrichment

$$q' \equiv \frac{\text{concentration in } V_+ \text{ obtained by enrichment}}{\text{concentration prior to enrichment}} .$$

Though q is closely related to the TD properties of the gas and to the TD column, q' will be the quantity of practical interest for radiocarbon dating.

We first treat the simple problems of the initial stage of the enrichment and the equilibrium situation and then discuss a practical approximation describing the transient behaviour during enrichment.

To start with, we have a homogeneous gas mixture. Consequently $\partial C_2/\partial z = 0$ and the *initial transport*

$$\tau_2 = HC_1C_2. \tag{2.6}$$

As long as the concentration gradient can be neglected, the heavy isotope is transported at a constant rate through the column and is concentrated linearly in V_+,

$$dC_2/dt = M_1\tau_2/M_2\, m_+ . \tag{2.7}$$

Here we assumed that $C_2 \ll C_1$ so $\rho \approx \rho_1$.

In the dynamic *equilibrium situation* the net transport is zero,

$$\tau_2 = HC_1C_2 - K\frac{dC_2}{dz} = 0. \tag{2.8a}$$

For a binary mixture $C_1 = 1-C_2$, so

$$\frac{dC_2}{C_2(1-C_2)} = \frac{H}{K}\,dz,$$

and

$$\frac{C_2(z)/C_1(z)}{C_2(z_o)/C_1(z_o)} = \exp\frac{H}{K}(z-z_o). \tag{2.8b}$$

The equilibrium separation factor then is:

$$q_e = \frac{C_2(L)/C_1(L)}{C_2(0)/C_1(0)} = \exp\frac{H}{K}L = \exp 2AL, \tag{2.9}$$

where $A = H/2K$.

q_e is constant for a certain column and certain operating conditions and independent of the volumes used. Although time consuming, the thermal diffusion constants can be determined from measurements of q_e (De Vries, 1956; Saviron et al., 1975, 1976).

The *transient behaviour* of the isotope separation and the enrichment must be derived from the transport equation (2.3) and the equation of continuity for species 2 (c.f. eq. 2.1):

$$\partial(\rho_2 C_2)/\partial t = -\operatorname{div}(J_2) = -\operatorname{div}\,(\rho_2 C_2 v - \rho_2 D \operatorname{grad} C_2 - \rho_2 D \alpha C_1 C_2 \operatorname{grad} \ln T). \tag{2.10}$$

The exact solution for a practical system is complex and has not been given. Solutions under certain simplifying assumptions are given by Bardeen (1940) and Jones and Furry (1946).

In a binary mixture with $C_2 \ll C_1$, so $C_1 = 1 - C_2 \approx 1$, τ_2 is linearly related to C_2. The solution presenting the concentration of the heavy isotope as a function of time and place in the column is a series expansion in terms of the final equilibrium value and a number of transient terms with rapidly decreasing time constants. In practice, often one transient term gives a sufficient approximation. Because of the complicated form of the exact solution, an approximate formula is to be preferred in most cases.

Felber and Pak (1974) developed an approximation method under the assumption that $C_2 \ll C_1$ for the practical case of a finite, large V_-, while V_c and V_+ are of the same magnitude. In their paper the treatment of Jones and Furry (1946) for $V_+ \gg V_c$ and $V_- = \infty$ is followed. The actual situation is accounted for by a correction of the mass m_+ in the positive reservoir both for the amount of enriched material present in the column and for the depletion of the column gas adjacent to V_-. This leads to the following equations for the transient behaviour of τ, q' and q:

$$\tau(t) = HC_{2o} \exp(-t/t_r); \tag{2.11}$$

$$q'(t) = q'_e - (q'_e - 1) \exp(-t/t_r); \tag{2.12}$$

$$q(t) = q_e \frac{q'_e - (q'_e - 1) \exp(-t/t_r)}{q'_e + (q_e - q'_e) \exp(-t/t_r)}. \tag{2.13}$$

Here

$$t_r = \frac{M_2}{M_1} \frac{m''_+}{H} (q'_e - 1) \tag{2.14}$$

is the time in which the initial transport would yield the equilibrium concentration of the rare heavy isotope in V_+ and m''_+ is the fictitious corrected mass consisting of the mass in V_+ and a term taking into account the enrichment in the column near V_+ and the depletion near V_- at equilibrium:

$$m''_+ = m_+ + \mu L \frac{m_-[(q_e - 1)/\ln q_e - 1] - m_+ [q_e - (q_e - 1)/\ln q_e]}{m_-(q_e - 1) + \mu L [q_e - (q_e - 1)/\ln q_e]} . \quad (2.15)$$

From a consideration of mass balance follows

$$q' = q(m_- + m''_+)/(m_- + qm''_+). \quad (2.16)$$

Felber and Pak (1974) found excellent agreement between the results of the approximation formulas 2.11–2.16 and those of the formulas derived more exactly.

The important question now is whether these equations describe the experimental results with sufficient accuracy to be used to predict the enrichment obtained. Comparing the theoretical and the experimental results Felber and Pak (1972) found considerable discrepancies. The experimental values of H and K_c were up to 40% smaller than the theoretical ones, that of t_r was about 40% higher. The enrichment, however, was fairly close to the theoretical value, indicating that the ratio V_+/V_- in this case probably has more influence on q'_e than H and K.
The apparatus was shown to work reproducibly. This means that, provided the experimental conditions (p, V, T_1, T_2) are kept constant, a few calibration runs can give the experimental parameters necessary to predict the enrichment.

If a more variable system is used (for instance a volume V_- depending on the amount of sample available), one can either make calibrations for a whole range of experimental conditions or determine the enrichment by measuring the simultaneous enrichment of a closely related molecule (De Vries, 1956; Grootes et al., 1975). This also has the advantage of being independent of the reproducibility of the column behaviour, provided a constant relation between the separation factors or enrichments of the two isotopic species exists.
The time dependence of the enrichment is given by eq. 2.12 in which both q'_e and t_r strongly depend on V_-. In eq. 2.13, which gives the separation factor as a function of time, q_e is volume independent (q'_e is only present in a correction factor).

In an earlier paper (Grootes et al., 1975) we used a simple approximate formula for the time dependence of the isotope separation,

$$(q-1) = (q_e - 1)(1 - e^{-t/t_r}),$$

and showed that the relation between the separation factors of different isotopic species could be given by a polynomial. In this way the influence of V_- and the depletion of the abundant molecule $C_1 = 1 - \sum_{i=2}^{n} C_i$ appears explicitly in the calculation of the enrichment.
The present more detailed treatment yields a relation for the enrichment of the same form (eq. 2.12).

From eq. 2.12 the relation between the enrichments of two different isotopic species I and II can be derived by elimination of t:

$$t = -t_r^{I} \ln\left\{1-\frac{q^{I'}-1}{q_e^{I'}-1}\right\}, \tag{2.17}$$

$$1-\frac{q^{II'}-1}{q_e^{II'}-1} = \left\{1-\frac{q^{I'}-1}{q_e^{I'}-1}\right\}^{t_r^{I}/t_r^{II}} \tag{2.18}$$

After rearrangement a series expansion gives

$$q^{II'}-1 = a_1(q^{I'}-1) + a_2(q^{I'}-1)^2 + a_3(q^{I'}-1)^3 + \ldots, \tag{2.19}$$

where $a_1 = \dfrac{(q_e^{II'}-1)t_r^{I}}{(q_e^{I'}-1)t_r^{II}} = \dfrac{m_+''^{I}H^{II}}{m_+''^{II}H^{I}}$,

$$a_2 = \frac{(q_e^{II'}-1)t_r^{I}(t_r^{II}-t_r^{I})}{(q_e^{I'}-1)^2\,2!(t_r^{II})^2} = \frac{m_+''^{I}H^{II^2}}{2!(m_+''^{II})^2H^{I}}\left\{\frac{m_+''^{II}}{H^{II}(q_e^{I'}-1)} - \frac{m_+''^{I}}{H^{I}(q_e^{II'}-1)}\right\},$$

$$a_3 = \frac{(q_e^{II'}-1)t_r^{I}(t_r^{II}-t_r^{I})(2t_r^{II}-t_r^{I})}{(q_e^{I'}-1)^3 3!(t_r^{II})^3}$$

$$= \frac{m_+''^{I}H^{II^3}}{3!(m_+''^{II})^3H^{I}}\left\{\frac{m_+''^{II}}{H^{II}(q_e^{I'}-1)} - \frac{m_+''^{I}}{H^{I}(q_e^{II'}-1)}\right\}\left\{\frac{2m_+''^{II}}{H^{II}(q_e^{I'}-1)} - \frac{m_+''^{I}}{H^{I}(q_e^{II'}-1)}\right\}.$$

Apparently the first coefficient a_1 only slightly depends (through m_+'') on the size of V_-, as opposed to a_2, a_3, ... (through q_e'). If the values of H and K are known for both isotopic molecules, the coefficients of the calibration relation can be calculated for each volume V_- used. These values (sect. 2.1.4) are to be compared with the experimental results (sect. 2.4).

2.1.4. Theoretical values

The enrichment parameters and the gas properties are given in table 2.1 and 2.2. To determine the dependence of the calculated enrichment on the specific interaction potential model, the shape factors (c.f. eq. 2.4) are calculated for three simple but more or less realistic models, viz. the Inverse Power repulsion (IP), the Lennard-Jones 12–6 (L-J 12–6) and the Buckingham exp. –6 (B exp. –6). Extensive tabulations for the IP model are given by Greene et al. (1966), for the L-J 12–6 model by McInteer and Reisfeld (1961). The shape factors for the B exp. –6 model

were supplied by Saviron (pers. communication). The shape factors and transport coefficients have to be calculated for a range of r_1 and T_1 values, because the column diameter varies from 0.89 cm near V_+ to 0.99 cm near V_-, and the cooling water temperature changes by at least 8 °C from V_+ to V_-. The shape factors are given in table 2.3.

Table 2.1. Parameters of the enrichment apparatus.

inner diameter columns	$0.89 < 2r_1 < 0.99$ cm
diameter wire	$2r_2 = 0.03$ cm
length of columns	$L \approx 600$ cm
temperature cold wall	$T_1 \approx 300$ K ($25\,^\circ\text{C} < T_1 < 35\,^\circ\text{C}$)
temperature hot wire	$T_2 \approx 920$ K
number of columns in parallel	9

Table 2.2. Gas properties at 300 K, 910 torr.

	CO			
$\rho_1 \approx \rho$		:	1.36×10^{-3} g/cm³	a
ρ_2	mass 29	:	1.41×10^{-3} g/cm³	
ρ_2	mass 30	:	1.46×10^{-3} g/cm³	
η		:	1.77×10^{-4} g/cm sec	a
D		:	0.187 cm²/sec	b
α	$^{13}C^{16}O/^{12}C^{16}O$	:	5.04×10^{-3}	c
	$^{14}C^{16}O/^{12}C^{16}O$	:	12.9×10^{-3}	c
	$^{12}C^{18}O/^{12}C^{16}O$	:	10.04×10^{-3}	c

a Handbook of Chemistry and Physics 49th ed. (1968) B 189 and F 43
b Amdur and Shuler (1963)
c Boersma-Klein and De Vries (1966)

Considering the fact that the shape factors for IP and L-J 12–6 were obtained by graphical interpolation from tabulated values, the application of different models presents good agreement (within 1% with the exception of h_{IP} and $h_{L\text{-}J}$). The values for the L-J shape factors may be somewhat large, since a direct computation of some of them by Saviron (pers. communication) yielded lower values ($\approx 4\%$ for h and $\approx 1\%$ for k_c and k_d).

We choose the L-J 12–6 interaction potential as our working model. Using eqs. 2.4 and tables 2.1–2.3 the transport coefficients were calculated for this potential model (table 2.4). Similar values were obtained for the other potentials. Using eq. 2.9 ($q_e = \exp\{H/(K_c + K_d)\}L$) we obtain the equilibrium separation factor q_e (table 2.5). Apparently small differences in transport coefficients yield considerably

Table 2.3. Shape factors for different interaction potential models.

I. Inverse Power Repulsion[a]

		h	$k_c \times 10^2$			k_d
T_1 (K)	T_2/T_1	r_1/r_2	r_1/r_2			r_1/r_2
		29.7–33.0	29.7	31.5	33.0	29.7–33.0
298	3.09	0.118	2.17	2.21	2.25	0.631
308	2.99	0.113	2.29	2.33	2.37	0.619
343†	2.68	0.102	2.35	2.39	2.43	0.601

II. Lennard-Jones 12–6

			h	$k_c \times 10^2$			k_d		
T_1 (K)	T_2/T_1 (=Θ)	$T_1{}^{*b}$	r_1/r_2 (=y_o)	r_1/r_2			r_1/r_2		
			29.7–33.0	29.7	31.5	33.0	29.7	31.5	33.0
298	3.09	3.39	0.138	2.21	2.26	2.30	0.633	0.635	0.637
308	2.99	3.50	0.132	2.28	2.33	2.37	0.625	0.627	0.629
343†	2.68	3.90	0.113	2.46	2.51	2.54	0.603	0.604	0.606

III. Buckingham exp. –6[c]

			h		$k_c \times 10^2$		k_d	
T_1 (K)	T_2/T_1 (=Z_o)	$T_1{}^{*c}$	r_1/r_2 (=y_o)		r_1/r_2		r_1/r_2	
			29.7	33.0	29.7	33.0	29.7	33.0
298	3.09	2.50	0.139	0.138	2.14	2.22	0.638	0.635
343†	2.68	2.92	0.114	0.113	2.40	2.48	0.606	0.604

a force $\sim r^{-\nu}$; the force index ν = 10.7 was calculated from the temperature variation of the viscosity, tabulated for the range 273 – 550 K (Handbook of Chemistry and Physics 49th ed. (1968) F 43) with $\rho \sim T^n$ giving n = 0.707 and $\nu = (2n+3)/(2n-1)$

b $T_1{}^* = kT_1/\epsilon$ is the reduced temperature at the cold wall of the column, ϵ/k = 88 K (Vasaru et al., 1969)

c shape factors calculated by Saviron (pers. communication) using Simpson integration routines, a steepness parameter a = 17 (Mason and Rice, 1954) and ϵ/k = 119 K at 298 K and 118 K at 343 K respectively

† maximum temperature of cooling water, occasionally reached; thermal protection switches off the power at this temperature

Table 2.4. Transport coefficients for the Lennard-Jones 12–6 model.

Molecule	T_1 (K)	$H \times 10^6$ (g/sec)			$K_c \times 10^4$ (g cm/sec)			$K_d \times 10^4$ (g cm/sec)		
		r_1/r_2			r_1/r_2			r_1/r_2		
		29.7	31.5	33.0	29.7	31.5	33.0	29.7	31.5	33.0
$^{13}C^{16}O$	298	2.54	3.16	3.89	2.61	4.14	6.38	2.07	2.31	2.57
	308	2.37	2.95	3.63	2.21	3.49	5.38	2.09	2.34	2.61
	343	1.81	2.25	2.77	1.21	1.91	2.92	2.19	2.45	2.72
$^{14}C^{16}O$	298	6.71	8.35	10.27	2.71	4.29	6.61	2.14	2.39	2.66
	308	6.25	7.78	9.58	2.28	3.61	5.56	2.17	2.42	2.70
	343	4.74	5.90	7.25	1.25	1.98	3.03	2.27	2.54	2.82
$^{12}C^{18}O$	298	5.27	6.56	8.07	2.71	4.29	6.61	2.14	2.39	2.66
	308	4.77	5.93	7.30	2.28	3.61	5.56	2.17	2.42	2.70
	343	3.35	4.17	5.12	1.25	1.98	3.03	2.27	2.54	2.82

Table 2.5. Equilibrium separation factors for different interaction potential models.

Molecule	T_1 (K)	q_e							
		Potential model							
		IP			L-J 12–6			B exp. –6	
		r_1/r_2			r_1/r_2			r_1/r_2	
		29.7	31.5	33.0	29.7	31.5	33.0	29.7	33.0
$^{13}C^{16}O$	298	16.8	12.9	9.7	26.0	18.9	13.5	27.6	14.6
	308	16.9	13.5	10.4	27.4	20.8	15.3		
	343	19.0	17.8	15.4	24.5	22.3	19.1	25.4	19.8
$^{14}C^{16}O$	298	1320	680	329	4060	1800	770	4720	929
	308	1350	755	387	4600	2290	1050		
	343	1700	1430	1000	3210	2540	1710	3510	1890
$^{12}C^{18}O$	298	284	168	95	685	362	186	771	215
	308	243	156	94	618	364	200		
	343	192	176	132	300	254	192	320	206

different separation factors. Considering the direct dependence of the transport coefficients on the column radius (r_1^4, r_1^8 and r_1^2 for H, K_c and K_d respectively, eqs. 2.4) a maximum value of q_e will be obtained for $K_d = 2K_c$. Because also the shape factors (slightly) vary with r_1, the true maximum of q_e will be found near this value. The column radii r_1 and r_2 have therefore been chosen near the value

maximizing q_e. A larger r_1 results in an increased rate of enrichment on the one hand and a lower q_e on the other. Therefore the optimum value of r_1 is somewhat larger than the value maximizing q_e.
Similarly a maximum of q_e as a function of T_1 is expected near $K_c = K_d$. An increase of q_e with T_1 is expected for $K_c > K_d$ and a decrease for $K_c < K_d$ (c.f. table 2.4 and 2.5).

Finally we can calculate the values of q'_e and t_r, using eq. 2.14, 2.15 and 2.16. In eq. 2.14 in combination with the total mass in V_+ we must use the total TD transport of 9 columns in parallel, i.e. $9H$. The q'_e values for standard and minimum volume and for the practical range of r_1 and T_1 are given in table 2.6. In fig. 2.3 and 2.4 the values of q'_e and t_r are shown as a function of V_- for the different isotopic molecules.

Table 2.6. Equilibrium enrichment factor and relaxation time for the Lennard-Jones 12–6 potential model.

Molecule	T_1 (K)	V_- = 201 l (standard)						V_- = 57 l (minimum)					
		q'_e			t_r (days)			q'_e			t_r (days)		
		r_1/r_2			r_1/r_2			r_1/r_2			r_1/r_2		
		29.7	31.5	33.0	29.7	31.5	33.0	29.7	31.5	33.0	29.7	31.5	33.0
$^{13}C^{16}O$	298	14.6	12.1	9.7	63.7	42.1	27.0	7.5	6.8	6.0	29.4	21.3	15.0
	308	15.1	12.9	10.6	70.3	48.0	31.7	7.6	7.0	6.3	32.0	23.6	17.0
	343	14.2	13.4	12.2	85.8	65.2	47.9	7.4	7.2	6.8	40.4	31.5	24.3
$^{14}C^{16}O$	298	34.2	33.6	32.6	56.6	45.0	35.7	10.7	10.6	10.5	16.1	12.9	10.4
	308	34.2	33.8	33.0	60.8	48.5	38.7	10.8	10.7	10.6	17.3	13.9	11.2
	343	34.2	34.0	33.7	80.0	64.1	51.8	10.7	10.7	10.7	22.8	18.3	14.8
$^{12}C^{18}O$	298	32.4	30.9	28.4	69.2	53.4	40.2	10.5	10.3	9.9	20.2	16.1	12.7
	308	32.2	31.0	28.8	76.2	59.1	44.9	10.4	10.3	10.0	22.4	17.8	14.1
	343	30.5	29.9	28.7	102.8	81.1	63.6	10.2	10.1	10.0	31.3	25.0	20.0

Apparently, the volume ratio V_t/V_+ ($V_t = V_+ + V_- + V_c$) is the factor determining the enrichment for large separation factors ($q_e > 10V_t/V_+$). Under these conditions the enrichment set-up will operate reproducibly, insensitive to small variations in operating conditions (T_1, T_2, p). The choice of the potential model has little influence on the calculated q'_e and t_r. This is evident from a comparison of table 2.5, showing that the influence of variations of r_1 and T_1 on q_e is equally large as that of the interaction potential model, with table 2.6 and fig. 2.3, showing that q'_e for

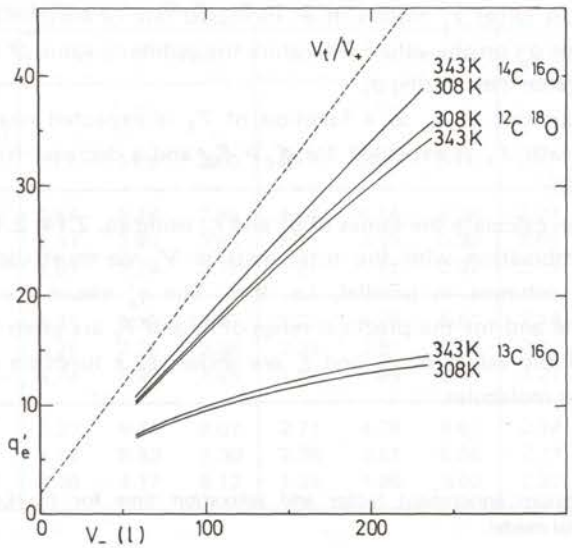

Fig. 2.3. Equilibrium enrichment q'_e as a function of the size of the storage volume V_-. V_t/V_+ — ratio of the total system volume ($V_- + V_+ + V_c$) and the enrichment volume.

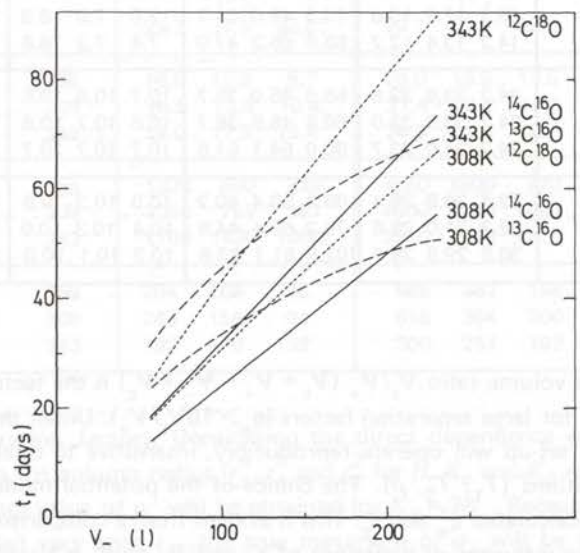

Fig. 2.4. Relaxation time t_r of enrichment as a function of the size of the storage volume V_-.

$^{14}C^{16}O$ and $^{12}C^{18}O$ is mainly determined by V_- ($\approx V_t$). Using the tabulated values of q'_e and t_r and eq. 2.11 and 2.12 the performance of the TD set-up can be calculated. In section 2.4.2 we give a comparison of this calculation with the enrichments observed.

Because of the similar enrichment of the $^{12}C^{18}O$ and $^{14}C^{16}O$ molecules (fig. 2.3 and 2.4) the former is considered to be a good indicator for the ^{14}C enrichment obtained. The figures show that the relation between $q^{14'}$ and $q^{18'}$ will slightly depend on V_- and the temperature. Values for the coefficients a_1, a_2 and a_3 of eq. 2.19 are given in table 2.7. It should be noted that these values only apply to the molecules $^{14}C^{16}O$ and $^{12}C^{18}O$. The experimental relation, on the contrary, will be based on a comparison of all ^{14}C containing isotopic molecules, including $^{14}C^{17}O$ and $^{14}C^{18}O$, with those of mass 30 ($^{12}C^{18}O + {}^{13}C^{17}O + {}^{14}C^{16}O$).

Table 2.7. Theoretical values for the coefficients a_1, a_2 and a_3 in the relation $(q^{14'}-1) = a_1 (q^{18'}-1) + a_2(q^{18'}-1)^2 + a_3(q^{18'}-1)^3$ for different storage volumes.

V_- (l)	T_1 (K)	a_1	$a_2 \times 10^3$	$a_3 \times 10^5$
57	308	1.338	−20.3	−52
	343	1.449	−28.9	−67
90	308	1.337	−12.5	−21
	343	1.448	−17.6	−28
119	308	1.337	− 9.2	−12
	343	1.448	−12.8	−16
169	308	1.337	− 6.1	− 6
	343	1.447	− 8.4	− 8
201	308	1.336	− 4.9	− 4
	343	1.447	− 6.7	− 6
231	308	1.336	− 4.1	− 3
	343	1.447	− 5.5	− 4

For mono-atomic molecules the theoretical models used above give satisfactory results. For poly-atomic molecules most properties of the gas can be described. The phenomenon of thermal diffusion, particularly the TD constant α, however, cannot be described accurately by these simple potential models, since it depends critically on the type of collisions. Therefore the 'theoretical' values calculated above were obtained from a theory that applies to spherically symmetric 'soft' molecules and experimental values of the thermal diffusion constant α. From the observation that

the choice of the potential model is of minor importance in the calculations given above, it follows that the main influence of the model is via α.

It has been shown (Boersma-Klein and De Vries, 1966; Stevens and De Vries, 1968) that the use of a non-spherical interaction potential fails to describe experiments satisfactorily. Rather, the difference in mass-distribution within the molecule is the determining factor. To explain the experimental results Schirdewahn et al. (1961) considered the influence of the moment of inertia of the molecules on the thermal diffusion behaviour. Van de Ree (1967) gave a discussion in which a spherical potential located in the centre of the molecule rotates around the centre of mass.

Another effort to account for the non-sphericity of the molecules is the description as rigid rotating ovaloids. In analogy to the model of rigid elastic spheres this model is partially successful, but cannot predict the temperature dependence of α. Recently Verlin et al. (1975a, b) calculated collision integrals for soft non-spherical molecules developed in terms of spherical Ω collision integrals. They found a satisfactory theoretical temperature dependence after the parameters had been fitted to experiments for CO at one temperature.

It was discussed above that the influence of the interaction potential on the shape factors and hence on q'_e and t_r is small. Therefore the theoretical refinements just mentioned are only needed when the thermal diffusion constant α must be obtained from theory because experimental values are not available.

2.1.5. The choice of CO

To qualify as a suitable molecule for the enrichment of a certain isotope, a molecule should be light (so as to obtain a large relative mass difference between the isotopic molecules), 'hard' (in behaviour closely resembling a rigid elastic sphere), relatively easy to prepare, and a closely related isotopic species should be available that allows a measurement of the enrichment. This last condition is necessary due to the often poor agreement between the theoretically predicted and the experimentally attained enrichment.

For carbon the most suitable molecules are CH_4 and CO. Radiocarbon samples are initially combusted to CO_2 that is either used directly as a counting gas, or subsequently converted to methane, acetylene or benzene before counting. The molecule CO has been chosen for the enrichment because: (i) the reduction of CO_2 to CO is relatively simple; (ii) the greater thermal stability and hardness of CO as compared to CH_4 compensate for the effect of smaller relative mass difference; (iii) the isobaric molecule $^{12}C^{18}O$ offers a possibility of indirectly measuring the ^{14}C enrichment mass spectrometrically. For CH_4 this is more difficult since the isobaric molecules of mass 18 are rare ($^{13}CH_3D$: $C \approx 6 \times 10^{-6}$ and $^{12}CH_2D_2$: $C \approx 1.3 \times 10^{-7}$). Isotopic molecules of mass 17 can in principle also be used to determine the ^{14}C enrichment. They have, however, the disadvantage of having a different mass.

Furthermore we have in natural samples a mixture of two different molecules of mass 17 ($^{13}CH_4$: $C \approx 10^{-2}$ and $^{12}CH_3D$: $C \approx 6 \times 10^{-4}$). Also the oxidation of CH_4 to CO_2 prior to mass spectrometric measurement presents complications.

2.2. The thermal diffusion columns

2.2.1. Description

The complete enrichment apparatus consists of 18 thermal diffusion columns; 2 single columns in series on top of each other, 9 of these double columns in parallel (fig. 2.5). Each column is of the Clusius-Dickel type and consists of a 3 m long pyrex glass tube with a diameter of 0.89 cm at the bottom increasing to 0.99 cm at the top. A 0.03 cm diameter Platinum-Iridium (80%–20%) wire is suspended in the centre. The wire is centered by triangular spacers (Pt-Ir 80–20; 0.01 cm thick), that have been soldered to the wire with gold, at regular distances of approximately 25 cm. The wall of the pyrex tube is cooled on the outside by water flowing from bottom to top between the wall and a second concentric pyrex tube of 3 cm diameter (fig. 2.6). The double columns are interconnected at the top (fig. 2.5) through which gas from any combination of 4 large storage bulbs of pyrex glass (volumes resp. 50 ± 0.5 l, 83 ± 1 l, 111 ± 1 l and 112 ± 1 l) can be circulated thermally. Each column has a 0.58 ± 0.01 l sample bulb at the bottom.

In order to increase the pumping speed the system was supplied with large-diameter (ϕ 5 cm) pumping tubes and two mercury diffusion pumps.

2.2.2. Pre-enrichment procedures

Prior to an enrichment the wires are heated to 500–600 °C in an oxygen atmosphere ($\approx$ 600 torr), in order to remove traces of carbon which may have been deposited on the wires as a result of the Bouduard reaction: $2CO \rightleftarrows CO_2 + C$ (Haubach et al., 1965). Then the columns are pumped to a vacuum of $\approx 10^{-5}$ torr and washed three times with approximately 1 l NTP of the CO sample.

2.2.3. The enrichment conditions

The whole system is filled with CO to a pressure of about 900 torr. Samples of the gas prior to enrichment are taken from the top and from the bottom of one of the columns for a mass spectrometer measurement. The power consumption during enrichment is about 3.5 kW (6 A at 190 V for each group of 3 double columns, fed

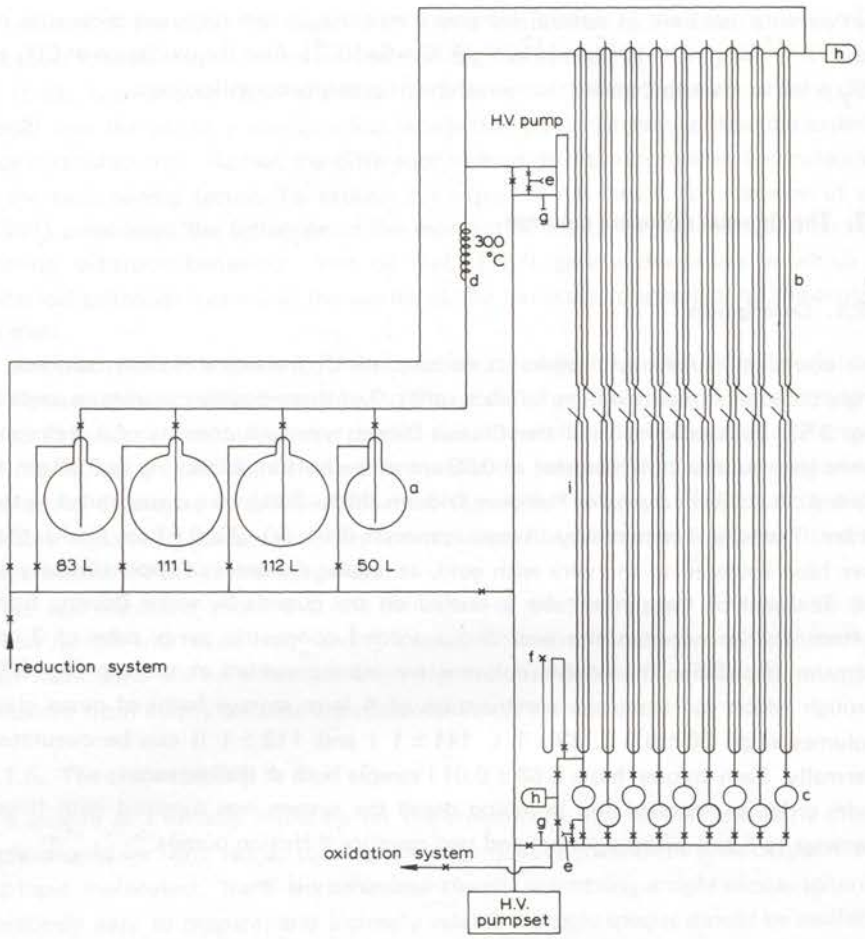

Fig. 2.5. Thermal diffusion enrichment system.
a — storage volume V_-, b — thermal diffusion columns, c — enriched sample volume V_+, d — thermal circulation, e — sampling point, f — mercury manometer, g — Pirani gauge, h — Penning highvacuum gauge.

from one power supply), resulting in a wire temperature of ≈ 650 °C (faintly red). The temperature of the cooling water shows a seasonal variation between 10 and 17 °C. The cold wall temperature is estimated to be in the range of 25 to 35 °C. Since the average change in temperature of the cooling water in the system for a flow rate of about 6 l/min is approximately 8 °C, the cold wall temperature will vary over the length of the column (the higher temperature at the top).
The apparatus is protected against overheating and water-leakage and against vacuum break-down during pumping.

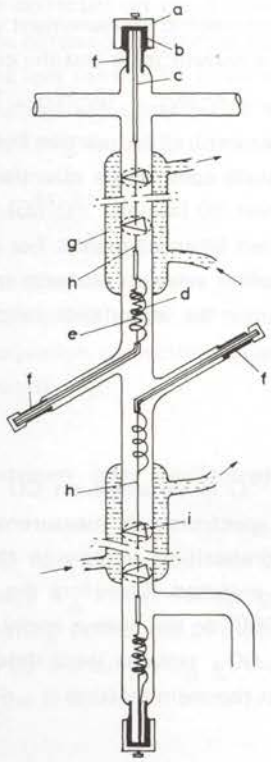

Fig. 2.6. Construction of the thermal diffusion column.
a — copper cap, b — tin solder, c — copper capillary, d — flexible copper wire, e — steel spring, f — kovar, g — pyrex glass diffusion column with cooling jacket, h — Pt-Ir (80% — 20%) wire, i — Pt-Ir (80% — 20%) triangle ('spacer').

2.3. Mass spectrometry

2.3.1. Introduction

We aim to find a relation to determine the ^{14}C enrichment of our samples from the enrichment of the stable isotopes. To this end we compare the behaviour of the isobaric molecules $^{14}C^{16}O$ and $^{12}C^{18}O$. In order to determine the isotopic enrichment by thermal diffusion, gas samples were analysed (i) for stable isotopic composition with a mass spectrometer (Varian MAT M86) and (ii) for radiocarbon with a proportional gas counter. The latter is discussed in chapter 3. The results of the different measuring techniques, however, are not directly comparable.

In principle, with a proportional counter a ^{14}C *mole fraction* ($^{14}CO_2$/total CO_2)

is determined, while mass spectrometric measurement yields an *isotopic abundance ratio* of isotopic molecules of a certain mass and the common isotopic species (viz. $(^{13}C^{16}O + {}^{12}C^{17}O)/^{12}C^{16}O$ or $(^{12}C^{18}O + {}^{13}C^{17}O + {}^{14}C^{16}O)/^{12}C^{16}O$). Because we do not have a simple binary mixture, the relation between these two quantities is somewhat complicated. To obtain comparable quantities the measured increase in isotopic abundance ratio of mass 30 (mainly $^{12}C^{18}O$) must be converted into the increase in $^{12}C^{18}O$ mole fraction (≡ enrichment). For this it is necessary to know the abundance ratios of the other relevant isotopic molecules (here $^{12}C^{17}O$ and $^{13}C^{16}O$ of mass 29). Accordingly the abundance ratio of both masses has to be determined.

2.3.2. Measuring procedures

The isotopic enrichment of ^{14}C is obtained on CO while the ^{14}C activities are measured on CO_2. The mass spectrometric measurements therefore involve both CO and CO_2. The isotopic composition relative to the standard gas ranges from strongly depleted to strongly enriched. Therefore the usual relations as presented by Craig (1957) and Mook (1968) do not always apply. The mass spectrometer and the measuring procedure for CO_2 samples were described before by Mook and Grootes (1973). We only repeat the main features.

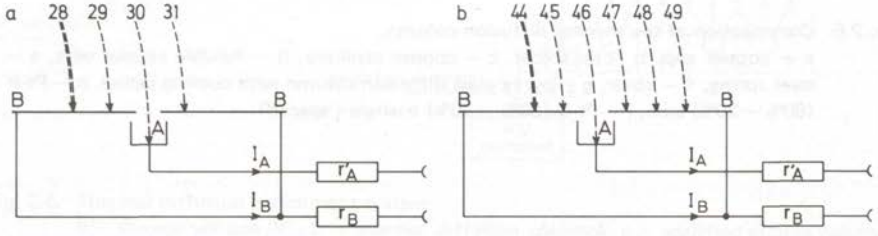

Fig. 2.7. Universal double collector.
a – carbon monoxide; masses collected during mass 30/mass 28 ratio measurement,
b – carbon dioxide; masses collected during mass 46/mass 44 ratio measurements,
I_A and I_B – ion current on A and B collector respectively.

The sample gas is ionized by electron bombardment and a number of ion beams of different mass are produced. The ions are collected in all measurements on a universal double collector (fig. 2.7). The voltage V_A generated over a resistor r_A by the ion beam of the mass considered is compensated by subtracting a fraction p of the voltage V_B generated by ion beams of all other masses of the isotopic mixture. For $V_A - pV_B = 0$, p represents the ratio of the ion beam of the mass considered to the

sum of all other ion beams collected on the B collector. Because of isotope fractionation occurring in the gas between the storage volume and the ion collector, the isotopic composition of the gas cannot be inferred directly from the ion beam ratios of the sample gas. The isotopic composition of the gas, however, is assumed to be affected always by the same factor β. Consequently the results obtained for the sample must be compared with those for a gas of known isotopic composition, measured under the same conditions.

In the following sections we derive, from the basic mass spectrometer function $V_A - pV_B$, an equation relating the relative difference in isotopic composition between a sample and the standard (δ value), to the output of the Varian MAT M86 mass spectrometer. In this equation corrections discussed separately by Mook and Grootes (1973) are incorporated.

2.3.3. General relations between mass spectrometer measurement and isotopic abundance ratio

The basic mass spectrometer function used in the determination of isotopic compositions is: $V_A - pV_B$ where V_A = the voltage generated by the rare ion beam current I_A and by the current i_A in the tails of other ion beams on the A collector, V_B = the voltage generated by the current I_B of the abundant and the current I_{Bi} of the other ion beams on the B collector, and p is a fraction which is chosen such that

$$(I_A + i_A)r'_A = p(I_B + \sum_i I_{Bi})r_B, \tag{2.20}$$

r'_A and r_B are high input resistances. These resistances are voltage dependent for large variations of the current.

The measuring procedure for samples of natural isotopic composition has been described in detail by Mook and Grootes (1973). For the CO_2 and part of the CO samples a pressure independent measuring procedure, described in that paper, was used.

The pressure of both standard and sample gas was adjusted to make the output V_B equal 24 V. Then

$$\frac{(I_A + i_A)_s r'_{As}}{p_s} = \frac{(I_A + i_A)_m r'_{Am}}{p_m}, \tag{2.21}$$

where s and m refer to standard and sample respectively. Defining the relative contribution of the tail of the abundant isotopic molecule line to the rare peak as $\chi = v_A/(V_A + v_A) = i_A/(I_A + i_A)$, eq. 2.21 is transformed into:

$$\delta = \frac{p_m}{p_s} \frac{1-\chi_m}{1-\chi_s} \frac{1+\sum_i R_i}{1+\sum_i S_i} \frac{r'_{As}}{r'_{Am}} - 1, \qquad (2.22)$$

where R and S are the true isotopic abundance ratios of sample and standard gas. Although generally δ values are presented in $^0/_{00}$, δ in our equations stands for the original number. This equation gives the exact relative difference in isotopic composition between sample and standard from the mass spectrometer output p. It contains corrections for the tail of the line of the abundant molecule, for the collector geometry and for voltage dependence of the resistors. For all practical cases this last effect is negligible.

In order to obtain a more practical equation for natural samples two simplifying approximations can be made: (i) Because all masses except 29, 30 respectively 45, 46 have a negligible abundance, the factor $(1 + \sum_i R_i)/(1 + \sum_i S_i)$, which corrects for the fact that all masses of the isotopic mixture except one are collected on the B collector (c.f. fig. 2.7), can be replaced by $(1 + R^\nu)/(1 + S^\nu)$, where ν is 29 or 30 for CO and 45 or 46 for CO_2 depending on which mass is collected on the A collector. (ii) The tail contribution i_A is the same for sample and standard since the total output voltage is taken constant (V_B = 24 V) and the isotopic compositon does not differ much. In that case $\chi_m = \chi_s p_s/p_m$.

In section 2.3.4. we will see that these approximations can be used generally.

For CO_2 as well as for CO we are interested in two isotopic abundances. With the simplifications given above we obtain from eq. 2.22

$$\delta^\mu = \frac{p^\mu_m}{p^\mu_s} \left[(1 - \chi^\mu_s \frac{p^\mu_s}{p^\mu_m}) / (1 - \chi^\mu_s)\right] \left[\{1 + S^\nu(1 + \delta^\nu)\}/(1 + S^\nu)\right] - 1,$$

$$\delta^\nu = \frac{p^\nu_m}{p^\nu_s} \left[(1 - \chi^\nu_s \frac{p^\nu_s}{p^\nu_m})/(1 - \chi^\nu_s)\right] \left[\{1 + S^\mu(1 + \delta^\mu)\}/(1 + S^\mu)\right] - 1.$$

From these δ^μ and δ^ν are solved,

$$\delta^\mu = \frac{\dfrac{p^\mu_m}{p^\mu_s} \dfrac{1}{1+S^\nu} \dfrac{1-\chi^\mu_s \dfrac{p^\mu_s}{p^\mu_m}}{1-\chi^\mu_s} \left(1 + \dfrac{p^\nu_m}{p^\nu_s} \dfrac{S^\nu}{1+S^\nu} \dfrac{1-\chi^\nu_s \dfrac{p^\nu_s}{p^\nu_m}}{1-\chi^\nu_s}\right)}{1 - \dfrac{p^\mu_m}{p^\mu_s} \dfrac{p^\nu_m}{p^\nu_s} \dfrac{S^\mu}{1+S^\mu} \dfrac{S^\nu}{1+S^\nu} \dfrac{1-\chi^\mu_s \dfrac{p^\mu_s}{p^\mu_m}}{1-\chi^\mu_s} \dfrac{1-\chi^\nu_s \dfrac{p^\nu_s}{p^\nu_m}}{1-\chi^\nu_s}} - 1. \qquad (2.23)$$

This equation can be used generally to convert the mass spectrometer output p to δ values corrected for tail contribution and geometry of the B collector. For CO the mass 29 (mainly $^{13}C^{16}O$) and mass 30 (mainly $^{12}C^{18}O$) abundances are obtained by inserting $\mu = 29$, $\nu = 30$ and $\mu = 30$, $\nu = 29$ respectively. Similarly for CO_2 the mass 45 (mainly $^{13}C^{16}O_2$) and mass 46 (mainly $^{12}C^{16}O^{18}O$) abundances by inserting $\mu = 45$, $\nu = 46$ and $\mu = 46$, $\nu = 45$.

Eq. 2.23 for CO_2 is identical with eq. 43 of Mook and Grootes (1973). The equations for the different isotopic masses of CO as well as of CO_2 differ only by their constants.

2.3.4. Enriched samples ($|\delta| > 0.1$)

The isotopic composition of enriched samples lies far outside the range of values normally encountered in natural samples. This influences the behaviour of the mass spectrometer and requires an adaptation of the measuring procedure as well as a reconsideration of the approximations used for the natural samples. In view of this we have to consider the following points:

(i) *Linearity:* For enriched samples the relation between the isotopic composition of the sample and the mass spectrometer output has to be established.

(ii) *Pressure:* The mass spectrometer output p generally depends on the gas pressure in the storage volume. This pressure is adjusted by varying the volume in such a way that $(I_B + \sum_i I_{Bi}) r_B = 24$ V. Since the fraction of the gas that is collected by the A collector ($\approx 1\%$ for natural samples, up to 5% for enriched gas) does not contribute to these 24 Volts over the B collector resistance the total gas pressure varies. Measuring p at the pressure independent position defined in the paper by Mook and Grootes (1973) eliminates the influence of this effect.

(iii) *Tail contribution:* In enriched samples the partial gas pressure of the less abundant masses is no longer negligible. This and the change in relative beam intensities might reduce the resolving power of the instrument by enlarging the tail contributions.

(iv) *Collector geometry:* The correction for the collector geometry is influenced by the relative increase of the abundance of the heavy isotopic molecules.

(v) *Memory effect:* Because of this effect the normal measuring procedure, in which the isotopic composition of sample and standard gas are measured alternately, cannot be followed. For the standard ratio p_s an average value is used, obtained from a series of previous measurements on natural samples performed on the same day, taking into account drift in p_s. Values for p_m^{29} and p_m^{30} (CO) respectively p_m^{45} and p_m^{46} (CO_2) are determined alternately twice during which time the sample gas flows uninterrupted. Only the last p_m values of a series are considered.

(vi) *Drift:* The fact that only samples are measured and no standard makes it impossible to detect a slow drift of the mass spectrometer setting during a series of

measurements. This means a decreased accuracy of the results obtained. Generally the relative drift in p values over a day is less than a few $^0/_{00}$. The influence of drift will be diminished by measuring the samples twice, at least a week apart and in a different sequence.

The points (i), (iii) and (iv) will be discussed in more detail.

2.3.4.1. Tail contribution

The tail contribution depends on the relative mass difference between isotopic molecules. This is larger for CO than for CO_2. Typical values are for CO: $0.4 \times 10^{-3} < \chi^{29} < 1.0 \times 10^{-3}$, $\chi^{30} < 0.4 \times 10^{-3}$; for CO_2: $4 \times 10^{-3} < \chi^{45} < 7 \times 10^{-3}$, $1.7 \times 10^{-3} < \chi^{46} < 5 \times 10^{-3}$. For a relative accuracy of $1\,^0/_{00}$ in the δ values the effect of the tail contribution may be neglected for CO. We therefore limit our discussion to CO_2.

For enriched samples the relative contribution of tails (mainly of that of the abundant ion beam) to the ion beam collected by the A collector, $\chi \equiv v_A/(V_A + v_A)$, decreases with increasing enrichment. At first sight the absolute value of the tail contribution, however, seemed to increase.

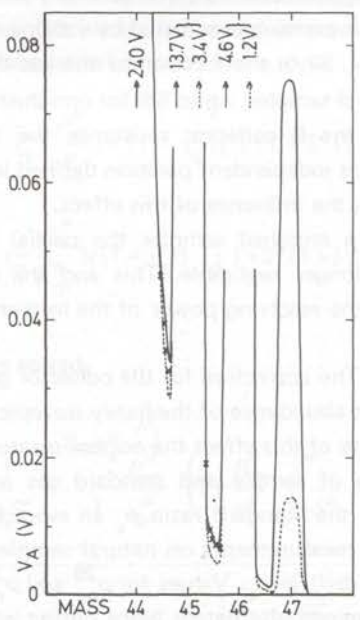

Fig. 2.8. Tail contributions; mass spectrum of CO_2 at high sensitivity.
----- sample of standard isotopic composition, ——sample enriched by a factor 4, x – calculated voltage of the enriched sample.

Fig. 2.8 shows a part of the mass spectrum (mass 44 to 47) at high sensitivity for a CO_2 sample of standard isotopic composition and for a sample enriched by a factor 4. If the spectrum consists of a number of separate lines, we can consider the intersections of these lines. For the enriched sample they are found at a higher voltage than for the standard.

Because the sample inlet pressure is adjusted to have a B collector voltage of 24 V, the gas pressure for the enriched samples is higher, in this case about 3% when measuring mass 45. From our previous work (Mook and Grootes, 1973) we know that a 3% increase in pressure has a negligible influence on the tail contribution.

It has been shown in the same paper, that the influence of the ion beam intensity on the tail contribution is negligible compared with ion scattering by gas molecules. Thus, the change in the mass 45 and 46 beam intensities cannot explain the observed effect either.

A third effect is the influence of the tails of the rare ion beams. We assume that beam intensity has no effect on the line shape. From the measured line shape of mass 44 for standard CO_2 and A collector peak heights of 240, 3.4 and 1.2 V for mass 44, 45 and 46 respectively, the tails of the different masses were calculated. The tail contribution of mass 45 is $\approx 10\%$ of the mass 44 tail under the mass 46 peak. Using the tails of mass 44, 45 and 46 and the spectrum of the standard CO_2 sample we calculated the voltage in the region of minimum intensity between the lines for the enriched sample (fig. 2.8). For the intersection of the mass 45 and 46 lines the calculated values are in good agreement with those observed. At the mass 44, 45 intersection the calculated values are still slightly lower. Our conclusion is that: (i) The absolute tail contribution to the mass 45 line is independent of the enrichment; this means that eq. 2.23 applies, for δ^{45}, to natural and enriched samples. (ii) The absolute contribution of tails to the mass 46 line increases with the enrichment ($\chi_m^{46} \approx \chi_s^{46}\,(0.9 + 0.1\ p_m^{45}/p_s^{45})p_s^{46}/p_m^{46}$) in accordance with the increasing tail contribution of mass 45. Since δ^{45} and δ^{46} are of the same magnitude for the thermal diffusion enriched samples, we can neglect the effect of this increase if a relative accuracy of about $1\,^0/_{00}$ is sufficient. Then also for δ^{46} the same equation 2.23 can be used.

2.3.4.2. Collector geometry

In samples of natural isotopic composition, the ion beams of mass 31, 32 respectively 47 to 50 can be neglected (c.f. table 2.8). Due to thermal diffusion isotopic enrichment the concentration of the heavy isotopic species in the gas increases. This increase depends on the relative mass difference between the rare, heavy and the abundant, light molecule. For mass 29 and 30 enrichments of approximately 5 and 10 respectively are obtained, which yield after oxidation enrichments of approxi-

mately 5 for both mass 45 and 46. For heavier isotopic species the separation factor will increase considerably with increasing mass difference. The enrichment, however, is limited by the volume ratio of the reservoir V_- and the enrichment volume ($\lesssim 40$) (c.f. fig. 2.3). Therefore, the enrichments of different isotopic masses differ much less than the separation factors would suggest; for mass 31 the enrichment is generally less than 20. Accordingly the contribution of the higher isotopic masses amounts to less than $1\,^0/_{00}$ of the abundant ion beam and will be neglected. The collector geometry correction for enriched samples is, consequently, identical to that for natural samples.

2.3.4.3. Linearity of the mass spectrometer

In order to establish the relation between the isotopic composition of a sample and the mass spectrometer output for enriched samples, a series of samples with different isotopic compositions was prepared by mixing standard CO_2 with enriched CO_2. The isotopic composition of each sample was measured twice. The values of δ^{45} and δ^{46} were corrected for the tail contribution and the geometry of the B collector. Using the δ values of standard and enriched CO_2, we can calculate the δ values of the mixtures. If we mix α parts of standard CO_2 with β parts of enriched CO_2 we have to convert the *isotopic abundance ratios* of the isotopic species in the two gases to *mole fractions.* From them we find the relative difference in isotopic abundance ratio between the mixture and the standard

$$\delta^{\nu} = [(\alpha C^{\nu} + \beta C^{\nu *})/(\alpha C^{44} + \beta C^{44*}) - S^{\nu}]/S^{\nu}, \tag{2.24}$$

where C^{ν} is the mole fraction of the isotopic species ν and the asterisk indicates the enriched gas. When two gases of which the δ values have been measured relative to the same standard are mixed, eq. 2.24 can be transformed into:

$$\delta^{\nu} = [\{\alpha(1+\delta_1^{\nu})C_1^{44} + \beta(1+\delta_2^{\nu})C_2^{44}\}/(\alpha C_1^{44} + \beta C_2^{44})] - 1, \tag{2.25}$$

where $C^{44} = (1+\sum_i R_i)^{-1} \approx [1 + S^{45}(1+\delta^{45}) + S^{46}(1+\delta^{46})]^{-1}$.

In fig. 2.9 we show that the isotopic abundance ratio of the mixture is a non-linear function of the mixing ratio. To this end we compared the δ values calculated for the mixed samples with the result of a linear combination of the original δ values ($\delta^{\nu\dagger} = (\alpha\delta_1^{\nu} + \beta\delta_2^{\nu})/(\alpha+\beta)$). The difference between the two values was plotted against the mixing ratio. In the same figure we give the differences between δ_{exp} and $\delta^{\dagger}$.

We estimate that the pressures of the mixed quantities of gas were read to $\pm$ 0.5 mm Hg giving a relative uncertainty between 0.5 and 1.7% in the mixing ratio.

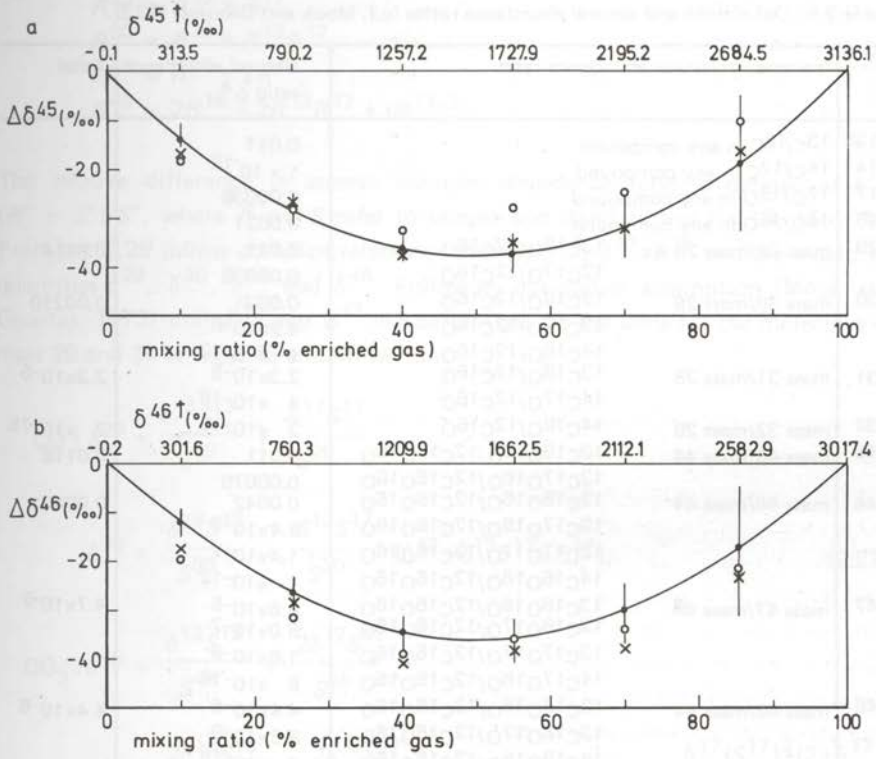

Fig. 2.9. Isotope ratio of a gas mixture as a function of the mixing ratio. The difference ($\Delta\delta$) between the calculated δ value of the mixture and a linear combination of the individual δ values of the components of the mixture ($\delta\dagger$) is given as a function of the mixing ratio for δ^{45}(a) and δ^{46}(b). $\dagger$ — uncertainty in calculated value of $\Delta\delta$, x and o — experimental values for $\Delta\delta$.

The calculated differences agree well with those observed over the whole range: the relation between mass spectrometer output and isotopic composition of the CO_2 sample is, within the measuring accuracy, linear for the range considered.

The differences between the duplicate measurements indicate, that the relative reproducibility of the measurements over the whole range is about $4^0/_{00}$.

The experiment does not permit the conclusion that the mass spectrometer yields the true isotopic composition since the composition of the enriched gas was measured with the same machine and is therefore subject to the same systematic errors. It proves, however, that the machine can be used to compare samples of widely varying isotopic compositions, as is required for determination of thermal diffusion isotopic enrichments.

Table 2.8. Definitions and natural abundance ratios (c.f. Mook and Grootes, 1973).

	Isotopic/molecular abundance ratio		Natural abundance ratio Δ [a]	Total
R^{13} [b]	$^{13}C/^{12}C$ in any compound		0.011	
R^{14}	$^{14}C/^{12}C$ in any compound		1×10^{-12}	
R^{17}	$^{17}O/^{16}O$ in any compound		0.00038	
R^{18}	$^{18}O/^{16}O$ in any compound		0.0021	
R^{29}	mass 29/mass 28 viz.	$^{13}C^{16}O/^{12}C^{16}O$	0.011	0.0114
		$^{12}C^{17}O/^{12}C^{16}O$	0.00038	
R^{30}	mass 30/mass 28	$^{12}C^{18}O/^{12}C^{16}O$	0.0021	0.00210
		$^{13}C^{17}O/^{12}C^{16}O$	4.2×10^{-6}	
		$^{14}C^{16}O/^{12}C^{16}O$	1×10^{-12}	
R^{31}	mass 31/mass 28	$^{13}C^{18}O/^{12}C^{16}O$	2.3×10^{-5}	2.3×10^{-5}
		$^{14}C^{17}O/^{12}C^{16}O$	4×10^{-16}	
R^{32}	mass 32/mass 28	$^{14}C^{18}O/^{12}C^{16}O$	2×10^{-15}	2×10^{-15}
R^{45}	mass 45/mass 44	$^{13}C^{16}O^{16}O/^{12}C^{16}O^{16}O$	0.011	0.0118
		$^{12}C^{17}O^{16}O/^{12}C^{16}O^{16}O$	0.00076	
R^{46}	mass 46/mass 44	$^{12}C^{18}O^{16}O/^{12}C^{16}O^{16}O$	0.0042	0.00421
		$^{13}C^{17}O^{16}O/^{12}C^{16}O^{16}O$	8.4×10^{-6}	
		$^{12}C^{17}O^{17}O/^{12}C^{16}O^{16}O$	1.4×10^{-7}	
		$^{14}C^{16}O^{16}O/^{12}C^{16}O^{16}O$	1×10^{-12}	
R^{47}	mass 47/mass 44	$^{13}C^{18}O^{16}O/^{12}C^{16}O^{16}O$	4.6×10^{-5}	4.7×10^{-5}
		$^{12}C^{18}O^{17}O/^{12}C^{16}O^{16}O$	8.0×10^{-7}	
		$^{13}C^{17}O^{17}O/^{12}C^{16}O^{16}O$	1.6×10^{-9}	
		$^{14}C^{17}O^{16}O/^{12}C^{16}O^{16}O$	8×10^{-16}	
R^{48}	mass 48/mass 44	$^{12}C^{18}O^{18}O/^{12}C^{16}O^{16}O$	4.4×10^{-6}	4.4×10^{-6}
		$^{13}C^{18}O^{17}O/^{12}C^{16}O^{16}O$	8.8×10^{-9}	
		$^{14}C^{18}O^{16}O/^{12}C^{16}O^{16}O$	4×10^{-15}	
		$^{14}C^{17}O^{17}O/^{12}C^{16}O^{16}O$	1×10^{-19}	
R^{49}	mass 49/mass 44	$^{13}C^{18}O^{18}O/^{12}C^{16}O^{16}O$	4.9×10^{-8}	4.9×10^{-8}
		$^{14}C^{18}O^{17}O/^{12}C^{16}O^{16}O$	8×10^{-19}	
R^{50}	mass 50/mass 44	$^{14}C^{18}O^{18}O/^{12}C^{16}O^{16}O$	4×10^{-18}	4×10^{-18}

a values from Nier (1950) quoted by Craig (1957)
b for a standard sample S is used

2.3.5. Atomic isotopic abundance ratios

So far we have only considered isotopic molecules. This is sufficient to determine the enrichment for radiocarbon dating. If we want to know precisely the variation in the carbon and oxygen isotopic composition we have to go into more detail.
The rare isotopic molecules of CO and CO_2 contain one or more of the rare isotopes ^{13}C, ^{17}O and ^{18}O (the amount of ^{14}C ($S^{14} \approx 10^{-12}$) is negligible). In fact the molecules of one mass consist of a mixture of different isotopic molecules (table 2.8). The relations between the atomic and the molecular isotopic abundance ratios are

$$
\begin{aligned}
R^{29} &= R^{13} + R^{17}, \\
R^{30} &= R^{18} + R^{13}R^{17}, \\
R^{45} &= R^{13} + 2R^{17}, \\
R^{46} &= 2R^{18} + 2R^{13}R^{17} + (R^{17})^2.
\end{aligned} \tag{2.26}
$$

The relative difference in atomic isotopic abundance ratio is defined as $\delta^{\nu} \equiv (R^{\nu} - S^{\nu})/S^{\nu}$, where R and S refer to sample and standard and $\nu = 13$, 17 or 18. From eq. 2.26 follow complex relations between δ^{13}, δ^{17}, δ^{18} and the measured quantities δ^{29}, δ^{30}, δ^{45} and δ^{46}. Following our earlier assumption (Mook and Grootes, 1973) that R^{13} and R^{17} in a certain gas are the same for the molecules of mass 29 and 30 or mass 45 and 46 we find

$$
\begin{aligned}
\mathrm{CO}: \delta^{29} &= \frac{\delta^{13}S^{13}}{S^{29}} + \frac{\delta^{17}S^{17}}{S^{29}}, \\
\delta^{30} &= \frac{\delta^{18}S^{18}}{S^{30}} + \frac{S^{13}S^{17}}{S^{30}} \quad (\delta^{13} + \delta^{13}\delta^{17} + \delta^{17}); \\
\mathrm{CO_2}: \delta^{45} &= \frac{\delta^{13}S^{13}}{S^{45}} + \frac{2\delta^{17}S^{17}}{S^{45}}, \\
\delta^{46} &= \frac{2\delta^{18}S^{18}}{S^{46}} + \frac{2S^{13}S^{17}}{S^{46}} \quad (\delta^{13} + \delta^{13}\delta^{17} + \delta^{17}) + \frac{\delta^{17}(S^{17})^2(2+\delta^{17})}{S^{46}}.
\end{aligned} \tag{2.27}
$$

With two measurements (δ^{29}, δ^{30} or δ^{45}, δ^{46}) we have a system of two equations with three variables. A third relation is obtained if we assume that isotope effects are only caused by mass differences (Bigeleisen, 1952; Craig, 1954) so that we may use the expression $\alpha \sim \exp(\Delta m C)$ for the fractionation factor (here Δm is the mass difference between the isotopic molecules and C is a constant). This gives for the isotope fractionations of ^{17}O and ^{18}O

$$
(R^{17}/S^{17})^2 = R^{18}/S^{18} \text{ or } \delta^{17} = \sqrt{1 + \delta^{18}} - 1. \tag{2.28}
$$

The values of δ^{13}, δ^{17} and δ^{18} can now be solved from the sets of equations. This gives for CO

$$
\begin{aligned}
\delta^{13} &= \frac{S^{29}}{S^{13}}\delta^{29} - \frac{S^{17}}{S^{13}}\delta^{17} = \frac{S^{29}}{S^{13}}\delta^{29} - \frac{S^{17}}{S^{13}}(\sqrt{1+\delta^{18}} - 1), \\
&\mathrm{A}_1^2(\delta^{18})^2 - (2\mathrm{A}_1\mathrm{B}_1 + \mathrm{C}_1^2)\delta^{18} + (\mathrm{B}_1^2 - \mathrm{C}_1^2) = 0,
\end{aligned} \tag{2.29}
$$

where $A_1 = S^{18} - (S^{17})^2$, $B_1 = S^{30}\delta^{30} + S^{17}S^{29}$ and $C_1 = S^{17}S^{29}(1+\delta^{29})$,

and for CO_2

$$\delta^{13} = \frac{S^{45}}{S^{13}}\,\delta^{45} - \frac{2S^{17}}{S^{13}}\,(\sqrt{1+\delta^{18}} - 1),$$

$$A_2^2(\delta^{18})^2 - (2A_2B_2 + C_2^2)\delta^{18} + (B_2^2 - C_2^2) = 0, \qquad (2.30)$$

where $A_2 = 2S^{18} - 3(S^{17})^2$, $B_2 = S^{46}\delta^{46} + 2S^{17}S^{45}$ and $C_2 = 2S^{17}S^{45}(1+\delta^{45})$.

If natural samples are considered, the equations 2.29 and 2.30 can be approximated by:

$$2\delta^{17} = \delta^{18},$$

for CO:

$$\delta^{13} = \frac{S^{29}}{S^{13}}\,\delta^{29} - \frac{S^{17}}{2S^{13}}\,\delta^{30},$$

$$\delta^{18} = \delta^{30} - \frac{S^{17}S^{29}}{S^{18}}\,\delta^{29}; \qquad (2.31)$$

and for CO_2:

$$\delta^{13} = \frac{S^{45}}{S^{13}}\,\delta^{45} - \frac{S^{17}}{S^{13}}\,\delta^{46},$$

$$\delta^{18} = \delta^{46} - \frac{S^{17}S^{45}}{S^{18}}\,\delta^{45}. \qquad (2.32)$$

Absolute isotopic abundance ratios for carbon and oxygen have been determined by Nier (1950) with a relative accuracy of 2 ‰ or better. From these measurements absolute isotope ratios for a number of international standards have been defined by Craig (1957) (table 2.9). In the same reference system we know the ratios of the CO_2 laboratory working standards which have been measured relative to NBS20–CO_2 (Solenhofener limestone, NBS reference sample no. 20). For CO a working standard was obtained by reduction of tank CO_2. CO reference samples are not available. Because during reduction and oxidation oxygen isotope fractionation can take place, we can only estimate the values of S^{17} and S^{18} for the CO working standard. The value of S^{13} is not affected by reduction or oxidation provided the process is quantitative.

Table 2.9. Absolute isotopic abundance ratios (Craig, 1957).

	PDB–CO_2	NBS20–CO_2	CO/T_o*
s^{13}	0.0112372	0.0112253	0.01100
s^{17}	0.0003800	0.0003792	0.000378
s^{18}	0.0020790	0.0020704	0.002059

* estimated values for the laboratory CO standard based on comparison of CO_2 and CO measurements

The isotopic abundance ratios for the different elements in samples can now be calculated. Using eq. 2.23 and 2.29 resp. 2.30 the results are correct for any isotopic composition as long as the assumptions made are allowed. The relation between δ^{17} and δ^{18} which is only based on mass differences, however, may not be valid for the enriched samples. It has been shown, that thermal diffusion isotope fractionation not only depends on the relative mass difference between isotopic molecules, but also on the intramolecular mass distribution (Boersma-Klein and De Vries, 1966; Stevens and De Vries, 1968). This is demonstrated by the difference in enrichment between $^{14}C^{16}O$ and $^{12}C^{18}O$. Therefore eq. 2.28 is not strictly valid for enriched samples obtained by thermal diffusion, which means that the atomic isotopic abundance ratios cannot be found precisely. We need further experiments to decide whether eq. 2.28 can still be used with sufficient accuracy.

If the aim of the measurements is only the determination of the ^{14}C enrichment for dating purposes, this is no serious problem. The ^{14}C enrichment can be read with sufficient accuracy from a calibration curve relating a number of directly measured ^{14}C enrichments (mainly $^{14}C^{16}O$) to the corresponding enrichments of mass 30. In doing so, the use of the atomic isotopic abundance ratios is avoided and part of the systematic errors is cancelled.

2.3.6. Calculation of the enrichment

The enrichment of a sample is found by comparing the δ values of the original and the enriched gas (eq. 2.23). Here allowance has to be made for the decrease in concentration of the light abundant molecule in the enriched gas.

Although this applies to CO_2 as well as to CO, we can use a simpler procedure for CO. Here the tail contribution is negligible (sect. 2.3.4.1). For the correction for collector geometry the relative abundance of the masses 28, 29 and 30 is required. These abundances also determine the correction of the enrichment for a decrease in concentration of the abundant molecule. It turns out that a simple equation can be obtained relating the enrichment q' directly to the mass spectrometer output p_m before and after enrichment. Using the definition of p^ν (eq. 2.20) and $q^{\nu'}$ $(=C^{\nu *}_{V+}/C^{\nu}_{o}$, where C is the mole fraction) we find

$$q^{\nu\prime} = (p_m^{\nu *}/p_m^{\nu})/[1 + C_o^{\nu}\{(p_m^{\nu *}/p_m^{\nu}) - 1\}], \tag{2.33}$$

where the asterisk refers to the enriched gas.

If we assume that the oxidation of the enriched CO sample in the CuO furnace only involves the addition of one oxygen atom per molecule of CO from an oxygen reservoir of standard isotopic composition, and that no fractionation nor exchange of the CO or CO_2 oxygen with this reservoir takes place, the mass 29 and 30 enrichments can be calculated from the CO_2 measurements. If C_g^{17}, C_g^{18} and $C_g^{16} = 1 - C_g^{17} - C_g^{18}$ refer to the mole fractions of the added oxygen,

$$\begin{aligned} C^{44*} &= C^{28*} C_g^{16}, \\ C^{45*} &= C^{28*} C_g^{17} + C^{29*} C_g^{16}, \\ C^{46*} &= C^{28*} C_g^{18} + C^{29*} C_g^{17} + C^{30*} C_g^{16}. \end{aligned} \tag{2.34}$$

Using the definitions of q' ($q' = C^*/C_o$), R (≡ concentration rare isotopic species/ /concentration abundant isotopic species) and δ ($\delta = (R - S)/S$ we find

$$\begin{aligned} q^{29\prime} &= [\{(1 + \delta^{45*})S^{45} - R_g^{17}\}/(1 + \delta_o^{29})S^{29}] \times \\ &\quad \times (1 - C_{V_+}^{29*} - C_{V_+}^{30*})/(1 - C_o^{29} - C_o^{30}), \\ q^{30\prime} &= [\{(1+\delta^{46*})S^{46} - R_g^{18} - [(1+\delta^{45*})S^{45} - R_g^{17}]R_g^{17}\}/(1+\delta_o^{30})S^{30}] \times \\ &\quad \times (1 - C_{V_+}^{29*} - C_{V_+}^{30*})/(1 - C_o^{29} - C_o^{30}), \end{aligned} \tag{2.35}$$

where $C_{V_+}^{\nu *}$ is the mole fraction of the isotopic molecule of mass ν in the enriched sample.

The enrichment can thus be calculated both from CO and from CO_2 measurements. This provides a check for contamination in a CO sample (for instance by air) on the one hand and for any exchange of oxygen in the CuO furnace on the other.

2.4. Experiments and discussion

In section 2.1 expressions were given for the equilibrium enrichment of a thermal diffusion column from which no gas is drawn (eq. 2.9 combined with eq. 2.16) and for the way the enrichment approaches this value (eq. 2.12).

In this section we first compare the performance of the individual columns and we shall see that small variations in the column parameters lead to different thermal diffusion results. Next we consider the enrichment as a function of time for one

column and find that differences between theory and experiment exist due to an insufficiently refined theory and/or knowledge of the experimental conditions. Finally we discuss the determination of the ^{14}C enrichment from the mass spectrometrically determined mass 30 enrichment.

2.4.1. Individual column performance

On 6 occasions a sample was taken from the positive (= heavy isotopes) storage volume of each separate column (c.f. fig. 2.5) after completion of the enrichment procedure. The enrichment q' of each sample relative to the original gas is calculated from the mass spectrometric measurements using eq. 2.33. Thus, corrections are made for a decrease in concentration of the abundant molecule of mass 28 in the enriched gas and for the collection of ions of mass 28 to 31 by the B collector of the mass spectrometer. The average enrichment time was 34 days (minimum 21 days and maximum 44), giving average enrichments $q^{29'} = 4.7$ and $q^{30'} = 8.4$ (minima 3.8 and 6.7 and maxima 5.0 and 9.8, respectively). The enrichment of each column separately for both mass 29 and mass 30 is calculated from the measurements relative to the mean enrichment of all columns for each run.

For each column the average performance for 6 enrichments is given with its standard deviation in fig. 2.10. The values range from 91% ± 1% to 111% ± 1.5%. This indicates the large influence of small differences between 'identical' columns. It also demonstrates the limited value of a theoretical calculation of the enrichment in a Clusius-Dickel thermal diffusion column.

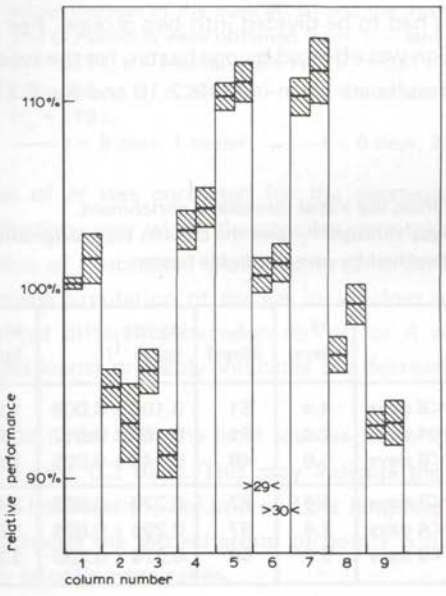

Fig. 2.10. Enrichment in the individual columns relative to the average enrichment of all columns.

2.4.2. Enrichment as a function of time

Knowledge of the enrichment in V_+ as a function of time is of practical importance for choosing an appropriate enrichment time for the ^{14}C samples. Moreover, the initial transport provides information on the TD transport coefficient H (eq. 2.6 and 2.7). This and the increase of the enrichment in the transient state enable us to compare the performance of the actual TD enrichment set-up with the calculations of sect. 2.1.4.

From the sampling facility of column no. 1 (c.f. fig. 2.5) samples were drawn of the enriched gas in the storage volume of column no. 1 during 7 of the enrichments. The minimum amount of gas necessary for a mass spectrometric analysis was taken, i.e. 3 ml or 0.5% of the amount of gas in the enrichment reservoir of one column. We may therefore assume that the disturbance introduced by the sample extraction is small. The mass spectrometric measurements yield the isotopic enrichment factors $q^{29'}$ and $q^{30'}$.

From the increase of the enrichment in the *initial phase* we can calculate H. As long as the influence of the depletion of V_- and the concentration gradient along the column is negligible we find from eq. 2.7 and the definition of q', taking into account the gas in the column,

$$dq'/dt = \frac{M_1}{M_2}\,\frac{H}{m_+''}\exp(-t/t_r) \approx \frac{M_1}{M_2}\,\frac{H}{m_\gamma''}\,. \qquad (2.36)$$

The data for the first 8 days are given in fig. 2.11.a,b and from them $dq^{29'}/dt$ and $dq^{30'}/dt$ were calculated. The data had to be divided into two groups. For the first V_- = 231 l and the thermal circulation was effected by one heater, for the second V_- = 201 l and two heaters were used. Results are given in table 2.10 and fig. 2.11.a,b.

Table 2.10. TD transport coefficient H from the initial increase in enrichment.
The circulation of the CO gas through V_- and the column tops, originally effected by one heater, was later intensified by using a double heater.

Mass		$\bar{t}$ (days)	t_r (days)	dq'/dt (days^{-1})	$H \times 10^6$ (g/sec)
29 ($\approx {}^{13}C^{16}O$)	1 heater, V_- = 231 l, t<8 days	4.4	51	0.150 ± 0.006	1.96 ± 0.08
	1 heater, V_- = 231 l, t<4 days	2.4	51	0.165 ± 0.017	2.07 ± 0.21
	2 heaters, V_- = 201 l, t<8 days	5.9	48	0.140 ± 0.025	1.89 ± 0.34
30 ($\approx {}^{12}C^{18}O$)	1 heater, V_- = 231 l, t<8 days	4.4	67	0.278 ± 0.008	3.48 ± 0.10
	1 heater, V_- = 231 l, t<4 days	2.4	67	0.295 ± 0.026	3.58 ± 0.32
	2 heaters, V_- = 201 l, t<8 days	5.9	59	0.274 ± 0.039	3.54 ± 0.50

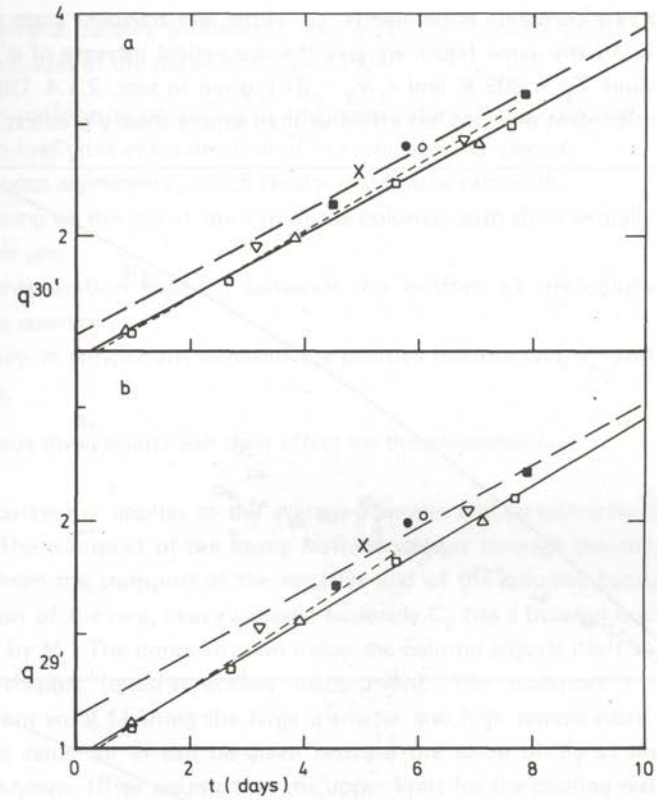

Fig. 2.11. Initial increase of the mass 30 (a) and the mass 29 (b) enrichment in column no. 1. The CO samples were obtained from: □ — tank CO_2, V_- = 90 l; Δ — marine shells (I), V_- = 231 l; ▽ — marine shells (V), V_- = 231 l; ■ — anthracite I, V_- = 201 l; ● — peat, Odderade I, V_- = 201 l; x — peat, Odderade II, V_- = 201 l; ○ — peat, Aschersleben, V_- = 119 l.
—— $t < 8$ days, 1 heater; – – – – $t < 8$ days, 2 heaters; ------- $t < 4$ days, 1 heater.

The value of H was corrected for the decrease of the TD transport with time, because the time over which the samples were taken is not negligible compared with t_r. The value of H obtained is of the correct order of magnitude (c.f. table 2.4).
The increased circulation of the gas in V_- does not show a significant effect on H. The observed difference between dq'/dt for 4 and 8 days (although statistically hardly significant) probably indicates the decreasing transport during the transient phase.
It should be noted that the least squares fit to the first group gives a value $q' = 1$ during the first 0.3 days. This may indicate the existence of a time delay of this magnitude between the column and the sampling volume. The different position of the line through the second group of points is to be explained by the later time at which the samples were taken.

The data for the complete enrichments, i.e. *initial and transient state* are given in fig. 2.12.a, b. In the same figure we give the theoretical increase of q', calculated using the values T_1 = 308 K and r_1/r_2 = 31.5 given in sect. 2.1.4. Obviously the actual TD enrichment set-up is less effective than simple theory predicts.

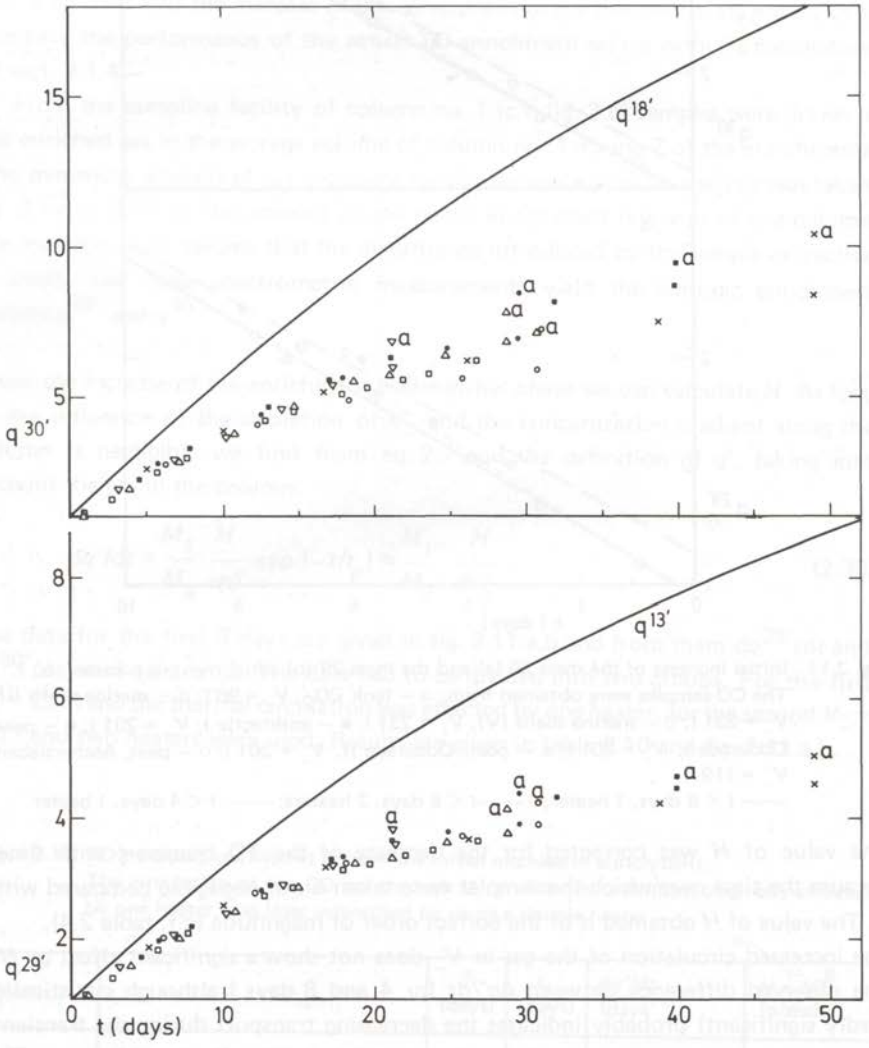

Fig. 2.12. Enrichment as a function of time for mass 30 and mass 29 in column no. 1.
The CO samples were obtained from: □ — tank CO_2, V_- = 90 l; Δ — marine shells (I), V_- = 231 l; ▽ — marine shells (V), V_- = 231 l; ■ — anthracite I, V_- = 201 l; ● — peat, Odderade I, V_- = 201 l; x — peat, Odderade II, V_- = 201 l; ○ — peat, Aschersleben, V_- = 119 l.
—— enrichment calculated from eq. 2.12 for $^{12}C^{18}O$ ($q^{18'}$) and $^{13}C^{16}O$ ($q^{13'}$) for V_- = 201 l. a — enrichment of mixed sample of all 9 columns.

There are several factors influencing the separation process that have not been taken into account in the theoretical calculation:

(i) the non-uniformity of the radius and temperature of the cold wall;
(ii) the non-negligible concentration of the rare isotopic species;
(iii) the column asymmetry, which results in parasitic remixing;
(iv) the mixing of the gas at the top of the columns with the thermally circulating reservoir gas;
(v) the concentration gradient between the bottom of the columns and the positive reservoir;
(vi) the delay in enrichment between the positive column end, V_+ and the sample volume.

We will discuss these points and their effect on the enrichment.

(i) The calculated q' applies to the average diameter and an estimated temperature of 308 K. The transport of the heavy isotopic species through the column can be calculated from the transport at the negative end of the column, because here the concentration of the rare, heavy isotopic molecule C_2 has a (nearly) constant value, determined by V_-. The concentration inside the column adjusts itself so as to give a constant transport (quasi-stationary assumption). The transport τ therefore is obtained from eq. 2.11 using the large diameter and high temperature value of H. No accurate value for H can be given because the value of T_1 at the top is not accurately known. If we assume that the upper limit for the cooling water temperature corresponds to T_1, this gives a decrease of H and τ relative to the values chosen for the calculated curve shown in fig. 2.12.a and b of 7%, 14% and 6% for $^{14}C^{16}O$, $^{12}C^{18}O$ and $^{13}C^{16}O$, respectively. After 30 days the decrease in q' amounts to 5%, 12% and 5% respectively.

(ii) Jones and Furry (1946) and Felber and Pak (1974) assumed that $C_2 \ll C_1$, so $C_1 = 1 - C_2 \approx 1$. For the enrichment of natural CO, containing $\approx 1.1\%$ of mass 29 (table 2.8), the approximation $C_1 = 1$ is no longer allowed. The separation factor q is no longer equal to the ratio of the concentrations of the rare isotopic species in V_+ and V_- but it contains also the ratio of the concentrations of the abundant isotopic species in both reservoirs (c.f. eq. 2.9). This means that a correction must be applied to our equations 2.11–2.16.
A more exact treatment of eq. 2.16 gives

$$q' = q(m_- + m_+'')/(m_- C_{1-}/C_{1+} + q m_+''). \qquad (2.37)$$

The same correction factor C_{1-}/C_{1+} appears both in the nominator and denom-

inator of eq. 2.15 in such a way that its effect is negligible. The relaxation time t_r changes proportional with q'_e (from eq. 2.37 instead of 2.16) and consequently also eqs. 2.11–2.13 containing t_r and q'_e give different values. From eq. 2.37 it appears that this correction will only be important if $m_- > q\, m''_+$, which means that it is negligible for $q^{14'}$ and $q^{18'}$ for the values of V_- and V_+ used, but it affects $q^{13'}$. For the standard conditions chosen for the calculation in fig. 2.12.a and b and V_- = 201 l the correction in $q^{13'}$ is 2.5% at 30 days.

In the theoretical discussion of sect. 2.1 as well as in the correction above only binary mixtures of abundant and rare isotopic species have been considered. In a multicomponent mixture this is allowed provided the chance of an interaction between rare isotopic molecules is negligible relative to that of the interaction between a rare and an abundant molecule. In practice $^{13}C^{16}O$ and perhaps even $^{12}C^{18}O$ might become concentrated to the extent that a correction is necessary. This effect, however, cannot easily be quantified.

(iii) The influence of column asymmetry and the resulting parasitic remixing is expressed by an extra mixing term in eq. 2.3 with a transport coefficient K_p which can be of the order of 20% of $(K_c + K_d)$ (Vasaru et al., 1969, p. 40). The influence of K_p will be relatively small in the early phase of the enrichment, because the initial enrichment is exclusively determined by H and m''_+ (see eq. 2.6 and 2.7). In a later stage, when the effect of a smaller q_e and q'_e is no longer balanced by the correspondingly smaller t_r, parasitic remixing results in a lower enrichment.
The degree of asymmetry of our columns is unknown. It is therefore impossible to determine K_p for our system. To estimate the influence of the parasitic remixing we calculate the effect of $K_p = 0.2\, K$. After 30 days the effect is a decrease of 2.3%, 4.3% and 12.4% in $q^{14'}$, $q^{18'}$ and $q^{13'}$ respectively for V_- = 201 l and of 1.5%, 3.4% and 10.6% for V_- = 57 l (calculated from eqs. 2.9, 2.12 and 2.14–2.16). From these figures it is evident that asymmetry in our columns may seriously reduce the enrichment.

(iv) The negative reservoir could not be placed directly on top of the columns due to a limited laboratory space. A thermal circulation loop connects the columns with the reservoir. The circulation must be sufficient to keep the gas in the top of the columns and the reservoir well mixed. The thermal circulation was at first provided by a 250 W heating tape wrapped around one of the tubes connecting the reservoir with the columns (c.f. fig. 2.5). Samples taken from the gas in the connecting tube near the columns and from the reservoir gas showed, that the circulation was insufficient and that accordingly a concentration gradient had been built up between the column tops and the reservoir (table 2.11). The effect of a concentration difference between the columns and the negative reservoir has been theoretically treated by Bardeen (1940). The rate of enrichment is lowered.

Table 2.11. Inhomogeneity of the gas in V_- when a single heater is used to effect the circulation.

	Lab. no.	$\delta^{29}(‰)$[a]	$\delta^{30}(‰)$[a]
Shells IV	CO/M97 (tube)	− 175.6	− 376.7
	CO/M97A (V_-)	− 118.6	− 244.2
Shells V	CO/M116 (tube)	− 83.5	− 168.2
	CO/M119 (V_-)	− 64.8	− 136.7

a δ values calculated relative to the sample taken from the top of the columns before enrichment

After a second 250 W heater had been added, no difference in isotopic composition between the gas at the sampling point and in the reservoir was found anymore (starting with Anthracite I GrN-6533, 3/12/1971). It cannot be excluded, however, that the gas in the column tops is slightly depleted because (a) the samples were taken 'upstream' from the column and (b) the circulating gas from V_- might not be completely mixed with the gas in the top of the columns (c.f. Rutherford and Kaminski, 1967).

(v) Because of a lack of space and to obtain a good accessibility, the positive reservoirs are situated at some distance from the lower end of the columns. Here no thermal circulation is used, so the isotope transport from the column to V_+ is effected only by concentration diffusion. At the start of the enrichment a simple system is considered, which includes only the volume adjacent to the positive end of the column (for each column 20 cm of tubing with ϕ = 10 mm inner diameter). For this system q'_e and t_r are calculated from H and q_e (table 2.4 and 2.5) using eqs. 2.14–2.16. The results are given in table 2.12.

Table 2.12. Concentration difference between the lower end of the TD column and V_+, and the time delay Δt of enrichment in V_+ (T_1 = 308 K, r_1/r_2 = 31.5).

V_- (l)	Molecule	q'_e	t_r (days)	$\Delta C_2/C_{2_0}$	Δt (days)
201	$^{14}C^{16}O$	337	42.0	2.74	0.22
	$^{12}C^{18}O$	144	28.6	2.09	0.22
	$^{13}C^{16}O$	16.1	8.9	1.08	0.04
57	$^{14}C^{16}O$	112	13.4	2.74	0.21
	$^{12}C^{18}O$	73.6	14.1	2.09	0.21
	$^{13}C^{16}O$	14.0	7.5	1.08	0.05

The TD transport builds up the concentration at the lower end of the column until the concentration difference between the bottom of the column and the reservoir gives an equally large concentration diffusion transport.
When TD and diffusion transport balance,

$$HC_{2_o} \exp(-t/t_r) = -\rho_2 DO \text{ grad } C_2. \tag{2.38}$$

Because the positive reservoir is large compared with the volume of the connecting tube, we can assume a constant transport and thus a linear concentration gradient over the tube, $-\text{grad } C_2 = \Delta C_2/l$. Then we have

$$\Delta C_2/C_{2_o} = H l \exp(-t/t_r)/\rho_2 DO. \tag{2.39}$$

For our set-up $l \approx 75$ cm and $O \approx 0.78$ cm^2. With ρ_2 and D from table 2.2 and H from 2.4 we calculate $\Delta C_2/C_{2_o}$ (table 2.12). The time Δt necessary to build up the concentration gradient is then obtained from eq. 2.12 and the values of q'_e and t_r. After this time the concentration diffusion transport is established and the complete volume V_+ takes part in the enrichment. The concentration gradient in the column has little influence on the TD transport (a decrease of about 1% for $^{14}C^{16}O$ and $^{12}C^{18}O$ and 0.5% for $^{13}C^{16}O$) and consequently on the rate of enrichment. This was to be expected from the large values of q_e.
The decrease of $\approx$ 10% in transport τ calculated from eq. 2.11 and 2.12 for a similar enrichment in the total reservoir V_+ therefore is mainly caused by the depletion of V_-.

(vi) We separately consider the diffusion from the bottom of the column to the positive reservoir. It takes some time before the concentration gradient in the connecting tube is established. From the dimensions of the tube and D we obtain a relaxation time of the order of 0.2 days. This is of the same order of magnitude as the time needed to build up the concentration at the bottom of the column. Therefore enrichment in the positive reservoir effectively starts about 0.2 days after the beginning of the enrichment. Similarly the relaxation time for concentration diffusion from the reservoir to the sampling point is $\approx$ 0.1 day. The total time delay for the samples is of the order of 0.2 to 0.3 days. This value is in good agreement with the experimental result in fig. 2.11 (0.3 to 0.4 days).

The corrections discussed above are summarized in table 2.13. For the initial transport the cold wall radius and temperature provide the only important correction. A relative difference between predicted and experimental value of 26% (H^{18}) and 27% (H^{13}) remains unexplained. This is outside the experimental standard deviation of about 10%.
For the enrichment obtained in 30 days the values of r_1 and T_1 ((i)) again give an

Table 2.13. Corrections to be applied to the theoretical values of the TD transport coefficient H and the enrichment q'.

Correction	(i) (%)	(ii) (%)	(iii) (%)	(iv) (%)	(v) (%)	(vi) (%)	Total (%)	Observed discrepancy (%) *
H^{14}	7	–	–	–	1	–	8	
H^{18}	14	–	–	–	1	–	15	41
H^{13}	6	–	–	–	0.5	–	7	34
$q^{14'}$ (30 days)	5	–	2.3	–	1	0.9	9	
$q^{18'}$ (30 days)	12	–	4.3	–	1	0.5	18	41
$q^{13'}$ (30 days)	5	2.5	12.4	–	0.5	0.3	21	36

* this includes the discrepancy between the theoretical values which apply to $^{12}C^{18}O$ and $^{13}C^{16}O$ and the experiment which measures mass 30 (mainly $^{12}C^{18}O$, but also $^{13}C^{17}O$) and mass 29 (mainly $^{13}C^{16}O$, but also $^{12}C^{17}O$)

important correction. Here also column imperfections giving rise to parasitic mixing result in a lower enrichment. Discrepancies between the predicted and the observed enrichment of 23% ($q^{18'}$) and 15% ($q^{13'}$) remain unexplained if we assume K_p = 0.2 K.

A comparison of the enrichment in the final sample drawn from column no. 1 with the average enrichment of all columns shows that in the first $q^{29'}$ is on the average 8% and $q^{30'}$ is 15% lower (or 6% and 10%, respectively, if related to the theoretical values). The discrepancy with the result of sect. 2.4.1 might be explained by variations in cooling water circulation (affecting T_1) and the effect of gas extraction.

The remaining discrepancy between the corrected theoretical enrichments (assuming K_p = 0.2 K), and the observed average values is 9% for $q^{29'}$ and 13% for $q^{30'}$. A similar difference may result for the H values. The agreement between theory and experiment can be called satisfactory considering the experimental uncertainties in the measured enrichment (± 2%), in the parameters used in the theoretical calculation and its corrections, and the fact that the theoretical enrichment applies to $^{12}C^{18}O$ and $^{13}C^{16}O$ while the experimental values include also $^{13}C^{17}O$ respectively $^{12}C^{17}O$.

2.4.3. Calibration of the ^{14}C enrichment

The ^{14}C enrichment of a sample is calculated from the mass spectrometrically determined mass 30 enrichment. In this way the influence of variations in thermal diffusion parameters and of discrepancies between TD theory and reality is minimized.

In order to establish a relation between the ^{14}C and the mass 30 enrichment of a sample a series of enrichments was made using CO_2 gas prepared from marine shells. The average radiocarbon activity of 4 CO_2 samples was 77.15 ± 0.17 pmc

(percent modern carbon). Where possible the ^{14}C enrichment was calculated from a comparison of the same sample before and after enrichment. For the others the average ^{14}C activity given above was used. A total of 5 successful calibration enrichments was carried out. The ^{14}C enrichment was measured with the proportional counter RZ. The enrichment of the masses 29 and 30 was calculated from mass spectrometer measurements using eq. 2.33. The composition of the gas before enrichment was determined from a sample taken from the top of the column. The gas taken from the bottom generally yielded a similar isotopic composition, unless the columns were filled with the residue gas of the reduction system. In that case the bottom sample turned out to be $20^0/_{00}$ or more heavier due to isotope separation during the evaporation of the condensed CO (Rayleigh distillation). A correction based on the theoretical values of the coefficients of eq. 2.19 (table 2.7) was applied to $q^{14'}$ to standardize the results to $V_- = 201$ l.

In fig. 2.13 $q^{14'} - 1$ is presented as a function of $q^{30'} - 1$. The best parabolic fit $y = ax + bx^2$ is obtained for

$$(q^{14'}-1) = (1.309 \pm 0.014)(q^{30'}-1) + (2.9 \pm 3.0) \times 10^{-3}(q^{30'}-1)^2. \quad (2.40)$$

The standard deviations of a and b are obtained from the scattering of the data.

For the estimated relative uncertainties of 2% in the mass spectrometric measurements and 0.5% in the ^{14}C measurements we obtain $\sigma_a \approx 0.04$ and $\sigma_b \approx 0.005$. The result is therefore consistent with a 1% uncertainty in the enrichment of the stable isotopes.

A comparison of eq. 2.40 with the theoretical values of the coefficients (table 2.7) shows, that the first coefficient is 2 σ smaller and the second 2.6 σ larger than that calculated for L-J 12–6 at 308 K and $r_1/r_2 = 31.5$. For the calibration samples the relative difference between theory and experiment is −0.6 to +1.9%, thus showing a good agreement between the experimental and the theoretical relation. This close agreement between theory and experiment allows the use of the theoretical values of the coefficients from table 2.7 to calculate $q^{14'}$ for small V_-.

The relative difference between the experimental results and the values calculated using the relation given by Grootes et al. (1975) is 2.5 to 7.5%. Although considerable compared with the measuring precision of the calibration experiment this difference gives a negligible error in the ^{14}C dates obtained using this relation.

In fig. 2.13 we also give $q^{30'}$ values obtained from the measurements on enriched CO_2 samples using eq. 2.35. The $q^{30'}$ thus derived is generally lower than that obtained from CO. This is probably due to exchange of oxygen during the oxidation of the enriched CO. The recalculated calibration runs of the enrichment

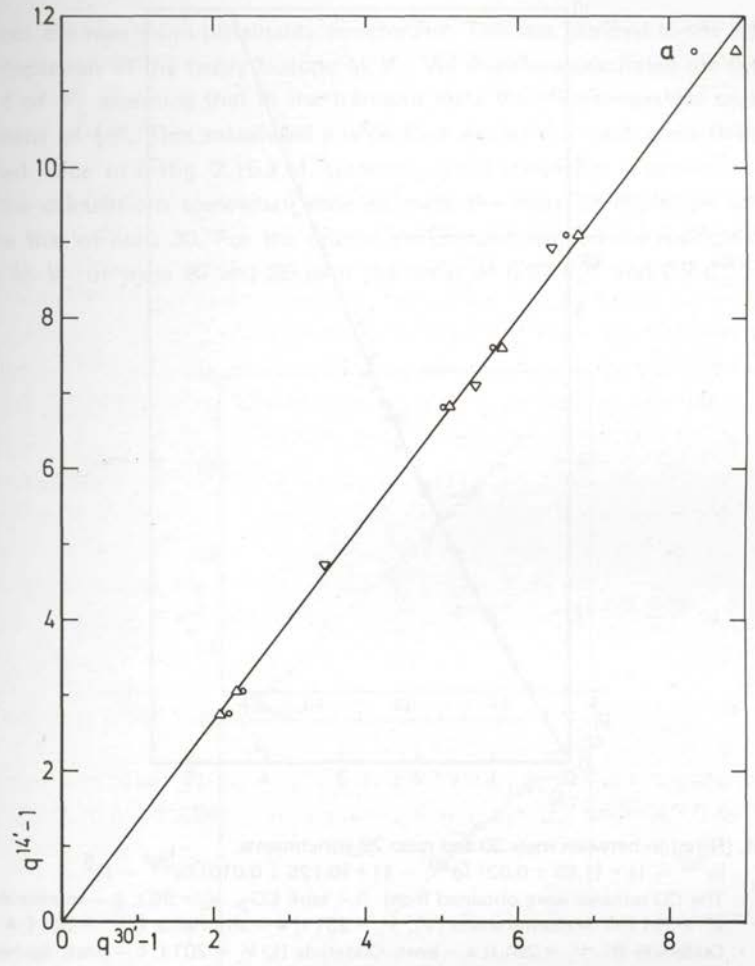

Fig. 2.13. Calibration for determination of the ^{14}C enrichment.
$(q^{14'}-1) = (1{,}309 \pm 0.014)\ (q^{30'}-1) + (2.9 \pm 3.0) \times 10^{-3}\ (q^{30'}-1)^2$. Enrichments were calculated from CO (Δ) and from CO_2 (○) measurements; ∇ — calibrations before 1967. a — leakage during enrichment, value not used for the calculation.

set-up as it was operating in Amsterdam (c.f. appendix) are in good agreement with our results.

In fig. 2.14 the relation between $q^{30'}$ and $q^{29'}$ is shown for the samples discussed in sect. 2.4.2. A least squares parabolic fit $y = ax + bx^2$ yields

$$(q^{30'}-1) = (1.69 \pm 0.02)(q^{29'}-1) + (0.125 \pm 0.010)(q^{29'}-1)^2. \qquad (2.41)$$

The standard deviations of a and b are obtained from the scattering of the data.

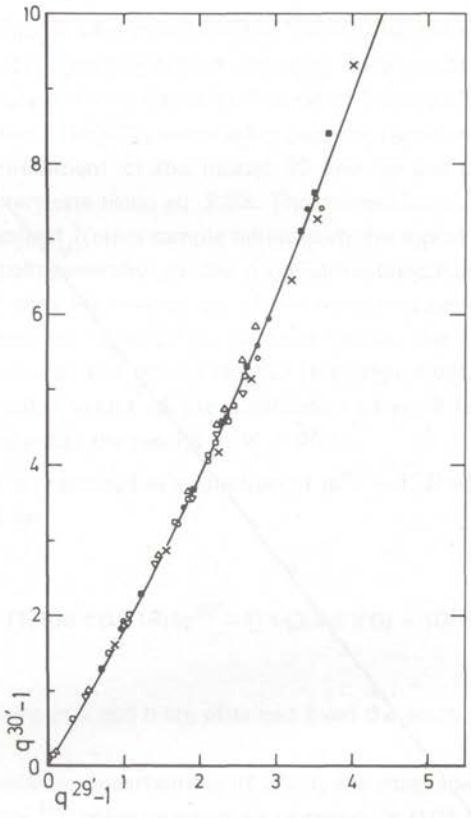

Fig. 2.14. Relation between mass 30 and mass 29 enrichments.
$(q^{30'}-1) = (1.69 \pm 0.02)\,(q^{29'}-1) + (0.125 \pm 0.010)\,(q^{29'}-1)^2$.
The CO samples were obtained from: □ — tank CO_2, $V_- = 90$ l; Δ — marine shells (I), $V_- = 231$ l; ▽ — marine shells (V), $V_- = 231$ l; ■ — anthracite I, $V_- = 201$ l; ● — peat, Odderade (I), $V_- = 201$ l; x — peat, Odderade II, $V_- = 201$ l; ○ — peat, Aschersleben, $V_- = 119$ l.

From eq. 2.19 and the values of q'_e and t_r of sect. 2.1.4 we find

$$(q^{18'}-1) = 2.123(q^{13'}-1) + 0.014(q^{13'}-1)^2 + 4.7\times10^{-4}(q^{13'}-1)^3,$$

for $T_1 = 308$ K, $r_1/r_2 = 31.5$ and $V_- = 201$ l.

The difference between the experimental and the theoretical results can probably be attributed to the difference between the theoretical and experimental values as discussed in sect. 2.4.2 and the relatively large difference in enrichment between $^{12}C^{18}O$ and $^{13}C^{16}O$.

In section 2.1.4 we provided arguments that the volume ratio V_t/V_+ strongly

influences the maximum obtainable enrichment. This was ascribed to the influence of the depletion of the heavy isotope in V_-. We therefore calculated the depletion factor ϵ of V_- assuming that in the transient state the column gas has an average enrichment of $\frac{1}{2}q'$. This calculated ϵ is plotted against the mass spectrometrically measured value of ϵ (fig. 2.15.a,b). Generally good agreement is obtained. Apparently the calculations somewhat underestimate the mass 29 depletion and overestimate that of mass 30. For the normal enrichment samples the residual concentration in V_- of mass 29 and 30 is of the order of 0.87 C_o^{29} and 0.7 C_o^{30} respectively.

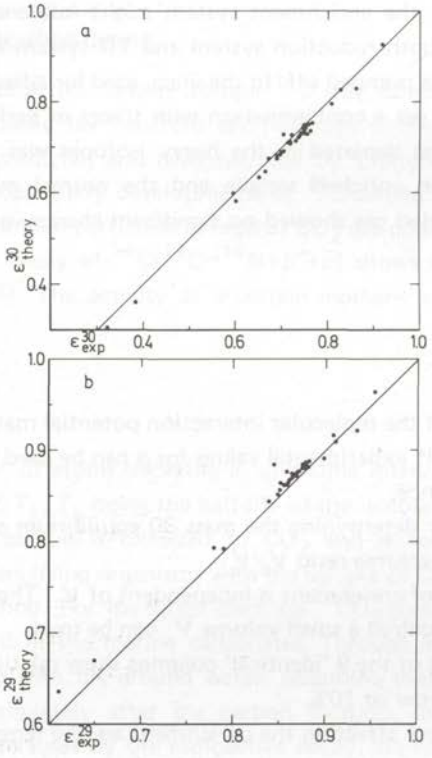

Fig. 2.15. The measured and calculated depletion of the isotopes of mass 30 (a) and mass 29 (b) in V_- for the samples enriched up till June 1976.

2.4.4. Back diffusion and memory effect

In case of power failure, the TD transport ceases. Then the concentration gradient built up by the TD transport decreases because of diffusion. In order to determine this effect the decrease of the concentration of the heavy isotopes in V_+ was

measured as a function of time, after switching off the power. We obtained relaxation times of 900 h (quasi-stationary concentration distribution in the column and connecting tubes re-established overnight, no convection of V_-), 300 h (the same, but with convection of V_-) and 200 h (experiment started 2 hours after admitting enriched column gas to V_+, with convection of V_-). The second experiment, yielding t_r = 300 h, closely resembles the situation of a power failure during an enrichment. From dimensional considerations we estimate a value t_r = 800 h, which is of the same order of magnitude. Obviously, the enrichment will hardly be influenced if the column is switched off for not more than a few hours.

A memory effect in the enrichment system might influence the ^{14}C results. To eliminate this effect both reduction system and TD system are washed three times with sample CO that is pumped off. In the silica, used for adsorbing the enriched CO sample, we may also get a contamination with traces of earlier samples. To check this possibility CO gas depleted in the heavy isotopes was adsorbed in the silica after treatment of an enriched sample and the normal pumping and degassing procedure. The depleted gas showed no significant change in isotopic composition.

2.5. Conclusions

(i) The influence of the molecular interaction potential mainly shows itself in the TD constant α. If experimental values for α can be used the potential model is of little importance.

(ii) The main factor determining the mass 30 equilibrium enrichment of our TD apparatus is the volume ratio V_t/V_+.

(iii) The initial rate of enrichment is independent of V_-. Therefore, if only a small enrichment is required a small volume V_- can be used.

(iv) The enrichments of the 9 'identical' columns show relative deviations from the average of the order of 10%.

(v) Important factors affecting the enrichment are the temperature and diameter of the negative column end and possibly also a column asymmetry giving rise to parasitic mixing.

(vi) The discrepancies between theory and experiment are about 10%, which is of the same order of magnitude as the uncertainty introduced by experimental errors.

(vii) There is a good agreement between the experimental and the theoretical relation between $q^{14'}$ and $q^{30'}$. This indicates that the theoretical relation can be used for volumes that differ considerably from the standard volume of 201 l.

Chapter 3

RADIOCARBON DATING

3.1. The limits of radiocarbon dating

The existence of a radioactive carbon isotope ^{14}C due to reactions between low energy (<1000 eV) cosmic ray neutrons and nitrogen in the lower stratosphere (^{14}N (n, p) ^{14}C) was predicted and demonstrated by Libby et al. (Libby, 1946; Anderson et al., 1947a,b). Early developments of ^{14}C dating are described in the book of Libby (1965) and in particular as regards CO_2 gas counting in the thesis of Barendsen (1955). The decay of $^{14}C(^{14}C \rightarrow {}^{14}N + \beta^- + \bar{\nu})$ shows a half-life of 5730 ± 40 years (Olsson, 1968). The activity at a certain moment is given by the decay formula

$$A(t) = A_0 e^{-\lambda t}, \tag{3.1}$$

where A is the number of atoms decaying in unit time interval at time t and the decay constant $\lambda = \ln 2/T_{\frac{1}{2}}$, $T_{\frac{1}{2}}$ being the half-life of the isotope considered.

The newly formed carbon is oxidized to CO_2 and mixes with atmospheric carbon dioxide. ^{14}C enters living organisms with the uptake of CO_2 from the atmosphere or with organic food. For the larger part the $^{14}CO_2$ goes to the ocean where it becomes incorporated in the marine carbonates. Through infiltrating precipitation ^{14}C is also carried into the ground water. Assuming that exchange with the surroundings ceases completely after the carbon fixation, the ^{14}C content of a certain material only decreases by the radioactive decay. We can thus easily determine the time elapsed since the carbon uptake by comparing the actual radioactivity in a sample with the original activity. We have, however, no means to determine the original ^{14}C activity. Thus the use of radiocarbon for absolute age determinations can only be based upon a number of assumptions, mainly concerned with establishing the best estimate for the original activity A_0.

Once the value of A_0 has been established, the age can be found from eq. 3.1 as

$$T = -\frac{1}{\lambda} \ln(A/A_0). \tag{3.2}$$

In age calculations the conventional (Libby) half-life $T_{\frac{1}{2}} = 5568$ years is used, instead of the more recent and accurate value of 5730 years. The continued use of the old value has been agreed upon by the Fifth Radiocarbon Dating Conference at Cambridge (Godwin, 1962) and by subsequent conferences (the last time at La Jolla, 1976) in order to avoid the necessity of recalculating all earlier dates and, even more, of having to repeat this for each future more accurate value of $T_{\frac{1}{2}}$.

3.1.1. The basic assumptions

With respect to the validity of ^{14}C ages we have to consider the underlying assumptions of the ^{14}C dating method. These assumptions are:

1. The production rate of ^{14}C has been essentially constant over a long period of time (the last 10^5 years).
2. The carbon reservoirs (atmosphere, biosphere and the ocean, divided in mixed layer and deep sea) are in a stationary state, have a turn-over time which is short in comparison with $T_{\frac{1}{2}}$ and are thus essentially well mixed.
3. The living organisms and the carbonates during deposition are in exchange equilibrium with their surroundings.
4. After organic carbon fixation and carbonate deposition, the exchange ceases completely (the 'closed system' assumption).
5. Radioactive decay proceeds at a constant rate irrespective of its chemical or physical surroundings.

Since fluctuations in the ^{14}C production rate do occur, the extra assumption has to be made that:

6. The distribution of ^{14}C over the different reservoirs is rapid compared with $T_{\frac{1}{2}}$. Thus the effect of a change in ^{14}C production rate is distributed over the total exchangeable carbon inventory instead of only over the relatively small atmospheric carbon reservoir ($\approx$ 1% of total carbon). This greatly reduces fluctuations in the atmospheric ^{14}C level.

Much research has been done in order to find out to what extent these assumptions are realistic. In view of the expansion of the routine dating range of about 50 000 years to approximately 75 000 years especially the assumptions 1 and 4 are essential.

Ad 1. Measurements of wood samples of which the age had been determined by tree ring counting and of organic material associated with varves (Stuiver, 1970; Yang and Fairhall, 1972) showed that both short- and long-term variations of the initial ^{14}C content occur. The short-term fluctuations do not exceed $3^0/_{00}$ (Lerman et al., 1970; Damon et al., 1973). For the age range considered these are negligible. As far as the long-term trend is concerned, a variation in ^{14}C concentration of about

10% has been detected over the age range investigated thus far (0–8000 years BP) (Suess, 1970a; Ferguson, 1970; Michael and Ralph, 1972; Damon et al., 1972).
The fluctuations are usually considered to represent changes in the ^{14}C production rate, caused by fluctuations in the cosmic radiation penetrating the earth's atmosphere. These fluctuations can be of extra-terrestrial origin (e.g. solar activity and supernovae) or result from changes in the intensity of the earth magnetic field (Lingenfelter and Ramaty, 1970). Evidence for the latter is given by the great similarity between a curve representing the intensity of the earth magnetic field during the Holocene obtained by Bucha (1970) and the dendrochronologically determined atmospheric ^{14}C activity curve. The magnetic measurements indicate intensity fluctuations with a period of approximately 9000 years and thus predict for older samples periodical fluctuations of the ^{14}C production rate and, accordingly, of the atmospheric ^{14}C level of the order of 5 to 10 percent. This seems to be confirmed by varve measurements.

Measurements on different cosmic ray produced isotopes in meteorites and sediments independently lead to the conclusion that the cosmic ray intensity has been constant within a factor 2 both in space and in time for at least the last 10^6 years (Oeschger et al., 1970).

It is thus unlikely from a geophysical point of view that the ^{14}C production over the last 10^5 years should have changed more than $\approx 10\%$; it has almost certainly not varied by a factor of more than 2.

Ad 4. The closed system assumption has turned out to be only partly valid in the case of materials containing exclusively inorganic carbon. Organic materials, on the contrary, do not exchange carbon with the surroundings. They occur, however, mixed with both inorganic and organic matter of different age, referred to as contaminants. In practice it is often possible to eliminate the contaminants and to develop criteria by which can be decided that this has been accomplished (sect. 4.2; ch. 5).

In conclusion we feel confident that the assumptions, although not completely valid, apply to the extended range, as well as they do to the 'normal' range. Meaningful dates in the age range from 50 000 to 75 000 years BP can therefore be obtained.

Here it is important to realize that the radiocarbon method is an absolute dating method only in the sense that the time as read from the radiocarbon clock is absolute on this clock. The correspondence between radiocarbon time and terrestrial time is based upon the assumptions 1–6 mentioned before.

Because of several complications, it has been shown necessary to precisely define the value of A_o, in order that the results of different laboratories be comparable. At the Fourth Radiocarbon Conference at Groningen (Godwin, 1959) the standard

recent activity of AD 1950 has been defined to be 95% of the activity of a certain batch of oxalic acid from the U.S. National Bureau of Standards. This was subsequently specified to apply to CO_2 prepared from the oxalic acid, having $\delta^{13}_{PDB} = -19.0\,‰$ (Flint and Deevey, 1961).

The unknown activity of a sample is then measured in a proportional gas counter or liquid scintillation counter under the same standard conditions as the activity A_o of the standard sample. A misassessment of the recent standard leads to a constant error in the ages obtained and thus to a shift of the complete time scale.

The use of the more recent value of the ^{14}C half-life ($T_{\frac{1}{2}} = 5730$ years) instead of the conventional value of 5568 years would lead to an expansion of the complete time scale with a constant factor (1.03). In both cases the relative position of measured samples on the ^{14}C time scale remains unaffected.

3.1.2. The instrumental limitations

With samples of very low ^{14}C activity (A) the standard deviation of the actual measurement ($A+B \approx B$) obscures the difference between $A+B$ and B, in other words makes it impossible to decide whether any ^{14}C activity is still present in the sample. Consequently every ^{14}C counter has a certain limit beyond which no ^{14}C activity can be established in a given time. Comparison of this minimum ^{14}C activity with the activity A_o of a recent sample under the same counter conditions yields the lowest fraction of the original ^{14}C activity that can be detected and, consequently, the upper age limit of the counter under the conditions chosen.

For the most sensitive counter set-ups presently in use, the range of the radiocarbon dating method, using a 48 hours counting period, is approximately 60 000 years (Stuiver et al., 1974).

The standard deviation for a sample of activity A measured during t minutes in a counter with background B is

$$\sigma = \sqrt{\frac{A+B}{t}} \text{ (cpm)}. \tag{3.3}$$

Here we assume that the number of counts detected is sufficiently large to have a Gaussian probability distribution of the true activity around the measured value. The net sample activity is

$$A = N/t - B \text{ (cpm)} \tag{3.4a}$$

with a standard deviation of

$$\sigma_A = \sqrt{(A+B)/t + B/t_B} \text{ (cpm)}. \tag{3.4b}$$

The background B is being measured frequently (t_B minutes with $t_B \gg t$), so that for samples where $A \ll B$ we can approximate eq. 3.4b by

$$\sigma_A \approx \sqrt{B/t} \,. \tag{3.5}$$

If we use the normal 2σ criterion, in which samples having an activity $A < 2\sigma$ are reported to have an activity smaller than $A+2\sigma$ (with 98% probability), the lowest measurable activity and thus the age range is determined by $A > 2\sqrt{\frac{B}{t}}$. The resulting maximum age then is (eq. 3.2)

$$T_{max} = +\frac{1}{\lambda} \ln \left[\tfrac{1}{2}\sqrt{t}\, \frac{A_o}{\sqrt{B}}\right]. \tag{3.6}$$

Obviously there are three ways to extend the range:

1. decrease the counter background (B);
2. increase the measuring time (t);
3. increase the specific activity of the sample.

An increase of the range by three to four half-lives is needed to date the early part of the Last Glacial.

A considerable amount of work has been done on the reduction of the background relative to the sample activity. A gain of, say, two half-lives, equivalent to a 16 fold reduction of B with constant A_o or a 4 fold increase in A_o by increasing the counter size and/or the gas pressure at a constant B would pose a serious problem. Increasing the measuring time to gain two half-lives is also impracticable. As far as these possibilities are concerned, the experimental limitation of the age range is 60 000 to 65 000 years.

Another way of extending the range is by increasing the specific activity of the sample. This can be achieved by means of thermal diffusion isotopic enrichment (Haring et al., 1958). In an enrichment of one month an increase in specific activity with a factor 10 is obtained, giving a gain in age range of somewhat more than three half-lives (18 500 years). With some additional increase in measuring time this leads to an instrumental dating range of 75 000 to 80 000 years.

3.1.3. Other limiting factors

Other factors limiting the maximum age that can be measured are the contamination of the samples *in situ* and in the laboratory and the *in situ* production of ^{14}C by cosmic ray and fission neutrons.

Generally the samples to be dated incorporate variable amounts of contaminating carbon having a specific activity different from that of the original material. This is a source of error for samples of any age, but its importance increases with age (see

fig. 3.1). A sample with an age of 75 000 years contains about 0.01% of the original (recent) ^{14}C activity. This is equivalent to a contamination with 0.01% of recent organic material. Therefore, a very critical evaluation of possible sources of contamination as well as a careful estimate of the *in situ* production of ^{14}C is required.

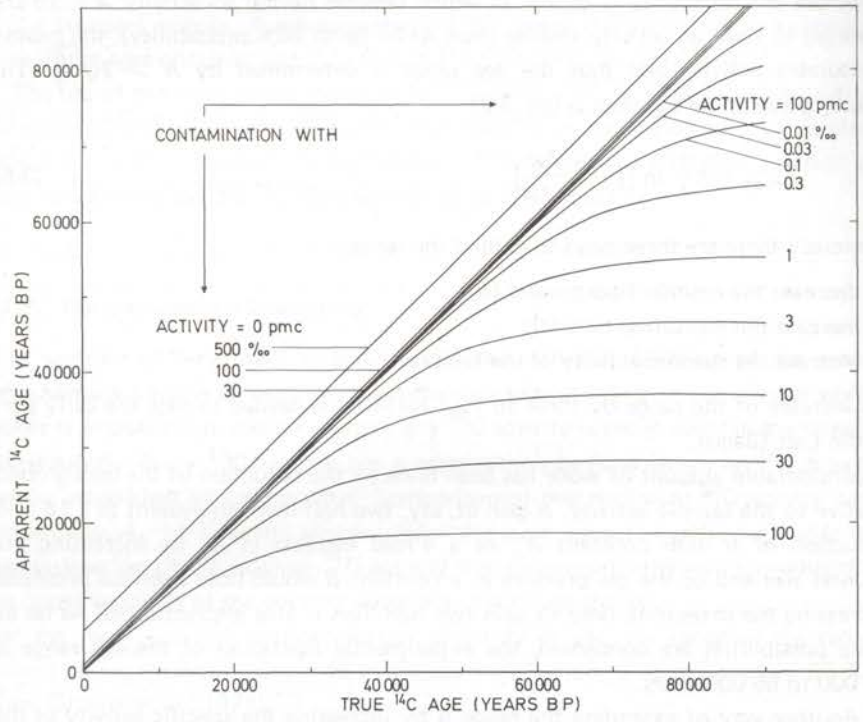

Fig. 3.1. The apparent as a function of the true sample age for various degrees of contamination with contaminants of zero radiocarbon activity (0 pmc), and of recent activity (100 pmc).

We will distinguish between two kinds of contamination:

(i) *sample contamination*, by materials containing carbon with a ^{14}C content different from the sample material, that are introduced into the sample *in situ* (e.g. humic substances, rootlets, carbonates) or during sample collection, transport and storage;

(ii) *laboratory contamination*, by foreign carbon introduced during sample handling in the laboratory.

3.1.3.1. Sample contamination

The amount and nature of the contamination can vary greatly from sample to

sample. A careful choice of sample and a mechanical and acid-alkali-acid pretreatment, however, give satisfactory results in most cases, even for samples of 50 000 years and older.

The reliability of a ^{14}C date as far as contamination is concerned has to be concluded from:

1. A comparison of the ages of different samples from the same profile. The sequence of ages should be in accordance with the stratigraphical evidence, if a reliable stratigraphy has been established.
2. A consistent picture for equivalent samples from different related profiles. Samples of different profiles, which are considered to be of the same age on base of pollenanalytical, stratigraphical and/or other evidence should yield corresponding dates.
3. An investigation of the activity of the material extracted in different fractions of the chemical pretreatment. If the contaminant has been introduced into the sample by infiltrating ground water (e.g. humic substances and carbonates) it may be expected to be somewhat more soluble than the bulk of the sample material, if peat, lignite or wood samples are considered. In that case the contaminant will be found in the early extracted fractions, but not in the last. Accordingly the first extracts may show extra ^{14}C activity. The last extract should have an activity equal to that of the final pretreated sample or, in the case of enriched samples, no measurable activity.

Experiments on sample contamination are described in sect. 4.2. The correlation between the results of the different enriched samples is discussed in chapter 5.

One source of contamination is easily avoided. After the sample has been taken, it should not be brought into contact with carbon containing materials such as cotton wool, paper, cloth, oil, varnishes etc. Suitable packing materials are Al-foil, metal boxes, glass vessels and plastic sheets or bottles.

3.1.3.2. Laboratory contamination

During our study it turned out that also in the laboratory sources of contamination occur. We devote a separate section of the chapter 'Sample Treatment' to this (sect. 4.4).

3.1.3.3. *In situ* production of ^{14}C

Several authors have discussed the possibility that ^{14}C might be produced in the sample *in situ*. (Sawelski, 1968; Felber, 1971; Harkness and Burleigh, 1974; Cain and Suess, 1976). Harkness and Burleigh (1974) concluded from artificial neutron irradiation experiments that in the age range up to 10 000 years BP no measurable effect could be detected in bristlecone pine samples after normal chemical pretreat-

ment within a mean standard deviation of 0.3%. Since the residual activities measured after isotopic enrichment are smaller, in the range 0.01–0.1%, we estimated the possible *in situ* production for some of our samples independently.

The most important reaction we have to consider is $^{14}N(n, p)^{14}C$ induced by low-energy (< 1000 eV) neutrons. The contribution of fast neutrons to this reaction and that of reactions of the type $^{13}C(n,\gamma)\ ^{14}C$ is small (< 10%, Sawelski, 1968). The neutron flux ϕ through a sample buried underground is produced by cosmic radiation (at greater depths almost exclusively muons) and by spontaneous fission reactions of uranium in the soil. We can calculate the activity of the sample due to the *in situ* production of ^{14}C from

$$A_{is} = P(1-e^{-\lambda T}) \text{ (dpm/g carbon)},$$

where P is the production rate of ^{14}C:

$$P = 60\ \phi\ \sigma_N\ N\ f_N/(f_C\ M)\ (^{14}C \text{ atoms/min/g carbon}),$$

λ is the ^{14}C decay constant, T is the time of exposure to neutron irradiation, σ_N is the effective cross section of nitrogen for thermal neutrons, N is Avogadro's number, f_N and f_C are the relative nitrogen and carbon content of the sample expressed as weight fraction and M is the atomic weight of nitrogen (= 14). If not only the reaction $^{14}N(n, p)\ ^{14}C$ is considered but the combined production rate of all possible reactions, P has to be multiplied by a factor $R \approx 1.1$.

Data of the samples for which *in situ* production has been considered are given in table 3.1. They were chosen because:

(i) *Anthracite* is used for background measurements and provides an indication of possible laboratory contamination;

(ii) *Amersfoort III* lies at the base of our most important and complete series of samples;

(iii) *Beaverdam Creek* offers the possibility of a correlation between ^{14}C and K-Ar dating due to the presence of a volcanic ash layer immediately on top of the ^{14}C dated layer.

The cosmic neutron flux at the position of the sample was calculated as the sum of:

(a) the cosmic neutron flux at the air-land interface at 200 m altitude corrected for atmospheric attenuation and attenuation underground;

(b) the neutron flux produced by muons assuming a muon attenuation length of 4000 g/cm^2;

(c) the neutron flux produced by nucleons assuming a nucleon attenuation length of $\approx$ 160 g/cm^2.

Table 3.1. Description of samples and estimated *in situ* production of ^{14}C.

Sample		Anthracite	Amersfoort III	Beaverdam Creek
depth below surface	m		8.40	54.2 [a]
thickness of layer	m		0.35	0.22
sample composition				
total dry organic material [bc]	%	97	86.5	16
carbon content	%	88.5	54.2	7
hydrogen content	%	3.8	5.6	1.25
nitrogen content	%	0.83	1.1	0.48
uranium concentration ash [d]	ppm	26 ± 5	18 ± 5	5 ± 3
neutron flux ϕ:				
in thick sample layer [e]	n/cm^2 sec	1.9×10^{-5}	1.6×10^{-5}	6.9×10^{-5}
in embedded layer [f]	n/cm^2 sec	6.3×10^{-4}	4.4×10^{-4}	1.2×10^{-4}
due to cosmic rays	n/cm^2 sec		6.6×10^{-5}	1.1×10^{-5}
produced activity:				
thick layer	dpm/g carbon	8.3×10^{-7}	7.8×10^{-6}	2.6×10^{-5}
embedded layer	dpm/g carbon	2.8×10^{-5}	4.7×10^{-5}	4.2×10^{-5}
apparent age: [g]				
thick layer	yrs BP	1.34×10^5	1.15×10^5	1.06×10^5
embedded layer	yrs BP	1.05×10^5	1.01×10^5	1.02×10^5

a sample taken from steep exposure; below: almost vertical section reaching down to stream level 15.1 m below; on top: section with slope $\approx 45°$; residence time near surface accordingly assumed to be short (< 100 years)

b analyses carried out by J. Ebels of the analytical department, Chemical Laboratory, Univ. of Groningen; C, H and N content based on total sample

c the water content of the samples can be estimated from the fact that moist peat contains an amount of water equal to approximately three times the amount of dry organic material

d X-ray fluorescence spectrometry analysis by E. A. Th. Verdurmen of Z.W.O. Laboratory for Isotope-Geology, Amsterdam

e 'thick' means several attenuation lengths (170 g/cm^2) i.e. several metres; the neutron production over one attenuation length is assumed to contribute to the flux

f composition of the surrounding layers assumed to be equal to that of the ash

g calculated using a recent activity of 13.56 dpm/g carbon (Karlén et al., 1964)

The neutron flux due to uranium fission was estimated from the measured uranium concentration in the samples, the spontaneous fission decay constants, λ_{sf}, and the attenuation length of neutrons ($169 \, ^{+19}_{-16}$ g/cm^2). Parameters for these calculations are given in table 3.2.

For the calculation of the neutron flux from ^{238}U fission we assumed that the attenuation length of fission neutrons underground is comparable to that for cosmic ray neutrons in water. Since the neutron capture cross section for hydrogen is of the same order as for several of the more important rock elements this assumption seems reasonable.
Also for muons and nucleons we assumed, that the attenuation length underground is approximately equal to that in water.

Table 3.2. Neutron flux parameters.

		ref.
neutron flux ϕ at air-land interface 0.05–2.0 MeV	2.3×10^{-3} n/cm² sec	1[a]
relative μ meson contribution to ϕ	4%	2
decay constant for spontaneous fission of ^{238}U, λ_{sf}^{238}	2.7×10^{-24} sec^{-1}	3
decay constant for spontaneous fission of ^{235}U, λ_{sf}^{235}	$(1.1 \pm 0.7) \times 10^{-25}$ sec^{-1}	3
average number of neutrons from ^{238}U fission	2.2 ± 0.3	3
attenuation length of neutrons in air	≈ 120 g/cm²	4
attenuation length of neutrons in water	$169 \, ^{+19}_{-16}$ g/cm²	5
attenuation length of nucleons in water	≈ 160 g/cm²	2
attenuation length of μ mesons in water	≈ 4000 g/cm²	2
non cosmic neutron flux in rock	$(0.14–1.44) \times 10^{-3}$ n/cm² sec	6
thermal neutron capture cross section σ_H	$(332 \pm 2) \times 10^{-27}$ cm²	7
σ_N	$(1.8 \pm 0.1) \times 10^{-24}$ cm²	7

a measured at altitude 200 m; latitude 42° N, longitude 88° W; geomagnetic latitude 53° N
1. Gold (1968); 2. Cocconi and Cocconi Tongiorgi (1951) and estimate; 3. Segrè (1952); 4. Harkness and Burleigh (1974); 5. Bagge and Skorka (1958); 6. Sawelski (1968); 7. Handbook of Chemistry and Physics 53rd ed. (1972), B 247.

The assumption that the uranium content of the overlying and underlying inorganic layers is equal to that of the ash of the organic material probably provides an upper limit for the fission produced flux, since uranium tends to be enriched in organic material relative to its inorganic surroundings (Felber and Hernegger, 1971).

The neutron fluxes calculated for thin sample layers agree well with the measured neutron flux in bore holes (Sawelski, 1968).

The calculated ^{14}C activities due to *in situ* production are upper limits, since it has been assumed that the total neutron flux is captured by ^{14}N. Although neutron capture cross sections for most rock elements are much smaller, their presence will result in a decreased ^{14}C production rate. From the apparent ages it is clear that no interference due to *in situ* production is to be expected for the samples (i, ii and iii). This is even more so, because probably an important fraction of the ^{14}C produced is removed during sample pretreatment as indicated by the results of Harkness and Burleigh (1974).

In situ production by the reaction $^{11}B(\alpha,p)^{14}C$, discussed by Felber (1971), would yield a ^{14}C activity $\lesssim 3 \times 10^{-7}$ dpm/g carbon for anthracite (the uranium content of anthracite is about 100 times lower than that of his samples). This reaction does not contribute in a measurable way to the ^{14}C activity of the sample.

We conclude that in the age range up to 80 000 years BP *in situ* production of ^{14}C is negligible.

Problems due to *in situ* production of ^{14}C only occur if the measuring range were to be extended beyond 100.000 years.

3.1.4. Effect of enrichment on dating range and accuracy

If we denote the ^{14}C enrichment of the sample by $q^{14'}$ (sect. 2.1.3), the measured activity of the enriched sample by A_e and the sample activity prior to enrichment by A, then

$$A_e = q^{14'} A. \tag{3.7}$$

With eq. 3.2 the age of the sample is

$$T = -\frac{1}{\lambda} \left(\ln \frac{A_e}{A_o} - \ln q^{14'} \right), \tag{3.8}$$

where $1/\lambda$ is the mean conventional ^{14}C life-time (8033 years).
The gain in age range is $(\ln q^{14'})/\lambda$, which is 18 500 years for a ^{14}C enrichment by a factor 10.

The gain in dating range is accompanied by an additional uncertainty due to the determination of the mass 30 enrichment $q^{30'}$, and the calibration relation (sect. 2.4.3). The standard deviation in the sample activity A results from eq 3.7:

$$\sigma_A = \left\{ (\sigma_{A_e}/q^{14'})^2 + \left(-A_e \sigma_{q^{14'}}/(q^{14'})^2 \right)^2 \right\}^{\frac{1}{2}}. \tag{3.9}$$

This leads to the standard deviation in the measured age:

$$\sigma_T = -\frac{1}{\lambda} \ln \left(1 \mp \{ (\sigma_{A_e}/A_e)^2 + (\sigma_{q^{14'}}/q^{14'})^2 \}^{\frac{1}{2}} \right). \tag{3.10}$$

For samples with a low specific activity (A_e corresponding to a ^{14}C age $> 40\,000$ years) it follows from a series expansion that σ_T is asymmetrical around T. The second term is the standard deviation due to the statistical character of the counting process. The third represents the uncertainty in the determination of the enrichment, mainly that in the mass 30 enrichment. The relative precision for $q^{14'}$ is approximately 1% (sect. 2.4.3.).

For samples where σ_{Ae}/A_e is small, the enrichment introduces a sizeable additional uncertainty. If we neglect any contribution to σ_A smaller than 10%, we can neglect the contribution of the enrichment for samples having an activity $A_e < 0.0218\, A_o$ ($T_e > 31\,000$ years) counted for 48 hours. Thus under the present circumstances, the inaccuracy of the enrichment factor does not influence the age determination of old samples ($> 60\,000$ years).

Thermal diffusion enrichment can be used to improve the measuring precision for old samples. From numerical calculations it follows that an improvement is obtained for samples having an activity $A < 0.06\,A_0$ ($T > 23\,000$ years) which are counted for 48 hours. If the counting period would be increased and taken equal to the time needed for enrichment plus 48 hours, then improved precision would be obtained for $A < 0.009\,A_0$ ($T > 38\,000$ years).
The amount of work involved in an enrichment dating makes it, however, unattractive to pursue a better precision in this way.

3.2. Proportional gas counting

3.2.1. Introduction

The β^- particles emitted in the decay of ^{14}C have a continuous energy distribution with a maximum energy of 156 keV and a top at approximately 25 keV (Sonntag et al., 1970). The energy is dissipated by collisions with the counter gas molecules, causing excitation and the so called *primary ionization*. The average energy required for the production of an ion-electron pair in CO_2 is about 33 eV. Therefore, approximately 750 ion-electron pairs are created by a β particle of 25 keV in CO_2.

To detect the primary ionization, we use counters with CO_2 as a counting gas. In the counter the electrons produced by primary ionization drift towards the wire in an electrostatic field. In the region of high field strength near the wire the energy gained by the electrons between consecutive collisions with gas molecules is sufficiently large to cause further ionizations. This avalanche effect is called *charge multiplication*. The gas multiplication is $M = n/n_0$, where n is the final and n_0 the original number of electrons. If M is independent of n_0, the final number of electrons n resulting from a β particle is proportional to its energy. Then the counter is operating in its *proportional* range. The decay of the ^{14}C atom is thus detected by the voltage pulse produced by charge collection.

The main problem of ^{14}C dating is to detect the very small number of ^{14}C decays in the presence of other ionizing radiation (cosmic ray and natural radioactivity) giving a counting rate 10 to 10 000 times higher than the ^{14}C decay. The design of a counter set-up requires a quantitative knowledge of (i) the processes that determine the voltage pulse and (ii) the composition and properties of the other ionizing radiation. The latter is discussed in sect. 3.2.3.3 and 3.2.3.4.

The magnitude of the voltage pulse resulting from a primary ionization is determined by the following processes: (i) a certain loss of primary electrons as they drift to the wire, resulting from the formation of negative ions by electron attachment; (ii) the gas multiplication caused by the electrons near the wire; (iii)

the movement of the positive ions to the counter wall and (iv) the capacity and resistance of the counter and its electrical connections.

The *electron attachment* especially to electronegative gases results in a decrease in the height of the voltage pulses produced in the counter. The part of the pulses below a pre-set discriminator level will be lost (c.f. sect. 3.2.2).
Electron attachment is essentially a three-body process. The primary electron is only permanently attached after the excited negative ion has transmitted its excitation energy to a colliding CO_2 molecule. Assuming the rate of electron loss to be proportional to the number of electrons n, the density of the impurity gas n_i and that of the CO_2 n_c we may write (Brenninkmeijer and Mook, 1976)

$$dn/dt = -n\, n_i\, n_c\, K_3. \tag{3.11}$$

K_3 is the reaction constant for the 'three-body collision' between the primary electron, the impurity gas molecule and a CO_2 molecule. The loss due to stabilization of the negative ion by the collision with a second impurity gas molecule (K_2) has been neglected since $n_i \ll n_c$. The total electron loss through attachment results from integration over the drift time of the primary electrons from their origin at r_o to the wire:

$$\ln \frac{n_o}{n} = \frac{c^2 f\, K_3 p^3 (r_o^2 - a^2) \ln (b/a)}{2\mu V}\,, \tag{3.12}$$

where a and b are the wire and counter radius respectively, n_o and n the number of primary electrons before and after electron attachment, f is the impurity fraction (n_i/n_c), c the ratio of density and pressure (n_c/p), μ the mobility coefficient and V the counter voltage.

The value of K_3 depends on the electronegative impurity considered. Measurements by Brenninkmeijer and Mook (1976) indicate that the values of K_3 for different gases (O_2, SO_2, NO, NO_2) are of the same magnitude ($\approx 10^{-30}$cm^6/sec).

Large-radius counters operating at high pressure will be particularly sensitive to electronegative impurities.

The correction of the measured ^{14}C activity for the presence of small amounts of electronegative impurities is discussed in sect 3.2.3.5.

Gas multiplication is limited to a small region near the wire where the field strength ($E(r) = V/r \ln(b/a)$, r being the distance from the counter axis) is high enough. In this region the electron attachment is negligible. Therefore we can consider the electron attachment and the gas multiplication as two independent processes.

Rossi and Staub (1949) have shown that any expression relating gas multiplication to counter parameters must satisfy the condition

$$M = f[a,p,V/\ln(b/a)] = f(a,p,E_a), \tag{3.13}$$

where E_a is the field strength at the wire surface.

Rose and Korff (1941) developed a generally accepted theory of gas multiplication, which was subsequently modified by Curran and Craggs (1949). A relationship for the lower-pressure range (a few hundred torr) was derived by Diethorn (1956). For higher CO_2 pressures (up to 2 atmosphere) Zastawny (1966) gave the following expression

$$(\ln M)/aE_a = K + B\{\ln(E_a/pS_0)+(pS_0/E_a)-1\}. \tag{3.14}$$

Here K, B and S_0 are constants for a particular gas. In section 3.2.3.2 we give the results of our gas multiplication measurements and make a comparison with eq. 3.14. In proportional counters M is generally of the order of 10^3 to 10^4. As a result virtually all ionization takes place within a distance of one wire radius from the wire.

The *pulse formation* in a proportional counter is determined by two processes: (i) the drift of ions and electrons in the electrostatic field in the counter producing a change in the counter voltage and (ii) the return of the counter voltage to its original value, determined by the effective capacity and resistance of the counter and its connections.

The change $v_i(t)$ in the counter voltage is determined by the capacity C of the anode-cathode system, and by the charges q induced by the positive and the negative charge carriers. The pulse due to one ion-electron pair is (Wilkinson, 1959)

$$v_i(t) = \{q_-(t)+q_+(t)\}/C, \tag{3.15}$$

where

$$q_{\mp}(t) = \mp e \ln\{b/r_{\mp}(t)\}/\ln(b/a),$$

e is the electron charge.

The positions r_- and r_+ at time t are determined by the position at which the ion-electron pair was formed (r_0), the field strength and the migration velocities of the electron and the ion respectively:

$$r(t) = \{[2\mu Vt/p\ln(b/a)] + r_0^2\}^{\frac{1}{2}}. \tag{3.16}$$

The relation $V_d = \mu E/p$ for the drift velocity, used in deriving eq. 3.16, is valid for

both ions and electrons everywhere in the counter volume except very close to the wire. The value of μ is 5.6 x 10^5 cm^2 torr/Vsec for electrons (Pack et al., 1962) and 840 cm^2 torr/Vsec (Raether, 1964) for CO_2^+ ions in CO_2. Since virtually all electrons originate close to the wire, they are collected very rapidly. The change in the counter voltage is primarily determined by the drift process of the positive ions to the wall. For one ion-electron pair we have

$$v_i(t) = -(e/C)\ln\{[2\mu Vt/a^2 p \ln(b/a)]+1\}/2\ln(b/a). \qquad (3.17)$$

The maximum pulse height is $v_{i\,max} = -e/C$. This is obtained after a time

$$t = (b^2 - a^2)\, p\, \ln(b/a)/2\mu V.$$

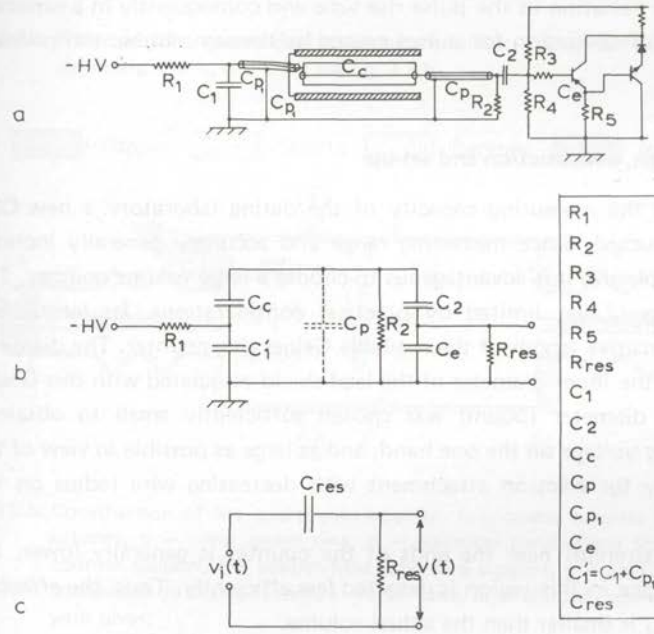

R_1	:	20 MΩ
R_2	:	20 MΩ
R_3	:	180 kΩ
R_4	:	220 kΩ
R_5	:	22 kΩ
R_{res}	:	99 kΩ
C_1	:	4700 pF
C_2	:	100 pF
C_c	:	7 pF
C_p	:	29 pF
C_{p_1}	:	100 pF
C_e	:	2 pF
$C_1'=C_1+C_{p_1}$	:	4800 pF
C_{res}	:	28 pF

Fig. 3.2. Proportional counter GRADA (no. 6) and its electrical connections.
a – actual situation; b – electrical equivalent of a); c – simplified form of b); C_p – parasitic capacitance, C_{p1} – parasitic capacitance of counter high-voltage connection ($C_1' = C_1 + \Sigma C_{p1} \approx C_1$), HV – negative high-voltage, $v_i(t)$ – change in counter voltage without RC filter, $v(t)$ – pulse reaching the amplifier.

The counter is coupled to an amplifier to increase the pulse size. The counter and its electrical connections (fig. 3.2.a) are represented by fig. 3.2.b which can be simplified to fig. 3.2.c. By the connection, capacitance and resistance are

introduced into the circuit, leading to a differentiation of the voltage $v_i(t)$ to a pulse $v(t)$ at the amplifier. If the primary ionization is considered to be concentrated in a point, the differentiated pulse $v(t)$ is still proportional to the amount of ionization. Depending on the RC-time of the differentiating circuit, $v(t)$ varies between $v_i(t)$ and, for small RC, the differentiated form (Wilkinson, 1959)

$$v(t) = \frac{v_{i\,\max} RC}{2 \ln (b/a) \{t + a^2 p \ln (b/a)/2\mu V\}} . \qquad (3.18)$$

Although this expression is only an approximation, it still provides a reasonable estimate for the decay of the pulse.

In reality the charge carriers are distributed along a track in the counter. The preceding discussion, therefore, has to be extended to include the effect of different arrival times of the primary electrons in the region of gas multiplication. This results in some variation in the pulse rise-time and consequently in a variation in pulse size after differentiation for pulses caused by the same amount of primary ionization.

3.2.2. Counter design, construction and set-up

In order to expand the measuring capacity of the dating laboratory a new CO_2 counter was constructed. Since measuring range and accuracy generally increase with increasing sample size it is advantageous to choose a large volume counter. The counter size, however, was limited by practical considerations. Its length was chosen to fit the sensitive length of the available Geiger ring counter. The diameter was determined by the inner diameter of the lead shield associated with this Geiger counter. The wire diameter (50μm) was chosen sufficiently small to obtain a reasonable operating voltage on the one hand, and as large as possible in view of the increasing sensitivity for electron attachment with decreasing wire radius on the other (eq. 3.12).

Since the field strength near the ends of the counter is generally lower, the ionization taking place in this region is detected less efficiently. Thus, the *effective counter volume* V_{eff} is smaller than the actual volume.

Using the diameters of the wire and the counter tube we calculated the radii of the field tube/wire support and of the quartz insulator for which the electrostatic field at the ends will be least disturbed using a program developed by Groeneveld (1977). The deviation in the field strength at a distance of one counter radius from the ends was calculated to be less than 1%. Thus a good ratio of effective to total volume is obtained. Moreover, the variation of counting rate with voltage in the plateau region is minimized.

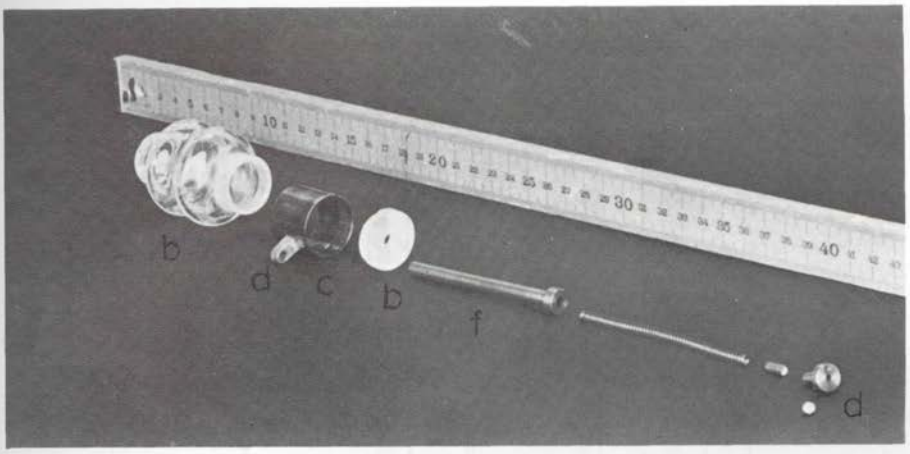

Fig. 3.3.a. Parts of the quartz-gold counter: insulator, electrical connections and wire mounting. For b, c, d and f see fig. 3.3.b.

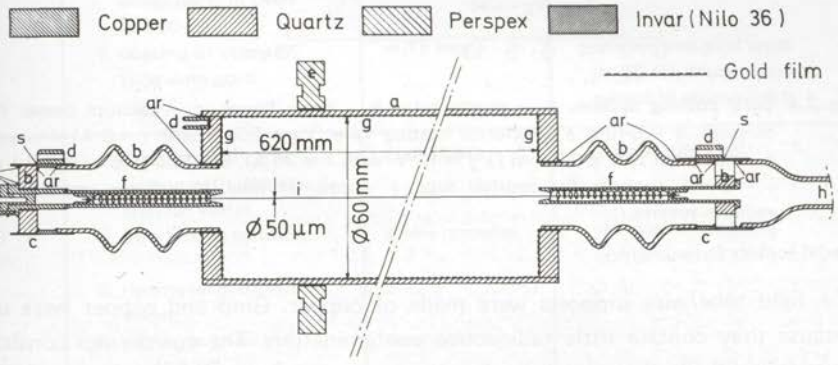

Fig. 3.3.b. Construction of the quartz-gold counter. a — quartz counter tube, b — quartz insulators, c — invar guard ring, d — electrical connections (copper), e — perspex counter support, f — copper field tube/wire support, g — gold layer (≈ 10 nm), h — connection to filling system, i — steel wire, ar — araldite connection, s — soldered with silver.

The counter design is given in fig. 3.3. The counter has been made of quartz. This can be purchased in a very pure form* (essentially free of radioactive contamination), has good vacuum properties and yields no electronegative impurities. The conducting layer on the inner wall of the counter consists of approximately 10 nm of fine gold deposited by evaporation using the method developed by Vogel (fig. 3.4).

* High purity quartz: 'Pursil 435'; Quartz & Silice.

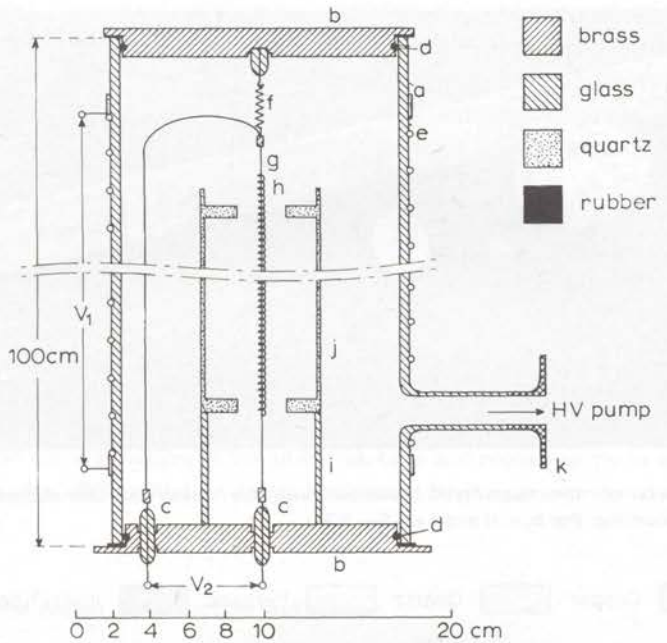

Fig. 3.4. Gold coating system. a — pyrex tube, b — brass flange, c — vacuum power feed-through, d — o-ring, e — external heating wire ($V_1 \approx 250$ V with $I \approx 8$ A), f — spring, g — tungsten wire ϕ 0.5 mm ($V_2 \approx 18$ V with $I \approx 30$ A), h — fine-gold wire ϕ 0.1 mm, i — pyrex support for counter tube, j — counter tube, k — flange connection to vacuum system.

The field tube/wire supports were made of copper. Gold and copper were used because they contain little radioactive contamination. The guard rings consist of Invar (nilo 36 alloy) to match the low thermal expansion of the quartz. A steel wire was used to provide sufficient strength. Since the total mass of the wire is small, a possible contamination will not seriously influence the counter background.

The parts of the counter manufactured by the glass and the mechanical workshop of the laboratory, were cleaned according to the procedure in table 3.3. The counter was subsequently assembled using 1-component (200°C) araldite in a special dust-poor counter-construction room (Vogel) in order to minimize the contamination of the counter by radioactive dust particles adhering to the inside of the counter wall.

The set-up for the new counter GRADA (= Groningen Radiocarbon Activity Detection Apparatus) (counter no. 6) is given in fig. 3.5.a,b. The massive iron shield stops all radiation except the cosmic ray mesons. Neutrons are moderated to thermal energies while passing through the paraffin and subsequently captured by boron near the base of the paraffin layer. The shield has been described by Barend-

Table 3.3. Pretreatment of counter parts.

Material	Treatment	Time	Effect
quartz	1. detergent solution, rinsing with demineralized water.	overnight	general cleaning.
	2. heating at ≈ 700 °C.	≈ 1 h	oxidation organic compounds.
	3. etching of the inside of the counter tube with 4% HF.	≈ 30 min	removal of outermost quartz layer with possible contaminants.
	4. Aqua regia.	overnight	dissolving of all metal contaminants.
	5. rinsing with: 10% HNO_3, 1% HNO_3 and distilled water consecutively.		
	6. drying of counter tube in coating oven in vacuum at ≈ 200 °C, other parts in oven at 100 °C.	overnight	
	7. coating of counter tube with gold.	≈ 15 min	conducting gold layer (≈ 50 Ω), bluish transparent in strong light.
metal	1. detergent solution, rinsing with demineralized water.	overnight	general cleaning.
	2. 20% HNO_3 solution.	a few minutes	removal of possibly contaminated surface layer.
	3. rinsing with distilled water.		
	4. drying in oven at ≈ 100 °C.	overnight	

sen (1955) and De Vries (1957). It was rebuilt by Vogel. The radiation inside the shield mainly consists of muons. It is discussed in more detail in sect. 3.2.3.4.

The muons are detected by the multiwire Geiger ring counter. This counter has been described by Barendsen (1955). It was refilled with ≈ 12 torr of ethanol vapour and 125 torr of argon. The Geiger plateau begins at approximately 1050 V, has a length of almost 200 V and a slope of 1.6 ± 0.5% per 100 V.

The proportional counter is placed inside the Geiger ring inside a cylinder of specially selected old (i.e. low radioactivity) lead. The gas pressure in the counter is read from a Wallace and Tiernan manometer type 62–075. The temperature is measured with a calibrated NTC sensor in a bridge circuit.

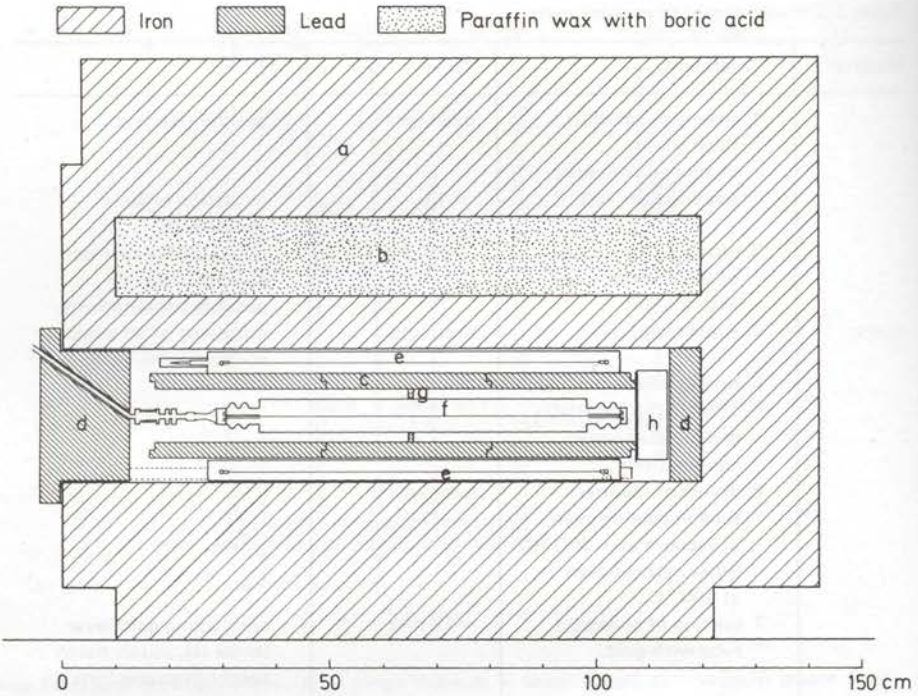

Fig. 3.5. a. Arrangement of the new counter GRADA (no. 6) and shielding. a – iron shield, b – paraffin with boric acid, c – segmented 'old' lead cylinder, d – lead endpieces, e – Geiger ring counter, f – proportional counter, g – perspex counter support, h – high voltage *RC* filter and preamplifier.

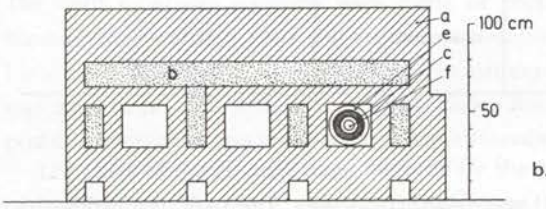

b. Cross-section of iron shield with the new counter.

The *electronic circuitry* is of a modified standard type for low level counting (fig. 3.6). Three discriminator-univibrator units (D–2 to D–4) are used to give block pulses of a chosen length and a fixed height for counter pulses exceeding the discriminator levels. D–2 determines the size of the smallest counter pulses that are detected. The level is sufficiently high to cut out the electronic noise. Virtually all ^{14}C pulses fall below the level of D–3. These two levels define the ^{14}C β channel. D–3 also sets the lower level of the α channel. Electromagnetic noise pulses picked

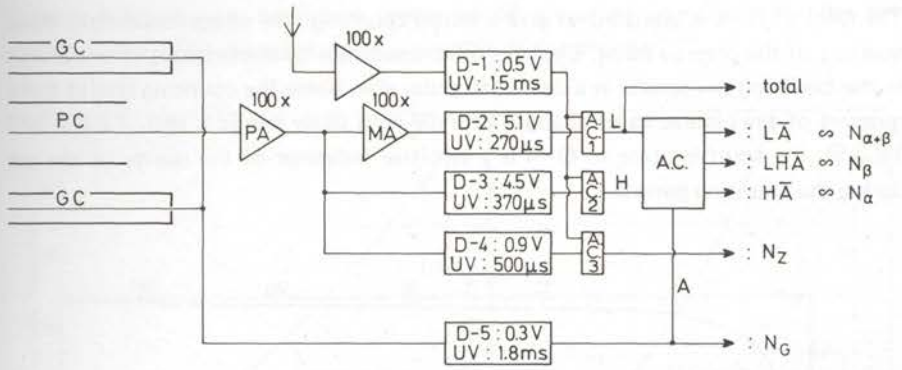

Fig. 3.6 Block diagram of the electronic system of the new proportional counter GRADA. PC – proportional counter, GC – Geiger ring counter, PA – preamplifier, MA – main amplifier, D – discriminator, UV – univibrator, AC – anti-coincidence circuit.

up by an antenna are fed to D–1 and used to block coincident counter pulses in 3 anti-coincidence circuits AC 2, 3 and 4. The pulses from AC 2–4 are counted directly (AC 2 and 4) and led to an anti-coincidence circuit (AC 2 and 3). The pulses produced in the Geiger ring counter are fed directly to discriminator-univibrator unit D–5. The resulting block pulses are counted directly and also fed to the anti-coincidence circuit. The timing of the block pulses of D 1–5 is shown in fig. 3.7.

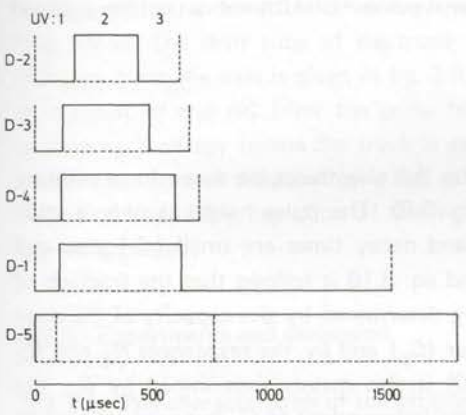

Fig. 3.7. Timing of the univibrator pulses D1–5. D–1: pick-up, D–2: lower discriminator level β channel, D–3: α-discriminator = upper level β channel, D–4: 'purity' channel, D–5: Geiger.

The discriminator-univibrator units each contain 3 univibrators (Groeneveld, 1977). The timing of the individual univibrators is adjusted such that the pulse to be blocked falls entirely within the period of the second blocking univibrator.

The level of D–4 is adjusted to give a muon counting rate of approximately three quarters of the plateau value. Electron attachment due to electronegative impurities in the counting gas results in a decreased pulse size. Since the counting rate at three quarters of the plateau value changes strongly with pulse size (c.f. sect. 3.2.3.1. and 3.2.3.5), the counting rate of D–4 is a sensitive indicator of the purity of the gas during the counting period.

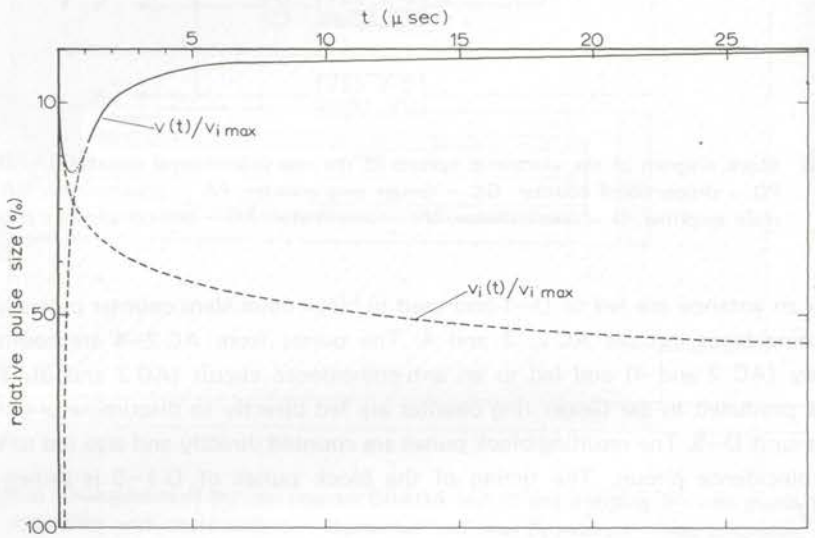

Fig. 3.8. Calculated pulse shape of the proportional counter GRADA without ($v_i(t)/v_{i\,max}$) and with RC filter ($v(t)/v_{i\,max}$).

Eq. 3.17 and 3.18 and the constants in fig. 3.2 give the pulse shape for a primary ionization concentrated in one point (fig. 3.8). The pulse height is only a small fraction of $v_{i\,max}$ ($\approx 23\%$) but the rise and decay times are small (< 1 μsec and ≈ 10 μsec respectively). From fig. 3.2 and eq. 3.18 it follows that the fraction of $v_{i\,max}$ obtained at the amplifier is mainly determined by the capacity of the coax cable from the counter to the preamplifier (C_p) and by the resistances R_3 and R_4 of the preamplifier. Since $v_{i\,max}(= -e/C)$ is also mainly determined by C_p, the absolute pulse size for small RC is virtually independent of C_p but proportional to R. For larger values of RC, $v(t)$ approaches $v_i(t)$.

Since a short pulse is desired we minimize C_p and choose R_3 and R_4 sufficiently large to include the rapid initial rise of $v_i(t)$ in our pulse but on the other hand small enough to obtain a rapid decay of the pulse and to match the emitter follower

output resistance to the input resistance of the amplifier. Obviously the pre-amplifier should be placed as close as possible to the counter.

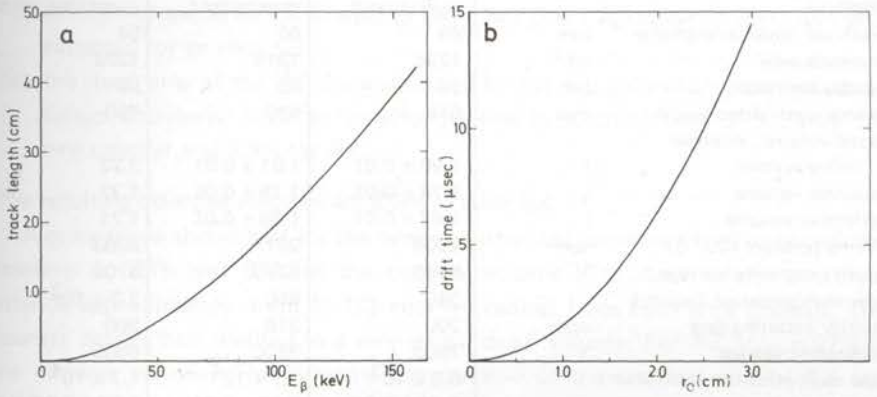

Fig. 3.9. a. Track length of ^{14}C β radiation as a function of the β energy in CO_2 gas at 2917 torr pressure, 20 °C.
b. Electron drift time as a function of the distance r_0 from the counter axis (operating conditions: 2917 torr CO_2 at 20 °C, 7800 V, wire radius 25 μm, counter radius 30 mm).

In order to estimate quantitatively the influence of the *RC* filter on the height of the ^{14}C β pulses for the case of primary ionization along a track of finite length, the average track length of β rays in CO_2 gas of 2917 torr, 20°C (actual operating conditions) as a function of energy was calculated (Katz and Penfold, 1952) (fig. 3.9.a). The drift time of electrons to the wire as a function of their original distance from the axis is given in fig. 3.9.b. From figs. 3.8 and 3.9 it is evident that as a result of the *RC* filter the pulse height will increase less than linearly with increasing β energy unless the track is exactly parallel to the wire. Also the probability that part of the β energy is lost to the counter wall increases with energy. As a result an apparent depletion of the high energy part of the β energy distribution can be expected.

3.2.3. Experiments and discussion

3.2.3.1. The characteristics of the proportional counters

The characteristics of the new proportional counter and its predecessor I (which disintegrated explosively) are given in table 3.4. For comparison also the characteristics are given of the Groningen counter RZ (= no. 2), which has been in routine operation since 1963 (Vogel and Waterbolk, 1967).

Table 3.4. Description of the proportional counters.

Counter		I (6A)	GRADA (6)*	RZ (2)
material		quartz/gold	quartz/gold	quartz/tin oxide
cathode, internal diameter	mm	60	60	54
cathode area	cm^2	1206	1215	1272
anode diameter	μm	50	50	50
anode unshielded length	mm	615	620	750
total volume, inclusive filling system	l	1.90 ± 0.01	1.91 ± 0.01	2.22
counter volume	l	1.74 ± 0.01	1.75 ± 0.01	1.77
effective volume	l	1.67 ± 0.01	1.69 ± 0.01	1.71
filling pressure (20 °C)	torr	2906	2917	2063
purity counting voltage	V	6450	6750	5700
gas multiplication (purity)		340	860	2.2×10^3
purity counting rate	cpm	200	216	200
operating voltage	V	7500	7800	6300
gas multiplication (operation)		6.5×10^3	1.7×10^4	1.7×10^4
background counting rate B	cpm	2.49 ± 0.01	2.63 ± 0.01	1.80 ± 0.01
slope of background plateau	%/100 V	1.4 ± 0.1	1.92 ± 0.05	5.5
variation B with atmospheric pressure	cpm/cm Hg	−0.087 ± 0.031	−0.079 ± 0.024	−0.055
	%/cm Hg	−3.5 ± 1.2	−3.0 ± 0.9	−3.1
variation B with filling pressure	‰/torr	≈ 0.2		
net recent sample counting rate A_0	cpm	42.36 ± 0.06	43.09 ± 0.04	30.81 ± 0.03
slope of ^{14}C plateau	%/100 V	0.40 ± 0.01	0.51 ± 0.02	1.3
muon channel counting rate N_μ	cpm	260.8 ± 0.3	269.4 ± 0.3	290
slope of muon plateau	‰/100 V	3.9 ± 0.3	3.1 ± 0.5	3.9 ± 0.9
maximum increase muon counting rate	cpm/V	0.691 ± 0.009	0.709 ± 0.009	0.943 ± 0.053
variation N_μ with atmospheric pressure	%/cm Hg	−2.15 ± 0.24	−1.61 ± 0.12	
variation operating voltage with filling pressure $(dV/dp)_\mu$	V/torr	1.39 ± 0.06	1.52 ± 0.07	
$(dV/dp)_\beta$	V/torr	1.56 ± 0.06	1.60 ± 0.07	
figure of merit, $A_0/\sqrt{B}$		26.8	26.6	23.0
range in a 2 days counting period	years	52 700	52 600	51 400

* presently 30 cm of iron and 20 cm of paraffin have been added to the counter shield and about 20 cm of concrete and soil to the roof above; this resulted in a background of 2.30 ± 0.04 cpm, a muon channel counting rate of about 250 cpm, a purity counting rate of ≈ 200 cpm and a figure of merit of 28

Using the measured standard counting rate A_0 (95% of the activity of CO_2 from NBS oxalid acid) and the specific disintegration rate (13.56 ± 0.07 dpm/g C in 1950 AD, Karlén et al., 1964) the *effective volume* can be calculated, considering that

(i) the decay since 1950 gives at present (1976) a specific disintegration rate of 13.52 ± 0.07 dpm/g C;

(ii) the Van der Waals interaction between the CO_2 molecules at 20 °C causes the amount of gas to be 1.7% larger at 2917 torr and 1.2% larger at 2063 torr than expected for an ideal gas;

(iii) the dead time of the ^{14}C channel caused by the anti-coincident blocking of the Geiger counter(s) leads to an effective loss in counting time of 3.2% for the new counter and 2.8% for RZ.

The resulting effective volumes are given in table 3.4.

A comparison shows that for the newly constructed counters the effective volume amounts to 96% and 97% of the counter volume. The dead volume therefore extends approximately 1 cm ($\sim$1/3 counter radius) from both ends inwards. The counter design thus resulted in a very small 'dead' volume. For RZ V_{eff} is 97% of the counter volume. The different construction of the counter ends in RZ and GRADA resulted in the same ratio $V_{eff}/V_{counter}$.

The *filling pressure* was limited by the calibrated range of the manometer (2950 torr).

The *operating voltage* was chosen such as to minimize the variation with voltage of the β^- and the background counting rate. In order to determine this voltage the counting rate in a narrow channel defined by two discriminator levels, apart by a factor $\sqrt{2}$, in anti-coincidence, was measured as a function of the voltage applied to the counter for a sample of CO_2 from oxalic-acid and for a background sample (fig. 3.10). The channel corresponds with an increase of $\approx$ 130 V in counter voltage. The use of the channel (Vogel, personal communication) enables a sensitive and fast determination of the increase in counting rate with increasing voltage in and near the plateau region. The plateau region deduced from these measurements (7.6–8.1 kV) is smaller than that estimated from the change in the integral anti-coincidence counting rate (7.3–8.2 kV). The voltage dependence of $N_{\alpha+\beta}$ and of the background counting rate B as deduced from these channel measurements is accordingly smaller.

3.2.3.2. Gas multiplication and energy calibration

For the new counters we determined the gas multiplication factor M as a function of the voltage applied to the counter and the filling pressure, using a method developed by Groeneveld (1977). In this method the cosmic ray muons are used to obtain M *indirectly*. M is determined from a series of measurements of the muon counting rate as a function of the counter voltage V (c.f. fig. 3.10.a) for different filling pressures p and discriminator levels D. This is done by comparing the voltages for which a certain counting rate N is obtained. A detailed discussion of this

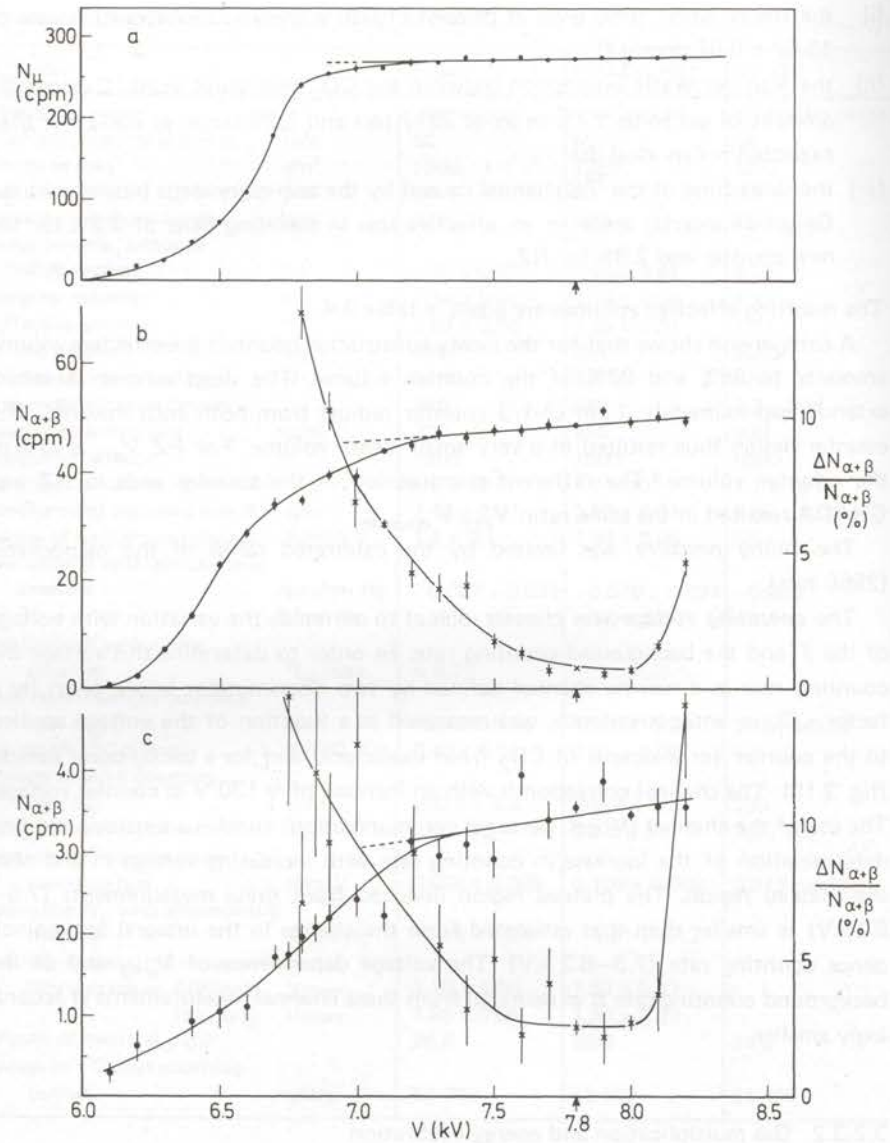

Fig. 3.10. Counting rate as a function of the voltage applied to counter GRADA, 2917 torr CO_2, 20 °C.
a — coincidence channel counting rate; b — total anti-coincidence counting rate (†) and its fractional increase in a 130 V channel (*) for an oxalic acid CO_2 sample; c — total anti-coincidence counting rate (†) and its fractional increase in a 130 V channel (*) for a background sample; ↑ operating voltage chosen.

procedure and of the results will be published elsewhere (Groeneveld and Grootes, 1977).

The pressures and discriminator levels used for counter I and counter GRADA differed by a factor $\sqrt{2}$. For counter I 6 pressures (520 to 2945 torr) and 4 discriminator levels of D–2 (1.8 to 5.0 V) were used. For counter GRADA we used 5 pressures (728 to 2919 torr) and 5 discriminator levels (1.3 to 5.1 V). M was determined for each of the measurements and $(\ln M)/aE_a$ was plotted as a function of E_a/p (fig. 3.11). The points obtained for the different counters lie on one line. This is to be expected for counters using the same gas. It indicates that the two series have not seriously been influenced by impurities of the counter gas or the difference in electronic amplification (c.f. table 3.5). In fig. 3.11 the function $f(E_a/p)=(\ln M)/aE_a = c_1+c_2(E_a/p)^{-1}+c_3 \ln(E_a/p)$ (c.f. eq. 3.14) has been fitted to the experimental points. Over the entire experimental range the best fit was obtained by

$$(\ln M)/aE_a = -0.108 + 1.298(E_a/p)^{-1} + 0.0216 \ln(E_a/p). \qquad (3.19)$$

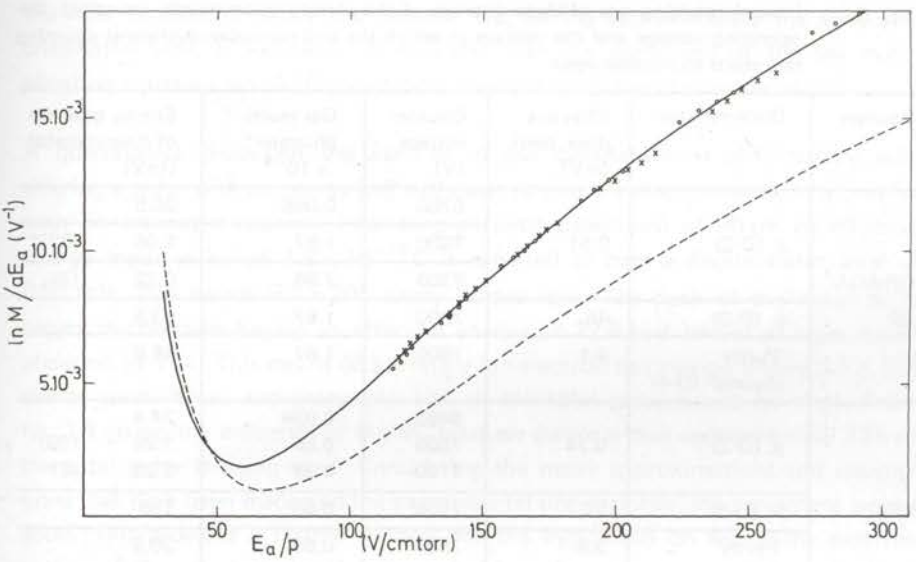

Fig. 3.11. $(\ln M)/aE_a$ as a function of E_a/p (Zastawny plot). — least squares fit of $f(E_a/p) = c_1 + c_2(E_a/p)^{-1}+c_3 \ln E_a/p$ to the experimental data of counter I (o) and counter GRADA (x); - - - - - calculated from measurements of Zastawny (1966).

The gas multiplication curve for CO_2 obtained by Zastawny (1966) has been drawn in the same figure for comparison. This curve turns out to be consistently lower. From the behaviour of the function given by eq. 3.19 at low E_a/p values it is

obvious that eq. 3.19 is only an approximation useful for the E_a/p range considered. In our region of interest, however, it gives sufficiently accurate results to be used to calculate the influence of pressure, counter voltage and counter and wire radius on the pulse height.

The discriminator levels of the β, α and 'purity' channel (*D–2,3* and *4* respectively) were determined experimentally on basis of the electronic noise level and the counting rates. To relate discriminator levels to beta energies, the number of primary ion-electron pairs necessary to produce a pulse just passing the discriminator must be found.
Ethane enriched in tritium was used as an internal source giving a primary ionization virtually concentrated in a point. In this case the pulse height distribution corresponds with the beta energy distribution. From the known energy spectrum of ^3H and eq. 3.19 an energy calibration of the discriminator levels was obtained. The results are given in table 3.5.

Table 3.5. Discriminator levels of the various counters at the voltage giving a coincidence (muon) counting rate of three quarters of the plateau value (purity counting), the operating voltage and the voltage at which the anti-coincidence channel counting rate starts to increase again.

Counter	Discriminator	Effective discr. level (mV)	Counter voltage (V)	Gas multiplication* $\times 10^{-4}$	Energy position of discriminator (keV)	
GRADA (6)	β (D-2)	0.51	6750	0.086	20.5	
			7800	1.67	1.06	(32)**
			8300	7.96	0.22	(7)
	α (D-3)	45	7800	1.67	93.5	
	'Purity channel' (D-4)	9.1	7800	1.67	18.9	
I (6A)	β (D-2)	0.24	6450	0.034	24.4	
			7500	0.65	1.28	(39)
			8100	4.34	0.26	(8)
	α (D-3)	25	7500	0.65	133	
	'Purity channel' (D-4)	3.9	7500	0.65	20.8	
RZ (2)	β	0.50	5700	0.22		
			6300	1.71		

* calculated using the counter specifications given in table 3.4, the gas multiplication equation for the individual counters I (6A) and GRADA (6) separately and the combined result, eq. 3.19, for counter RZ (2)

** equivalent number of primary ion-electron pairs

The discriminator settings used for measuring the purity of the sample at three quarters of the plateau muon counting rate are slightly below the energy of the peak of the effective muon energy loss distribution (22.8 ± 0.3 keV). This gives a strong dependence of the counting rate on electronegative impurities. The term effective energy is used to indicate the energy of a point ionization source yielding the same pulse height. For ionizations with non-negligible track length the actual energy is higher (c.f. fig. 3.8 and 3.9).

An α discriminator level passing approximately 0.5% of the β pulses seems reasonable, especially if the high energy depletion of the distribution is taken into account.

An increase in counting rate in the anti-coincidence channel can be expected when single electron pulses pass the discriminator level. From the observed values of 8300 V and 8100 V for the onset of anti-coincidence counting increase in GRADA and I respectively, we calculate an average value of about 7 primary ion-electron pairs for a pulse just passing the discriminator. This value does not seem unreasonable.

The agreement of the gas multiplication factor under operating conditions for the new counter GRADA and counter RZ, having approximately the same discriminator level, is excellent. It indicates that the usefulness of the gas multiplication equation (eq. 3.19) extends to counters of different construction.

A quantitative check on the validity of our calculations is obtained by considering a pulse with an energy just sufficient to pass the discriminator. In a counter with an estimated capacity (including parasitic capacities) of 30 pF an effective charge input pulse of 1.5×10^{-14}C is required to pass a discriminator level of 0.51 mV. This means 9.5×10^4 singly loaded ions. The peak of the muon pulse height distribution having an effective energy of 22.8 keV passed at a gas multiplication of 774. This means 693 primary ion-electron pairs giving finally 5.4×10^5 charge pairs. Thus, approximately 18% of the total pulse has to be used. From fig. 3.8 giving the influence of the *RC* filter we estimate that approximately 23% of the total pulse is being used. Considering the many approximations and assumptions that have been made and the experimental uncertainties, the agreement is very good. This provides a further support for the hypothesis on which the determination of the gas multiplication factor has been based and for the veracity of the energy calculations.

3.2.3.3. Effect of filling pressure on counter performance

From a series of measurements at different filling pressures we can estimate the various counting rate components. The counting rate depends on the counter voltage, even in the plateau region. It is therefore necessary to determine the

equivalent operating voltages at different pressures. The gas multiplication in each case is calculated from eq. 3.19.

The coincidence (muon) and the anti-coincidence (background) counting rates as a function of voltage were measured for counter I at 7 different filling pressures from 99 to 2843 torr. To compare the results the voltage required to obtain a coincidence channel counting rate of 200 cpm was read from the experimental results and calculated from eq. 3.19 for the different pressures used. Here it was assumed that the primary muon ionization is proportional to the filling pressure. The results are given in fig. 3.12. The correspondence between experiment and the results of eq. 3.19 supports the usefulness of eq. 3.19 for calculating operating voltages. The increasing difference at low pressures probably reflects the increasing loss in pulse size due to wall effects and electron drift time.

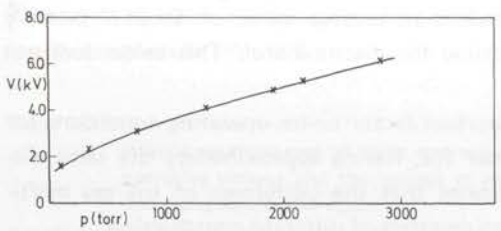

Fig. 3.12. Voltage for which the coincidence channel counting rate of counter I equals 200 cpm as a function of the filling pressure, calculated using eq. 3.19; x – experimental values.

The corresponding operating voltages on the plateau can now be calculated for the different pressures from eq. 3.19 and the consistent voltage differences observed (fig. 3.12). The relation between the coincidence (muon), the anti-coincidence (background) channel counting rate and the filling pressure is found from the experiments by reading the plateau counting rate at the calculated operating voltage. The results are given in fig. 3.13.a,b.

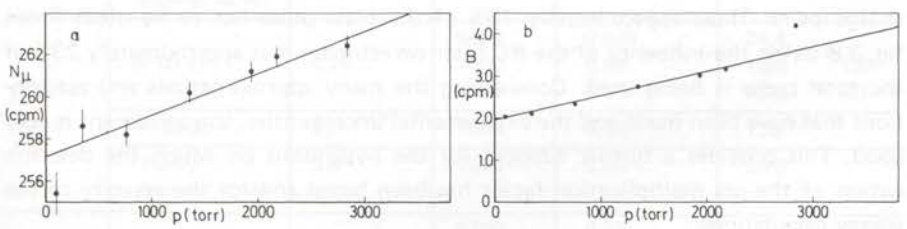

Fig. 3.13. Coincidence channel (muon) (a) and background (b) counting rate as a function of the CO_2 filling pressure for counter I.

The pressure dependence for the *coincidence (muon) channel* is

$$dN/dp = (2.0 \pm 0.3) \times 10^{-3} \text{ (cpm/torr)}$$
$$= (7.7 \pm 1.2) \times 10^{-3} \text{ (}^{0}/_{00}\text{/torr)} .$$

The coincidence channel counting rate thus is practically independent of the filling pressure. This means either that the passing muon on the average undergoes several interactions with the counter gas even at low pressures (100 torr), so that the probability of no interaction is small, or that interactions in the counter wall contribute to the primary ionization in the gas. Two additional measurements at 50 and 25 torr did not show a marked decrease of the coincidence channel counting rate, although a decrease of 13% and 37% respectively was expected from the observed decrease of 2% from 2840 to 100 torr if only muon interaction in the gas produced the muon pulses. Therefore we have to conclude that interactions in the counter wall contribute to the primary ionization. Since good results were obtained with the assumption that the primary muon ionization is proportional to the filling pressure (c.f. fig. 3.12), this means that at higher pressures the primary ionization in the counter gas due to muon interactions in the wall is small compared with that due to interactions in the gas itself. At very low pressures, however, the walls give an important contribution.

The *anti-coincidence (= background) channel counting rate* for a CO_2 filling with presumably no ^{14}C activity was determined as a function of filling pressure, assuming the energy distribution of the background pulses to be proportional to the filling pressure. This assumption applies to a possible direct contribution to the background counting rate by muons and nucleons, that escaped detection by the Geiger ring and to the contribution by neutrons and γ radiation. The result is given in fig. 3.13.b. The value at 2843 torr deviates significantly from a straight line determined by a least squares fit and causes a large χ^2 (67 for 7 points). Discarding the 2843 torr point gives for the pressure dependence

$$dB/dp = (0.58 \pm 0.03) \times 10^{-3} \text{ (cpm/torr)},$$

$$B_{p=0} = 1.94 \pm 0.05 \text{ (cpm)}.$$

At 2900 torr we find $B = 3.64$ cpm and accordingly

$$dB/dp = (0.16 \pm 0.01)(^{0}/_{00}\text{/torr}).$$

The χ^2 of the new least squares fit was 5.7 giving a probability $P \approx 0.22$ for obtaining $\chi^2 \geqslant 5.7$. The anti-coincidence (background) channel counting rate varied with a

factor two over the pressure range considered. Interactions in the gas obviously give an important contribution. When decreasing the pressure, the operating voltage was adjusted so as to produce a constant pulse height while the primary ionization decreased. By this procedure the pressure dependence might be slightly underestimated, because some pulses of which the size is independent of the gas pressure increase in size with the increasing multiplication. The above results give only a qualitative indication of the behaviour of the background counting rate since at a later stage the background counting rate was reduced from ≈ 3.6 cpm to ≈ 2.5 cpm (c.f. table 3.4). The observed dependence of B on the filling pressure is of the same order of magnitude as reported by Barendsen (1955) (10%/atm for his counter II).

The calculated operating voltages as a function of pressure for the present counters correspond well with the experimental results of Barendsen, obtained for his counter with a uranium γ source. In analogy to his work we calculate for:

$$\text{Counter I} \quad : V = 7.09\ (p\,a + 4.24\ \text{n}) \ln(b/a); \tag{3.20.a}$$

$$\text{Counter GRADA}: V = 7.19\ (p\,a + 4.06\ \text{n}) \ln(b/a); \tag{3.20.b}$$

$$\text{Barendsen (1955)}: V = 7.54\ (p\,r_i + 4.4\ \text{n}) \ln(r_u/r_i).$$

Here $b(=r_u)$ and $a(=r_i)$ are the inner counter and the wire radius respectively, both expressed in microns, p is the filling pressure in atmospheres and n is a fixed number of free paths over which gas multiplication occurs. The difference in the second term is at least partly attributable to a difference in effective discriminator setting. The correspondence therefore is very good. This indicates that eq. 3.19, which was obtained for our two counters, has a more general applicability.

The *anti-coincidence counting rate of an active sample* (8 times the standard ^{14}C activity) was measured as a function of the operating voltage for filling pressures of 2180, 1936 and 760 torr. The ^{14}C pulse height distribution was assumed to be independent of filling pressure. Corresponding operating voltages were calculated as before. From these voltages the ^{14}C counting rates (N_β) at the different pressures were found after subtraction of the background. A least squares fit of a straight line gave

$$N_\beta = (0.1153 \pm 0.0003)p - (2.66 \pm 0.41)\,(\text{cpm}).$$

Since N_β must be zero for $p = 0$ the negative value of N_β for $p = 0$ indicates a more than linear increase of the ^{14}C counting rate with pressure. This can be caused (i) by the non-ideal character of the gas and (ii) by a decrease in the ionization track length with increasing pressure. Using the Van der Waals equation of state it appears

that the amount of gas in the counter had been underestimated by 1.27%, 1.13% and 0.44% respectively. Applying the Van der Waals correction we obtain

$$N'_\beta = (0.1135 \pm 0.0003)p - (1.65 \pm 0.33)\ (\text{cpm}).$$

Although N'_β is closer to zero for p=0 and the decrease in σ indicates a better linearity, the significantly negative value of N'_β for p=0 may indicate the influence of the variation of the ^{14}C β ionization track length with filling pressure on the counting rate for the pressure range considered.

3.2.3.4. Background

A low and stable background counting rate is essential for determining the low residual radiocarbon activities of samples older than 30 000 years. The optimum construction of the counter shielding depends on the nature of the background radiation. Therefore it is important to consider the different factors that constitute the total background counting rate.

Possible components of the total background counting rate are given in table 3.6. The intensities of the cosmic muons and nucleons depend on the atmospheric pressure. Since the variations of these two components with atmospheric

Table 3.6. The background components and the atmospheric pressure dependences.

Source of radiation		dB/db
Cosmic muons: (CM)		
direct ('leak' in anti-coincidence ring)	B_μ	
neutrons produced in shield by muons	$B_{\mu n}$	−2.3%/cm Hg[a]
γ radiation produced in shield by muons	$B_{\mu\gamma}$	
Cosmic protons: (CP)		
direct ('leak')	B_p	
protons produced in shield by protons	B_{pp}	
neutrons produced in shield by protons	B_{pn}	
γ radiation produced in shield by protons	$B_{p\gamma}$	
Cosmic neutrons: (CN)		−9.6%/cm Hg[b]
direct	B_n	
protons produced in inner shield by neutrons	B_{np}	
neutrons produced in shield by neutrons	B_{nn}	
γ radiation produced in shield by neutrons	$B_{n\gamma}$	
Radioactive contamination of the counter and its immediate surroundings	B_c	
Electronic imperfections like pick-up and instabilities	B_e	0%/cm Hg

a Wada (1962); high latitude value
b Mathews (1959)

pressure are different, the dependence of B on this pressure can be used to distinguish different background components.

The analysis of the background comprizes the following:

(i) The variation of the Geiger Müller counting rate and that of the coincidences in GM and proportional counter with atmospheric pressure. From this the relative contributions of muons and protons to the flux of ionizing radiation inside the shield are estimated and accordingly also their relative *direct* contribution to the background counting rate B.

(ii) The variation of B with atmospheric pressure and with coincidence (muon) counting rate. This indicates the relative contribution to B of nucleons and muons, both *direct and through secondaries* produced in the shield (see table 3.6).

(iii) An estimate of the muon and proton flux after different amounts of shielding and of their relative contribution to neutron production at this position. This verifies the measurements of (i) and (ii).

(iv) The change of B as a result of 30 cm of iron and 20 cm of paraffin placed on top of the existing shield.

We shall now discuss points (i) to (iv) in some detail.

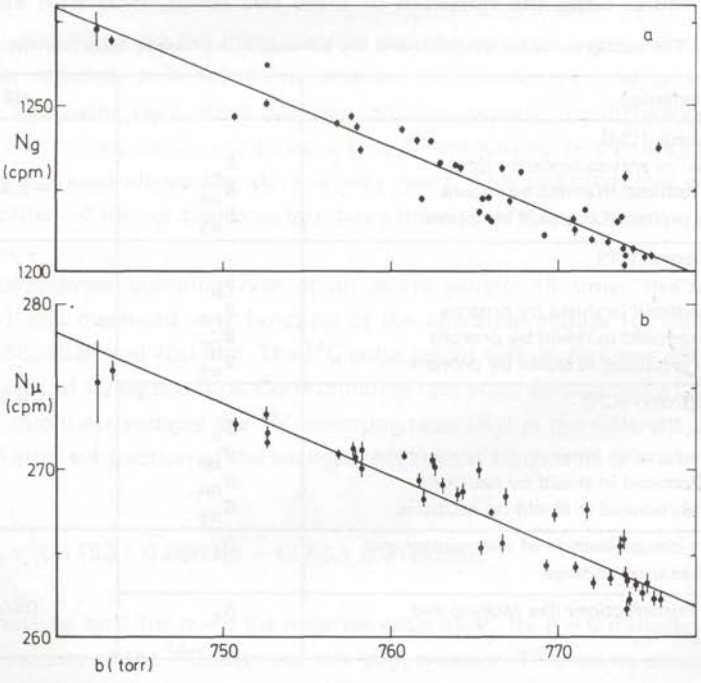

Fig. 3.14. Geiger (a) and coincidence channel (muon) (b) counting rate as a function of the atmospheric pressure for the period 19/1–10/3/'76.

(i) The measured atmospheric pressure dependences of the GM and the coincidence channel (CC) counting rate are shown for a number of periods in fig. 3.14.a and b and table 3.7. It is obvious from the pressure dependence that the direct proton contribution (−9.6%/cm Hg) to the counting rate within the shield is small. Actually, the experimental slopes are even below the value quoted for muons at high latitude. The direct neutron flux is still unknown because of the low detection efficiency for neutrons of the GM and proportional counters. Since fast neutrons and protons in the cosmic radiation are approximately in exchange equilibrium at sea level and their attenuation lengths are of the same order of magnitude, we conclude from the absence of a measurable direct proton flux that also the direct cosmic neutron flux is negligible.

The counting rate–pressure relations were taken from data collected during relatively short periods in order to minimize the influence of aging of the Geiger counter filling and of seasonal variations in cosmic ray intensity.

The results for different periods show a considerable variation. Furthermore, Poisson statistics would predict relative standard deviations for the GM and the CC counting rate of $0.8\,{}^{0}/_{00}$ and $1.9\,{}^{0}/_{00}$ respectively, for a one day counting period. The observed values, however, were $5.0\,{}^{0}/_{00}$ and $5.5\,{}^{0}/_{00}$ respectively. The relation between the CC and the GM counting rates (fig. 3.15) was found to be within Poisson statistics. Therefore the large standard deviations of the data in table 3.7 must be caused by fluctuations in cosmic ray intensity, apart from variations due to the atmospheric pressure.

The variations in primary cosmic radiation generally are of the order of a few tenths of a percent or less (Regener, 1962; Bagge and Binder, 1962). The possibility of incidental large fluctuations (a factor 27 in the neutron producing component), however, cannot be excluded (De Vries, 1956a).

As was mentioned before (table 3.6), the atmospheric influence is different for the nucleonic and the (μ) mesonic component of the cosmic radiation. The first (−9.6%/cm Hg) is determined by mass absorption alone, the latter varies with the height of production in the atmosphere because of the decay of the muon and with the density of the atmosphere in the production region and along the track (Duperier, 1949; Trefall, 1955; Mathews, 1959). The difference between the actual and the Poisson standard deviations in table 3.7 indicates, that the use of only an atmospheric pressure correction leaves a non-Poisson standard deviation of approximately 0.5%, ascribed to variations in primary cosmic radiation and the existence of other atmospheric influences as discussed above. The differences in the atmospheric pressure dependence for the different periods can be attributed to the same cause (c.f. Duperier, 1949, p. 692).

Obviously the CC counting rate is a better indication for the atmospheric and cosmic influence on the number of ionizing events caused by muons than the atmospheric pressure b. If nucleons dominate b is to be considered.

Table 3.7. Variation of Geiger (GM) and coincidence channel (CC) counting rate with atmospheric pressure (b).

	Period	N_{GM}[a]	dN_{GM}/db (%/cm Hg)	N_{CC}[a]	dN_{CC}/db (%/cm Hg)
counter 6A – I	3/12/'74 – 13/1/'75	1211.5 ± 1.2 (0.3)*	−2.00 ± 0.15 (0.04)*		
	10/ 2/'75 – 27/3/'75	1209.7 ± 0.9 (0.2)	−1.57 ± 0.08 (0.02)		
	2/ 4/'75 – 13/5/'75	1204.0 ± 1.7 (0.2)	−2.03 ± 0.23 (0.03)		
	15/ 5/'75 – 20/6/'75	1218.0 ± 1.4 (0.2)	−2.02 ± 0.23 (0.04)	260.8 ± 0.3 (0.1)*	−2.15 ± 0.24 (0.08)*
counter 6 GRADA	3/12/'75 – 12/1/'76	1239.7 ± 1.9 (0.2)	−1.59 ± 0.42 (0.02)	268.8 ± 0.71 (0.15)	−1.83 ± 0.37 (0.08)
	19/ 1/'76 – 10/3/'76	1236.8 ± 1.2 (0.2)	−1.64 ± 0.11 (0.04)	269.5 ± 0.27 (0.09)	−1.61 ± 0.12 (0.04)
	11/ 3/'76 – 29/3/'76	1237.6 ± 1.6 (0.3)	−2.00 ± 0.24 (0.04)	269.8 ± 0.39 (0.13)	−2.30 ± 0.25 (0.08)
	5/ 4/'76 – 6/5/'76	1222.9 ± 1.5 (0.3)	−1.57 ± 0.19 (0.03)	269.3 ± 0.10 (0.13)	−1.57 ± 0.06 (0.08)

* the values in parentheses are the standard deviations due to Poisson counting statistics

a counting rate for standard conditions and atmospheric pressure 760 torr

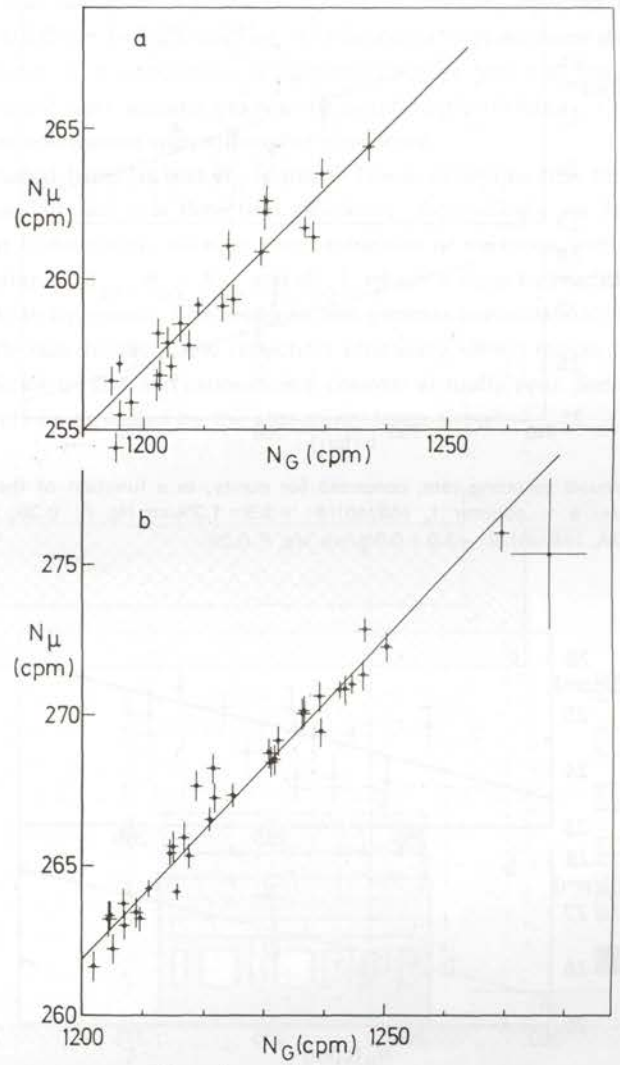

Fig. 3.15. Coincidence channel (muon) counting rate as a function of the Geiger counting rate for: a — the period 13/5–20/6/'75 , counter I; b — the period 19/1–10/3/'76, counter GRADA.

(ii) B is plotted as a function of atmospheric pressure b (fig. 3.16) and as a function of the CC (muon) counting rate (fig. 3.17). The relative muon and nucleon contribution to the background counting rate is obtained from this plot. First, from the relative variation of B with atmospheric pressure b (table 3.6) and the CC counting rate (≈ 1 and ≈ 4 for muons and nucleons respectively). Since the relative variation will be influenced by the presence of a constant contribution B_c and/or

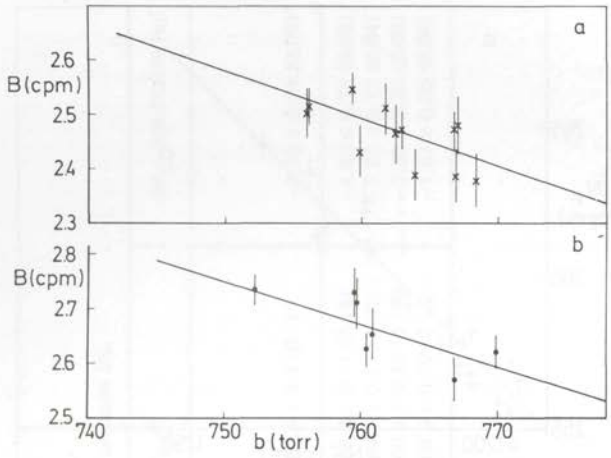

Fig. 3.16. Background counting rate, corrected for purity, as a function of the atmospheric pressure. a — counter I, $(dB/db)/B$: $-3.5 \pm 1.2\%$/cm Hg, P: 0.36; b — counter GRADA, $(dB/db)/B$: $-3.0 \pm 0.9\%$/cm Hg, P: 0.29.

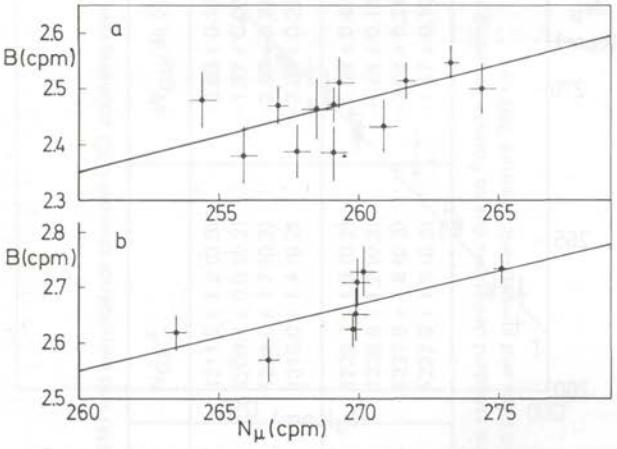

Fig. 3.17. Background counting rate, corrected for purity, as a function of the coincidence channel (muon) counting rate. a — counter I, $(dB/dN_\mu)N_\mu/B$: 1.30 ± 0.49, P: 0.30; b — counter GRADA, $(dB/dN_\mu)N_\mu/B$: 1.24 ± 0.40, P: 0.24.

B_e, also the correlation of B with the variations in b and the CC counting rate is considered. The atmospheric pressure dependences for the two counters are in good agreement with each other and with that for RZ (−3.1%/cm Hg). Also the earlier result of De Vries (1957) (-2.1 ± 0.6%/cm Hg) and the values determined by Nydal et al. (1975) (−2.3 and −2.2%/cm Hg) are of the same magnitude.

Because our values of $(dB/db)/B$ exceed the values expected from a purely muonic contribution (−2.3%/cm Hg), it is probable that *nucleons do contribute to the background*. This conclusion is supported by the fact that the probabilities P for the different least squares fits are not significantly different, although slightly better for the correlation with atmospheric pressure.

We concluded from (i) that B_p is small. The same will be true for B_n due to the low flux (see (i)) and low detection efficiency. Accordingly we have an indirect contribution by nucleons through the production of neutrons and gammas in the shielding material (B_{pn}, $B_{p\gamma}$, B_{nn} and $B_{n\gamma}$), which is done by nucleons much more effectively than by muons. The neutrons and gammas contribute to the background counting rate due to their low detection efficiency which makes cancellation by anti-coincidence of GM and proportional counter virtually zero. Secondary protons will effectively be cancelled by the anti-coincidence circuit.

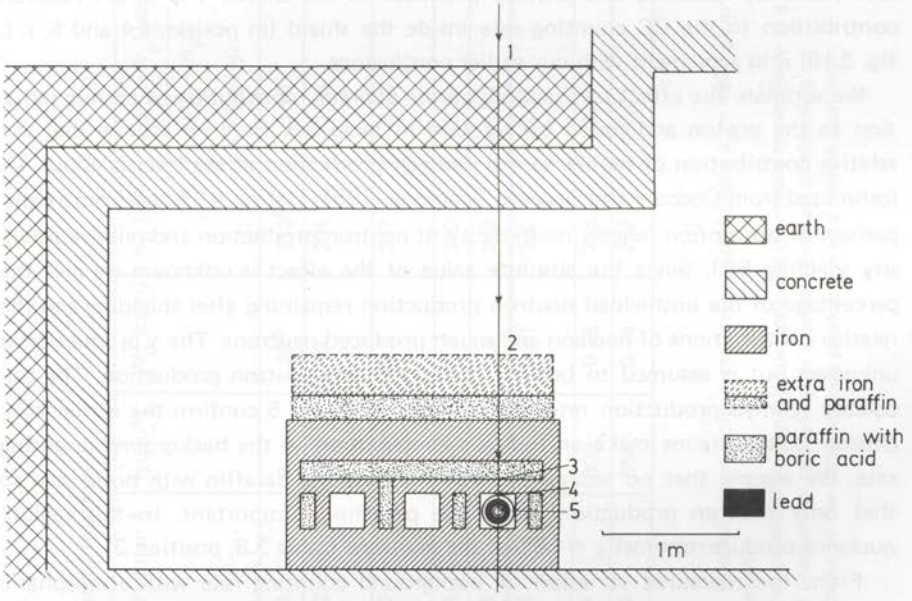

Fig. 3.18. The shielding of the new counting set-up. The numbers indicate the positions for which the effect of the shielding on vertical cosmic radiation is calculated.

(iii) The influence of different elements of the shielding is calculated from $N = N_o \exp(-d\rho/\lambda)$, where N is the fraction of the unshielded value N_o traversing d cm of shielding material with a density ρ g/cm^3 (table 3.8). We use an attenuation length $\lambda_\mu = 4000$ g/cm^2 for muons and $\lambda_N = 160$ g/cm^2 for nucleons at sea level given by Cocconi and Cocconi Tongiorgi (1951) and contributions of the muon and the nucleon component to the cosmic radiation at sea level of 80% and 20%, based

on their intensity values ($I_\mu \approx 1.3 \times 10^{-2} cm^{-2} sec^{-1}$ and $I_N \approx 4 \times 10^{-3} cm^{-2} sec^{-1}$) and on measurements by Meshkovskii and Solokov (1957) (2.4% protons after 15 cm Pb).

From the CC counting rate of our counter we now estimate its muon counting rate N_μ at sea level without shielding to be 312 cpm. The nucleon component is assumed to consist of equal amounts of protons and neutrons. This indicates an unshielded nucleon counting rate N_N of about 40 cpm. The values of N_μ and N_N agree well with the surface of the counter cross section (372 cm^2) and the cosmic ray intensities at sea level.

The *direct nucleon component* of the cosmic radiation is reduced to about 2% by the use of the underground laboratory and the iron shielding. An extra 30 cm of iron with 20 cm of paraffin virtually eliminates this component. An important contribution to the nucleon component of the radiation inside the shield is therefore made by neutrons and protons produced in the shield. The direct nucleon contribution to the CC counting rate inside the shield (in positions 4 and 5, c.f. fig. 3.18) is in agreement with our earlier conclusions.

We estimate the effect of shielding on the *indirect contribution* of cosmic radiation to the proton and muon background in table 3.8. Here we assume that the relative contribution of muons to the neutron production at sea level is about 4% (estimated from Cocconi and Cocconi Tongiorgi (1951) stating $\approx 2\%$ and from a comparison of absorption length, multiplicity of neutron production and relative intensity yielding 5%). Since the absolute value of the effect is unknown we give the percentage of the unshielded neutron production remaining after shielding and the relative contributions of nucleon and muon produced neutrons. The γ production is unknown but is assumed to behave similarly to the neutron production. The calculated relative production rates in positions 3, 4 and 5 confirm the earlier conclusion that nucleons make an indirect contribution to the background counting rate. We assume that no secondary neutrons pass the paraffin with boric acid so that only neutron production below the paraffin is important. In this region, nucleons produce maximally $\approx 58\%$ of the neutrons (table 3.8, position 3).

From the measured variation of background counting rate with atmospheric pressure (-0.087 ± 0.031 and -0.079 ± 0.024 cpm/cm Hg) and the calculated neutron variation ($\leqslant 6.5\%$/cm Hg, table 3.8) we estimate a minimum value of 1.34 ± 0.48 cpm for the cosmic ray contribution to the background counting rate of counter I and 1.22 ± 0.37 cpm for counter GRADA. If muons contribute to the background in any other way, the total cosmic ray contribution to B will be larger.

(iv) If an extra amount of 30 cm of iron and 20 cm of paraffin with boric acid is added on top of the existing shield, the nucleon intensity is reduced by a factor 4.9 and the muon intensity by a factor 1.07 (c.f. table 3.8). The neutron production immediately below the paraffin is expected to decrease with a factor 2.0.

Table 3.8. Effect of different amounts of shielding.

	Position [a]	(g/cm²)	N_p (cpm)	N_μ (cpm)	$\frac{d(N_p + N_\mu)/db}{(N_p + N_\mu)}$ (%/cm Hg)	$\boldsymbol{N}_N$ (%)[c]	$\boldsymbol{N}_\mu$ (%)[c]	f (%)[d]	$\frac{d\boldsymbol{N}/db}{\boldsymbol{N}}$ [e] (%/cm Hg)
sea level, no shielding	1	0	39[b]	312[b]	−3.10	96	4	100	−9.3
40 cm concrete + 80 cm soil above underground laboratory	2	224	10	295	−2.53	86	14	27.5	−8.6
+ 30 cm Fe and 15 cm paraffin with boric acid	3	475	2.0	277	−2.35	58	42	8.4	−6.5
+ 10 cm Fe	4	554	1.2	272	−2.33	46	54	6.4	−5.7
+ 1.5 cm Fe and 3 cm Pb	5	599	0.9	269	−2.32	40	60	5.7	−5.2
+ 60 cm Fe and 35 cm paraffin with boric acid	3	729	0.41	260	−2.31	23	77	4.3	−4.0
+ 10 cm Fe	4	808	0.25	255	−2.31	16	84	3.9	−3.5
+ 1.5 cm Fe and 3 cm Pb	5	853	0.19	252	−2.31	13	87	3.7	−3.2

a see fig. 3.18

b calculated from the coincidence channel counting rate, the attenuation lengths $\lambda_\mu = 4000$ g/cm² and $\lambda_N = 160$ g/cm² (Cocconi and Cocconi Tongiorgi, 1951) and 10% proton intensity

c $\boldsymbol{N}_N$ and $\boldsymbol{N}_\mu$ are the relative neutron production rates by nucleons and by muons respectively at a certain position

d f is the fraction of the unshielded production rate left after a certain amount of shielding

e the atmospheric pressure dependence of the total neutron production at a certain position

However, neutrons are also produced in the side walls of the shield and in the shield below the counter. Here the effective amount of shielding material is larger and the nucleon influence accordingly smaller. The nucleon contribution to the total secondary neutron flux might be of the order of 30%. The additional 30 cm of iron and the paraffin are estimated to reduce the total neutron flux by a factor 1.4.
A further increase of the amount of shielding will be less effective since the muons, which now form the main contribution, have much larger attenuation lengths.

Table 3.9. Influence of 30 cm of iron and 20 cm of paraffin with boric acid on the counting rates.

	old shield	+ 30 cm Fe and 20 cm par.	predicted
Geiger: N_G	1238 ± 1 cpm	1163 ± 1 cpm	1163 cpm
Coincidence: $N_\mu + N$	269.4 ± 0.3 cpm	252.9 ± 0.2 cpm	252.2 cpm
Background: B	2.63 ± 0.01 cpm	2.44 ± 0.02 cpm	

The effect of the extra shielding on the counting rates of Geiger, coincidence and anti-coincidence channel is given in table 3.9. The predicted CC counting rate is given in table 3.8, position 5.
From the cross sectional area of the effective part of the Geiger ring (ϕ 23 cm, length 68 cm, which gives 1564 cm^2) and the calculated values for the proportional counter at position 4 without extra iron, we estimate a Geiger counting rate due to passing nucleons and muons of 1150 cpm. This amounts to about 93% of the total measured counting rate N_G = 1238 ± 1 cpm. The contribution of natural radioactivity in the Geiger counter and its surroundings and of cosmic ray produced neutrons and gammas is about 90 cpm or 7%. In a similar way we calculate for the GM counting rate with the extra iron and paraffin 1073 cpm due to direct cosmic radiation and N_G = 1163 cpm. The agreement between the measured and the calculated values of GM and CC counting rate is good.

From the experiments (i), (ii) and (iv) discussed above we now calculate the contribution of muons, nucleons, radioactive impurities and electronic imperfections to the total background counting rate. From the equations (c.f. table 3.6, 3.8) for the total background,

$$(B_{p\ldots} + B_{n\ldots}) + B_{\mu\ldots} + (B_c + B_e) = 2.63 \pm 0.01, \qquad (3.21.a)$$

the atmospheric pressure dependence,

$$-0.096\,(B_{p\ldots} + B_{n\ldots}) - 0.023\,B_{\mu\ldots} = -0.079 \pm 0.024, \qquad (3.21.b)$$

and the effect of iron and paraffin,

$$0.797(B_{p\ldots}+B_{n\ldots}) + 0.0618\, B_{\mu\ldots} = 0.19 \pm 0.02, \qquad (3.21.c)$$

we derive:

nucleon contribution $(B_{p\ldots}+B_{n\ldots})$	: -0.041 ± 0.119 cpm
muon contribution $(B_{\mu\ldots})$	: $+3.60 \pm 1.63$ cpm
radioactivity and electronics contribution (B_c+B_e)	: -0.93 ± 1.64 cpm.

The range of physically possible solutions is: $0 \leqslant$ nucleon contribution $\leqslant 0.08$ cpm; $1.97 \leqslant$ muon contribution $\leqslant 2.63$ cpm and $0 \leqslant$ radioactivity contribution $\leqslant 0.66$ cpm.

Although no definite value for the different contributions is obtained, the results indicate that the direct and indirect nucleon contribution is small and that the main part of the background counting rate is caused by muons and their secondaries. The background contribution of radioactive impurities and electronic imperfections probably is less than 30%.

From the experiments it is impossible to find the separate contribution of the muon and nucleon component of the cosmic radiation and that of their secondaries. From the measurements of the CC counting rate, however, we concluded that the primary nucleon flux was negligible compared with the muon flux. Therefore the nucleon contribution must be ascribed to secondary nucleons. The muon contribution to the total production of secondary neutrons and gammas was estimated to be about 70%. This gives an indirect muon contribution $B_{\mu n}+B_{\mu\gamma}$ of about 0.2 cpm ($\approx 10\%$). Then the main muon contribution ($\approx 90\%$) is made directly by muons 'escaping' detection by the Geiger anti-coincidence ring. The standard deviation of the muon and nucleon contribution is large. The ratio of the muon and the nucleon contribution to the production of secondaries is only a rough estimate and might be wrong by a factor three. The true values of the direct and indirect muon contribution accordingly remain uncertain and await further experiments.

Measurements by Groeneveld (1977) with a copper counter similar in size and construction to our quartz counter, installed in the neighbouring hole of the shield gave a similar decrease in background counting rate due to the extra 30 cm of iron and the paraffin. The measured atmospheric pressure dependence of this counter is not significantly different from that of our counters.

A direct muon contribution of $\geqslant 1.67$ cpm indicates that 0.62% or more of the muons passing the counter escape detection by the anti-coincidence ring ('leak'). This agrees well with the leak value of $0.50 \pm 0.02\%$ estimated by Barendsen (1955) for a similar Geiger ring counter using a proportional counter with an effective length of 16 cm. Our value is somewhat higher than the value of $0.17 \pm 0.06\%$ calculated by Puite (1965) for the anti-coincidence ring of 34 separate Geiger counters (a complete ring of 24 counters with half a ring on top of this) used for

the routine counters LZ (no. 1) and RZ (no. 2). The effective length of these Geiger counters is 100 cm instead of the 68 cm of the ring counter.

Measurements of De Vries (1956b, 1957) on the background of a counter with similar cross section for cosmic radiation (360 cm^2) and CC counting rate (272 cpm, counter III, Barendsen, 1955) in the same shield yielded a larger decrease in background counting rate upon addition of 30 cm of iron (0.56 cpm). During these experiments the shield was situated at ground level with no additional shielding of concrete or soil. Therefore, the nucleon contribution is higher by at least a factor 3.

We conclude that muons probably make the most important contribution to the background counting rate by direct 'leak' through the anti-coincidence ring. With 70 cm of iron shielding the direct influence of nucleons has virtually disappeared. The addition of more shielding iron or lead will not have much effect because of the large attenuation length for muons. Our conclusion is that the amount of radioactive impurities in properly selected and processed counter materials (quartz and copper) is low. This is in good agreement with the results obtained with counters situated underground (Stuiver et al., 1974; Oeschger and Wahlen, 1975; Vogel, personal communication).

The *background counting rate of counter RZ* (Vogel and Waterbolk, 1967) *and its stability* have been carefully analyzed, since our enriched samples were measured in this counter. Generally the background counting rate was measured each weekend. These measurements are given in fig. 3.19 for the period 11/12/'71–31/7/'76. During this time the background counting rate decreased from $\approx$ 2.21 cpm to $\approx$ 1.77 cpm. This decrease is caused mainly by the decay of a radioactive contamination introduced into the counter on 28/10/1970 when the CO_2 freezing trap was broken during the filling procedure (at that time $B \approx 1.70$ cpm).
The period can be subdivided into 7 periods during which the background seems rather stable. A least squares fit for a straight line has been made for each of these periods. The results are given in fig. 3.19.
The probability values P obtained from the χ^2 (table 3.10) indicate a reasonable agreement between the straight line assumption and the experiments. A comparison of the calculated standard deviations with those expected from counting statistics only indicates that other factors affect the background counting rate. Their contribution to the total standard deviation, however, is generally smaller than that of the counting statistics. This instrumental standard deviation sets a lower limit to the standard deviation that can be obtained by a longer measurement. It seems that for counter RZ a period of 2 to 4 days is the best compromise between standard deviation and measuring time. This of course only applies to the stable periods when all parts of the equipment function properly.

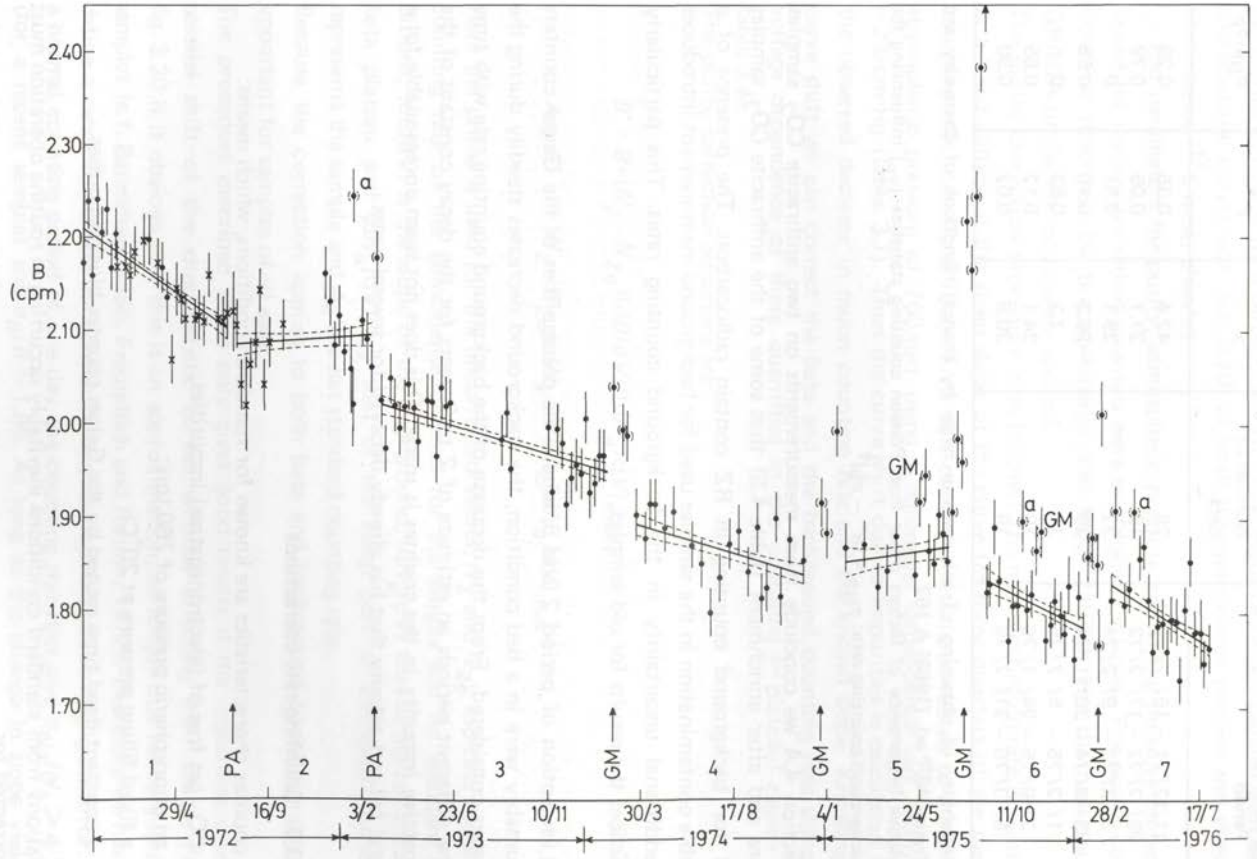

Fig. 3.19. Background counting rate of counter RZ. PA — preamplifier defect, GM — increase in background counting rate caused by a change of the Geiger plateau, a — not considered for least squares fit.

Table 3.10. The background counting rate of RZ; results of the least squares fits for a line $y = ax + b$.

	Period	Number of data	χ^2	P [a]	σ_{NP}/σ_P*
1	11/12/'71 – 15/ 7/'72	28	42.4	0.35	0.29
2	29/ 7/'72 – 17/ 2/'73	19	27.7	0.05	0.79
3	3/ 3/'73 – 9/ 2/'74	32	29.1	0.51	0
4	23/ 3/'74 – 30/11/'74	20	26.3	0.10	0.68
5	1/ 2/'75 – 5/ 7/'75	11	7.2	0.62	0
6	3/ 9/'75 – 24/ 1/'76	19	24.1	0.12	0.65
7	6/ 3/'76 – 31/ 7/'76	19	30.8	0.02	0.90

a probability of obtaining χ^2 this large or larger by chance, Handbook of Chemistry and Physics 49th ed. (1968) A 162

* relative importance of factors other than Poisson counting statistics (σ_P) influencing the background counting rate: $\sigma_{NP} = (\sigma^2 - \sigma_P^2)^{\frac{1}{2}}$

In section 4.4 we conclude from measurements on two anthracite CO_2 samples before and after enrichment (table 4.5) that some of the anthracite CO_2 samples used for background counting in RZ contain radiocarbon. The presence of a variable contamination in the samples used for background measurement introduces an additional uncertainty in the background counting rates. This particularly influences the results for old samples.

With exception of period 2 and 5, where the preamplifier or the Geiger counters presumably were in a bad condition, the background decreases steadily during the $4\frac{1}{2}$ years considered. From the decrease of the background counting rate with time in the different periods an estimate of 2 to 3 years for the decay constant of the radioactive impurity in the counter is made. This does not seem unreasonable for a natural fall-out activity that has already decayed for several years.

3.2.3.5. Counting rate corrections

The counter characteristics are known for standard conditions, which means:

(i) CO_2 gas free of (electronegative) impurities;
(ii) an atmospheric pressure of 760 torr;
(iii) a fixed filling pressure at 20°C;
(iv) a constant dead time caused by the Geiger counter blocking pulses.

Deviations from standard conditions inevitably occurring in routine operation must be corrected for.

The *purity correction* compensates for the influence of electronegative im-

purities in the counting gas (c.f. eq. 3.11). Their effect is essentially equivalent to lowering the operating voltage (a certain decrease in voltage causes a decrease of the gas multiplication M by a certain factor). Thus impurities give a parallel shift of the characteristic curves (c.f. fig. 3.10) of both the coincidence (muon) and the anti-coincidence (^{14}C beta) channel.

The parameters for purity, atmospheric pressure and filling pressure correction in use for the routine dating counters were established by Vogel. The purity correction was described by Brenninkmeijer and Mook (1976). For the new counter GRADA similar corrections are applied.

The purity correction procedure is as follows: The muon counting rate is measured at a fixed voltage at the steep slope of the curve (at three quarters of the plateau counting rate, c.f. fig. 3.10.a). First this counting rate is corrected to a standard atmospheric pressure of 760 torr using a barometer dependence $(dN_\mu/db)/N_\mu = -2\%/\text{cm Hg}$ (table 3.7). Then the curve shift due to impurities is calculated from the observed decrease in muon counting rate and the known slope. Knowing the curve shift we can correct the beta and the background counting rate using the voltage dependence of these quantities in the operating (= plateau) region (c.f. table 3.4).

The purity correction equations are:

$$B' = B + (N_Z - N_{Zo})(dB/dV)/(dN_\mu/dV)_{max}, \qquad (3.22.a)$$

$$A = A' \{1 - (N_Z - N_{Zo})(dN_\beta/dV)/A_o(dN_\mu/dV)_{max}\}. \qquad (3.22b)$$

Here the prime is used for the uncorrected values, N_Z and N_{Zo} indicate the purity counting rate of the coincidence channel for the sample and for standard conditions, (dB/dV) is the slope of the background, (dN_β/dV) that of the net standard beta plateau and $(dN_\mu/dV)_{max}$ that of the steep part of the muon curve, A represents the sample and A_o the net standard counting rate.

Because the correction applies to both beta and background counting rate it is important for samples of all ages.

The procedure described above only gives good results if the impurities cause a parallel shift of the characteristic curves without affecting their shape. From fig. 3.20 it is obvious that this is an approximation, no longer true for very impure samples (c.f. Barendsen, 1955; Freundlich and Rutloh, 1972). Therefore we have to define a range for which the constant slope assumption gives a negligible error. For a normal counting period of one day the counting statistics give $\sigma_{N\beta}/N_\beta \geq 4\ ^0/_{00}$ (for a recent sample) and $\sigma_B/B \approx 1.8\%$. As long as the change in slope yields a relative difference of $< 1\ ^0/_{00}$ resp. $< 4\ ^0/_{00}$, the error introduced by taking a constant slope is 3% or less of the total standard deviation and is therefore negligible.

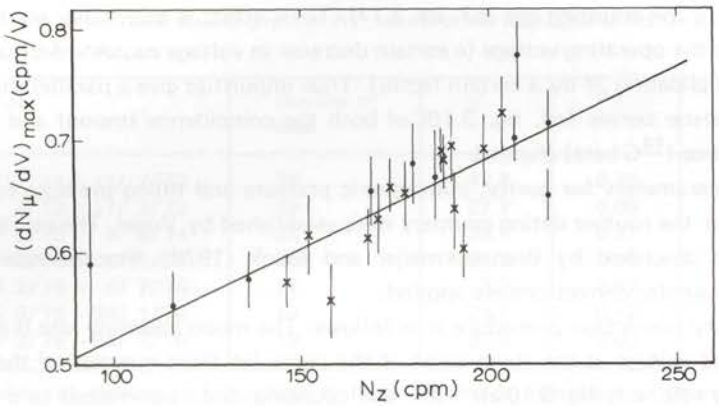

Fig. 3.20. Relation between the maximum slope of the muon characteristic curve $(dN_\mu/dV)_{max}$ and the 'purity counting rate' N_Z; ✱ – counter I, † – counter GRADA.

The maximum increase of the muon counting rate with voltage $(dN_\mu/dV)_{max}$ varies with the purity counting rate as

$$(dN_\mu/dV)_{max} = (1.61 \pm 0.26) \times 10^{-3} N_Z + (0.361 \pm 0.084). \qquad (3.23)$$

The constants for the purity correction for the different counters are summarized in table 3.11. From this table and eq. 3.23 we choose a counting rate of 70% of N_{Z_0} (= 150 cpm for counter GRADA) as the lower limit of applicability of the purity correction. Here the use of the constant slope assumption gives an error of $0.8^0/_{00}$ and $3^0/_{00}$ in N_β and B respectively.

The *atmospheric pressure correction* must be applied to the background counting rate. The components of the background counting rate and their variation with atmospheric pressure were discussed in a previous section. The P value of the least squares fit of the background counting rate as a function of the atmospheric pressure is slightly better than as a function of the muon counting rate. In view of this and to conform to the correction procedure in use at the Groningen laboratory the background was corrected using the barometer reading only. If high accuracy is required, however, also the muon counting rate should be considered.
The atmospheric pressure correction is:

$$B_b = B - (76 - b)\,dB/db, \qquad (3.24)$$

where b is the barometer reading in cm Hg. The constants are given in table 3.11. The correction is important for low activity samples. For recent samples it is usually negligible.

The *filling pressure* affects the counting rate in two different ways. In the first place, for a constant operating voltage, the gas multiplication factor changes with filling pressure. If we calculate the change in voltage necessary to compensate for the pressure variation we find 1.60 ± 0.07 V/torr for beta radiation in the operating region (V = 7800 V, p = 2917 torr). This effective change in operating voltage, however, need not be corrected for separately since it is already included in the purity correction.

The second effect is the change in the amount of gas in the counter. In a first approximation this only affects the beta counting rate which is corrected by

$$A = A' p_o/p, \tag{3.25}$$

where A' is the measured ^{14}C activity of the sample and p_o is the standard filling pressure.

The *dead time* caused by the anti-coincidence blocking pulses of the Geiger counter leads to a loss in anti-coincidence counting rate in the proportional counter. Since the total dead time is directly proportional to the Geiger counting rate N_G, the anti-coincidence counting rate of the proportional counter (N/t) has to be corrected for variations in the Geiger counting rate

$$N_o/t = N/t\{1-(N_G-N_{Go})\tau/60\}, \tag{3.26}$$

where the subscript o indicates standard conditions, $(N_G-N_{Go})/60$ is the deviation from the standard Geiger counting rate in counts per second and τ is the dead time due to the blocking pulse ($\approx$ 1 msec) triggered by a Geiger count in seconds per count.

Since the Geiger counter mainly detects cosmic ray muons, one source of variations in Geiger counting rate is the variation of the atmospheric pressure. With a dead time of 3.2% for GRADA and 2.8% for RZ (c.f. sect. 3.2.3.1) and an atmospheric pressure dependence of −2.3%/cm Hg for muons, this gives a correction of 0.7 resp. 0.6‰/cm Hg for the anti-coincidence channel counting rate.

This correction has to be taken into account only with high precision analyses of young samples (e.g. tree ring calibration).

The four corrections discussed above can be combined into one correction equation:

$$A = \left\{ \frac{N}{t[1 - (N_G - N_{Go})\,\tau/60]} - [B + \frac{N_Z - N_{Zo}}{(dN_\mu/dV)_{max}}\, dB/dV + (b - 76)dB/db] \right\} \times$$

$$\times \left\{ 1 - \frac{N_Z - N_{Zo}}{(dN_\mu/dV)_{max}} \times \frac{dN_\beta/dV}{A_o} \right\} \frac{p_o}{p}. \qquad (3.27)$$

Table 3.11. Counting rate corrections.

Counter		I (6A)	GRADA (6)	RZ* (2)
B	cpm	2.49 ± 0.01	2.63 ± 0.01	1.80 ± 0.01
N_{Zo}	cpm	200	216	200
$(dB/dV)/(dN_\mu/dV)_{max}$		$(50.4 \pm 3.7) \times 10^{-5}$	$(71.2 \pm 2.1) \times 10^{-5}$	10^{-3}
$(dN_\beta/dV)/(dN_\mu/dV)_{max}\, A_o$	cpm^{-1}	$(5.78 \pm 0.17) \times 10^{-5}$	$(7.20 \pm 0.30) \times 10^{-5}$	2×10^{-4}
dB/db	cpm/cm Hg	−0.087 ± 0.031	−0.079 ± 0.024	−0.055
p_o	torr	2906	2917	2063
N_{Go}	cpm	1210	1240	2400
τ	sec/count	1.5×10^{-3}	1.5×10^{-3}	0.7×10^{-3}

* parameters as determined by Vogel

3.2.4. Conclusions

(i) From the results for the counters I and GRADA (no. 6A and 6) it appears that counters with a background counting rate of approximately 2.5 cpm at an effective volume of 1.7 l can be reproducibly constructed. Using these counters at a pressure of almost 4 atmospheres poses no serious problems and gives a figure of merit of 27 resulting in an age range of about 53 000 years for a two days counting period.

(ii) An indirect determination of the gas multiplication factor makes possible a quantitative interpretation of the counter operating conditions. Standard conditions are a gas multiplication of 1.7×10^4 at 7800 V and 2917 torr at 20 °C with a lower discriminator level corresponding to a primary energy of ≈ 1.0 keV or 30 primary ion-electron pairs.

(iii) Since the gas multiplication equation found gives good results when applied to the earlier work of Barendsen as well as to RZ it is of probably more general validity for CO_2 proportional counters.

(iv) Interactions in the gas and in the wall of the counter both contribute to the background counting rate.

(v) For muons interactions in the counter gas dominate at moderate and high pressures. Interactions in the counter wall become important only at very low pressures (< 100 torr).

(vi) The background counting rate of the counter is mainly caused by cosmic radiation, especially muons. The radioactivity of the counter contributes $< 30\%$ to the background. This emphasizes the importance of using heavily shielded (underground) counting rooms.

Chapter 4

SAMPLE TREATMENT

4.1.1. Introduction

The sample treatment in the laboratory can be divided into (i) the mechanical and chemical pretreatment necessary to eliminate sample contamination and (ii) the conversion of the carbonaceous sample material into CO_2 gas suitable for proportional gas counting.

The reliability of a ^{14}C age obtained depends on the instrumental reliability of the measurement but, even more, on the quality of the sample material finally used for the activity measurement. The sample quality is determined by the amounts of various contaminants incorporated in the sample and by the possibility of eliminating them. With contaminant we mean any carbon which has a specific ^{14}C activity different from that of the original material.

In the mechanical pretreatment the outer (more contaminated) part of the sample is cut away and visible contaminants like rootlets are picked out by hand. The chemical pretreatment is based on the assumption that contaminants that have been introduced into the sample by infiltrating ground water (e.g. humic substances and carbonates), will dissolve more readily than the bulk of the sample material. This is probably true for peat, lignite* and wood samples.

Apart from sample contamination, which has to be eliminated by pretreatment, we may have to deal with a laboratory contamination due to contaminants introduced into the sample during pretreatment and/or subsequent laboratory treatments (combustion to CO_2, purification, reduction to CO for enrichment and oxidation of the enriched gas to CO_2).

4.1.2. The effect of contamination

In fig. 4.1 we give the apparent age that will be obtained for a sample of given true age containing a certain amount of contamination.

* The term lignite is used here for the German 'Schieferkohle', a glacially strongly compressed peat, having a lignite like appearance but a carbon content below that of true lignite.

The effect of contamination with 'dead' carbon is independent of the age of the sample. In the age range beyond 50 000 years the error introduced is below the standard deviation σ_T for contamination $< 100^0/_{00}$.

The effect of contamination with modern carbon is large. Only $\approx 0.03^0/_{00}$ can be tolerated for a sample having an age of 75 000 years, if the error introduced should be smaller than σ_T.

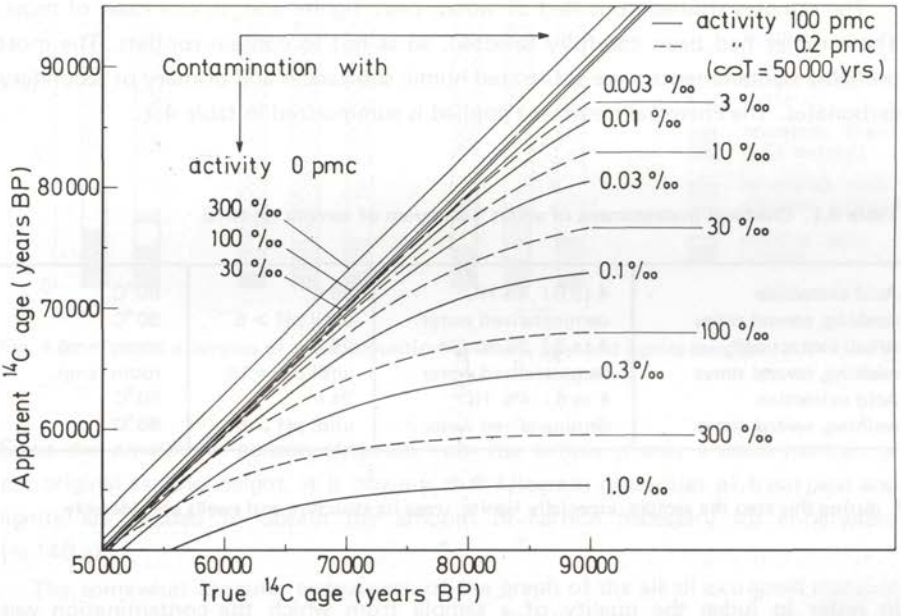

Fig. 4.1. Apparent age for samples older than 50 000 years as a function of the true sample age for various degrees of contamination with contaminants (i) without ^{14}C activity (0 pmc), (ii) of recent ^{14}C activity (100 pmc) and (iii) having a ^{14}C age of 50 000 years (0.2 pmc).

The material extracted from the sample during chemical pretreatment is tested for its radiocarbon activity following the procedure for routine ^{14}C dating. Most extracts did not show a measurable radiocarbon activity (c.f. tables sect. 5.2) and accordingly yielded ages $>$ 50 000 years BP. The effect on the apparent ^{14}C age of a contamination having a radiocarbon age of 50 000 years is also shown in fig. 4.1. The tolerance for this type of contamination is approximately 500 times larger than that for modern carbon in accordance with the specific activity of the contaminant (0.2 pmc, percent of modern carbon). The absence of a measurable ^{14}C activity in the extracted material adds to our confidence that the age determined for the sample is reliable.

4.2. The pretreatment: sample contamination

The mechanical and chemical pretreatment routinely used in our laboratory to eliminate contaminants from the sample (table 4.1) has been described by De Vries et al. (1958), Vogel and Waterbolk (1963) and Vogel (1969). Because only an extremely low level of contamination could be tolerated (less than 0.1 $^{0}/_{00}$) a rigorous treatment was decided upon; a partial loss of sample material is considered to be less serious than incomplete removal of contaminants.

The samples studied consisted of wood, peat, lignite and, in one case, of moss. The samples had been carefully selected, so as not to contain rootlets. The most probable contaminants were infiltrated humic substances and primary or secondary carbonates. The chemical treatment applied is summarized in table 4.1.

Table 4.1. Chemical pretreatment of about 1 kilogram of sample material.

Acid extraction	4 to 6 l 4% HCl	48 h	80°C
washing, several times	demineralized water	until pH $\geqslant$ 5	80°C
Alkali extraction*	4 to 6 l 3% NaOH	24 h	room temp.
washing, several times	demineralized water	until pH $\approx$ 10	room temp.
Acid extraction	4 to 6 l 4% HCl	24 h	80°C
washing, several times	demineralized water	until pH $\geqslant$ 5	80°C

* during this step the sample, especially lignite, loses its structure and swells considerably

In order to judge the quality of a sample from which the contamination was removed as well as possible, it is important to have information about the amount of contaminants removed and about the radiocarbon activity of the material extracted. The organic carbon extracted during the hydrochloric acid treatment is obtained by evaporating the brown acidic extract almost to dryness and washing with demineralized water until pH $\geqslant$ 5. The alkali extracted material (NaOH and subsequent water extractions) is precipitated by acidifying with concentrated hydrochloric acid and subsequently washed with demineralized water until pH $\geqslant$ 5 or until the precipitate begins to dissolve. The alkali extract and the alkaline water extractions are processed separately to be able to follow the extraction quantitatively. The amount of dry extracted material recovered in each step is expressed as a percentage of the original amount of dry organic matter. The dry weight is determined after drying at 110°C, while the amount of sand and clay originally present is estimated from the amount of ashes left after the combustion of the purified sample (i.e. the residue of the extraction). Some typical examples of sample composition and extraction results are given in fig. 4.2 and 4.3 respectively.

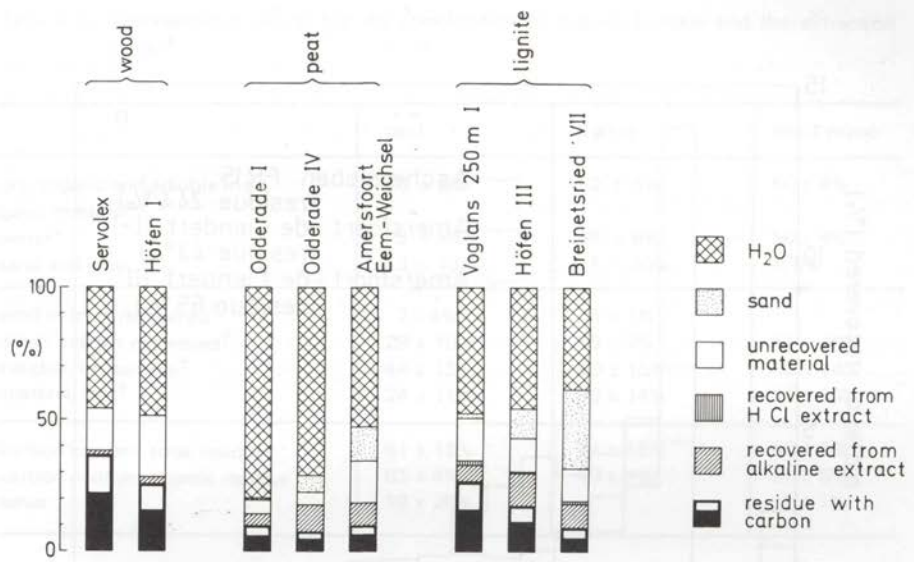

Fig. 4.2. Typical examples of the composition of wood, peat and lignite samples.

Since the amount of carbon obtained from the sample is only a small fraction of the original sample weight, it is obvious that kilogram quantities of fresh peat and lignite are needed to obtain the amount of carbon necessary for enrichment ($\approx$ 140 g).

The somewhat irregular appearance of the graph of the alkali extracted material might be caused by different extraction times. The first extract occasionally is small due to strong absorption of the alkali solution in the sample. Then only a small amount of liquid can be decanted.

Representative values for sample composition as well as the amounts of the extract are given in table 4.2. The large variations in the recovery after the alkali extraction are probably caused by a different degree of degradation of the original organic material. The high carbon content of the organic residue might be caused by a certain degree of carbonization during the pretreatment.

The radiocarbon activity of several of the extracts was measured according to our routine procedures. The results are given together with the dates obtained for the purified samples in the tables of sect. 5.2. It is obvious that the careful selection of the material resulted in samples having a low degree of contamination. Most extracts showed no measurable radiocarbon activity. Therefore it was impossible to determine the effect of successive stages of the extraction procedure. In the few cases where ^{14}C activity was detected, most of it was eliminated during the first series of acid extractions and the first alkali extraction.

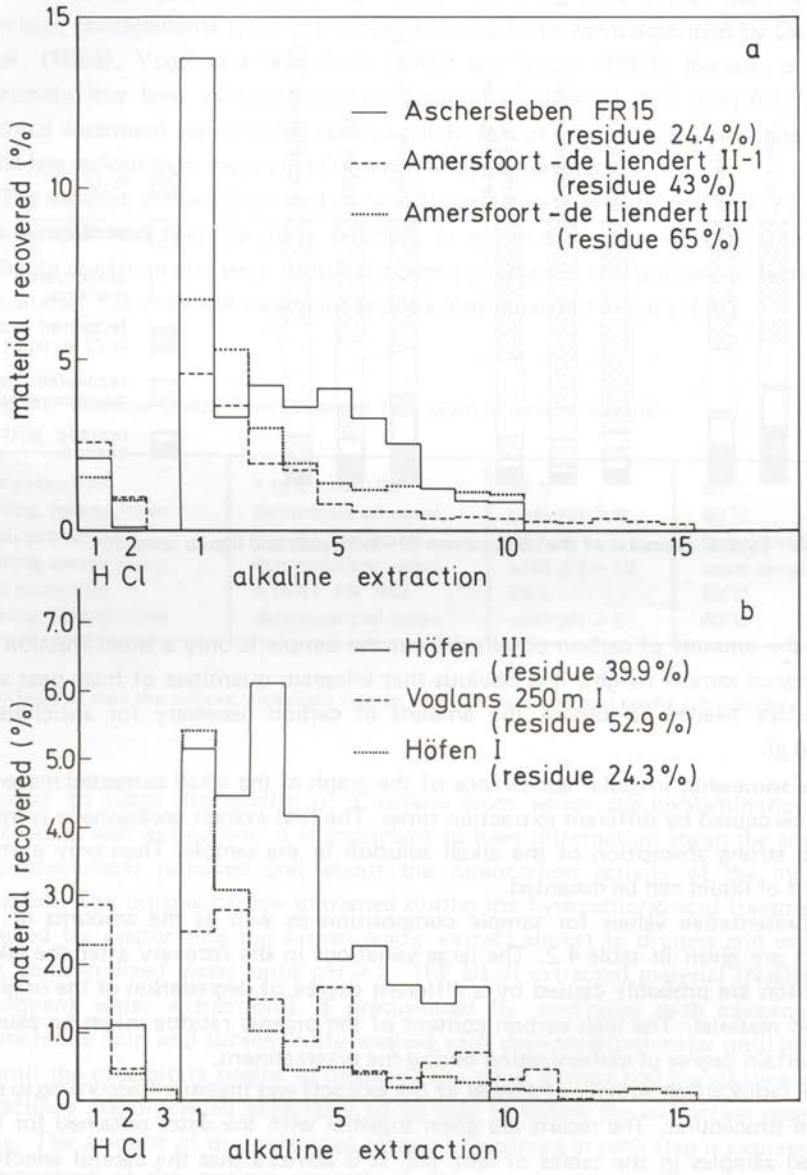

Fig. 4.3. Typical examples of the relative amount of material recovered from the extract during chemical pretreatment of peat (a) and lignite (b) samples.

Table 4.2. Representative values for the composition of organic samples and the extraction yields.[a]

	peat	lignite	fossil wood
dry organic and soluble inorganic material *	25 ± 8%	52 ± 6%	50 ± 4%
water*	75 ± 8%	48 ± 6%	50 ± 4%
sand and clay	0.3 – 13%	1 – 30%	≈ 0%
acid extract recovered†	2–4%	3 ± 1%	
alkali extract recovered†	29 ± 10%	19 ± 7%	11 ± 12%
residue, i.e. sample†	44 ± 13%	40 ± 15%	52 ± 14%
material lost†	24 ± 11%	39 ± 14%	37 ± 8%
carbon content total residue	51 ± 13%	44 ± 16%	60 ± 5%
carbon content organic residue	63 ± 4%	60 ± 1%	61 ± 5%
ashes	18 ± 20%		1 ± 1%

a based on the results of the chemical pretreatment of 12 peat, 9 lignite and 5 wood samples
* based on an ash-free sample
† based on dry ash-free material

4.3. Sample treatment

4.3.1. Combustion

The standard procedure for the conversion of carbonaceous material into pure CO_2 in use at the Groningen Laboratory has been described earlier by De Vries and Barendsen (1953), Barendsen (1955) and by Vogel and Waterbolk (1967). Our new version of the combustion system is presented in fig. 4.4. After flushing the combustion tube containing the organic sample with nitrogen to remove foreign CO_2, the sample material in the inner tube is first carbonized by heating in a stream of nitrogen gas. The volatile compounds are converted into CO_2 when the hot nitrogen enters the oxygen atmosphere in the concentric outer tube. Finally oxygen is led directly through the sample until the combustion is complete. After several purifications the sample is collected in two CO_2 traps at liquid air temperature. The traps containing the solid CO_2 sample are evacuated. The CO_2 is further purified by passing it a number of times through a water trap at – 80 °C and copper and silver at 450 °C. After each passage the CO_2 is frozen at liquid air temperature and pumped.

The system has been designed to produce large quantities of CO_2 for enrich-

ment. The combustion tube has a capacity of an equivalent of 70 to 100 l NTP of CO_2. This production can be obtained in one day.

Some special features of the system are:
(i) The use of high purity gases* for the combustion, making any additional removal of CO_2 by alkali wash bottles superfluous.
(ii) The additional purification of these gases from moisture and hydrocarbons by passing them through two traps at $-80\,^{\circ}C$ prior to combustion.
(iii) The heating of the sample material at $1000\,^{\circ}C$ by means of an electrical furnace with automatic transport.
(iv) The use of glass spikes in the CO_2 traps to reduce the possibility of laminar gas flow and ensure a good collecting efficiency. Several measurements indicate that more than 98.5% of the CO_2 is retained in the first trap and thus more than 99.9% of the total CO_2 is collected.
(v) The omission of the radon purification. This is possible since the time between the combustion and the completion of the enrichment procedure (>30 days) is long compared with the radon half-life (3.8 days), ensuring a sufficient decay.
(vi) The low pressure in the CO_2 traps (kept at approximately 100 torr by continuously pumping off the non-condensable gases) preventing the condensation of oxygen.

The sample is stored after combustion in a 1 l CO_2 cylinder.

4.3.2. Reduction

The CO_2 sample is reduced to CO by passing it from a storage cylinder via a pressure regulator through a pyrex tube containing zinc–asbestos, heated to about $420\,^{\circ}C$ in a temperature-controled furnace (fig. 4.5). The asbestos, which facilitates the gas flow through the reduction furnace, is heated before use to $900\,^{\circ}C$ in air to remove possible organic contaminants and water. The zinc powder is washed with di-ethyl ether to remove grease. After complete evaporation of the ether, the asbestos and the zinc are mixed (1:10 by weight). The mixture is thoroughly degassed by prolonged pumping at $125\,^{\circ}C$. Some hours before starting the reduction, the temperature of the furnace is increased to $\approx 400\,^{\circ}C$ which results in additional degassing of the mixture. For each reduction a 6 cm diameter pyrex tube is packed rather loosely with ≈ 1.5 kg of this mixture over a length of approximately 35 cm. At temperatures above $420\,^{\circ}C$ the reduction is faster, but melting of the zinc (at $419.4\,^{\circ}C$) and softening of the pyrex set an upper limit to the temperature used. The system is flooded three times with about 100 ml NTP of CO_2

* L'Air Liquide N.V. high purity gases. Nitrogen A28 ($H_2O \leq 5$ vpm; N_2 + noble gases 99.999%); Oxygen A40 ($H_2O \leq 5$ vpm; $C_nH_m \leq 5$ vpm; O_2 99.99%).

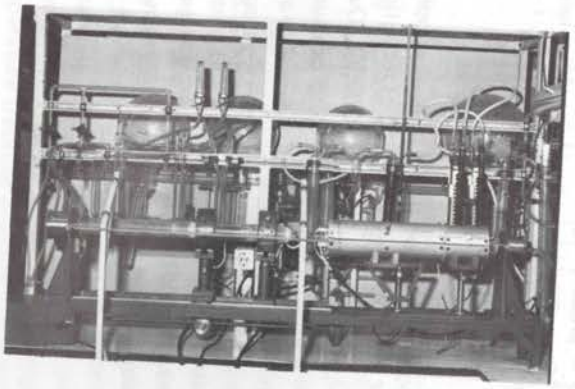

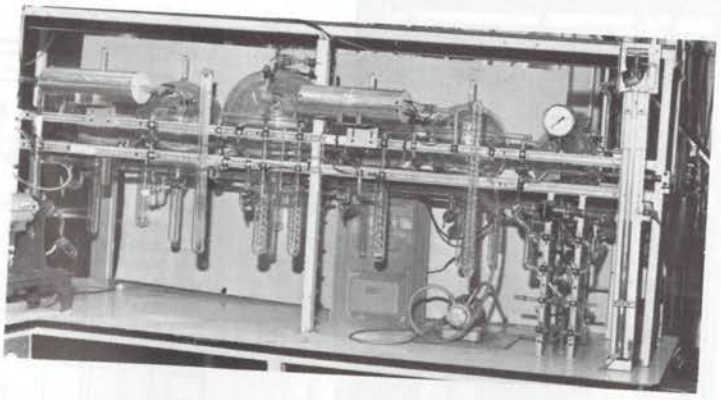

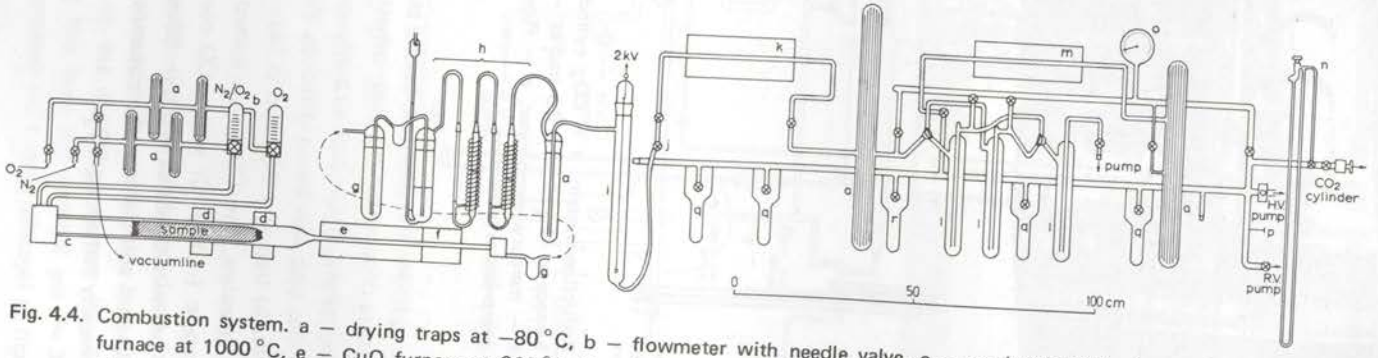

Fig. 4.4. Combustion system. a – drying traps at –80 °C, b – flowmeter with needle valve, c – combustion tube (quartz), d – combustion furnace at 1000 °C, e – CuO furnace at 800 °C, f – Ag furnace at 500 °C, g – water trap, h – $KMnO_4$ wash bottles, i – Cottrel electrostatic dust collector, j – needle valve, k – Ag furnace at 450 °C, l – CO_2 traps at liquid air temperature, m – Cu and Ag furnace at 450 °C, n – mercury manometer, o – Bourdon manometer, p – Pirani gauge, q – 10 l storage bulbs, r – 20 l storage bulb.

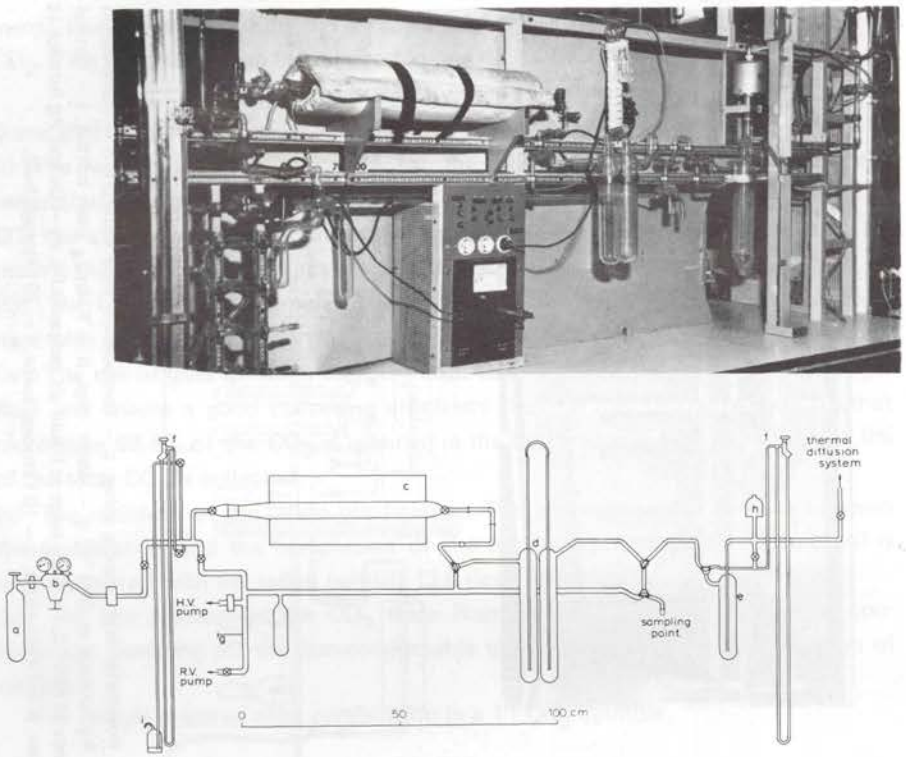

Fig. 4.5. Reduction system. a – CO_2 cylinder, b – pressure regulator, c – zinc-asbestos furnace at 420 °C, d – CO trap at –195 °C, e – CO_2 trap at liquid air temperature, f – mercury manometer, g – Pirani gauge, h – Penning highvacuum gauge, i – overpressure protection.

from the cylinder and pumped, before starting the reduction of the bulk of sample. At a pressure drop across the zinc–asbestos of some 400 torr the speed of reduction is approximately 10 l/h and virtually no CO_2 passes the furnace ($< 0.1\%$). Over 60% of the zinc can be oxidized to ZnO in this way. In order to keep pressures moderate, to trap any CO_2 and to have the possibility of filling the columns to any desired pressure, the CO gas is passed through a double trap at liquid nitrogen temperature (– 196 °C) where CO condenses to a colourless clear liquid with a vapour pressure of about 470 torr. When the reduction has been completed, the CO is evaporated and led into the columns through a trap at liquid air temperature to condense any remaining CO_2.

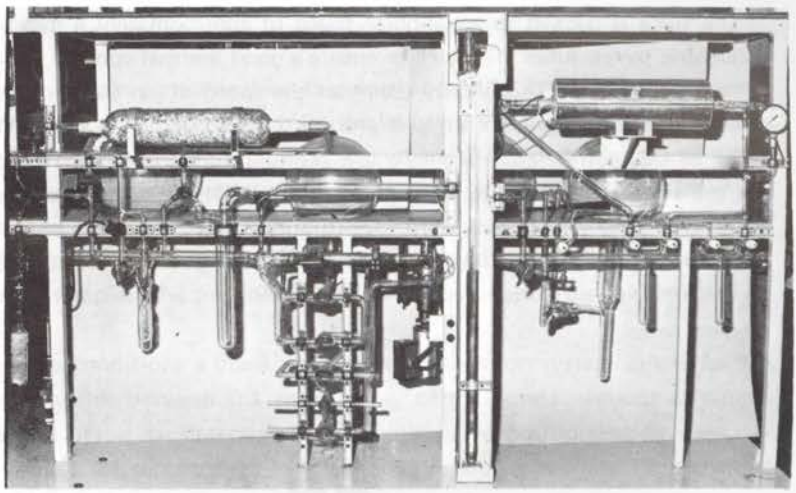

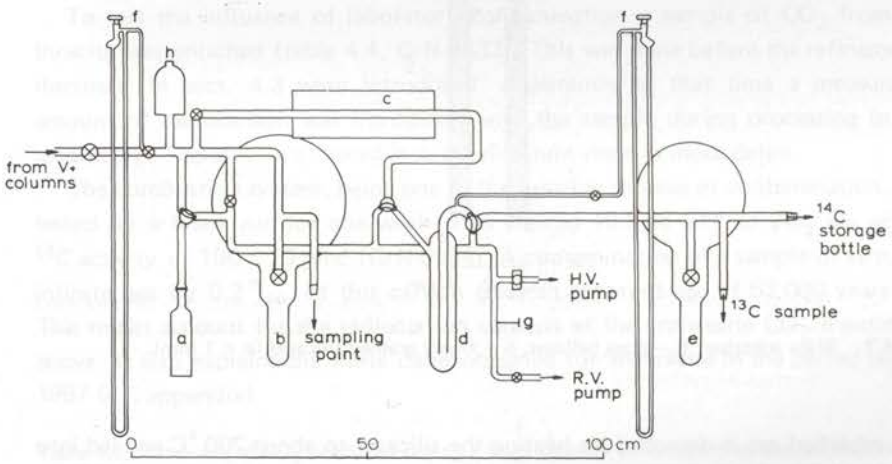

Fig. 4.6. Oxidation system. a – silica adsorber, b – 10 l storage bulb, c – CuO furnace at 450 °C, d – CO_2 trap at liquid air temperature, e – 6.5 l calibration volume, f – mercury manometer, g – Pirani gauge, h – Penning highvacuum gauge.

4.3.3. Oxidation

Since the enriched sample has to be counted by our standard procedures, it has to be reoxidized to CO_2. The enriched gas, collected in 9 sample bulbs at the bottom of the enrichment columns is admitted to the oxidation system (fig. 4.6) by expanding into a 10 l bulb. After closing this bulb the residual gas ($\approx$ 30%) is quantitatively adsorbed in 40 g of finely grained ($<$ 1 mm) silicagel at liquid air temperature (residual pressure $< 5 \times 10^{-3}$ torr).

The silica is packed in an annular space of approximately 4 mm between two concentric pyrex tubes (fig. 4.7) to ensure a good thermal contact with the cooling or heating medium. This greatly enhances the speed of gas ad- and desorption. By gradually raising the liquid air level around the adsorber a large amount of gas (> 2 l NTP of CO) can be adsorbed to a low residual pressure ($< 5 \times 10^{-3}$ torr). Before use the silica is treated with hot concentrated HNO_3 and washed thoroughly in order to remove radioactive impurities (uranium) that produce radon. Prior to the oxidation run the silicagel has been evacuated overnight at about 200 °C.

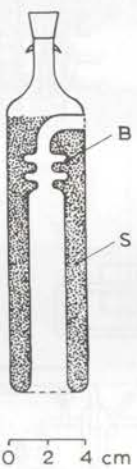

Fig. 4.7. Silica adsorber. B – glass bellows, S – finely grained silicagel ($\phi < 1$ mm).

The adsorbed gas is desorbed by heating the silicagel to about 200 °C and led into the 10 l bulb. From this gas mixture a sample is taken to measure the enrichment that has been obtained.

The gas is oxidized by passing it through a CuO furnace at 450 °C and condensing the CO_2 in a trap at liquid air temperature. Although some CO passes the furnace, reduction can be made quantitative by recirculating this CO through the CuO furnace. After recycling twice, the pressure in the system remains constant, indicating that the oxidation is complete. Some non-condensable gases can be pumped off (< 0.03% of the initial amount of gas), after which the enriched CO_2 sample is transferred to a storage bulb. The total procedure takes about 10 hours. After each oxidation the CuO furnace has to be regenerated by heating it at 450 °C in oxygen.

4.4. Laboratory contamination

Apart from the sample contamination discussed in sect. 4.2, there is a possibility that the sample becomes contaminated in the laboratory. This laboratory contamination may originate from several sources, e.g. chemicals and demineralized water used for the sample pretreatment, combustion gases, contamination or memory effect in the combustion line, leakages in the vacuum systems and contamination in the reduction and oxidation system. Because the laboratory treatment is essentially the same for all samples, the possible degree of contamination can be detected by blank runs.

Under routine conditions a blank run of the combustion system in use for the normal samples yields between 0.1 and 0.4 $^0/_{00}$ of the normal amount of sample CO_2. This is well below the detection limit of routine radiocarbon dating, even if it completely consists of recent carbon. It becomes serious, however, when thermal diffusion enrichment is to be used.

To test the influence of laboratory contamination a sample of CO_2 from anthracite was enriched (table 4.4, GrN-6533). This was done before the refinements discussed in sect. 4.3 were introduced. Apparently at that time a measurable amount of radiocarbon was introduced into the sample during processing in the laboratory. Therefore we looked into the different steps in more detail.

The *combustion system*, being one of the possible sources of contamination, was tested by a blank run for one week. This yielded 48.5 ml STP of CO_2 gas with a ^{14}C activity of 190 ± 15 pmc (GrN-6594). A contamination of a sample of virtually infinite age by 0.2 $^0/_{00}$ of this carbon gives an apparent age of 63 000 years BP. This might account for the radiocarbon content of the anthracite CO_2 mentioned above. It also explains the finite dates obtained for anthracite in the period before 1967 (c.f. appendix).

Table 4.3. Amounts of CO_2 produced during a (blank) run in various parts of the combustion system.

Source	Fraction of total gas used (vpm)			
	oxygen		nitrogen	
	CO_2	CO_2 from hydrocarbons	CO_2	CO_2 from hydrocarbons
Gas, technical quality	18	10 to 15	3	4
Gas, high purity, teflon membrane	–	≈ 15	–	–
The same with two cold traps −80 °C	–	≈ 8	–	–
Rubber membrane	–	≈ 8		
sodiumhydroxide solution	–	–	–	–
combustion tube		10 – 80		
potassiumpermanganate		0 – 10		
vacuum section		0		

A thorough investigation of the combustion system showed (table 4.3) that the technical grade combustion gases (N_2 and O_2) introduce foreign carbon into the sample, that cannot simply be removed by an alkali wash bottle, since part of it is present as hydrocarbons. The use of high purity gases containing no measurable amount of CO_2 and < 5 vpm C_nH_m (O_2, grade A40) gives some improvement, especially in combination with an additional purification in two cold traps at $-80\,^{\circ}C$.

The main source of contamination, however, appeared to be the combustion tube. Probably during the degassing procedure condensation of hydrocarbons in the 'cold' parts of the system takes place. Partial evaporation in subsequent combustions causes high blank runs and a memory effect. If the combustion tube is cleaned thoroughly before each combustion, the degree of contamination is reduced. A blank run gives: $CO_2 < 50$ vpm based on the volume of O_2 passed through the system. Because an excess of oxygen is used for the combustion the CO_2 contamination relative to the amount of sample CO_2 produced is higher. If, however, as an extra precaution, only 'old' samples are admitted to the combustion system the amount of radiocarbon introduced is negligible.

The *zinc–asbestos mixture* used for filling the reduction furnace also had to be considered as a potential source of contamination, especially because a new filling is used for each sample. Therefore the original cleaning procedure consisting of degassing by pumping at 125 °C was replaced by the more elaborate procedure described in sect. 4.3.2. This greatly reduced the degassing at 400 °C.

After these precautions had been taken three more anthracite samples were treated. The results are given in table 4.4 together with those of some other 'dead' samples. Obviously laboratory contamination has been reduced to below our present detection limit.

During the period 13/4/'73 to 10/5/'75 the anthracite samples III and IV before and after enrichment were measured in turn with the routine background determination. This gives an indication whether the anthracite CO_2 really contains no measurable radiocarbon. The activity of the samples relative to the routine anthracite CO_2 counting rate ('background') is given in table 4.5.

If the enrichment factor for the enriched sample is $q^{14'}$, the difference in activity between the CO_2 gas before and after enrichment is $(q^{14'} - 1)A$. From these results we conclude that the CO_2 gas prepared from anthracite, taking the special precautions for enriched samples outlined above, contains no measurable amount of ^{14}C. This proves the assumption, that a CO_2 sample from anthracite can provide a true background counting rate.

If we assume that the specific activity of the anthracite is zero, then the average activity value of 0.0026 ± 0.0024 pmc for III and IV indicates the degree of

Table 4.4. Results of anthracite CO_2 and samples with no statistically significant activity.

	Number	Activity measured (cpm)	Enrichment	A (pmc*)	Apparent age (yrs BP)	
					2σ criterion	1σ criterion
Anthracite	GrN-6533	0.082 ± 0.039	12.2 ± 0.2	0.022 ± 0.010		67 700 $^{+5200}_{-3100}$
	GrN-6680	0.023 ± 0.030	10.2 ± 0.4	0.0072 ± 0.0094	> 66 300	
	GrN-6808	−0.010 ± 0.010	12.8 ± 0.3	< 0.0050	> 79 600	
	GrN-7193	0.012 ± 0.012	14.5 ± 0.4	0.0028 ± 0.0026	> 75 900	84 300 $^{+22\,000}_{-5300}$
	GrN-7257	0.015 ± 0.022	11.3 ± 0.2	0.0043 ± 0.0063	> 69 700	
	GrN-7391	−0.077 ± 0.022	11.6 ± 0.2	< 0.012	> 72 200	76 400 $^{+6700}_{-3600}$
	GrN-7424	0.027 ± 0.016	12.3 ± 0.4	0.0071 ± 0.0042	> 70 400	
	GrN-7490	0.017 ± 0.020	8.6 ± 0.4	0.0066 ± 0.0076	> 67 700	
	GrN-7498	0.032 ± 0.020	11.1 ± 0.2	0.0093 ± 0.0059	> 68 000	74 500 $^{+8100}_{-4000}$
	GrN-7704	0.002 ± 0.021	12.4 ± 0.3	0.0004 ± 0.0056	> 72 800	

* samples counted in RZ having A_o = 30.81 cpm

Table 4.5. Results for anthracite CO_2 samples III and VI.

GrN	Sample	Activity (cpm)	$(q^{14'}-1)A$ (cpm)	$q^{14'}$	A^c (pmc)
6851	III, normal	-0.020 ± 0.007^a			
6808	III, enriched	-0.010 ± 0.010^a	0.009 ± 0.012	12.8 ± 0.3	0.0024 ± 0.0033
7152	IV, normal	$+0.0001 \pm 0.0087^b$			
7193	IV, enriched	$+0.012 \pm 0.012^b$	0.012 ± 0.014	14.5 ± 0.4	0.0029 ± 0.0035

a measured relative to RZ background samples of November 1972 and October 1973 in period 3, 4 (normal) respectively 3 (enriched) (table 3.10)

b measured relative to RZ background sample of August 1974 in period 4 and 5 (table 3.10)

c recent standard counting rate RZ: $A_o = 30.81$ cpm

laboratory contamination. The main contribution might be made by hydrocarbons from the oxygen used for combustion (table 4.3). A twofold excess of oxygen used for the production of CO_2 and a specific activity of the contaminant between 150 pmc (atmospheric) and 190 pmc (GrN-6594), would explain the results obtained. With 98% probability the laboratory contamination as determined from anthracite CO_2 III and IV is < 0.0074 pmc. If this amount of activity was added to a sample of practically infinite age, it would yield an apparent age of 76 400 years BP.

The sample results show that a low degree of laboratory contamination and sample contamination cannot only be obtained with anthracite, but also with other sample materials like peat (GrN-7424), wood (GrN-7257 and GrN-7498) and lignite (GrN-7391, GrN-7490 and GrN-7704). The results prove that as far as laboratory contaminations are concerned, radiocarbon dates up to 75 000 years can be obtained. Probably the contamination in the combustion system has been the main source of error.

If a further extension of the range is desired or if samples having an age close to 75 000 years are to be dated, a further investigation of laboratory contamination should be made.

Although the contamination in the combustion line can account for the finite anthracite ages obtained before 1967, it cannot explain some of the earlier erroneous results (Vogel and Zagwijn, 1967). These probably are to be ascribed to other causes, e.g. the filling of the zinc furnace (c.f. appendix).

The negative activity found for the normal anthracite CO_2 sample III (GrN-6851) indicates that the anthracite CO_2 samples of November 1972 and October 1973 used for the measurement of the RZ background counting rate contained a measurable amount of radiocarbon.

Considering the amount of CO_2 collected during blank runs of the routine combustion system (0.1 – 0.4 ‰) and the high activity measured for CO_2 from a blank run, the activity of the routine anthracite CO_2 sample seems quite reasonable. The result for anthracite IV (GrN-7152) indicates that the routine preparation of August 1974 contained no measurable radiocarbon activity.

The possibility that a small amount of radiocarbon-containing contaminant is present in the anthracite CO_2 used for background measurement introduces an additional uncertainty in the background counting rate. This becomes important for samples with a measured activity close to $2\sigma_B$.

The activity of the enrichment samples measured relative to the background anthracite samples of November 1972 and October 1973 has been corrected for the activity of these anthracite samples. For samples measured after August 1975 no information about the exact background anthracite contamination is available.

Chapter 5

SAMPLES DATED: DESCRIPTION, RESULTS AND DISCUSSION

5.1. Introduction

The aim of the expansion of the range of the radiocarbon dating method using thermal diffusion enrichment was to obtain a time scale for the climatic development in the early part of the Last Glacial. To this end samples from a limited and relatively well known area, viz. North-west Europe between the Scandinavian and the Alpine ice sheet, were collected. The samples were selected for enrichment when stratigraphical and/or pollenanalytical evidence suggested that they belonged to the early glacial period. A number of new samples were obtained from localities which had been dated using thermal diffusion enrichment before 1967 (Amersfoort and Odderade). The sites from which samples have been enriched up till June 1976 are given in table 5.1, their geographical distribution can be seen in fig. 5.1.
Thanks to much friendly cooperation of geologists and palynologists in the Netherlands and Germany it has been possible to obtain these samples.

In the preceding chapter the problem of contamination and its implications for the reliability of ^{14}C dates have been discussed.

The extreme sensitivity for 'recent' contamination in the age range of 50 000 to 75 000 years BP makes a single date in this range not sufficiently reliable. In section 3.1.3.1 we have concluded that the reliability of an age determination has to be inferred from:

(i) a comparison of the ages of different samples from the same profile;
(ii) a consistent picture for equivalent samples from different related profiles;
(iii) an investigation of the ^{14}C activity of the material extracted in different fractions during the chemical pretreatment.

Thus, in order to obtain a reliable time scale it is essential that a great number of samples are dated that have been correlated stratigraphically and pollenanalytically.

In section 5.2 we give a description of the geographical situation, the stratigraphy and the results of pollen analyses of the various samples, supplied by the collectors and investigators of the samples. These descriptions are supplemented by

Table 5.1. Dated sites up to June 1976.

Site	Samples collected by	Pollen analysis performed by
Amersfoort – De Liendert Amersfoort, boring Eemian	W. H. Zagwijn	W. H. Zagwijn
Voorthuizen	W. H. Zagwijn	T. A. Wijmstra
Odderade	F. R. Averdieck	F. R. Averdieck
Aschersleben	D. Mania	
Samerberg	E. Grüger	E. Grüger
Breinetsried Pömetsried Höfen	B. Frenzel	P. Peschke
Mauern	A. Brande	A. Brande
Voglans La Croix Rouge Pessey–Sonnaz Servolex } Val du Bourget	Ch. Hannss	W. H. E. Gremmen
La Flachère, Grésivaudan		S. Bottema Y. M. Koster
Padul	T. A. Wijmstra	T. A. Wijmstra
Beaverdam Creek	G. M. Richmond	

our ^{14}C results and a discussion of their reliability considering the criteria (i) and (iii). The consistency of the dates for samples from different related profiles (criterion (ii)) is discussed in sect. 5.3.

In the tables of section 5.2 we first give the ages of the enriched samples, then the conventional ages and finally those obtained for the extracted material. All enriched and part of the other samples have been measured in counter RZ (no. 2), the remaining samples in counter GRADA (no. 6) and counters I (no. 6A) and LZ (no. 1). The background counting rate of RZ was determined from a least squares fit to the background data (fig. 3.19) and, when possible, corrected for the residual radiocarbon activity of the anthracite CO_2 sample used for background determination. The ^{14}C enrichment was calculated from a mass spectrometrical determination of the mass 30 enrichment using the calibration relation, eq. 2.40. If the measured activity is less than two times the statistical uncertainty of the measurement (σ) a maximum ^{14}C activity and minimum age is given following the conven-

Fig. 5.1. Geographical distribution of sites from which samples for enrichment were taken.

tional 2σ criterion. If, however, the activity is smaller than 2σ but exceeds 1σ, also an age is calculated using a 1σ criterion. Obviously this age should be considered merely as an indication. All ages have been corrected for isotope fractionation using $\Delta T_{corr} = 16(\delta^{13}_{PDB} + 25.00)/(1-25.00 \times 10^{-3})$ where δ^{13}_{PDB} refers to the relative difference in isotopic abundance ratio between the sample and the PDB standard CO_2. The value of -25.00 is the δ^{13}_{PDB} value defined for standard wood (δ value given in $^0/_{00}$), to which all samples are conventionally related.

5.2. Sample descriptions and ^{14}C results

5.2.1. Amersfoort

5.2.1.1. Introduction

The Eem valley near Amersfoort (52° 09′ N Lat, 5° 24′ E Long) in the province of Utrecht, The Netherlands, originated as a glacier tongue basin during the Saalian glaciation. Subsequently, during the Last Interglacial (Eemian) the sea invaded the area and left its deposits. During the Last Glacial (Weichselian) the valley was further filled with non-marine sediments. The locality Amersfoort near the north-western edge of the valley is the type-area of both the Eemian Interglacial and the Amersfoort Interstadial of the Last Glacial (Zagwijn, 1961).

5.2.1.2. Lithostratigraphy (by W. H. Zagwijn)

The oldest sediments filling the basin are fluvioglacial sand and gravel of Saalian age. They are overlain by sediments of the Eem Formation. Four members can be recognized in this area within this formation: locally a lower peat member, overlain by a marine sand member, and a marine clay member. At the top of the formation a peat member, indicating freshwater conditions, is generally found. The top of the Eem Formation is at about 10 to 13 metres below the present valley floor.

The deposits of the Eem Formation are overlain by those of the Twenthe Formation, mainly consisting of aeolian sands (coversands) and other sands laid down under periglacial conditions, alternating with some peat beds.

The general sequence of the Twenthe Formation, as deduced from borings and some exposures, is as follows.

At the base about 1.5–2 m of aeolian sand is found, overlain by a peat member of general occurrence; in some places, however, we are dealing with a podsolic soil with cryoturbations. On top of this bed another layer of aeolian sand occurs, in some places very thin, often more than one metre thick. This sand is overlain by another podsolic soil, but in an area just east of the town of Amersfoort a peat bed of about one metre thickness is found in the same stratigraphic position. In one exposure (Amersfoort–De Liendert) this peat bed was immediately on top of the afore-mentioned lower podsolic soil and corresponding peat bed.

In this particular exposure a thin bed of aeolian sand was found in the upper part of the second peat bed. Overlying this sequence are loamy coversands, about 1.5 to 2 metres thick. These loamy coversands have very large frostwedges at their base, and are overlain by a cryoturbatic peat bed. The uppermost part of the Twenthe Formation shows several metres of loamy and less loamy coversands up to the surface. In the exposure Amersfoort–De Liendert no traces of leaching and humic infiltration reaching down to the sample levels were observed.

5.2.1.3. Pollen analysis (by W. H. Zagwijn)

Several pollen diagrams from the above mentioned sequence were published before (Zagwijn, 1961). In addition pollenanalytical data were obtained from sections which have been especially sampled for radiocarbon dating after isotope enrichment. These samples come from the uppermost peat bed of the Eem Formation in a special boring (32B/119 bis), and from the above mentioned peat beds of the Twenthe Formation, exposed in 1967 in a construction pit at Amersfoort–De Liendert. A simplified pollen diagram of these sections is presented in fig. 5.2.
The peat between 12.63 and 12.13 m shows a local dominance of *Alnus* at the bottom and an increase of *Pinus* characteristic of the Eemian pollen zone E 6a higher up (Zagwijn, 1961). A thin sand layer at 12.25 m probably represented an unconformity. Above this level the pollen spectrum shows a high percentage of pollen of Ericales (*Calluna*), whereas among the tree pollen only *Betula* and *Pinus* are present. This assemblage is characteristic of the first Early Weichselian pollen zone (EW Ia). Therefore the Eemian-Weichselian boundary is at the hiatus at 12.25 m. The pollen spectra at the base of the lowermost peat bed of the Twenthe Formation (8.50–8.32 m) are similar in composition as they show high values of herbs, especially Ericales. These spectra too, indicate the presence of beds of pollen zone EW Ia age. A decrease of herbs and a maximum of *Salix* mark the final phase of this pollen zone (EW Ib). Pollen zones EW Ia and EW Ib represent the first cold Stadial (I) of the Early Weichselian (Zagwijn, 1961). On top of these beds an increase in tree pollen indicates the beginning of the Amersfoort Interstadial. Two pollen zones reflect this interstadial: a lower one with a dominance and maximum of *Betula* (EW IIa) and an upper one with equal values of *Betula* and *Pinus* (EW IIb). No signs of climatic deterioration are found at the top of the peat bed, which may indicate that part of the sequence is missing.

The pollen spectra from the base of the next peat layer (7.60–6.60 m) again have high values of herbs, pointing to the presence of pollen zone EW III, reflecting the Second Stadial of the Early Weichselian. Following this zone a decrease of herbs to circa 30% and dominance of *Pinus* over *Betula* mark the first zone (EW IVa) of the Brørup Interstadial. As compared with the spectra from the higher part of this interstadial observed in a boring nearby (Zagwijn, 1961), a hiatus must be present in the higher part of the peat bed. Spectra of subzone EW IVb showing a characteristic dominance of *Picea omorikoides,* are absent. Two spectra obtained from a thin clay layer (6.90–6.87 m) resemble those of the deeper layers except for the presence of thermophilous trees like *Corylus* and *Carpinus*. Therefore, they probably correspond to zone EW IVc as described by Zagwijn (l.c.) from the top of the Brørup Interstadial. The remaining part of the peat bed (6.87–6.60 m) represents a pollen zone, which has not been described with the previous borings and exposure. The lower part of this zone (EW Va) has a stadial character (high values

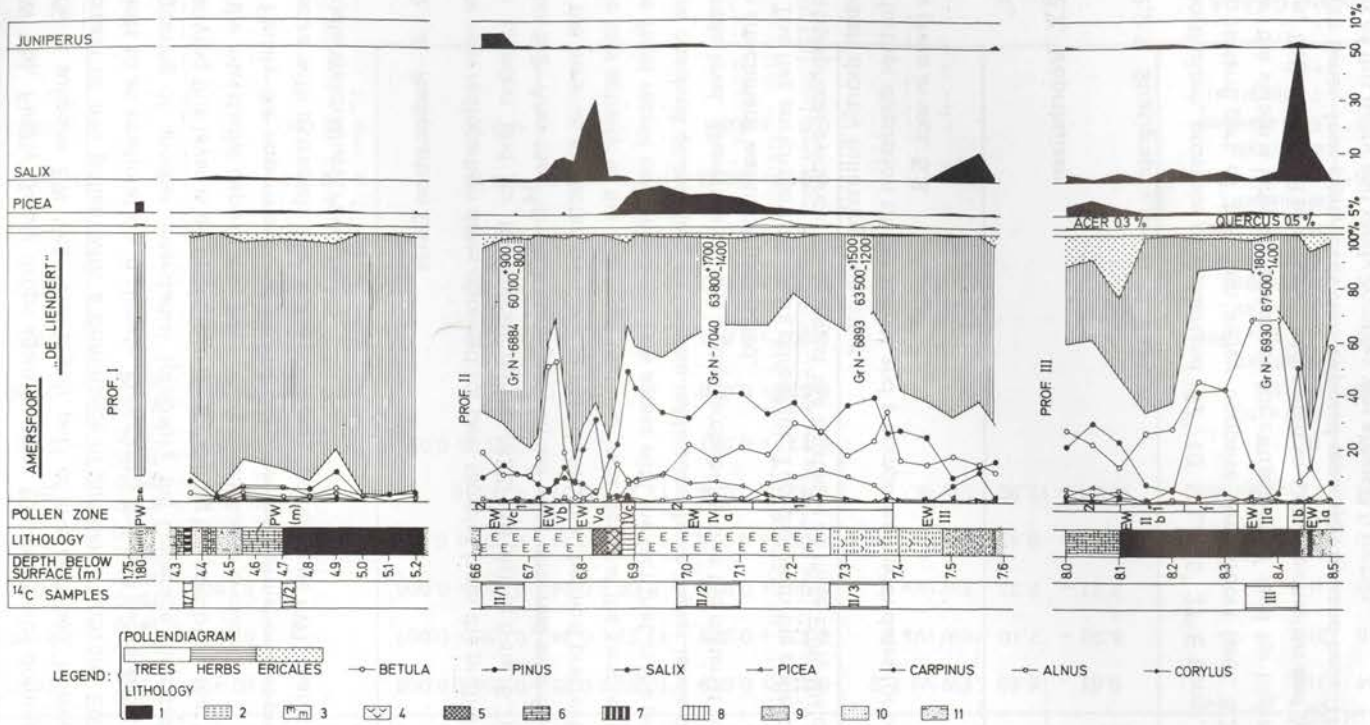

Fig. 5.2. Pollen diagram and lithology of the exposure Amersfoort–De Liendert.
1 – peat, 2 – *Phragmites*-peat, 3 – *Carex*-peat, 4 – wood-peat, 5 – gyttja, 6 – humic clay, 7 – peaty clay, 8 – clayey, 9 – fine sand, 10 – coarse sand, 11 – humic sand.

of herbs and a maximum of *Salix*). Then *Betula* reaches a maximum of circa 50% (EW Vb). Finally *Betula* drops again to circa 10% and herbs dominate with circa 80% in subzone EW Vc1. The higher part of the peat bed, however, shows an increase of tree pollen with a dominance of *Juniperus* (subzone EW Vc2), which points to an amelioration in climate. Presumably this part of the section reflects the beginning of another interstadial (probably the Odderade Interstadial). Directly overlying this layer is an unconformity indicating the possibility that the main part of the interstadial deposit may have disappeared due to erosion.

Finally the uppermost peat bed of the Twenthe Formation has provided pollen spectra with extremely high values of herbs (pollen zone PW), characteristic of the Middle Weichselian (Pleniglacial).

5.2.1.4. Radiocarbon Dates

The new radiocarbon dates obtained for peat samples from the profile Amersfoort–De Liendert and for the special boring (32B/119 bis) (c.f. fig. 5.2) are given in table 5.2. Also the ^{14}C results are given which were obtained on different fractions of the material extracted from the sample during the chemical pretreatment.
The low activity in the extracted material indicates that the samples were virtually free from recent contaminants. This agrees with the fact that in the profile no signs were observed of leaching and humic infiltration from higher levels down into the sample level. Therefore there is a good probability that the material finally used for the enrichment was uncontaminated.

The five enrichment dates are consistent. Together with the pollenanalytical and stratigraphical evidence they suggest the existence of three Early Weichselian Interstadials shortly following each other.
A further discussion of the results and a comparison with dates for other localities are given in sect. 5.3.

5.2.2. Voorthuizen

5.2.2.1. Stratigraphy (by W. H. Zagwijn)

Voorthuizen, province of Gelderland (52° 10′ N Lat, 5° 37′ E Long), is situated in the eastern part of the Eem valley opposite Amersfoort (sect. 5.2.1). In 1969 near the village a large pit was made for extraction of sand for highway construction. Below about 8 m of sands, deposited in Late Weichselian and Middle Weichselian times, four peaty beds were exposed separated by sand-beds. The total thickness of this peaty and sandy complex was about 3.5 metres.

Table 5.2. Results from Amersfoort.

GrN	Sample Code	Depth (m)	Pollen zone	Measured activity (cpm)	Enrichment	Sample activity (pmc)[a]	Age (yrs BP)		δ^{13}_{PDB} (‰)
							2σ criterion	1σ criterion	
6884	II-1	6.61 – 6.69	EW Vc 1, 2	0.187 ± 0.019	10.82 ± 0.22	0.056 ± 0.006		60 100 $^{+\ 900}_{-\ 800}$	– 24.23
7040	II-2	6.98 – 7.10	EW IVa 2	0.133 ± 0.025	12.22 ± 0.24	0.035 ± 0.007		63 800 $^{+1700}_{-1400}$	– 27.80
6893	II-3	7.27 – 7.37	EW IVa 1	0.091 ± 0.015	8.06 ± 0.24	0.037 ± 0.006		63 500 $^{+1500}_{-1200}$	– 26.36
6930	III	8.33 – 8.43	EW IIa–EW Ib	0.094 ± 0.018	13.83 ± 0.41	0.022 ± 0.004		67 500 $^{+1800}_{-1400}$	– 29.55
7424	Eem-Weichsel I	12.04 – 12.30	EW Ia	0.027 ± 0.016	12.27 ± 0.37	< 0.016	> 70 400	76 400 $^{+6700}_{-3600}$	– 28.61
7377*	II-1 1st acid extr.			0.177 ± 0.021		0.41 ± 0.05		44 100 $^{+1000}_{-\ 900}$	– 25.37
7378*	II-1 1st alkali extr.			0.036 ± 0.028		< 0.21	> 49 300	56 800 $^{+11\,800}_{-4600}$	– 28.00
7150	II-1 11–14th alkali extr.			0.002 ± 0.037		< 0.25	> 48 200		– 28.51
7907*	II-2 8–9th alkali extr.			0.009 ± 0.022		< 0.12	> 53 800		– 28.23
7149	II-3 14–16th alkali extr.			0.007 ± 0.037		< 0.26	> 47 700		– 28.78
7906*	III 6th alkali extr.			0.010 ± 0.033		< 0.18	> 50 900		– 28.34
7951*	Eem-Weichsel 7–8th alkali extr.			0.0 ± 0.02		< 0.1	> 56 000		– 28.21

* counter GRADA

a percent of modern carbon

The pollen content of the peaty beds indicated very open, tundra-like conditions. A ^{14}C sample taken from the very top of the upper peat-bed (peat-bed I) resulted in: greater than 44 450 BP (GrN-5923); a date from the base of peat-bed III was: greater than 50 800 BP (GrN-5940). On the basis of this result, the pollenanalytical data and the general stratigraphy the peaty complex has been assigned to the lower part of the Middle Weichselian. Comparison with other sections showing peaty beds, dating from this part of the Weichselian, makes it probable that the complex under discussion belongs to the Moershoofd Interstadial (Zagwijn and Paepe, 1968). A large sample for ^{14}C enrichment was taken from a thin moss layer (peaty bed IV) at the very base of the peaty complex (335–341 cm below the top).

5.2.2.2. Pollen analysis (by T. A. Wijmstra)

The enrichment sample from Voorthuizen is taken from a moss layer in a predominantly sandy sequence. Above this moss layer two peat layers are found. For a detailed discussion of the vegetational succession see Kolstrup et al., 1977 (in press). The moss layer is formed by remnants of *Calliergon turgescens* (T. Jens) *Kindb.*, a moss with arctic distribution. The pollen found in this layer also point to an open vegetation with plant life only on favourable sites.
The palynological analysis of this layer does not give information on the stratigraphical position of the site, other than that this layer must have been developed under arctic conditions during the Weichselian.

5.2.2.3. Radiocarbon Dates

The enrichment date obtained together with two results on the extracted material are given in table 5.3.
The higher activity obtained for the extracted material of the last fractions is somewhat unexpected. The radiocarbon activity measured in the last fractions indicates that the final material might still be contaminated. The enrichment date is slightly younger than expected from stratigraphy and earlier radiocarbon dates.
A further discussion is given in sect. 5.3.

5.2.3. Odderade

5.2.3.1. Introduction (by F. R. Averdieck)

Odderade, known as a type locality of an Early Weichselian Interstadial (Averdieck, 1967), is a village near the western coast of Schleswig-Holstein. At 750 m west-

Table 5.3. Results from Voorthuizen.

GrN	Sample Code	Depth (m)	Measured activity (cpm)	Enrichment	Sample activity (pmc)	Age (yrs BP) 1σ criterion	δ^{13}_{PDB} (‰)
6821	VH IV	10.30	0.635 ± 0.021	9.17 ± 0.37	0.225 ± 0.012	49 000 ± 400	
7411*	VH IV 1st alkali extr.		0.129 ± 0.029		0.299 ± 0.067	46 600 $^{+2100}_{-1600}$	− 30.33
7379*	VH IV 4-6th alkali extr.		0.261 ± 0.032		0.606 ± 0.074	40 900 $^{+1100}_{-1000}$	− 30.34

* counter GRADA

north-west of the village centre, on the edge of the sandy uplands towards the marsh (the lowland of the river Miele), a sandpit exists. It is situated at 54° 8' 40'' N Lat and 9° 10' 48'' E Long; according to the Gauss-Krueger co-ordinate system, right 35 11 760, high 60 01 380, ordnance survey map (1:2500) 1821 Nordhastedt.

5.2.3.2. Stratigraphy (by F. R. Averdieck)

In 1960, two remarkably well preserved fossil podsolic soils, one lying upon the other, were discovered on the side of the pit. As the sands above the soils had been affected by a Weichselian periglacial congeliturbation, and Eemian soil occurred below the sand on Saalian till, the podsolic soils suggested themselves to be of interstadial origin. The pit is ditched in a series of sands covering the western flank of the slope, consisting of Saalian boulder clay, and submerging in the lowland below Holocene peat. By means of probings, the Saalian moraine district covered up by fen and sand turned out to have had a troubled morphology. Thus, a depression of −12 m (the lowland of the river Miele is about +2.5 m) stretches along and parallel to the verge bottom of the sandy uplands. Through the probings, it was discovered that the fossil soils visible in the pit continue in peat layers towards the former depression. The Saalian depression was filled up by a series of mud and peat layers over 8.5 m thick, with two intercalated sand layers. In 1962, the Geologisches Landesamt of Schleswig-Holstein carried out several core borings to obtain samples from the edge and the centre of the depression. Whereas on the edge (profiles 1–3) swamp peat overlain by raised bog peat was found alternated with sandlayers, the central boring (profile 5) produced a threefold succession of silting-up from gyttja to peat, each ending in raised bog peat. The intercalating sands in this area were, as expected, remarkably less thick than those on the verge.

Following the suggestion of the stratigraphic commission of the Deutsche Union Geologischer Wissenschaften (DUGW) to resume the research of stratigraphically significant type localities, four new borings were carried out near Odderade in 1974. They were made at the spot where the thickest organogene interstadial deposits could be expected (i.e. within the region of the old boring 5). The borings were supported by the DFG. Especially care was taken to obtain a sufficient quantity of sample material for ^{14}C dating. The lithology of the new cores obtained is shown in fig. 5.3. Material from cores 2 and 3 was used for radiocarbon dating at the Groningen Laboratory.

5.2.3.3. Pollen analysis (by F. R. Averdieck)

It has not yet been possible to perform the pollen analysis to the projected extent. Therefore, as a first step, the comparison between the new borings and the imme-

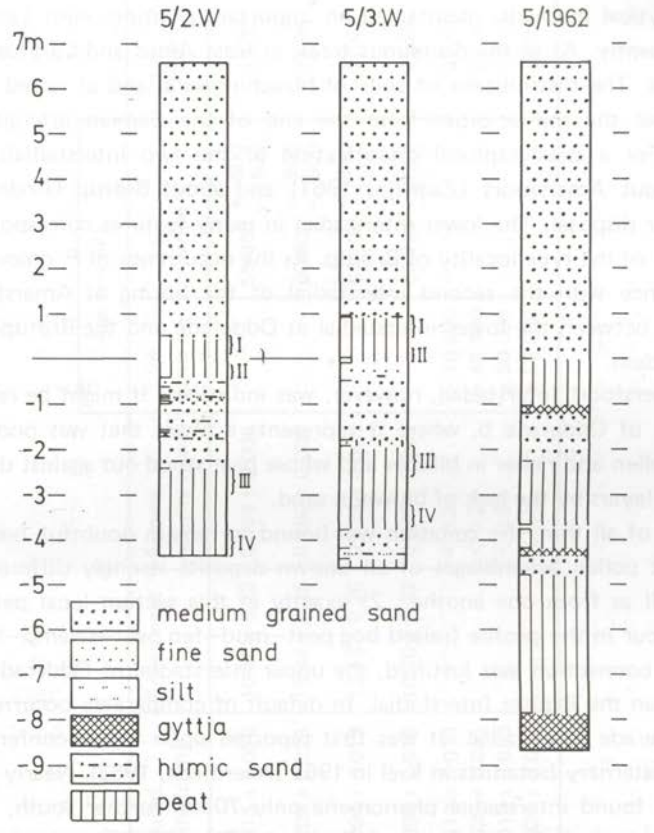

Fig. 5.3. Stratigraphy of the old boring 5 and the new borings 5/2W and 5/3W at Odderade. I to IV – enriched samples.

diately adjacent old profile 5 was guaranteed by survey diagrams (fig. 5.4). This old profile will be discussed.

The palynological analysis connected with lithological-pedological data brought forth the result that near Odderade Eemian deposits exist of sedimentary and sedentary nature from the time of *Corylus-Quercetum mixtum* (zone f according to Jessen and Milthers, 1928) until the end of the interglacial period; these deposits are overlain by two similar interstadial formations which are, however, clearly separated by sand beds.

Each interstadial peat bed was eroded during the following cold phase and buried under solifluction. This means that the first period of the development of vegetation only is reflected in the peat horizons.

In both interstadials the vegetation developed – corresponding to the fluctuating timber line – in quite a similar way: After a *Betula* phase *Pinus* and *Picea* became abundant. Among the latter genus the species *P. omorica*, which is determinable by

pollenanalytical methods, maintained an important position. Also *Larix* appeared more frequently. As to the deciduous trees, at least *Alnus* and *Corylus* remigrated to the area. The distribution of soils of bleaching sand and of raised bog growth characterizes the soil acidities from the end of the Eemian interglacial period onwards. For a stratigraphical classification of the two interstadials, the publications about Amersfoort (Zagwijn, 1961) and about Brørup (Andersen, 1961) were at our disposal. The lower interstadial in many features corresponded to the interstadial of the type locality of Brørup. As the occurrence of *P. omorica* was also in accordance with the second interstadial of the boring at Amersfoort 3, the parallelism between the lower interstadial at Odderade and the Brørup Interstadial seemed evident.

The Amersfoort Interstadial, however, was indistinct: it might be recognized in the profile of Odderade 5, where it represents a phase that was poorer in non-arboreal pollen and richer in birches and whose peat stood out against the over- and underlying layers by the lack of blown-in sand.

In spite of all that, the zonation was bound to remain doubtful, because 1) the Amersfoort pollen assemblages of all known deposits strongly differed from this one as well as from one another, 2) exactly in this section local petrographical changes occur in the profile (raised bog peat–mud–fen peat–swamp–forest peat). But if the connection was justified, the upper interstadial of Odderade had to be younger than the Brørup Interstadial. In default of comparable occurrences it was called Odderade Interstadial. It was first reported upon in the conference of the German quaternary botanists in Kiel in 1962 (Averdieck, 1963). Nearly at the same time, Selle found interstadial phenomena only 70 km further south, near Oerel, which were very similar to those of Odderade. Therefore, the parallel was easily drawn to the latter (Selle and Schneekloth, 1965). The correlation of the lower interstadials at the two sites with the Brørup Interstadial was, according to Schneekloth (1966), 'not to be rejected'. The minimum ages of both the localities found by ^{14}C measurements have not been in conflict with this interpretation.

5.2.3.4. Radiocarbon Dates

The new radiocarbon dates obtained for the peat samples indicated in fig. 5.3 are given in table 5.4.

The enrichment dates obtained are consistent. The samples II and I provide dates for the beginning and a developed phase of the Odderade Interstadial. The dates III and IV indicate an older interstadial with an age similar to the first interstadial at Amersfoort. The preliminary pollen analysis, however, indicates that samples III and IV belong to the pollen zones FW4 and FW2 respectively (c.f. fig. 5.4). These zones were paralleled with the Brørup and Amersfoort Interstadials respectively by Averdieck (1967). The lower peat bed in that case consists of material from two

Table 5.4. Results from Odderade.

GrN	Sample Code	Depth (m)	Pollen zone	Measured activity (cpm)	Enrichment	Sample activity (pmc)	Age (yrs BP) 2σ criterion	Age (yrs BP) 1σ criterion	δ^{13}_{PDB} (‰)
7054	5/2W + 5/3W, I	6.05 – 6.30 5.85 – 6.10	FW6	0.315 ± 0.020	10.85 ± 0.22	0.094 ± 0.006		55 900 $^{+\ 600}_{-\ 500}$	– 27.03
7123	5/2W + 5/3W, II	6.70 – 7.00 6.40 – 6.70	FW6	0.209 ± 0.023	13.44 ± 0.26	0.050 ± 0.006		60 900 $^{+\ 900}_{-\ 800}$	– 27.94
7077	5/2W + 5/3W, III	9.00 – 9.30 8.60 – 8.90	FW4	0.094 ± 0.019	13.13 ± 0.26	0.023 ± 0.005		67 100 $^{+1900}_{-1500}$	– 27.62
7442	5/2W + 5/3W, IV	10.60 – 10.85 10.00 – 10.30	FW2	0.056 ± 0.019	10.70 ± 0.32	0.017 ± 0.006		69 700 $^{+3300}_{-2300}$	– 29.98
7151	I alkali extr.			0.013 ± 0.038		< 0.29	> 46 900		– 27.44
7807*	II alkali extr.			0.028 ± 0.035		< 0.23	> 48 900		– 27.35
7808*	III alkali extr.			0.019 ± 0.033		< 0.20	> 50 000		– 27.13
7809*	IV alkali extr.			–0.024 ± 0.033		< 0.15	> 52 000		– 28.93

* counter GRADA

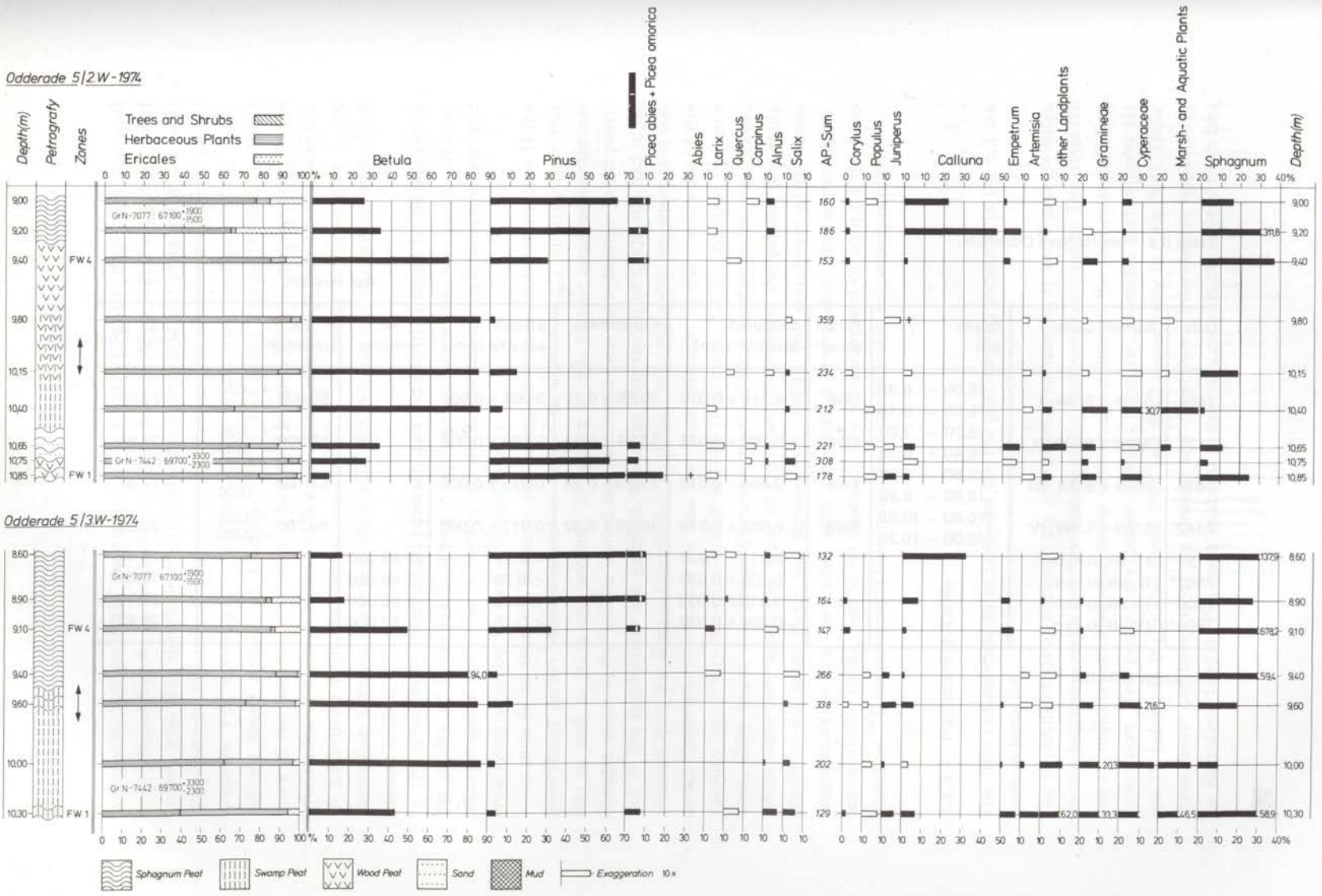
Odderade 5|2 W-1974
Depth(m)
Petrography
Zones
Trees and Shrubs
Herbaceous Plants
Ericales
Betula
Pinus
Picea abies + Picea omorica
Abies
Larix
Quercus
Carpinus
Alnus
Salix
AP-Sum
Corylus
Populus
Juniperus
Calluna
Empetrum
Artemisia
other Landplants
Gramineae
Cyperaceae
Marsh- and Aquatic Plants
Sphagnum
Depth(m)
Gr N-7077 : 67100 +1900 -1500
Gr N-7442 : 69700 +3300 -2300
FW 4
FW 1
9,00
9,20
9,40
9,80
10,15
10,40
10,65
10,75
10,85
160
186
153
359
234
212
221
308
178
311,8
30,7
Odderade 5|3 W-1974
8,60
8,90
9,10
9,40
9,60
10,00
10,30
132
164
147
266
338
202
129
94,0
137,9
678,2
59,4
21,6
20,3
62,0
33,3
46,5
58,9
Sphagnum Peat
Swamp Peat
Wood Peat
Sand
Mud
Exaggeration 10 x

Fig. 5.4. a. Pollen diagram of boring Odderade 5/1962.
b. Survey diagrams of the lower peat layer in boring 5/2W and 5/3W at Odderade.

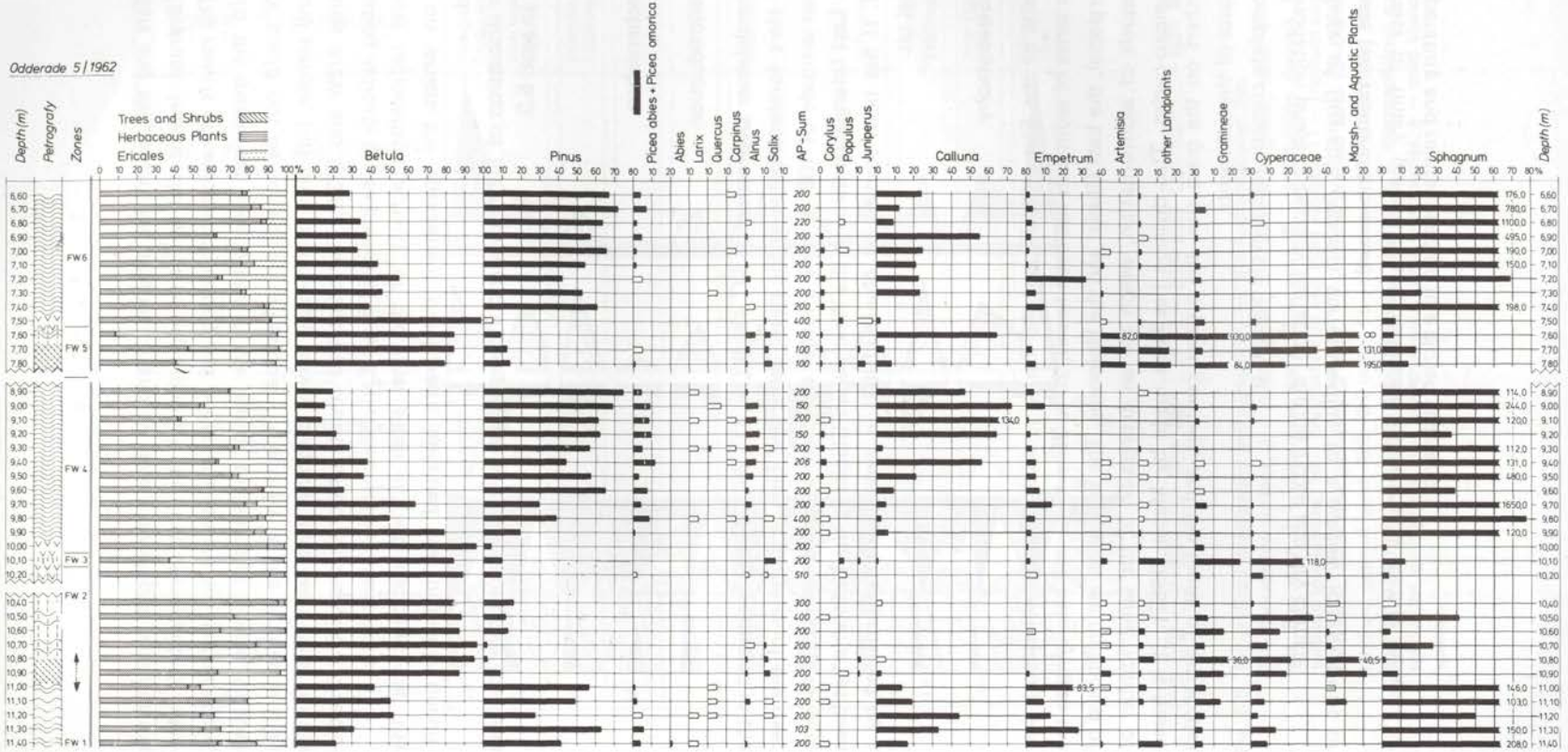

interstadials and the results for samples III and IV date a developed phase of the second (Brørup) Interstadial and the beginning of the first (Amersfoort) Interstadial. The results of radiocarbon dating and pollen analysis are not incompatible, because (i) the measuring uncertainty in the age of the samples is large, (ii) Odderade IV could not be corrected for residual ^{14}C activity in the anthracite CO_2 background sample, (iii) only preliminary survey diagrams have been made for the new borings 5/2W and 5/3W. The combined results of pollen analysis and radiocarbon dating indicate the existence of three Early Weichselian interstadials.

The low radiocarbon activity of the final alkali extracts indicates that the material on which the enrichment dates were obtained was probably uncontaminated.

A further discussion of the results and a comparison with dates for other localities are given in sect. 5.3.

5.2.4. Aschersleben

5.2.4.1. Introduction

The Aschersleben Depression (≈ 51° 47′ N Lat, 11° 25′ E Long) is situated in the northern Harz foreland between the rivers Selke and Eine, tributaries of the river Elbe, at an altitude of 108 m. Here a rather complete series of sediments ranging from the Last Interglacial through the Weichselian Glacial to the Holocene has been preserved. It has been studied by Mania (1967) in large exposures provided by a brown coal pit.

5.2.4.2. Stratigraphy

On deposits of the Elster Glacial and the Tertiary, showing a distinct denudation surface, a series of sediments has been found, 20 to 25 m thick and belonging to the Last Interglacial, the Last Glacial and the Holocene. The sediments are composed of eleven sequels of sedimentation, which are an expression of the same number of climatic micro-cycles. This division has been made by Mania (1967). It is based among others on the grain size, the organic content, and the fauna of ostracodes and molluscs of the sediments.

One complete climatic micro-cycle consists of:

(i) a denudation phase (especially deflation) during a cold and dry climate.
(ii) a phase of fluviatile deposits corresponding to a gradual improvement of climate (warmer and more rain).
(iii) a phase of finely grained limnic sediments caused by a further increase of temperature and rainfall leading to a closed vegetation.

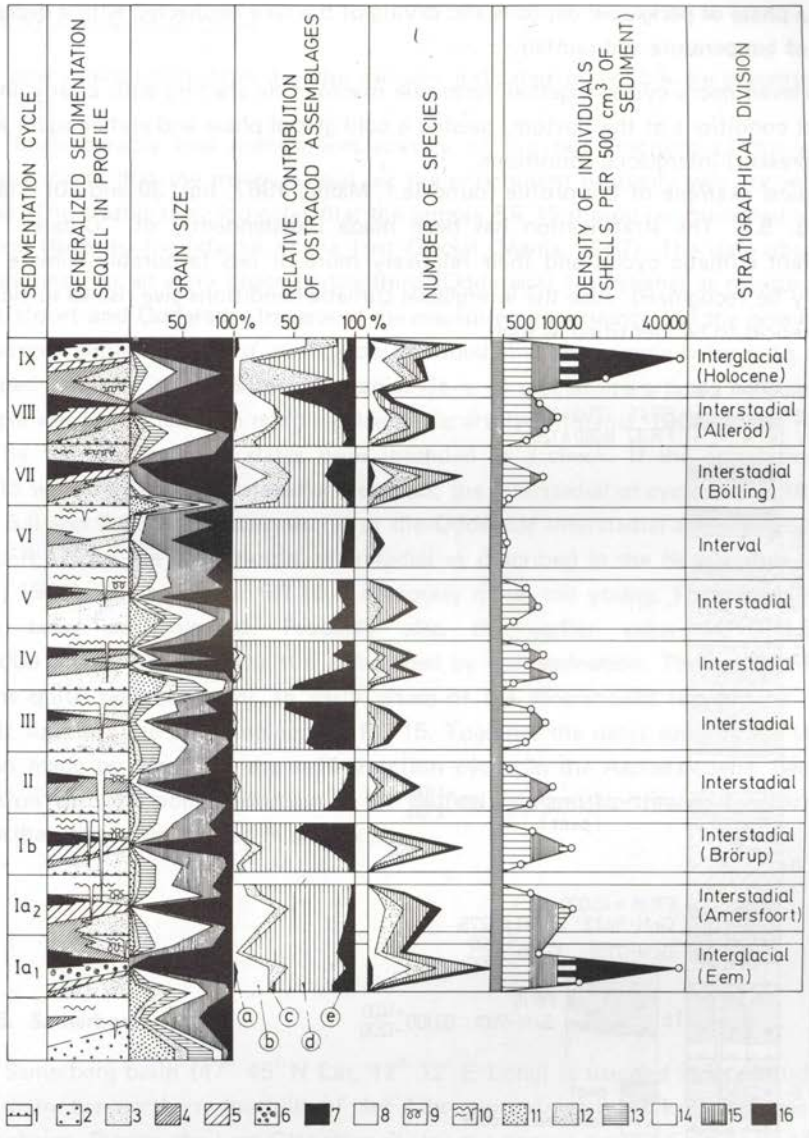

Fig. 5.5. Generalized stratigraphy and periodicity for the Ascherslebener See.
1 – denudation surface, 2 – sandy gravel, 3 – sand with gravel, sand, 4 – sand and silt, 5 – clay, 6 – calcareous ooze, 7 – peat, 8 – solifluction deposit, 9 – cryoturbatic involutions, 10 – cryoturbation and frost wedges, 11 – medium coarse gravel (> 6 mm), 12 – fine gravel (6–2 mm), 13 – coarse grained sand (2–0.6 mm), 14 – medium grained sand (0.6–0.2 mm), 15 – fine sand (0.2–0.06 mm), 16 – silt and clay (< 0.06 mm), a – warm stenothermous species, b – thermophilous species, c – species of spring-time, d – eurythermous persistent species, e – cold stenothermous species.

(iv) a phase of periglacial deposits and drying of the lake connected with a decrease of temperature and rainfall.

The eleven micro-cycles together form one macro-cycle starting with clearly interglacial conditions at the bottom, passing a cold glacial phase and ending again with (the present) interglacial conditions.

A typical example of the profile found (c.f. Mania, 1967, figs. 39 and 40) is given in fig. 5.5. The stratification has been made independently of ^{14}C dates. The different climatic cycles and their relatively more or less favourable climate can clearly be recognized. Also the interglacial climatic conditions give rise to sufficient differences to be identified as such.

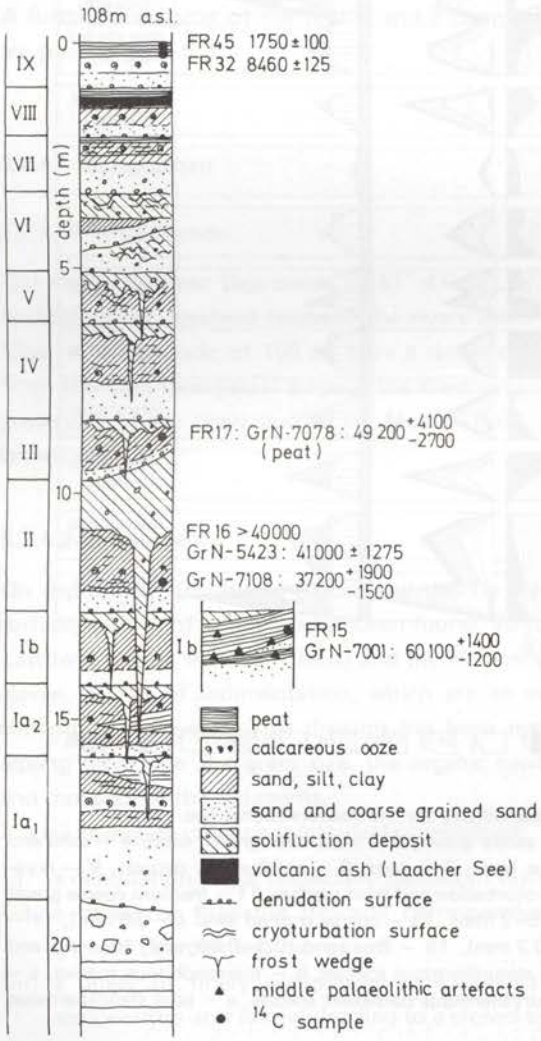

Fig. 5.6. Stratigraphy of the sampled profile Aschersleben.

5.2.4.3. Radiocarbon Dates

The new radiocarbon dates for the samples indicated in fig. 5.6 are presented in table 5.5.
The unmeasurably low radiocarbon activity of the two fractions of the alkali extract shows that the material used for the enrichment probably was uncontaminated. The stratigraphy indicates that the sample FR 15 should be attributed to the second (Brørup) Interstadial of the Last Glacial (Mania, 1967). The date obtained corresponds to an early phase of the third (Odderade) Interstadial as measured at Amersfoort and Odderade. In view of the measuring uncertainty and the possibility of sample contamination it cannot be excluded that the sample belongs to a developed phase of the Brørup Interstadial. It is of special importance because the sample was associated with middle-palaeolithic artefacts (Mania, 1967).

The two conventional dates were intended as a check. If the correlation of FR 15 with the Brørup Interstadial is correct, the interstadial of cycle II (FR 16; c.f. figs. 5.5 and 5.6) should correspond to the Odderade Interstadial and that of cycle III (FR 17) to the Moershoofd Interstadial as described in the Netherlands (Zagwijn, 1961). The result for FR 16 is obviously much too young. The sample must have been contaminated. Probably also the earlier value of GrN-5423 (41 000 ± 1275 yrs BP) was still influenced by contamination. The age of FR 17 seems quite reasonable for an early phase of the Moershoofd Interstadial. This result supports the one obtained on FR 15. Together the dates support the correlation made by Mania of the sedimentation cycles in the Aschersleben See Depression with the pollen zonation in the Netherlands and North-west Germany.
A further discussion is given in sect. 5.3.

5.2.5. Samerberg

The Samerberg basin (47° 45′ N Lat, 12° 12′ E Long) is situated at an altitude of 600 m in the northern foothills of the Alps approximately 15 km south-east of Rosenheim. During the Last Glaciation it was the tongue basin of a branch of the Inn glacier.

5.2.5.1. Lithostratigraphy (by E. Grüger)

About 19 m of pollen containing fine sands and silts belonging both to an interglacial and to the early part of a succeeding glaciation are lying on till from an older glaciation. This sequence is covered by 2 to 3 m of till from the Last Glaciation.

Table 5.5. Results from Aschersleben.

GrN	Sample Code	Depth (m)	Measured activity (cpm)	Enrichment	Sample activity (pmc)	Age (yrs BP) 2σ criterion	Age (yrs BP) 1σ criterion	δ^{13}_{PDB} (‰)
7001	FR 15	15	0.152 ± 0.023	8.83 ± 0.35	0.056 ± 0.009		$60\,100\ ^{+1400}_{-1200}$	− 28.75
7108*	FR 16	14	0.129 ± 0.027		0.97 ± 0.20		$37\,200\ ^{+1900}_{-1500}$	− 23.94
7078	FR 17	8.70	0.068 ± 0.027		0.22 ± 0.09		$49\,200\ ^{+4100}_{-2700}$	− 23.45
7616**	FR 15 1st alkali extr.		−0.023 ± 0.032		< 0.15	> 52 300		− 28.28
7381**	FR 15 9 + 10th alkali extr.		0.018 ± 0.023		< 0.15	> 52 200		− 28.65

* counter LZ; A_o = 13.27 cpm
** counter GRADA

5.2.5.2. Pollen analysis (by E. Grüger)

The basal part of the sediments shows a complete interglacial vegetational cycle characterized by high values of mixed-oak forest and hazel, the early expansion of spruce, a *Taxus* phase and finally a fir, spruce, horn-beam phase. A similar vegetational development was found in Zeifen and Eurach in the Alpine foreland of Bavaria (Jung et al., 1972; Beug, to be publ.). There it was attributed to the Riss-Würm Interglacial. The overlying early glacial sediments are approximately 18 m thick. They comprise three forest phases, which most likely represent three interstadials, and the corresponding stadial periods. Although the pollen flora of the

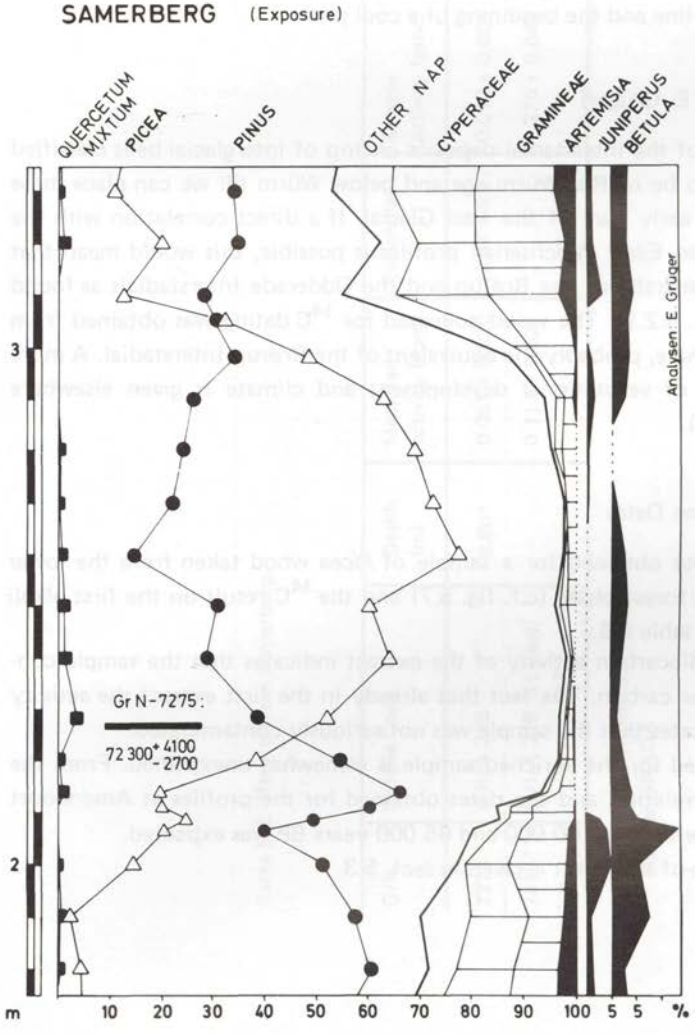

Fig. 5.7.

Pollen diagram for the second forest phase at Samerberg.

stadials is very similar, the interstadials can be discerned on basis of their vegetational development. The simplified pollen diagram of the middle forest phase is given in fig. 5.7.

After a rather long period with open vegetation, characterized by relatively high values of NAP with regular occurrence of *Artemisia, Helianthemum, Thalictrum, Selaginella selaginoides* etc., the forest vegetation in this area begins with a slight increase of *Betula* and *Juniperus* values. During the following expansion of *Pinus* the NAP values decrease to less than 5%. After this *Picea* becomes dominant. Apart from these conifers also pollen of *Larix* and the different species of the mixed-oak forest (especially *Quercus*) was found in small numbers. *Abies* pollen is completely missing. A subsequent increase of the NAP values above the 3 m level reflects the lowering of the tree-line and the beginning of a cool phase.

5.2.5.3. Dating (by E. Grüger)

From the position of the interstadial deposits on top of interglacial beds classified on good evidence to be of Riss-Würm age and below Würm till we can place these interstadials in the early part of the Last Glacial. If a direct correlation with the North-west European Early Weichselian profiles is possible, this would mean that we have here the Amersfoort, the Brørup and the Odderade Interstadials as found in Amersfoort (sect. 5.2.1). The wood collected for ^{14}C dating was obtained from the second forest phase, probably the equivalent of the Brørup Interstadial. A more detailed discussion of vegetational development and climate is given elsewhere (Grüger, to be publ.).

5.2.5.4. Radiocarbon Dates

The enrichment date obtained for a sample of *Picea* wood taken from the lower part of the middle forest phase (c.f. fig. 5.7) and the ^{14}C result on the first alkali extract are given in table 5.6.

The measurable radiocarbon activity of the extract indicates that the sample contained some younger carbon. The fact that already in the first extract the activity was rather low indicates that the sample was not seriously contaminated.

The date obtained for the enriched sample is somewhat unexpected. From the pollenanalytical correlation and the dates obtained for the profiles at Amersfoort and Odderade an age between 60 000 and 65 000 years BP was expected.

A further discussion of the result is given in sect. 5.3.

Table 5.6. Results from Samerberg.

GrN	Sample Code	Depth (m)	Measured activity (cpm)	Enrichment	Sample activity (pmc)	Age (yrs BP) 1σ criterion	δ^{13}_{PDB} (‰)
7275	F II/A 226	8.80*	0.051 ± 0.020	13.41 ± 0.27	0.012 ± 0.005	$72\,300\ ^{+4100}_{-2700}$	− 24.82
7415**	F II/A 226 1st alkali extr.		0.117 ± 0.021		0.270 ± 0.048	$47\,500\ ^{+1600}_{-1300}$	− 26.43

* depth below Würm till
** counter GRADA

5.2.6. Murnau–Penzberg area

5.2.6.1. Introduction (by Peter Peschke)

The presence of lignites in the Murnau–Penzberg area is a well-known fact. Generally we find rather thin seams (approximately 20–50 cm) of strongly compressed woodpeat with abundant remains of wood. The lignite seams are exposed in several gravel pits and especially within the last few years during the construction of a new highway they have also been found in several other places. The most prominent lignite seam known today (thickness about 200 cm) is located at Grossweil. It has been mined for many years. According to the pollenanalytical investigations by H. Reich (1953) these lignites were looked upon as being deposits of a warm period and they were attributed to the Last Interglacial. Until recently they were considered to be the only definite proof of the existence of this interglacial in the northern Alpine foreland. All other lignites found in this area were held as being an equivalent of those of Grossweil.

5.2.6.2. Geography (by Peter Peschke)

The lignites described here are those of *Breinetsried, Höfen* and *Pömetsried.* They are all located in the glacial tongue basins of the former Kochelsee and Loisach glaciers respectively, being parts of the Isar foreland-glacier. They are met with at an altitude between 600 and 650 m above sea level (fig. 5.8).

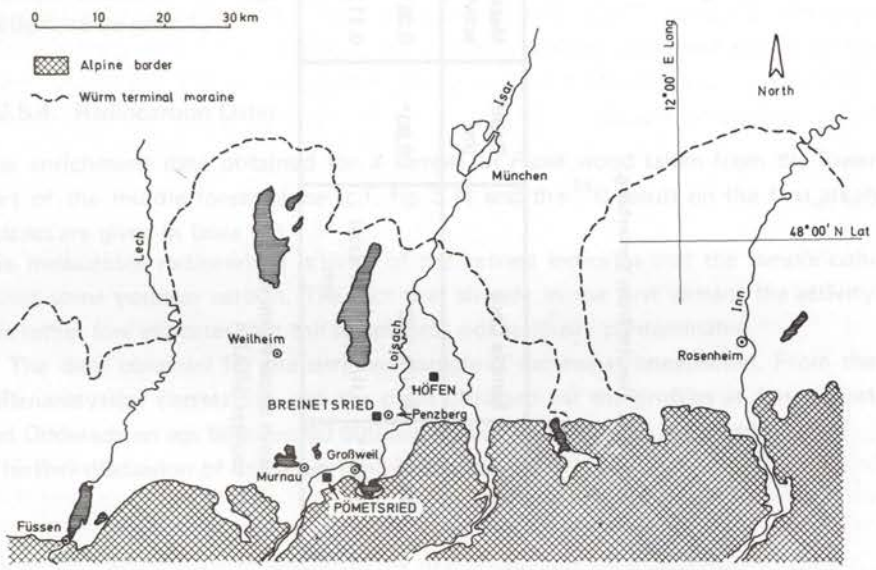

Fig. 5.8. The Murnau–Penzberg area.

The lignite seams were exposed in gravel pits (Breinetsried, Höfen) or came to light during road construction (Pömetsried). Always the lignite seams were easily accessible. This enabled us to obtain samples of good quality in an amount sufficient for pollen analysis and radiocarbon dating.

The lignite seams of Breinetsried and Höfen are intercalated in outwash gravels, the lignite of Pömetsried cropped out in the upper part of a very thick layer of lacustrine clays. Several prominent east-west oriented Molasse ridges prevented the erosion of these sediments of a warmer climate by the Loisach and Kochelsee glaciers during pleniglacial times (as to a more detailed geological information see Zeil, 1954; Jerz, 1969).

5.2.6.3. Stratigraphy (by Peter Peschke)

a. Breinetsried

The lignite seam has a thickness of 45 cm and consists mainly of woodpeat with many remnants of brown mosses and of *Cyperaceae*. It is situated between layers of bluish grey clay. Only the clay layers adjacent to the lignite contain pollen in amounts sufficient for analysis. On top of the uppermost clay which has a thickness of approximately 20 cm several metres of gravel occur, which are covered by Würm till. Due to glacial tectonics the gravel bed has been tilted seriously in several places. The pebbles of the gravel bed mainly consist of Alpine limestone, igneous material being rare (Stephan, 1970). The clay and silt layer below the lignite is approximately 30 cm thick and gradually changes into medium and coarse grained sands followed by a gravel bed of approximately 3 m thickness. Below this one finds Oligocene Molasse deposits.

b. Pömetsried

The lignite seam of approximately 20 cm thickness was exposed during the construction of a highway bridge. It consists of woodpeat with remnants of brown mosses like that of Breinetsried. The lake sediments above have a thickness of 20–30 cm and are overlain by gravel and till which, however, have been removed during the highway construction. The clay deposit below the lignite has a thickness of more than 30 m. Because there are up to now no borings at our disposal and because only a few exposures are available, the exact thickness of these sediments and the position of the Flysch bedrock is unknown. Geologists have long considered the clay deposit to be of interglacial origin (Zeil, 1954). Preliminary pollen-analytical investigations of the upper 5 m of these sediments (Peschke, unpubl.) gave, however, no indication of an interglacial forest vegetation.

c. Höfen

The exposure in the gravel pit of Höfen is a remarkable one. The investigated lignite seam has a thickness of 25 cm. It runs horizontally and has not been disturbed by glacial tectonics. The same holds true for the overlying and underlying gravel beds. The lignite consists once more of woodpeat with remnants of brown mosses and of *Cyperaceae.*

Above and below the lignite seam one finds approximately 30 cm of yellowish brown sandy silt, respectively silty sand (fig. 5.9), which proved to be nearly devoid of pollen grains. The gravel bed above the lignite is several metres thick and in many places forms a 'Nagelfluh'-like conglomerate. This gravel bed is covered by Würm till and melt water deposits.

Below the lignite seam and its underlying silty sand a coarse gravel occurs, the uppermost layers of which are strongly weathered. The colour of this weathering horizon is reddish yellow. It is strongly enriched in clay and silt. Below this horizon the normal pro-glacial gravel deposit, consisting of Alpine limestone pebbles, is cropping out (Stephan, 1970).

Recently a boring in the gravel pit revealed the stratigraphy of the underlying deposits (fig. 5.9, thanks to the Bayerisches Geologisches Landesamt, Munich). Thick clay and silt layers are alternating twice with tills containing many striated boulders. The palynological investigation of the lake sediments still in progress does not warrant the view of an interglacial age of these sediments (see sect. 5.2.6.4.).

5.2.6.4. Pollenanalytical investigations (by Peter Peschke)

After prolonged soaking in 10% HNO_3 the lignite material was subjected to normal pollen preparation methods. For peat samples with a high mineral content and for clay samples 45% HF had to be used. Samples were taken each 5 cm. Contamination by younger or older material was thoroughly avoided by cutting away several centimetres thick outer layers of the peat monoliths. The results given in the pollen diagrams are based upon the total pollen sum (arboreal pollen (AP) plus non-arboreal pollen (NAP) averaging 100%). Spores are not included in the pollen sum.

a. Breinetsried

The pollen diagram of Breinetsried covers a length of 65 cm (fig. 5.10.a). It comprises not only the lignite seam proper but parts of the silts and clays above and below, the pollen content of which was high enough to enable pollenanalytical work. The NAP amounts to 50% of the pollen sum with a strong preponderance of *Cyperaceae*. Among the AP *Pinus* strongly predominates (repeatedly about

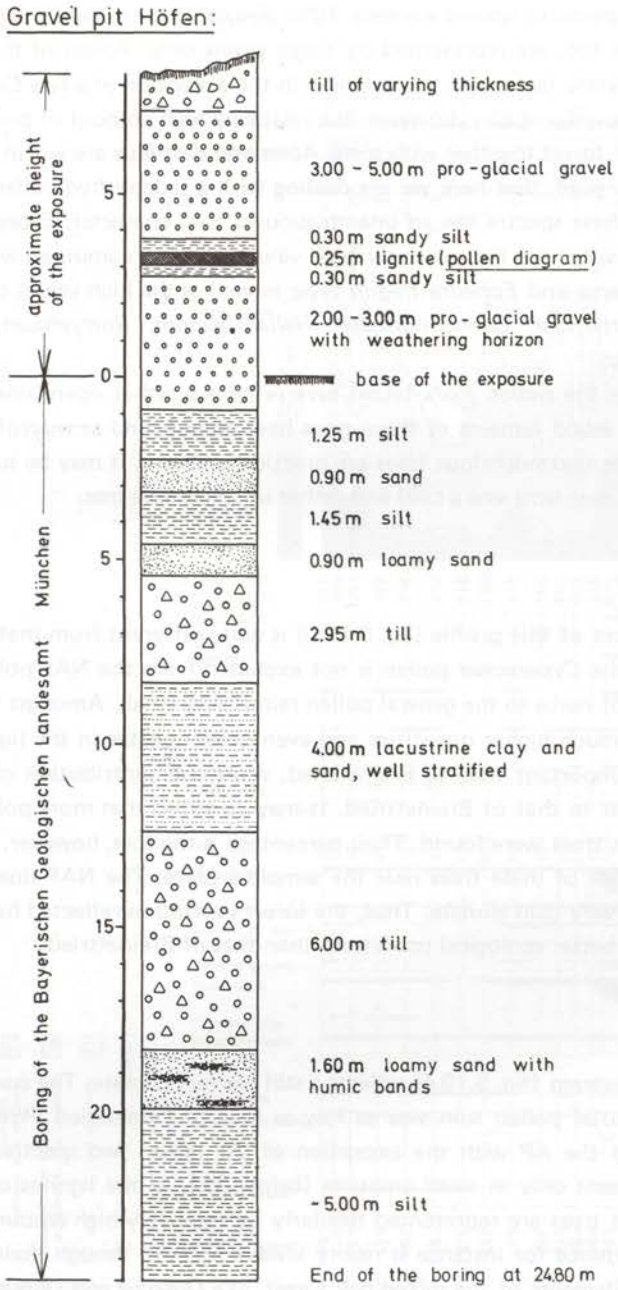

Fig. 5.9. Stratigraphy in the exposure and boring Höfen.

80–90%). Second in importance is *Picea*, which shows an uninterrupted curve, but only in one spectrum spruce exceeds 10%. *Betula*, and in the upper part of the diagram *Alnus* too, are represented by single grains only. Pollen of thermophilous trees is completely lacking in the lignite with the exception of a few *Corylus* pollen grains. In the overlying clay, however, the relatively high amount of pollen grains of the mixed-oak forest together with some *Abies* and *Carpinus* are worth mentioning. It should be argued, that here we are dealing with a redeposited pollen flora, since the NAP of these spectra has an unambiguously cool character. Especially significant in this respect are the relatively high values of *Salix* combined with the presence of *Juniperus* and *Ephedra fragilis*-type as well as the high values of heliophilic herbs like *Artemisia, Chenopodiaceae, Helianthemum, Botrychium, Selaginella selaginoides* etc.

As a whole the pollen flora found here reflects a rather open pine forest with some spruce; wood remains of these trees have been found as macrofossils (Jung, unpubl.). Since thermophilous trees are practically absent, it may be suggested that the climate at that time was a cold and rather unfavourable one.

b. Pömetsried

The pollen flora of this profile (fig. 5.10.b) is quite different from that of Breinetsried. Even if the *Cyperaceae* pollen is not excluded from the NAP pollen sum, the contribution of herbs to the general pollen rain is very small. Amongst the AP *Picea* is present in much higher quantities and even predominates in the lignite spectra. *Pinus* is less important than in Breinetsried, while the contribution of *Betula* and *Alnus* is similar to that of Breinetsried. It may be added that more pollen grains of thermophilous trees were found. Their percentage is too low, however, to prove the former existence of these trees near the sampling place. The NAP does not favour the view of a very cold climate. Thus, the forest vegetation reflected here may have existed under better ecological conditions than that of Breinetsried.

c. Höfen

This pollen diagram (fig. 5.10.c) reflects a still warmer climate. The contribution of NAP to the total pollen sum was as low as that of Pömetsried. *Picea* dominates again amongst the AP with the exception of the upper two spectra. *Betula* and *Alnus* are present only in small amounts (below 3%). In the lignites of Höfen, the thermophilous trees are represented regularly by relatively high amounts. Pollen of *Abies* and *Carpinus* for instance is nearly always present, though their percentages remain low. Elements of the mixed-oak forest, like *Quercus* and *Ulmus*, are present rather regularly. *Tilia* is rare, *Fraxinus* and *Acer* are lacking. Among the NAP heliophytes and so called 'glacial indicators' were either only weakly represented or

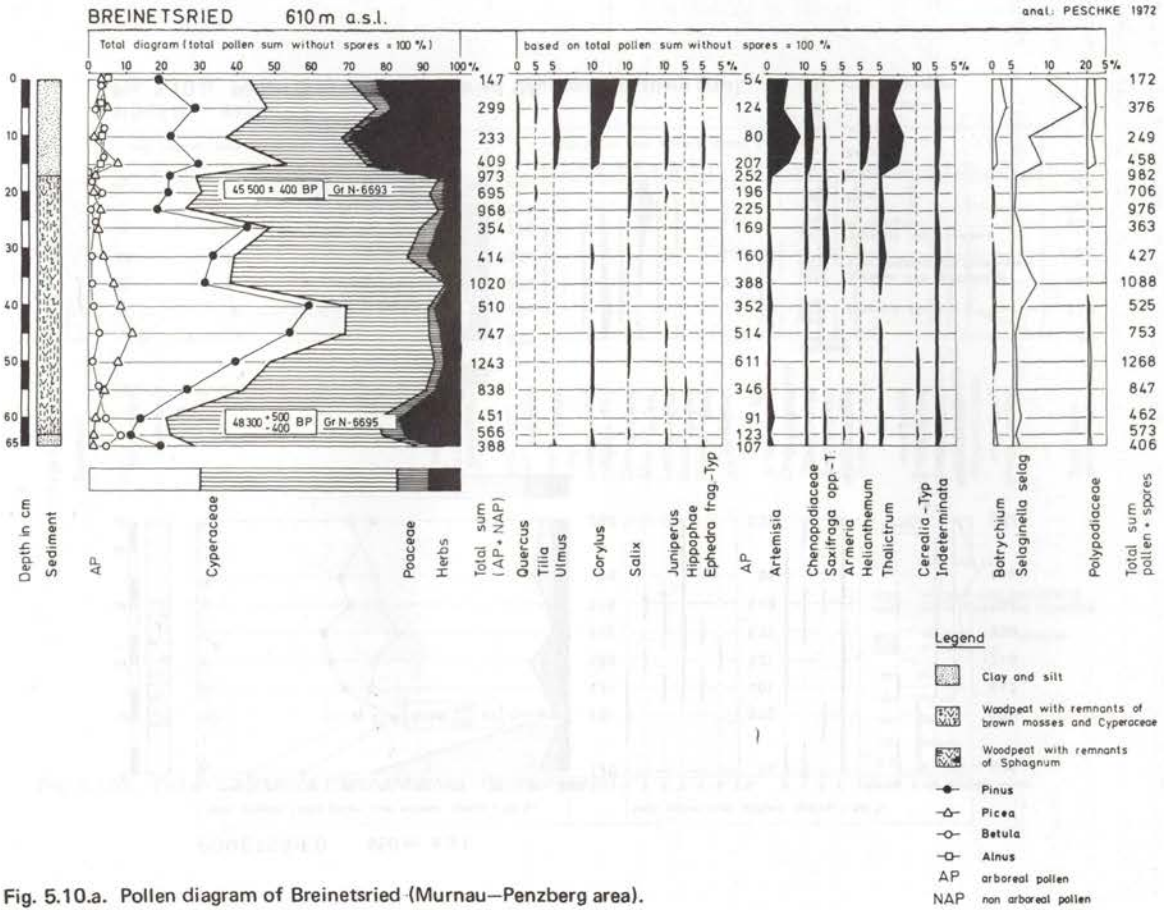

Fig. 5.10.a. Pollen diagram of Breinetsried (Murnau–Penzberg area).

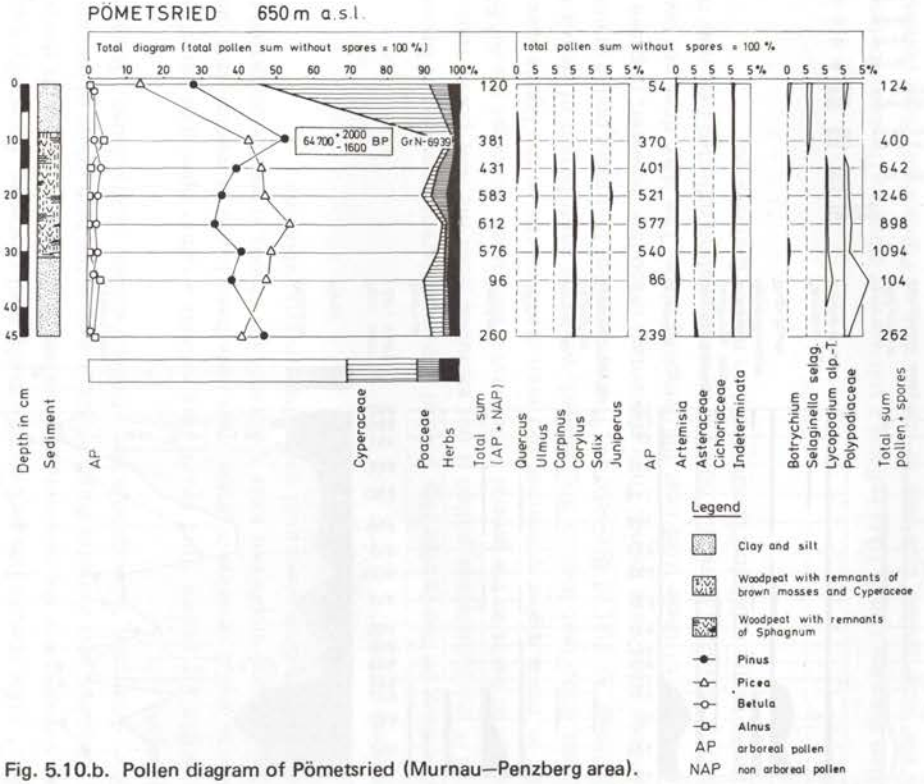

Fig. 5.10.b. Pollen diagram of Pömetsried (Murnau—Penzberg area).

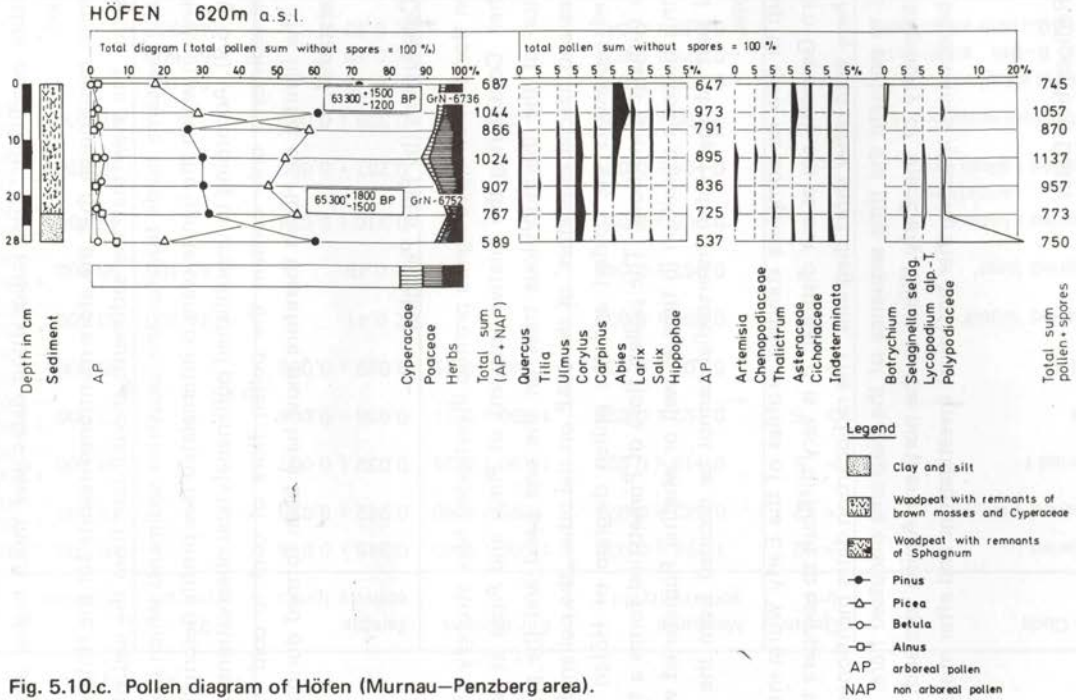

Fig. 5.10.c. Pollen diagram of Höfen (Murnau–Penzberg area).

could not be detected regularly. So it should be suggested that the climate then was much better than during the formation of the Pömetsried or Breinetsried woodpeats, respectively. Yet the composition of the forest at Höfen can only be sketched very tentatively. Probably we have to deal with a spruce–pine forest with some larch and fir. Some thermophilous trees seem to have thrived under edaphically favourable conditions. Two radiocarbon dates gave much higher ages than at Breinetsried.

It is worth mentioning that the afore-mentioned results for the Höfen exposure do not favour the view that the sediments should date from the end of the Last Interglacial. The same holds true for the lacustrine sediments which underlie the glacial gravels in which the lignite seam is intercalated (see profile description of the boring, fig. 5.9). According to unpublished pollenanalytical observations by Frenzel these lake sediments only contain the pollen flora of cool to cold interstadial climates. The lignites of Höfen therefore must have been formed during an Early Würm interstadial.

5.2.6.5. Conclusions (by Peter Peschke)

The pollen floras of all three lignite profiles investigated here strongly differ from one another. Considering the relative amounts of *Pinus* and *Picea* as well as the contribution of the thermophilous trees on the one hand and the presence of heliophytes and 'glacial indicators' of the NAP on the other, the pollen diagram of Breinetsried represents the coldest and the pollen diagram of Höfen the most temperate climatic conditions. The pollen flora of Pömetsried forms a transition. Whether this means a transition in time as well or whether Pömetsried was rather the initial part of the Höfen Interstadial cannot be decided from the botanical record alone.

Since up to now no complete standard profiles of the Early Würm interstadials in Southern Germany are at our disposal, it is very difficult to compare the results obtained here with other short diagrams. The radiocarbon dates mentioned are very important to evaluate the time sequence of the diagrams discussed here. A precise pollen stratigraphy of the Early Würm in the northern Alpine foreland, however, can only be obtained after further botanical investigations and after more absolute dates.

5.2.6.6. Radiocarbon Dates

The enrichment and recent conventional radiocarbon dates for samples of the lignites from Breinetsried, Pömetsried and Höfen are given in table 5.7. In the same table the ^{14}C results on material extracted from the enrichment samples during chemical pretreatment are listed.

Table 5.7. Results from the Murnau–Penzberg area.

GrN	Sample Code	Depth (m)	Measured activity (cpm)	Enrichment	Sample activity (pmc)	Age (yrs BP) 2σ criterion	Age (yrs BP) 1σ criterion	δ^{13}_{PDB} (‰)
6693	Breinetsried I	≈ 12	1.176 ± 0.030	11.06 ± 0.40	0.345 ± 0.015		45 500 ± 400	− 29.43
6695	Breinetsried VII	≈ 12	0.742 ± 0.029	9.96 ± 0.40	0.242 ± 0.013		48 300 $^{+\ 500}_{-\ 400}$	− 30.39
6939	Pömetsried I	≈ 5	0.116 ± 0.025	11.90 ± 0.24	0.032 ± 0.007		64 700 $^{+2000}_{-1600}$	− 27.19
6736	Höfen I	> 5	0.122 ± 0.020	10.50 ± 0.21	0.038 ± 0.006		63 300 $^{+1500}_{-1200}$	− 27.94
6752	Höfen III	> 5	0.103 ± 0.020	11.40 ± 0.22	0.029 ± 0.006		65 300 $^{+1800}_{-1500}$	− 28.95
6278	Breinetsried 'wood'		0.057 ± 0.034		< 0.41	> 44 200	50 500 $^{+7300}_{-3800}$	− 28.40
6476	Breinetsried 'peat'		0.057 ± 0.040		< 0.45	> 43 400	50 500 $^{+9700}_{-4300}$	− 28.82
6681	Breinetsried I before enrichment		0.095 ± 0.023		0.310 ± 0.074		46 300 $^{+2200}_{-1700}$	− 29.43
7620*	Breinetsried I alkali extr.		0.124 ± 0.021		0.287 ± 0.050		46 900 $^{+1500}_{-1300}$	− 29.85
6723	Höfen I before enrichment		0.100 ± 0.020		0.325 ± 0.063		46 000 $^{+1700}_{-1400}$	− 27.94
7619*	Höfen I 1st alkali extr.		−0.064 ± 0.026		< 0.12	> 54 100		− 27.88
7618*	Höfen I 6–9th alkali extr.		−0.075 ± 0.021		< 0.10	> 55 600		− 28.27
7380**	Höfen I 10–14th alkali extr.		0.035 ± 0.047		< 0.30	> 46 500		− 28.84

* counter GRADA
** counter I

The dates for the lignite seam at Höfen suggest that this interstadial deposit corresponds to the second (Brørup) Interstadial at Amersfoort (c.f. sect. 5.2.1).

The top of the lignite seam at Pömetsried is somewhat (although not significantly) older than the top of the lignite at Höfen. The dates obtained up till now suggest that both lignite seams belong to the same interstadial. A further date on the bottom section of Pömetsried, which is presently in preparation, might enable us to decide whether this is true or whether Pömetsried belongs to an older (the first) interstadial. The ages agree with the results of the pollen analysis and stratigraphy indicating an early glacial interstadial age for both. The deviations between the pollen diagrams may be caused by small differences in the position of the sample localities, by formation of the lignites during different phases of the same interstadial or by the fact that we really have two different interstadials.

The dates for the lignite of Breinetsried place its formation after the first main cooling of the Last Glacial. They resemble conventional dates obtained for a rather cool and weak interstadial described at Moershoofd in the Netherlands (Zagwijn and Paepe, 1968). This correlation is favoured by the cool character of the pollen diagram. The reliability of the enrichment dates for Breinetsried is supported by the similar age obtained for the extracted material (GrN-7620) and by three conventional dates. The first two were obtained from the middle part of the lignite seam. One sample was subjected to a rigorous ('wood'), the other to a less rigorous ('peat') chemical pretreatment. Both results show, that the samples contain no statistically significant ^{14}C activity. The third result on CO_2 from sample I prior to enrichment (GrN-6681) is within standard deviation of the enrichment date. An earlier routine date for Breinetsried (GrN-4998; 42 570 ± 1160, Vogel and Waterbolk, 1972) is somewhat younger. In spite of the good agreement between residue and extracted material for this sample some contamination may have persisted.

The results for the material extracted from Höfen I indicate that the sample was virtually uncontaminated, as was expected from the stratigraphy. The result prior to enrichment is not in serious disagreement with the above, considering the fact that it was measured in a period of unstable background.
A further discussion of the results and a comparison with other enrichment dates are given in sect. 5.3.

5.2.7. Mauern

5.2.7.1. Introduction (by A. Brande)

The pollen-bearing part of the profile Mauern I (circa 30 km N of Rennertshafen, 48° 46' N Lat, 11° 03' E Long) in the ancient Danube valley of Wellheim represents a sequence of more or less fluvial sediments with two main peat layers (strata 3 and

6). It lies on Danube gravel material, correlated till now with the Rissian glaciation complex, and below colluvial loess loam of last glacial age. The AP diagram (fig. 5.11) shows the tree vegetation changes of stadial-like and interstadial periods with high percentages of redeposited pre-quaternary and thermophilous pollen in the minerogenic strata. Main features of the total pollen diagram are zonation changes of the valley floor vegetation following the peat formation of the interstadial periods.

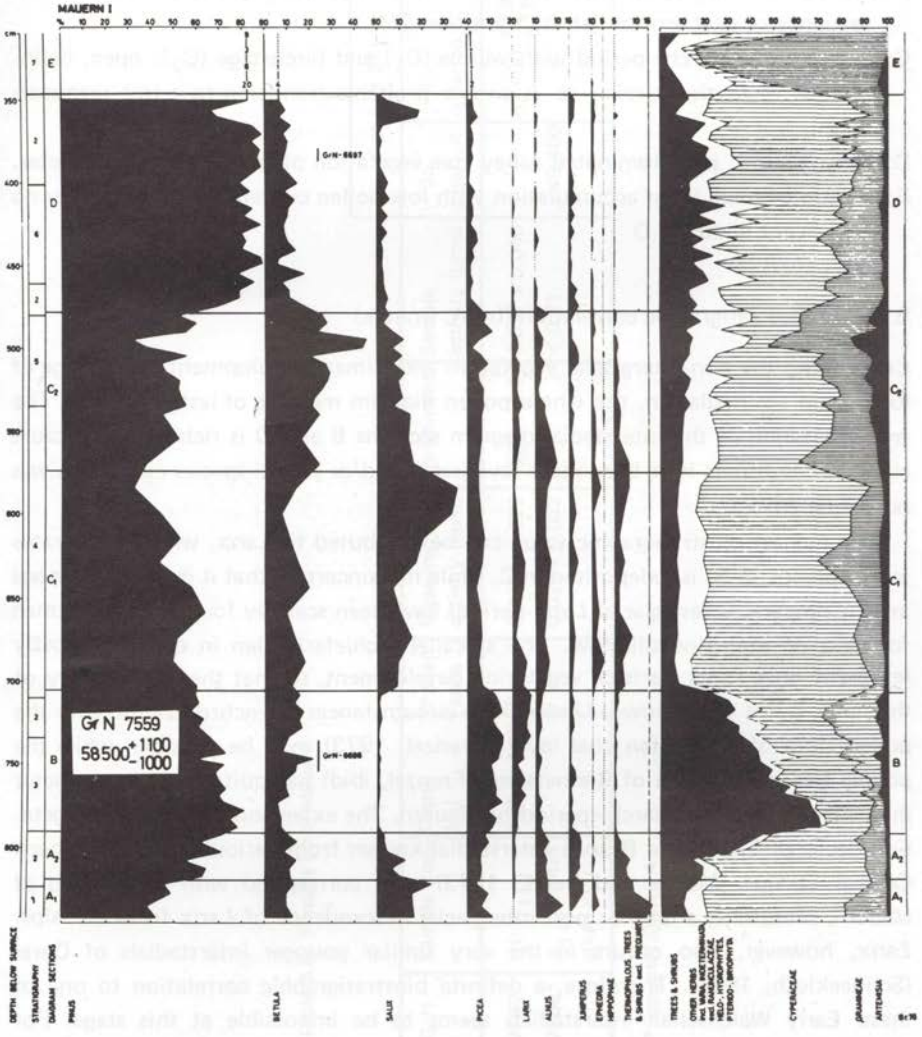

Fig. 5.11. Simplified AP and total pollen diagram of the profile Mauern I (Brande, 1975). Stratigraphy: 1 – sand with gravel, 2 – alluvial loam, partly humic/peaty, 3 – sedge peat, 4 – alluvial loam with sand layers, 5 – alluvial loam, mud-like, 6 – Bryales-peat, clayey, 7 – colluvial loess loam, mud-like.

5.2.7.2. Vegetation and climate development (by A. Brande)

The following diagram sections have been distinguished:

A: Pine–willow–juniper–period with willow-(A_1) and birchstage (A_2): open, heliophilous shrub-rich vegetation of stadial-like character with transition to tree spreading.

B: Pine–spruce–larch–period: coniferous valley vegetation of interstadial character. The deposits of this period are incompletely preserved as a consequence of peat erosion (strata transition 2/4).

C: Pine–willow–birch–period with willow-(C_1) and birchstage (C_2): open, heliophilous vegetation similar to A with a probable transition to a tree reappearance.

D: Pine–period: pine-dominated valley tree vegetation of an interstadial character.

E: Period of loess loam accumulation with low pollen content, but presumably no significant hiatus to D.

5.2.7.3. Biostratigraphic correlation (by A. Brande)

Considering the non-interglacial vegetation and climate development and the age of loess loam accumulation, the whole pollen diagram must be of last glacial age. The tree vegetation of the interstadial diagram sections B and D is richer in B, because climatic conditions have been more favourable and/or stadial species extinction was no yet far advanced.

The highest biostratigraphic value can be attributed to *Larix,* which immigrates in A, spreads in B, is redeposited in C, while it is uncertain that it is autochthonous in D. Comparable last glacial *Larix*-periods have been scarcely found in the German foreland of the Alps till now. The so-called Schieferkohlen in question mostly represent only short parts of vegetation development, so that the areal history of the larch is not well known. Under these circumstances a synchronization with the pollen flora of the Höfen coal layer (Frenzel, 1973) may be possible, while the poorer tree pollen flora of Breinetsried (Frenzel, ibid) has quite another character than the pine–spruce–larch–period of Mauern. The extension of *Larix* and vegetation development of the Brørup Interstadial known from various sites of northern Central Europe (Menke and Behre, 1973) may correspond with this period of Mauern, presuming a late- or post-interglacial descendence of *Larix* from the Alps. *Larix*, however, also occurs in the very similar younger interstadials of Oerel (Schneekloth, 1966). Therefore, a definite biostratigraphic correlation to one of these Early Weichselian interstadials seems to be impossible at this stage. For further arguments of datation we refer to Brande (1975).

Table 5.8. Results from Mauern.

GrN	Sample Code	Depth (m)	Pollen zone	Measured activity (cpm)	Enrichment	Sample activity (pmc)	Age (yrs BP) 2σ criterion	Age (yrs BP) 1σ criterion	δ^{13}_{PDB} (‰)
7652	III: A_{1+2}	7.35 – 7.55	B	0.149 ± 0.022	13.08 ± 0.26	0.037 ± 0.006		63 400 $^{+1300}_{-1100}$	– 28.91
7806*	A_{1+2} 1–4th alkali extr.			0.028 ± 0.032		< 0.21	> 49 400		– 28.00

* counter GRADA

5.2.7.4. Radiocarbon Dates

The enrichment date obtained for the top of the lower peat layer (fig. 5.11) as well as the result for the extracted material are given in table 5.8.
The age suggests that the lower peat bed at Mauern was deposited during the second (Brørup) Interstadial of the Last Glacial (c.f. sect. 5.2.1). This means that the lignites at Höfen (c.f. sect. 5.2.6) are probably of the same age. This is in good agreement with the pollenanalytical results. The absence of a measurable ^{14}C activity in the extracted material supports the reliability of the age.

The earlier dates (GrN-6697: 29 290 ± 260 for the upper peat bed and GrN-6696: > 49 970 for the lower one; Brande, 1975) agree with our conclusion and confirm the existence of a hiatus between the two peat beds.
A further discussion of the results is given in sect. 5.3.

5.2.8. Val du Bourget and Haut Grésivaudan

5.2.8.1. Introduction (by Ch. Hannss and P. M. Grootes)

In the Départements of Savoie and Isère in the French inner Alpine region and its foreland, numerous lignite deposits have been found (Bourdier, 1961, 1962). Samples for the Early Weichselian dating project were obtained from the *Val du Bourget* and the *Haut Grésivaudan* (fig. 5.12). These two valleys are connected by the Cluse de Chambéry. Its entrance from the Isère valley is obstructed by deposits of a medieval landslide, overlying sands, gravels and moraines. This region, the Seuil des Marches, extends approximately 50 m above the valley floor of the Isère situated at 270 m.

Val du Bourget

In the Val du Bourget, between Chambéry and the Lac du Bourget several lignite layers have been found on both sides of the valley at altitudes between 250 and 340 m (fig. 5.12; c.f. Bourdier, 1961, 1962). These lignites occur in late pleistocene deposits viz. the banquette du Tremblay on the west side and the banquette de Sonnaz on the east side of the valley. In the former we find lignites in the gravel pit of the airport of Bourget, north of Montarlet (265 m), near Servolex (275 m), in the valley of the Ruisseau de Chapitre (280–290 m) and near the Côte Chevrier (285 m). In the banquette de Sonnaz we find lignites in the gravel pit of Voglans (250 and 280 m), in Bouvard (260 m), near Le Fromaget (250 and 278 m), in the gravel pit of the Combe Noire (280 m), in Pessey–Sonnaz (between 312 and 322 m

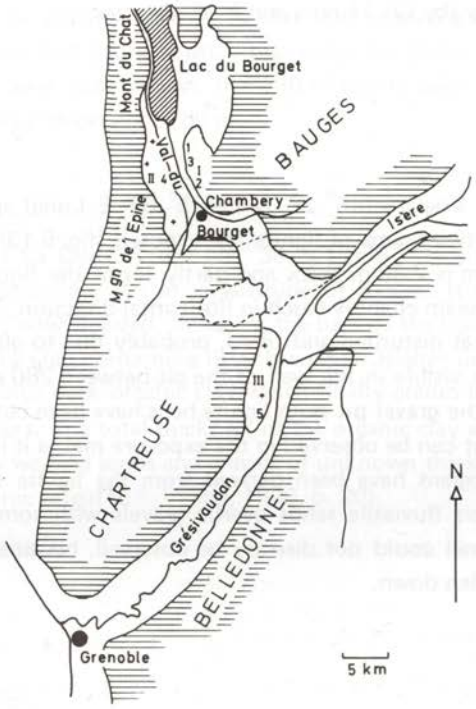

Fig. 5.12. Val du Bourget and Grésivaudan area.
I : banquette de Sonnaz; 1 – Voglans, 2 – La Croix Rouge, 3 – Pessey–Sonnaz.
II : banquette du Tremblay; 4 – Servolex.
III: banquette de Barraux; 5 – La Flachère.

and at 341 m) and north of La Croix Rouge (315 m). Most of these lignites have been mined.

Up till now age determinations using isotopic enrichment have been made for Voglans (250 and 280 m), La Croix Rouge (315 m), Pessey–Sonnaz (341 m) and Servolex (275 m) (fig. 5.12).

Haut Grésivaudan: La Flachère

La Flachère (45° 23′ N Lat, 5° 57′ E Long) is situated in the Haut Grésivaudan approximately 20 km south of Chambéry (fig. 5.12). The alluvial valley floor is situated at an altitude of approximately 250 m. Late pleistocene deposits reaching up to 400 m have been preserved on both sides of the valley. The deposits mainly consist of a succession of clays, sands and gravels in which in some places organic layers occur. At an altitude of 333 to 336 m lignites have been found on both sides of the valley (Bourdier, 1961, 1962; Hannss et al., 1976).

5.2.8.2. Stratigraphy (by Ch. Hannss and P. M. Grootes)

Val du Bourget

Voglans

In the gravel pit of Voglans (45° 37′ N Lat, 5° 55′ E Long) approximately 7 km north of Chambéry two seams of lignite are exposed (fig. 5.13). The lower one at an altitude of 250 m is 2.30 m thick and partly forms the floor of the gravel pit. The altitude of this seam changes much in horizontal direction. The western part of the seam is somewhat disturbed and tilted, probably due to glacial tectonics. The upper lignite seam is visible in the wall of the pit between 280 and 282 m altitude. To the westside of the gravel pit both lignite beds have been cut by glacial erosion. The stratigraphy that can be observed in the exposure makes it improbable that the lower lignites of Voglans have been derived from the lignite seam at 280 m. Between the two layers fluviatile sands overlie gravels with some sand lenses. The lower part of the wall could not directly be observed, because it was covered by material that had fallen down.

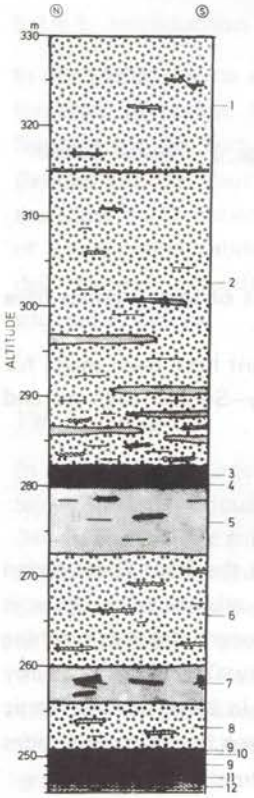

Fig. 5.13. Stratigraphy of the gravel pit of Voglans.
1 – coarse gravel with some sand lenses, 2 – gravel with sand lenses, number of sand lenses decreases in the higher part, the gravel becomes coarser, 3 – 280 m lignite, showing an erosion surface, 4 – dark coloured clay containing remnants of plants, 5 – stratified grey sands, 6 – medium coarse fluviatile gravel with sand lenses, 7 – cross bedded sand with gravel layers, 8 – gravel with many sand lenses, 9 – 250 m lignite, layer is disturbed and tilted, 10 – light grey unstratified clay, 11 – blue unstratified clay containing lignite lenses, 12 – grey unstratified clay.

Below the lignite at 250 m bluish grey clay was observed in many places. The thickness of this clay bed is unknown. Apparently the 250 m lignite is replaced by clay beds on the west side. Above the 280 m lignite again fluviatile sands and gravels occur, having a thickness of 50 m.

La Croix Rouge

The lignite seam of La Croix Rouge (45° 36′ N Lat, 5° 55′ E Long) approximately 3.5 km north of Chambéry lies at an altitude of 315 m. It is exposed in the entrance of a former, now flooded, mine. At the base of the lignite a bluish grey clay is overlain by a silty clay containing little branches. Higher up the bluish grey clay gradually changes into dark organic clay which finally grades into lignite with some embedded clay layers. The total thickness of the organic clay and lignite is approximately 2 m. Below we find sands and gravels of unknown thickness. This material is obviously of morainic origin (c.f. Vivien, 1896, p. 20).

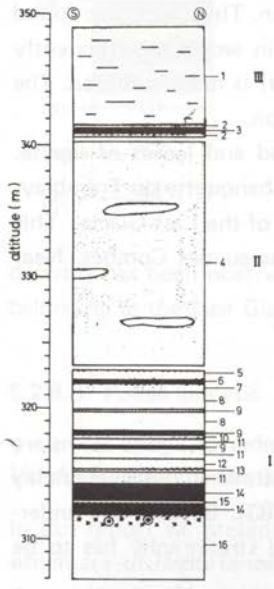

Fig. 5.14. Stratigraphy at Pessey–Sonnaz.
1 – fine sand, orange, well stratified, 2 – silty clay, light grey, 3 – lignite, rich in clay, containing molluscs, 4 – clay, locally exposed, containing sand lenses, 5 – bluish grey clay, increasingly sandy near the top, 6 – thin lignite layer, rich in clay, containing molluscs, 7 – dark blue compacted clay, 8 – sand, 9 – lignite, very rich in clay, 10 – clay containing plant remnants, 11 – stratified, bluish grey clay containing a few remnants of branches, 12 – unstratified gravel in sand bed, about 50% limestone pebbles, 13 – clay containing a 1 cm thick lignite layer, 14 – main lignite bed, 15 – dark silty clay containing wood remnants, 16 – silty, bluish grey clay.

Pessey–Sonnaz

In Pessey–Sonnaz (45° 37′ N Lat, 5° 55′ E Long) approximately 5 km north of Chambéry lignite seams have been found between 312 and 322 m and at 341 m (fig. 5.14). The lowest bed of lignite between 312 and 314 m has a considerable thickness. It has extensively been mined. It is probably the same seam as found near

La Croix Rouge about 1 km to the south. It was not exposed when the samples were taken. Under the principal lignite seam clays containing molluscs, thin lenses of lignite and bones of fishes and mammalia have been found (c.f. Mortillet, 1850a, p. 116; 1850b, p. 206–207). Between 314 and 318 m thin lignite layers alternate with beds of clay. These accumulations are covered by a sand layer of 3 m thickness and 2 m of clay. In the clay a thin band of lignite has been observed at 322 m.

At 341 m two thin (≈ 3 cm) layers of lignite, separated by 10 cm of clay rich in molluscs, are found embedded in a bluish grey, locally dark organic clay layer. The highest parts of the banquette de Sonnaz consist of sands and gravels. On top of these layers we find morainic material of the Last Glacial. Therefore the lignites most probably have been formed prior to the last large glacial extension.

Servolex

Near Servolex (45° 36′ N Lat, 5° 52′ E Long) approximately 6 km north-west of Chambéry lignites have been exposed at an altitude of 275 m in several places along the slopes of a highway and other roads under construction. They were also found in two borings. The lignite of Servolex is generally rich in wood and frequently contains pine cones. Among the fossil woods spruce (*Picea*) is most common. The lithology of the lignite changes rapidly in horizontal direction.

Below we find lacustrine clays containing pieces of wood and lenses of lignite. Generally, the lignite of Servolex is covered by gravels. The banquette du Tremblay, in which these lignites are found, is locally covered by till of the Last Glacial. This can especially be observed in the gravel pit of the Ruisseau des Combes. Near Servolex the till even contains small parts of lignite.

Haut Grésivaudan: La Flachère

Along the road between la Buissière and la Flachère a number of lignite seams are exposed at an altitude of 333 to 336 m intercalated in unstratified bluish grey clay containing molluscs (c.f. Depape and Bourdier, 1952, p. 83). Because the under- and overlying deposits are not exposed at this place the stratigraphy has to be deduced from observations at other localities (fig. 5.15).

Below the lignites probably sandy fluviatile deposits exist resting on till with boulders. These layers can be observed in the gravel pit in La Gache. Bourdier (1962, p. 24–25, fig. 24) considers the till to be of Rissian age. Hannss et al. (1976) favour the opinion that it belongs to a glacial advance during the beginning of the Würm. On top of the lignites 40 to 50 m of fluviatile gravel deposits are found, containing both limestone pebbles and igneous material. At 348 m these layers are interrupted by 0.5 m of unstratified clay. On top of the gravels a bank of pure limestone

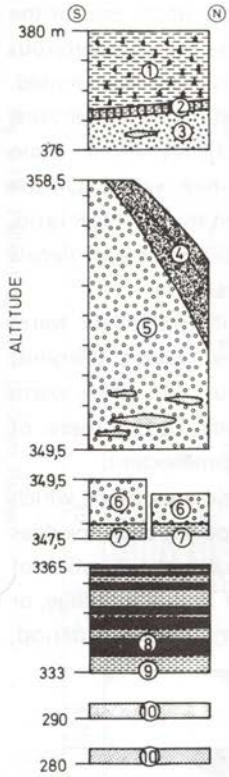

Fig. 5.15. Stratigraphy of the banquette de Barraux near La Flachère.
1 — slope deposit of angular limestone debris, 2 — band of loam and clay, 3 — unstratified gravel, almost without limestone, 4 — slope deposit consisting of reworked gravel, 5 — unstratified coarse gravel, 6 — gravel bed forming a conglomerate, 7 — unstratified clay, 8 — lignite, rich in wood, 9 — bluish grey clay, 10 — unstratified bluish grey clay with molluscs.

deposits has been observed. On the surface we find locally some morainic material belonging to the Last Glacial.

5.2.8.3. Pollen analysis

Val du Bourget (by W. H. E. Gremmen)

In this report we present simplified pollen diagrams. Only pollen curves are shown which are of importance for the purpose of this paper, viz. a short characteristic of the past vegetation and its climatic implications. The complete diagrams and a more comprehensive discussion will be published later.

La Croix Rouge

Pollen diagram 1 (fig. 5.16) shows results of the palynological examination of the lignite layer at La Croix Rouge, about 315 m above sea-level. The bottom zone of the diagram (samples 1–8) is characterized by a dominance of *Pinus*, while

Artemisia pollen values are high in the lowermost samples. In the upper part of the zone the *Pinus* values decrease. In the succeeding zone (samples 9–14) coniferous pollen values are low, whereas thermophilous trees are fairly well represented. Particularly *Corylus, Ulmus* and *Quercus* were frequently found. In the upper zone of the diagram (samples 15–32) coniferous pollen, specifically *Picea*, again dominates. In the upper part of this zone *Artemisia* reaches high values. On the basis of the fluctuations in the curves for *Pinus* and *Picea* and in the AP/NAP ratio, the upper zone can be subdivided into 4 subzones. In sample 25 the value of *Betula* pollen is calculated as a percentage of the pollen sum excluding *Betula*.

The middle zone of the diagram reflects the vegetation of a relatively warm period. In sample 11 the sum of thermophilous tree pollen values (*Corylus, Quercus, Ulmus, Fraxinus, Tilia* and *Acer*) amounts to about 80%. This warm period is preceded as well as succeeded by much colder periods. During these, of the thermophilous trees, only *Corylus* could maintain itself to some extent.

Although the middle part of the diagram points to climatic conditions which were favourable for the expansion of thermophilous trees, the pollen evidence does not point to an interglacial vegetation development. Very probably the duration of the warm period was rather short. Consequently, the lignite of La Croix Rouge, or at least its middle part, should have been deposited during an interstadial period, probably of Early-Weichselian age.

Voglans II

Near Voglans two lignite layers are found, viz. Voglans I at about 250 m above sea-level, and Voglans II at about 280 m. The layers are separated by about 30 m of coarse sands and gravels.

Some of the results of the palynological examination of the upper lignite (Voglans II) are shown in diagram 2 (figure 5.17.a). It should be mentioned that only the spectra with odd numbers are included in this diagram. At the bottom of the diagram a conspicuous *Alnus* dominance can be observed, while thermophilous trees, such as *Corylus, Carpinus, Ulmus* and *Acer*, show relatively high pollen percentages. Between spectra 3 and 5 *Picea* increases markedly, while the rise in the *Pinus* curve takes place above spectrum 5. From spectrum 5 onwards, up to the top of the diagram, coniferous pollen dominates. However, the continuous curves, with values of a few percent, for thermophilous trees indicate that these species could maintain themselves in the area.

The pollen percentages in spectrum 3 are biassed by the anomalously high local *Alnus* values. If *Alnus* is excluded from the pollen sum, thermophilous trees show fairly high percentages, whereas those of *Picea* and *Pinus* remain low. In view of the good representation of *Carpinus,* with a corrected pollen value of circa 33%, we are probably dealing with a section of the Eem Interglacial. In that case the larger part

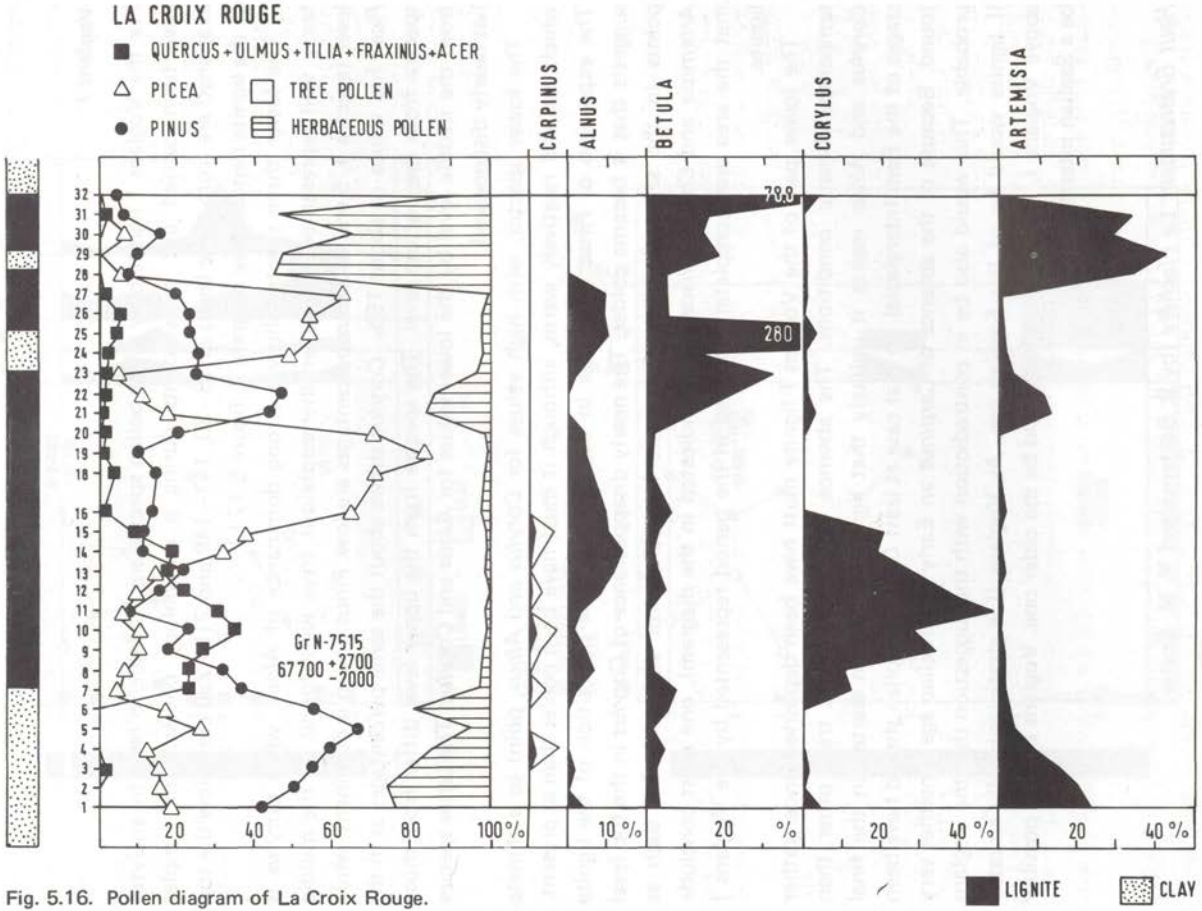

Fig. 5.16. Pollen diagram of La Croix Rouge.

of the lignite deposit, with high pollen percentages for *Picea* and *Pinus* (above spectrum 5), should either belong to the final, colder stages of the Eemian or to the Early Weichselian.

Voglans I

For the Voglans I lignite only a few pollen spectra are available so far. The analyses have been carried out by students during a palynology course. The samples examined are from three levels at 18–30, 141–149 and 215–230 cm below the top of the lignite deposit (see diagram 3, figure 5.17.b).

The lower three spectra show a strong dominance of *Alnus*, while *Corylus* is fairly well represented. No other thermophilous trees were found. In the middle level (spectra 4, 5 and 6) *Alnus* percentages are low. *Pinus* pollen is dominant, while *Picea* has values of about 15%. *Corylus* shows about the same percentages as in the spectra from the bottom level. The spectra from the upper level differ from those from the middle level by the lower values for *Alnus* and *Corylus*. The latter species has nearly disappeared.

The lower spectra, with high values for *Corylus* and *Alnus*, point to a climate which was still relatively warm, although it must have been cooler than at present. The expansion of *Pinus* and *Picea* in the course of the deposition of the lignite suggests that it became colder. The nearly disappearance of *Corylus* in the top level points in the same direction. From the low values for various herbs, such as *Artemisia* and *Chenopodiaceae* (not indicated in the diagram), one must conclude that the area was completely forested in the period represented by the Voglans I lignite.

The lower part of the Voglans I lignite must have been deposited under rather temperate climatic conditions. The absence of thermophilous trees other than *Corylus* and *Alnus* makes it unlikely that lignite deposition started in the final stages of the Eem Interglacial. In that case at least *Carpinus* pollen should have been found. Because of the absence of *Carpinus* an Early Weichselian age is neither very probable. This would also be in contradiction with the suggestion that the Voglans II lignite would be of late-Eemian age. As Voglans II is stratigraphically situated above Voglans I, the latter lignite should be the older one. Voglans I could possibly be a Saalian interstadial.

Haut Grésivaudan: La Flachère (by S. Bottema and Y. M. Koster)

Three and a half metres of sediment originating from near La Flachère was studied palynologically. The material represents alternating lignite and clay layers. A simplified diagram (fig. 5.18) shows some of the most important pollen curves.

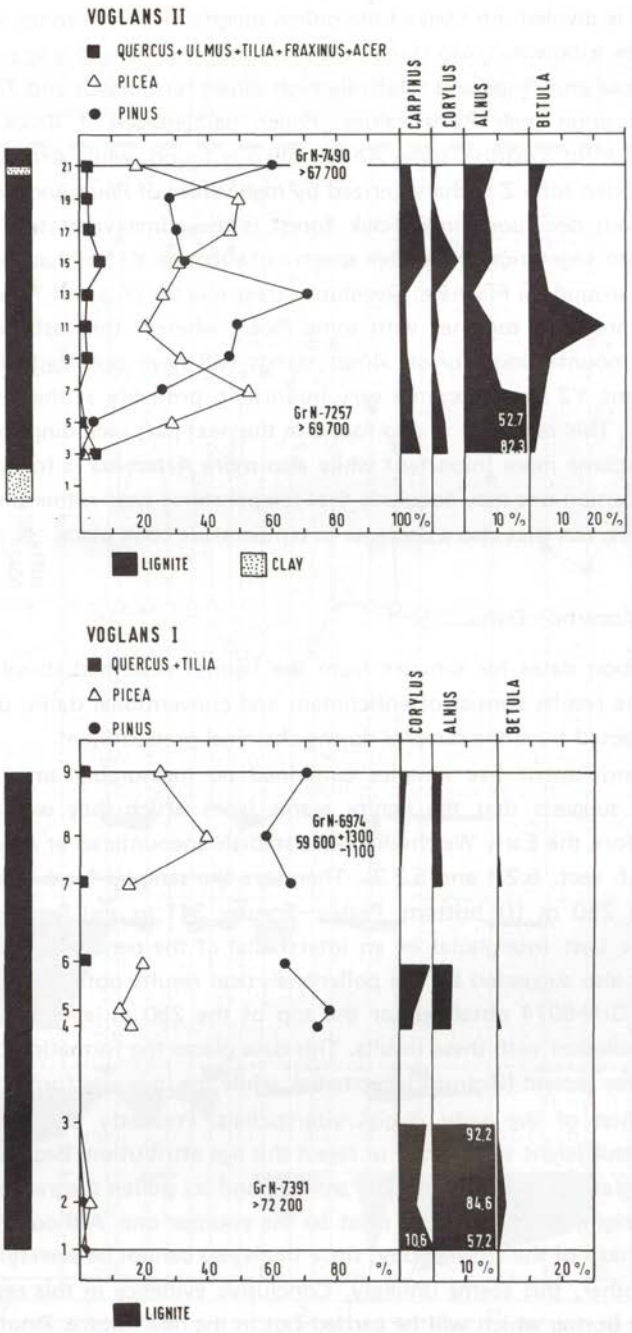

Fig. 5.17. Pollen diagrams of Voglans II (280 m) (a) and I (250 m) (b).

The diagram is divided, on basis of the pollen spectra, into two zones, *viz.* Y and Z. Zone Y can be subdivided into three subzones. Subzone Y1 is characterized by high values for *Picea* and *Pinus* and relatively high values for *Corylus* and *Tilia*. Subzone Y2 is based upon high *Picea* values. Pollen percentages of *Alnus* and *Betula* dominate the third subzone, some *Abies* pollen is found, while *Artemisia* becomes important. Pollen zone Z is characterized by high values of *Pinus* and *Betula*.
At the moment deciduous mixed-oak forest is the climaxvegetation in the area. Translated into vegetation the pollen spectra of subzone Y1 will have represented a dense forest around La Flachère. Deciduous trees like *Corylus* and *Tilia* covered the valley-floor, probably together with some *Picea*, whereas this last tree and *Pinus* formed the mountaneous forest. *Alnus* stands will have occurred in wet places. During subzone Y2 *Picea* becomes very important, probably as the result of lower temperatures. This tendency is also found in the next part including zone Z. *Betula* and *Pinus* become more important while also more *Artemisia* is found. From this pollen composition one may conclude that temperatures were rather low, compared with nowadays, but that also a decrease in temperature took place.

5.2.8.4. Radiocarbon Dates

The radiocarbon dates for samples from the lignites described above are given in table 5.9. The results consist of enrichment and conventional dates, partly on the material extracted from the samples during chemical pretreatment.
Even after enrichment five samples contained no measurable amount of radiocarbon. This suggests that the lignite seams from which they were taken were deposited before the Early Weichselian interstadials encountered at Amersfoort and Odderade (c.f. sect. 5.2.1 and 5.2.3). Therefore the samples from Voglans 280 m (II), Voglans 250 m (I) bottom, Pessey–Sonnaz 341 m and Servolex probably belong to the Last Interglacial or an interstadial of the penultimate Glacial. This conclusion is also suggested by the pollenanalytical results obtained by Gremmen.

The date GrN-6974 obtained for the top of the 250 m layer at Voglans is in strong contradiction with these results. This date places the formation of the top of the layer in the second (Brørup) Interstadial, while the base was formed somewhere before the first of the early glacial interstadials. Presently the pollenanalytical evidence is insufficient to approve or reject this age attribution. Because the 280 m lignite at Voglans gave no measurable activity and its pollen diagram suggested an interglacial origin, the lower layer must be the younger one. Although it cannot be excluded on basis of the stratigraphy, since the layers cannot be seen lying vertically above each other, this seems unlikely. Conclusive evidence in this respect should come from a boring which will be carried out in the near future. Another explanation is that the sample GrN-6974 has been contaminated. Because the top of the 250 m layer has been on the surface (= bottom of the gravel pit) for some time, this

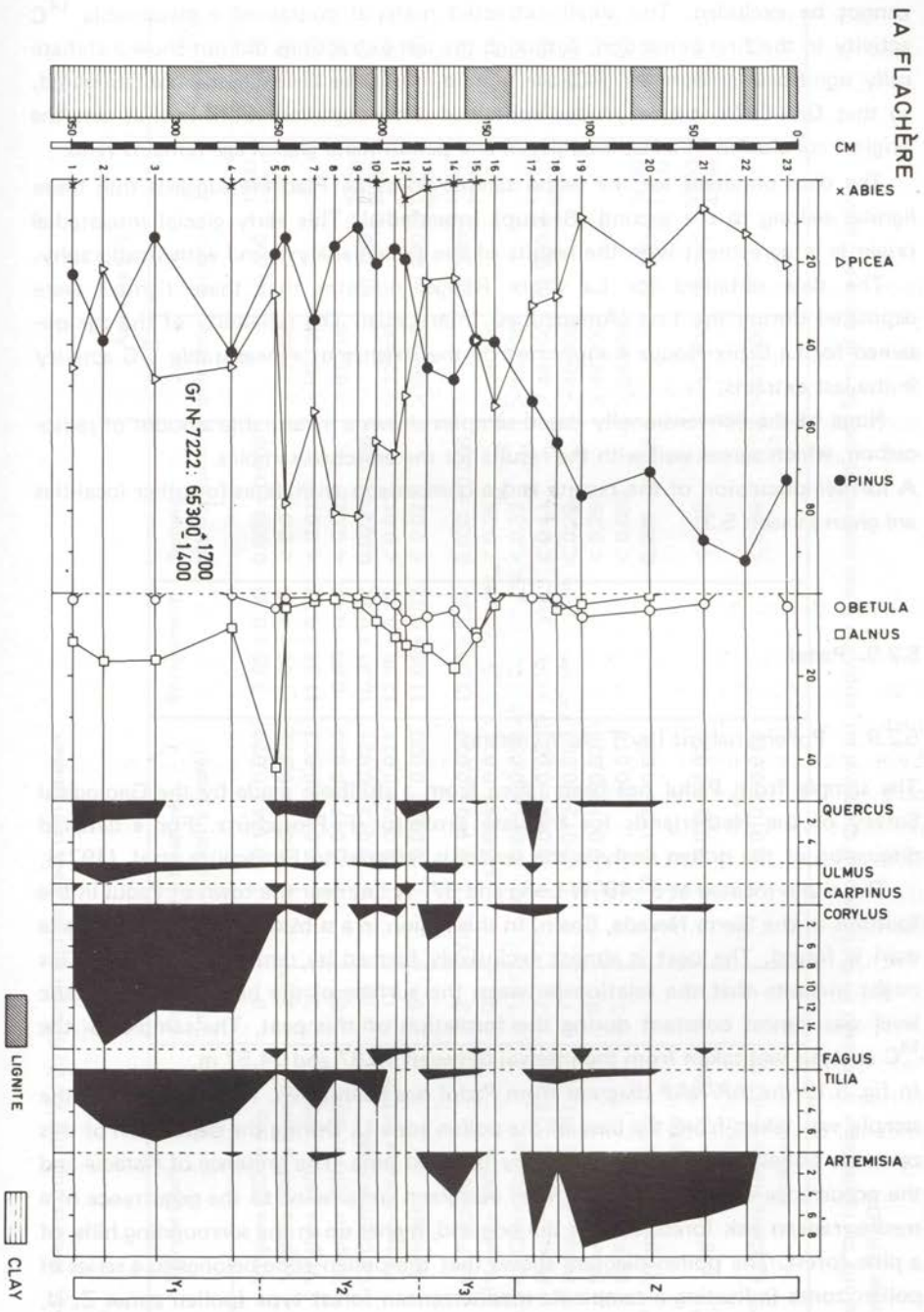

Fig. 5.18. Pollen diagram of La Flachère.

cannot be excluded. The alkali extracted material contained a measurable ^{14}C activity in the first extraction. Although the last extractions did not show a statistically significant amount of ^{14}C, the sample must have been slightly contaminated, so that GrN-6974 still may have contained some contamination. In that case the original conclusion of a last interglacial and penultimate glacial age remains valid.

The date obtained for the wood sample from La Flachère suggests that these lignites belong to the second (Brørup) Interstadial. This early glacial interstadial origin is in agreement with the results of the pollen analysis and with stratigraphy.

The date obtained for La Croix Rouge indicates that these lignites were deposited during the first (Amersfoort) Interstadial. The reliability of the age obtained for La Croix Rouge is supported by the absence of a measurable ^{14}C activity in the last extracts.

None of the conventionally dated samples shows a measurable amount of radiocarbon, which agrees well with the results for the enriched samples.
A further discussion of the results and a comparison with dates for other localities are given in sect. 5.3.

5.2.9. Padul

5.2.9.1. Pollen analysis (by T. A. Wijmstra)

The sample from Padul has been taken from a drillhole made by the Geological Survey of the Netherlands for the late professor F. Florschütz. For a detailed discussion of the pollen analysis the reader is referred to Florschütz et al. (1971).

The site is located at 3° 40' W Long and 37° N Lat near the town of Padul in the foothills of the Sierra Nevada, Spain. In this region in a subsiding basin peat and lake marl is found. The peat is almost exclusively formed by remnants of *Carex*. This might indicate that the relation between the surface of the bog and the phreatic level was almost constant during the formation of this peat. The sample for the ^{14}C analysis was taken from the interval between 13.67 and 14.57 m.
In fig. 5.19 the AP/NAP diagram from Padul has been given. It is obvious that the sample was taken from the base of the pollen zone U. During the deposition of this zone the pollen rain was dominated by oak and pine. The presence of *Pistacia* and the occurrence of pollen coming from evergreen oaks point to the occurrence of a mediterranean oak forest around the bog and, higher up in the surrounding hills, of a pine forest. The pollen diagram shows that the pollen zone belongs to a series of pollen zones indicating a temperate-mediterranean forest type (pollen zones Z, U, S, Q). The development of the forest vegetation during these zones Z and Q points to a succession occurring when for a long time optimum conditions exist as far as

Table 5.9. Results from the Val du Bourget and the Haut Grésivaudan.

GrN	Sample Code	Depth (m)	Pollen zone	Measured activity (cpm)	Enrichment	Sample activity (pmc)	Age (yrs BP) 2σ criterion	Age (yrs BP) 1σ criterion	δ^{13}_{PDB} (‰)
6974	Voglans 250 m top	0*		0.144 ± 0.020	7.85 ± 0.39	0.060 ± 0.009		$59\,600\ ^{+1300}_{-1100}$	− 28.23
7391	Voglans 250 m bottom	2.3*		−0.077 ± 0.022	11.62 ± 0.23	< 0.012	> 72 200		− 28.68
7257	Voglans 280 m: '968'	> 20		0.015 ± 0.022	11.34 ± 0.22	< 0.017	> 69 700		− 26.89
7490	Voglans 280 m: '967'	> 20		0.017 ± 0.020	8.60 ± 0.43	< 0.022	> 67 700		− 27.56
7515	La Croix Rouge	≈ 1½		0.073 ± 0.021	10.91 ± 0.22	0.022 ± 0.006		$67\,700\ ^{+2700}_{-2000}$	− 30.93
7704	Pessey–Sonnaz 341 m	≈ 1½		0.002 ± 0.021	12.35 ± 0.25	< 0.012	> 72 800		− 28.66
7498	Servolex	≈ 5		0.032 ± 0.020	11.06 ± 0.22	< 0.021	> 68 000	$74\,500\ ^{+8100}_{-4000}$	− 27.40
7222	La Flachère	≈ 3	Y-1	0.110 ± 0.020	12.09 ± 0.24	0.030 ± 0.006		$65\,300\ ^{+1700}_{-1400}$	− 25.61
7209	Voglans 280 m	> 20		−0.006 ± 0.038		< 0.25	> 48 200		− 28.27
7428	La Croix Rouge	≈ 1½		0.021 ± 0.038		< 0.32	> 46 200		− 29.56
7427	Pessey–Sonnaz 318 m	≈ 2		0.048 ± 0.039		< 0.41	> 44 100	$51\,900\ ^{+13\,500}_{-4800}$	− 29.55
7426	Pessey–Sonnaz 341 m	≈ 1½		0.012 ± 0.039		< 0.29	> 46 900		− 28.33
7181	Servolex	≈ 5		−0.001 ± 0.038		< 0.25	> 48 200		− 30.17
6652	La Flachère	≈ 3		0 ± 0.014		< 0.089	> 56 400		− 26.63
7413**	Voglans 250 m 1st alkali extr.			0.132 ± 0.024		0.306 ± 0.055		$46\,500\ ^{+1600}_{-1300}$	− 28.67
7414**	Voglans 250 m 11–12th alkali extr.			0.036 ± 0.026		< 0.20	> 49 800	$56\,900\ ^{+9900}_{-4300}$	− 28.67
7805**	La Croix Rouge 9–12 th alkali extr.			0.010 ± 0.014		< 0.09	> 56 500		− 29.73

* presently the lignite layer is exposed on the bottom of the gravel pit, originally it was covered by over 50 m of sands and gravels

** counter GRADA

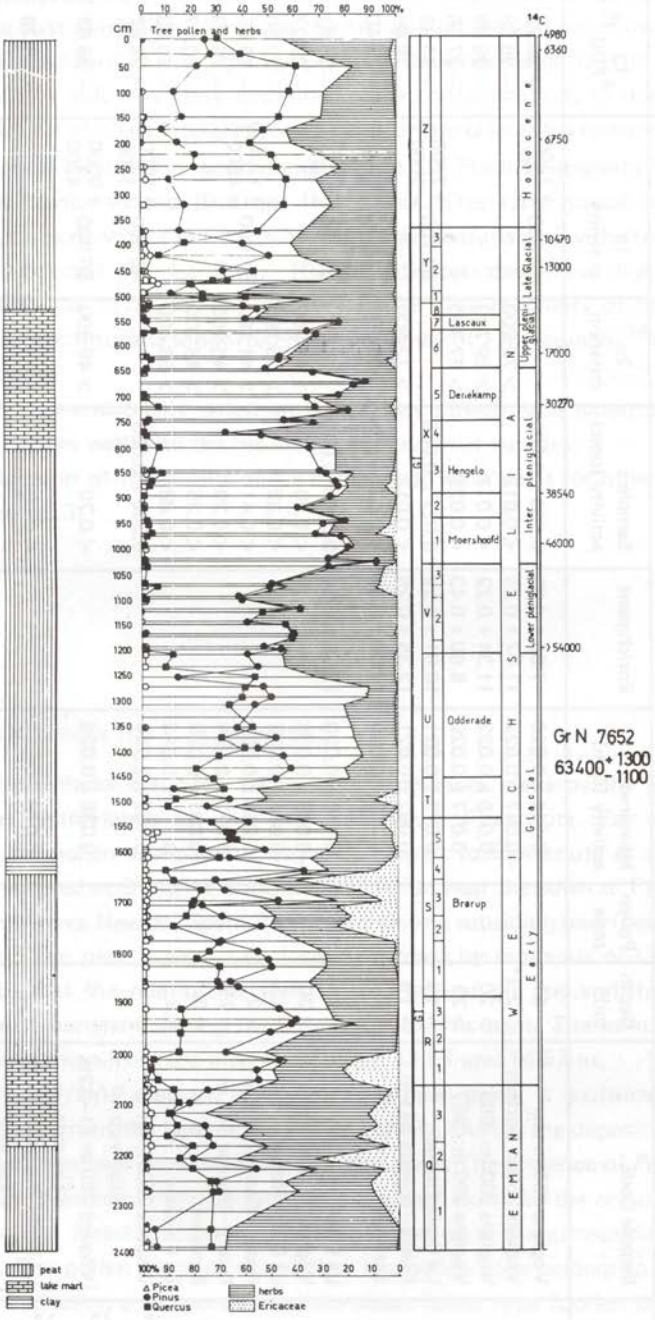

Fig. 5.19. Pollen diagram and stratigraphy of Padul.

temperature and precipitation are concerned. Under these conditions an equilibrium is developing between climate and vegetation (Iversen, 1975). These conditions are in principal restricted to interglacial conditions. For this reason it seems logical to correlate our zone Z and Q with the Holocene and the Last Interglacial (Eemian) respectively. The sedimentation in the Padul section seems to be continuous in the interval under discussion (a *Carex* peat). Therefore, there are only two forest phases after the Last Interglacial pointing to an amelioration of climate. In another case in Greece where also continuous sedimentation is present (Wijmstra, 1969), also two forest phases have been found after the Last Interglacial. On strength of these facts and the similarity of the forest development, the pollen zone U of the Padul section is correlated with the Elevtheroupolis Interstadial as defined in Greece (Wijmstra, 1969).

In areas in North-west Europe, where we have no continuous registration of the interaction of vegetation and climate, it has become evident that after the Last Interglacial at least two periods are encountered favourable for forest development. These periods are called Brørup and Odderade respectively (Andersen, 1961; Averdieck, 1963). For the time being the correlation Elevtheroupolis Interstadial–Odderade seems therefore a logical one.

5.2.9.2. Radiocarbon Dates

The enrichment dates both for the residue and for the extracted material of the Padul peat sample are given in table 5.10.

The date for the residue places the formation of the peat of pollen zone U in the third (Odderade) Interstadial dated at Amersfoort and Odderade. Since the core diameter of the sample was rather small and the peat already partly decomposed, a length of $\approx$ 1 m covering half of the interstadial pollen zone U had to be used for the sample. The date gives an average age for the lower half of zone U. This confirms the pollenanalytical correlation with Odderade.

The large amount of organic material recovered from the alkaline extracts enabled us to obtain an enrichment date for the extracted material. This turned out to be slightly younger pointing to a slight contamination in the original sample. The close agreement between the two results adds to the reliability of the age for the residue.

A further discussion is given in sect. 5.3.

5.2.10. Beaverdam Creek

5.2.10.1. Geologic setting of the Beaverdam Creek ^{14}C sample YG-70-20 in Yellowstone National Park (by Gerald M. Richmond)

Table 5.10. Results from Padul.

GrN	Sample Code	Depth (m)	Pollen zone	Measured activity (cpm)	Enrichment	Sample activity (pmc)	Age (yrs BP) 1σ criterion	δ^{13}_{PDB} (‰)
7559	I	13.67 – 14.57	U	0.159 ± 0.020	7.56 ± 0.23	0.068 ± 0.009	$58\,500\ ^{+1100}_{-1000}$	– 27.69
7611	I alkali extr.			0.345 ± 0.020	13.05 ± 0.26	0.086 ± 0.005	56 700 ± 500	– 27.16

Beaverdam Creek is tributary to the Southeast Arm of Yellowstone Lake in Yellowstone National Park (fig. 5.20). Yellowstone Lake lies in an ancient caldera that has been partly filled with rhyolite flows of late Quaternary age (U.S. Geological Survey, 1972). At least four times during the Pleistocene, glaciers developed at altitudes of about 3350 m in the high plateaus southeast of Yellowstone Lake and flowed down valleys into the lake (altitude 2358 m). Here they merged to form an icecap that filled and overflowed the basin to points near or beyond the boundaries of the Park (Richmond, 1969; U.S. Geological Survey, 1973).

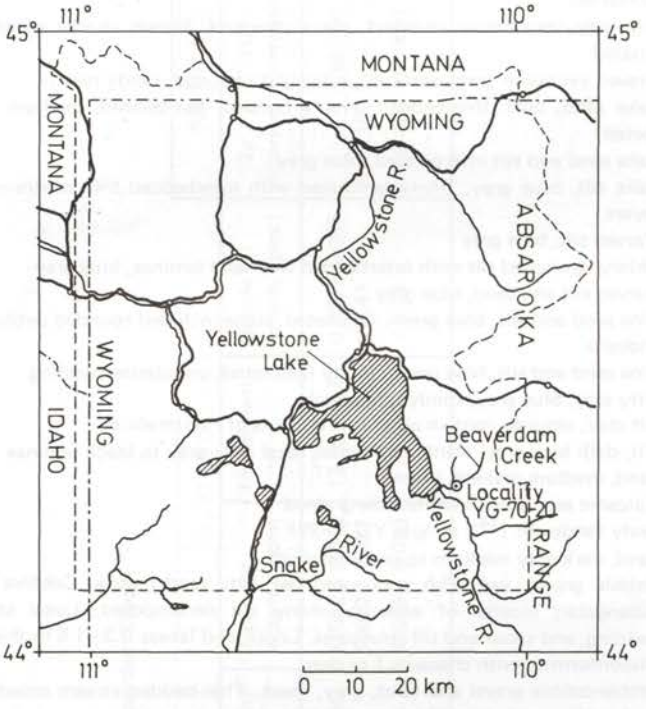

Fig. 5.20. Map of Yellowstone National Park showing location of ^{14}C locality YG-70-20.
——— roads, — · — · — · — state boundary, — — — park boundary.

At ^{14}C locality YG-70-20 (fig. 5.20) a peaty sandy silt bed, about 21.6 cm thick, occurs at the base of a thick sequence of interstadial and ice-dammed lake silts (Richmond and Pierce, 1972) overlain by proglacial gravel and till of the last major glaciation. This is the Pinedale Glaciation, believed to be correlative with the Main Würm (Richmond, 1970). ^{14}C locality YG-70-20 is at a point about 90 km toward the mountains from the end moraines of the last glaciation and about 10 km downvalley from the cirques. It lay beneath about 975 m of ice at the glacial maximum (Richmond, 1969).

The major units of the stratigraphic section at ^{14}C locality YG-70-20, as measured by hand level from top to bottom, are described below.

Table 5.11. Stratigraphic section at ^{14}C locality YG-70-20.

Thickness in m	Description
1.8	Colluvium, buff stony, silty
2.4	Sand, gray, clean, medium grained, stream crossbedded, local gravel lenses, locally contorted
7.0	Till, gray, very sandy compact, platy structure. Stones chiefly of andesite, some striated
2.1	Gravel, yellowish gray, unsorted, subround to round, sandy matrix
6.4	Lake sand, buff, thin-bedded, evenly bedded, flat-bedded, medium grained, well sorted
1.5	Lake sand and silt interbedded, blue gray
3.3	Lake silt, blue gray, thinly laminated with interbedded thin medium to fine sand layers
0.6	Varved silt, blue gray
4.1	Thinly laminated silt with interbedded fine sand laminae, blue gray
2.9	Varved silt and sand, blue gray
1.8	Fine sand and silt, blue green, laminated, some included rounded pebbles of andesite
7.6	Fine sand and silt, blue green, thinly laminated, undulating bedding
3.5	Silty clay, blue gray, thinly laminated
0.05	Silt clay, laminae contain abundant remains of *Fontinalis sp.*
9.1	Silt, dark blue gray, thinly laminated, local dark gray to black laminae
0.05	Sand, medium grained, clean
0.01	Volcanic ash, grayish white, fine grained
0.216	Peaty sandy silt (^{14}C sample YG-70-20)
0.25	Sand, dark gray medium to coarse grained
5.8	Cobble gravel, yellowish gray, unsorted; silty sand matrix. Cobbles subround to subangular; mostly of andesite; many are decomposed. Local stream foreset bedding, and scour and till structures. Local sand lenses 0.3–1.5 m thick Disconformity with channels 1 m deep
9.1	Pebble-cobble gravel and sand, gray, clean. Thin-bedded stream crossbedded. Sand beds well sorted, gravel beds poorly sorted
69.58 m	Total thickness of stratigraphic section

The lower gray gravel is probably related to the recession of an earlier glacier. The overlying yellowish gray silty gravel may represent interstadial stream conditions. The peaty layer is believed to have accumulated at or near a lake shore at an altitude of about 2440 m. The thin ash layer on the peat has recently been carefully collected and submitted for potassium-argon dating. The result when available will be interesting to compare with the ^{14}C date of the peaty layer.

Table 5.12. Results from Beaverdam Creek.

GrN	Sample Code	Depth (m)	Measured activity (cpm)	Enrichment	Sample activity (pmc)	Age (yrs BP) 2σ criterion	Age (yrs BP) 1σ criterion	δ^{13}_{PDB} (‰)
7332	YG-70-20	≈ 54	0.082 ± 0.019	13.20 ± 0.26	0.020 ± 0.005		68 300 $^{+2200}_{-1700}$	− 28.22
7292	YG-70-20		0.012 ± 0.057		< 0.41	> 44 100		− 28.35
7617*	YG-70-20 1st alkali extr.		0.039 ± 0.033		< 0.24	> 48 400	56 400 $^{+15\,600}_{-4900}$	− 27.32

* counter GRADA

5.2.10.2. Radiocarbon Dates

The enrichment date is given in table 5.12 together with the ^{14}C result obtained for the material recovered from the alkali extract.
The low radiocarbon activity of the latter indicates that the sample was probably uncontaminated.

The enrichment date gives the age of the base of a thick sequence of interstadial and ice-dammed lake silts predating the last major glacial advance in this region. The stratigraphical evidence is compatible with a correlation of this interstadial sequence with the Early Weichselian interstadials of North-west Europe. The date obtained also compares well with ^{14}C results for the first (Amersfoort) Interstadial of the Weichselian Glacial.

The sample is of special importance because a rhyolitic ash layer on top of it is believed to belong to one of the youngest rhyolitic eruptions in this region (Richmond, 1972, pers. communication). The youngest rhyolite flows in the Yellowstone Park are according to K-Ar dating approximately 70 000 years old (J. D. Obradovich, 1975, pers. communication). At present a K-Ar date on a sample from the ash layer itself is in preparation.

If the correlation given above is correct, the agreement between the ^{14}C enrichment date and the age determined by the K-Ar method is excellent (especially if the conventional ^{14}C age is corrected to the better value of the ^{14}C half-life: $T_{\frac{1}{2}}$ = 5730 years). As yet, however, no definite conclusion about the comparison of ^{14}C and K-Ar dating can be drawn.
Further discussion is given in sect. 5.3.

5.3. Discussion of the enrichment dates

The 28 enrichment dates discussed in the previous sections are summarized in fig. 5.21, together with the stratigraphical information given for their interpretation. This includes the position of the sample in the layer, the kind of material of the sample and whether the beginning or the end of a period of peat growth has been dated. In these cases the block is closed. Otherwise it is left open. The radiocarbon activity of most samples has been corrected for the residual activity of the anthracite CO_2 sample used for background measurements (c.f. sect. 4.4). For samples indicated with an asterisk this activity is not accurately known. Consequently, no correction could be applied, so that these dates may be slightly too old.

The locality *Amersfoort* provides our most complete sequence. We will discuss this first. At Amersfoort we have several peat layers in a well-known stratigraphy, while

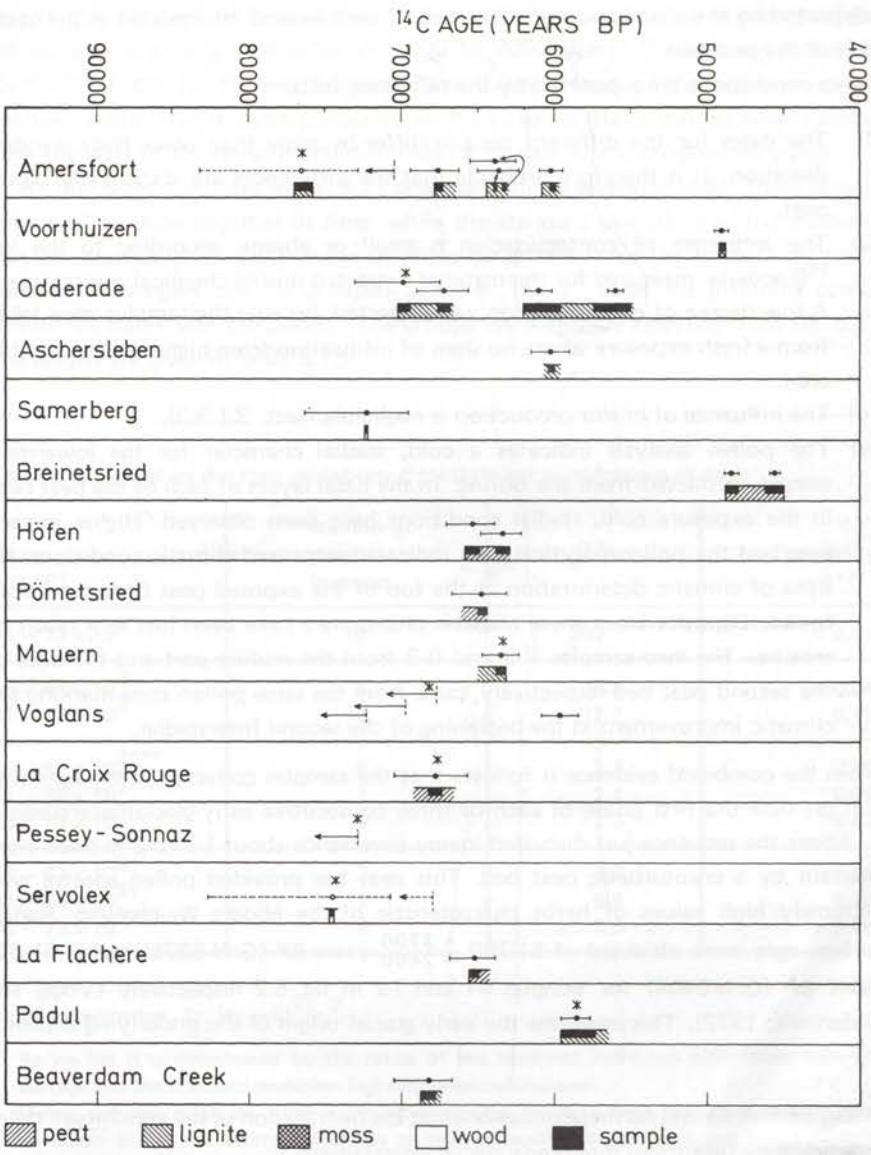

Fig. 5.21. Results for the enriched ^{14}C samples.
* dates not corrected for residual activity of the background CO_2 sample.

detailed pollen analyses are available. From the data (c.f. sect. 5.2.1) the following conclusions can be derived: (i) Four different periods of peat growth have been dated. (ii) The second (upper) early glacial peat bed in the exposure consists of the remnants of two peat layers deposited during two different interstadials. This is

supported by the observation of a thin bed of aeolian sand intercalated in the upper part of the peat bed.
These conclusions are supported by the following facts:

(i) The dates for the different periods differ by more than twice their standard deviation. It is therefore probable that the differences are statistically significant.
(ii) The influence of contamination is small or absent, according to the low ^{14}C activity measured for the material extracted during chemical pretreatment. A low degree of contamination was expected, because the samples were taken from a fresh exposure where no signs of infiltration from higher levels could be seen.
(iii) The influence of *in situ* production is negligible (sect. 3.1.3.3).
(iv) The pollen analysis indicates a cold, stadial character for the lowermost sample, extracted from the boring. In the basal layers of each of the peat beds in the exposure cold, stadial conditions have been observed. Higher in each peat bed the pollenanalytical data indicated improved climatic conditions. No signs of climatic deterioration at the top of the exposed peat beds have been found. Deposits from these climatic phases may have been lost as a result of erosion. The two samples II-2 and II-3 from the middle part and the base of the second peat bed respectively, came from the same pollen zone marking the climatic improvement at the beginning of the second Interstadial.

From the combined evidence it follows that the samples collected in the construction pit date the first phase of each of three consecutive early glacial interstadials.

Above the sequence just discussed loamy coversands about 1.5 to 2 m thick were overlain by a cryoturbatic peat bed. This peat has provided pollen spectra with extremely high values of herbs characteristic of the Middle Weichselian. Radiocarbon ages were obtained of 51 700 $^{+\,3700}_{-\,2400}$ years BP (GrN-5375) and $>$ 51 000 years BP (GrN-5404) for samples I-1 and I-2 in fig. 5.2 respectively (Vogel and Waterbolk, 1972). This confirms the early glacial origin of the underlying deposits.

In this section we will further discuss whether the distribution of the enrichment dates supports the existence of three early glacial interstadials.
Of the 28 samples that have been enriched 6 showed no measurable ^{14}C activity. Three yielded dates less than 50 000 years BP, well in agreement with the pleniglacial character of the deposits. The remaining 19 samples were dated between 56 000 and 73 000 years BP.

In the discussion we assume, that deposition under interstadial conditions started synchronously at different places. This need not be true, because local conditions and the migration velocity of different plant species have ultimately

determined the kind of deposit formed. The statistical uncertainty in the age of the old samples (σ_T) is of the order of 1000 to 2000 years. The migration of plant species over the North-west European area takes a time of the order of several hundred years. This is short compared with σ_T, so for statistical purposes samples from the start of the same interstadial may be treated as a homogeneous group.

At first sight the dates in fig. 5.21 seem to fall into several groups. These groups, however, are close together in time, while the standard deviations of the measured ages are considerable. To provide an objective criterion for the probability that a number of samples can be grouped together, the χ^2 value for different combinations of dates was calculated. The groups were visually selected from fig. 5.21. The results are given in table 5.13.

Table 5.13. χ^2 values and their probability P for different combinations of dates.

Group (yrs BP)	Number of dates in group	χ^{2*}	Probability P^{**}
$55 - 73 \times 10^3$	19	202	< 0.01
$55 - 61 \times 10^3$	6	36.3	< 0.01
$61 - 73 \times 10^3$	13	17.7	0.13
$55 - 61 \times 10^{3***}$	5	3.3	0.50
$61 - 66 \times 10^3$	7	2.1	0.92
$66 - 73 \times 10^3$	6	2.3	0.82
$55 - 61 \times 10^{3\dagger}$	3	3.2	0.20
$61 - 66 \times 10^{3\dagger}$	7	9.5	0.15
$66 - 73 \times 10^{3\dagger}$	6	3.3	0.66

* χ^2 is defined as $\sum_{i=1}^{n} (x_i - \bar{x})^2/\sigma_i^2$

As we see it is determined by the ratios of the observed individual differences from the average and the standard deviation (σ_i) estimated beforehand.

If the samples originate from a period of shorter duration than the estimated standard deviation and if the estimate includes all relevant sources of variation, we find a value of $\chi^2 \approx n - 1$. P gives the probability of finding a value of χ^2 larger than or equal to the one calculated.

A reasonable agreement between the experimental results and the estimated uncertainty requires $0.05 < P < 0.95$.

** Handbook of Chemistry and Physics, 49th ed. (1968), A 162

*** without top sample Odderade

† combination of dates based also on stratigraphical and/or pollenanalytical evidence: $55 - 61 \times 10^3$ without Voglans and Aschersleben; $61 - 66 \times 10^3$ with Aschersleben, without Pömetsried; $66 - 73 \times 10^3$ with Pömetsried, without Samerberg

Evidently there is more than one group. The high χ^2 value for the group 55–61 000 years BP is caused almost exclusively by the top sample of Odderade. Without this sample we find $\chi^2 = 3.3$ for 5 dates giving $P = 0.50$ and $\chi^2 = 3.2$ for 3 dates giving $P = 0.20$. The time span of the upper peat layer at Odderade is large compared with the standard deviation. Therefore top and base have to be considered separately. The other χ^2 values all have a reasonable probability.

The fact that much higher P values are obtained when the dates are divided into three groups indicates that we have probably found three interstadials. If we take into account the pollenanalytical and stratigraphical evidence (sect. 5.2), we obtain different groups of which, however, the χ^2 values still have a good probability.

From the statistical evidence we thus decide that the simplest explanation for the observed distribution of dates is the existence of a close succession of three early glacial interstadials between 73 000 and 56 000 years BP.

Because the distribution of the ages discussed above as well as the detailed analysis of the Amersfoort sequence point to the existence of three early glacial interstadials, we will further assume the reality of this division and discuss the position of the different samples in this interstadial sequence.

The *first* (= *oldest*) *Interstadial* has been found at *Amersfoort* and *Odderade* and, if a correlation of European and North-American interstadials is allowed, also at *Beaverdam Creek*. Furthermore, it has probably been observed at *La Croix Rouge* and possibly at *Pömetsried*. From the dates for the base of the deposits we obtain a ^{14}C age of 68 200 ± 1100 years BP for the beginning of the first Interstadial. Although the age for La Croix Rouge might be somewhat high, there is a good probability that this deposit was formed during the first Interstadial. The date obtained for Pömetsried seems to fit the second Interstadial better than the first. The date holds for the top of a lignite seam showing a pollen diagram somewhat cooler than that at Höfen nearby (c.f. sect. 5.2.6). This difference in pollen diagram would be explained by assuming that Pömetsried belongs to the first Interstadial. Considering the standard deviation this is quite well possible. The final classification has to await the result for the base of the lignites at Pömetsried which is in preparation.
No date has been obtained for the end of the first Interstadial.

The *second Interstadial* has been found at *Amersfoort, Höfen, Mauern* and *La Flachère*. It has possibly also been found at *Pömetsried* (see discussion above) and at *Aschersleben*. From the dates for the base of the deposits we obtain 64 400 ± 800 years BP for the beginning of the second Interstadial. The date for the top of the (lower) peat layer at Mauern might be somewhat high. It situates the formation of the peat, however, clearly in the second Interstadial. This is in agreement with the pollenanalytical correlation with Höfen and the Brørup Interstadial

as suggested by Brande (c.f. sect. 5.2.7). It will be interesting to obtain the date for the base of this peat layer which is at present in preparation.
The result for the peat layer at Aschersleben seems to fit the third Interstadial better than the second. It has been attributed to the second Interstadial by Mania (1967), based on the sequence of sedimentation cycles found in the former Aschersleben See. From the sample and profile description given by Mania it seems that the sample FR 15 has been taken at a place where only part of the profile was observed. Therefore the sample is attributed to the second Interstadial only on basis of its correlation with the complete standard sequence. On the other hand we found evidence for a considerable contamination in samples from younger peat layers taken from the main profile. A contamination of the sample can therefore not be excluded, although the dates for the extracted material do not favour this possibility. Finally we might have to explain the date as representing a late phase of the second Interstadial with a true age higher than the measured value due to the statistical uncertainty (σ_T: + 1400 and − 1200 years). Therefore no definite conclusion can be drawn.

The *third Interstadial* is found at *Amersfoort, Odderade* and *Padul* and, as the date suggests, possibly at *Aschersleben* (see above). The date obtained on *Voglans* is not considered as it is in contradiction with pollenanalytical and stratigraphical evidence as well as with the other results on the same profile.
From the two dates for the base of the deposits we obtain 60 500 ± 600 years BP for the beginning of the third Interstadial. According to the date for the top of the upper peat layer at Odderade this interstadial has lasted at least until 56 000 years BP, after which pleniglacial conditions developed.

The results on *Voorthuizen* and *Breinetsried* indicate that after 50 000 years BP the climatic conditions, although still pleniglacial, had improved sufficiently to allow the formation of organic deposits. Above the moss layer dated at Voorthuizen three more pleniglacial organic layers were found for which routine dates were obtained of > 44 450 years BP (GrN-5923, the top of the upper peat bed) and > 50 800 years BP (GrN-5940, the base of the third peat bed). At Amersfoort–De Liendert the two pleniglacial peat beds found above the early glacial sequence yielded similar dates. Obviously these deposits belong to a rather cool *pleniglacial Interstadial* which probably lasted from approximately 50 000 to 45 000 years BP. Because the date of the last extract from Voorthuizen IV indicates that the pretreated sample may still have been contaminated, the date of 49 000 ± 400 years BP provides a minimum age for the beginning of this interstadial.

Of the remaining samples only that of *Samerberg* gave a finite age (72 300 $^{+4100}_{-2700}$ years BP). From its position in a layer deposited during the second forest phase of

the Last Glacial (c.f. sect. 5.2.5), it was expected to give an age of approximately 64 000 years BP. The date obtained therefore indicates that (i) all other dates are too young (contaminated), or (ii) the forest phases of the Samerberg pollen diagram do not correspond to the interstadials discussed above, or (iii) the piece of wood does not belong to the layer in which it was found, but has been reworked from an older deposit. The consistent picture obtained from 17 dated samples makes the first explanation unlikely. The presence of large amounts of subfossil tree trunks in present-day river beds (Becker, 1976) makes the third explanation quite well possible.

The age of the *early glacial stadial* peat deposit at *Amersfoort* indicates that the Last Interglacial ended before 70 000 years BP. This date adds to the credibility of the finite ages obtained for the overlying layers. A minimum age (> 69 700 years BP) for the end of the Last Interglacial is also obtained from the Val du Bourget. Here pollen analysis suggests an interglacial origin for the 280 m lignites and an interstadial origin for the 250 m deposits at *Voglans*. Because the stratigraphy indicates that the beds lie on top of each other, no finite dates can be expected. The age for the top of the 250 m lignite is therefore probably the result of contamination. Similarly the fact that only a lower limit for the age of *Servolex*, lying at the same altitude, could be determined, was expected. Further pollenanalytical and stratigraphical evidence in this region is needed to assess the significance of these dates.

5.4. Radiocarbon time scale

From the dates discussed above and from the pollenanalytical investigations we can construct a radiocarbon time scale for the climatic fluctuations in the early part of the Last Glacial of North-west Europe. In combination with the climatic curve for the Last Glacial in the Netherlands published by Van der Hammen et al. (1967), which is valid up to 50 000 years BP, a complete time scale is obtained (fig. 5.22). Many dates have shown that the climatic trend for the Netherlands is valid for the whole of North-west Europe. It should be noticed, however, that the estimated temperature scale given was established for the Netherlands only. In other areas the whole pattern of varying temperatures may be found at a different level. In fig. 5.22 the interstadials have been indicated by names which have been established for the Weichselian glacial sequence of the Netherlands, Northern Germany and Denmark. For other areas local names should be used at least until the position of such stratigraphic units on an absolute time scale has been unambiguously established.

Because frequently only small sections of the stadial–interstadial cycle have been preserved in the pollen record, it is difficult to construct a complete and detailed climatic and vegetational picture for the area and the time interval considered.

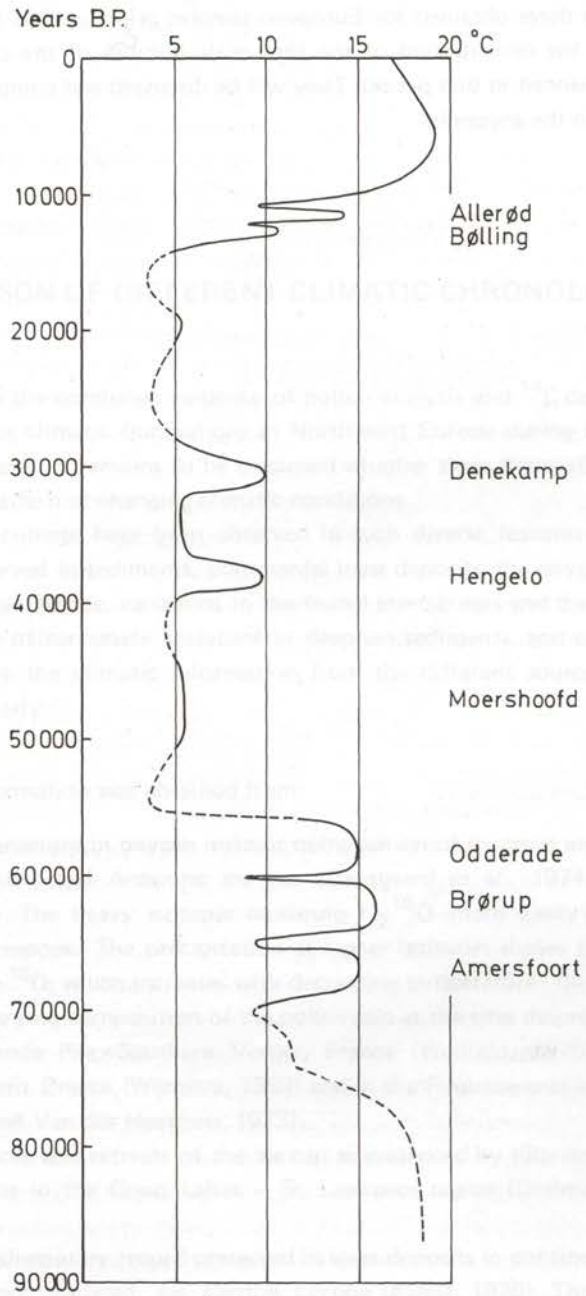

Fig. 5.22. Radiocarbon time scale for climatic fluctuations in North-west Europe during the Last Glacial. The temperature given is the estimated mean July temperature in the Netherlands.

The enrichment dates obtained for European samples prior to 1967 have not been considered for the construction of the time scale because of the contamination problems experienced in that period. They will be discussed and compared with the present results in the appendix.

Chapter 6

COMPARISON OF DIFFERENT CLIMATIC CHRONOLOGIES

In chapter 5 the combined evidence of pollen analysis and ^{14}C dates resulted in a time scale for climatic fluctuations in North-west Europe during the early part of the Last Glacial. It remains to be discussed whether these fluctuations formed part of a global pattern of changing climatic conditions.

Changes in climate have been observed in such diverse features as pollen distribution preserved in sediments, continental loess deposits, the oxygen isotopic composition of glacier ice, variations in the faunal assemblages and the oxygen isotopic composition of carbonate skeletons in deep-sea sediments, and coral terraces. We will compare the climatic information from the different sources, and the time scales separately.

Climatic information was obtained from:

(i) The variations in oxygen isotopic composition of ice cores extracted from the Greenland and Antarctic ice cap (Dansgaard et al., 1971; Johnsen et al., 1972). The heavy isotopic molecule $H_2{}^{18}O$ more easily condenses from water vapour. The precipitation at higher latitudes shows therefore a depletion in ^{18}O, which increases with decreasing temperature.

(ii) The varying composition of the pollen rain at the sites described in chapter 5, at Grande Pile, Southern Vosges, France (Woillard, 1975), in Macedonia, Northern Greece (Wijmstra, 1969) and in the Fuquene area in Colombia (Van Geel and Van der Hammen, 1973).

(iii) Advances and retreats of the ice cap as evidenced by tills, meltwater and lake deposits in the Great Lakes – St. Lawrence region (Dreimanis and Karrow, 1972).

(iv) The sedimentary record preserved in loess deposits in continental areas which were not glaciated, e.g. Central Europe (Kukla, 1970). The soils reflect the former existence of relatively warmer climatic conditions, whereas loess deposits reflect the cold periods.

(v) Palaeo sea levels obtained from old shore lines visible in regions of tectonic

uplift like Barbados (Mesolella et al., 1969; James et al., 1971) and New Guinea (Bloom et al., 1974). The formation of an ice cap on the continents leads to a drop in sea level. Contrarily a high sea level indicates reduced ice volume related to a relatively warmer climate.

(vi) The variations in the oxygen isotopic composition of the carbonate of fossil shells of foraminifera obtained from deep-sea cores from the Caribbean (Emiliani, 1966; Emiliani et al., 1975), the Pacific (Shackleton and Opdyke, 1973), the southern Indian Ocean (Hays et al., 1976) and other localities. The ^{18}O content of the shell carbonate reflects the oxygen isotopic composition and the temperature of the water in which it was deposited. The ^{18}O content of the oceans increases when a large amount of isotopically light water is fixed in an ice cap on the continents. A lower water temperature also favours the concentration of ^{18}O in carbonate, precipitated from the ocean.

(vii) The faunal assemblages found in deep-sea cores, e.g. from the Caribbean (Emiliani et al., 1975), the southern Indian Ocean (Hays et al., 1976) and the North Atlantic (Sancetta et al., 1973). The faunal assemblages of foraminifera and radiolaria may reflect the sea water temperature (Imbrie and Kipp, 1971).

(viii) The varying calcium carbonate content of the sediment in deep-sea cores, e.g. from the eastern equatorial Atlantic (Hays and Peruzza, 1972). The carbonate content of the sediment is determined by the production of organic carbonate and the rate of dissolution of the shells. Both are influenced by temperature.

The climatic patterns obtained from the sources mentioned above show different detail. The $^{18}O/^{16}O$ changes in ice cores provide the most detailed information. Also the pollen record may reflect climatic fluctuations in considerable detail. The information from loesses and sea levels is less detailed since here the difference between extremes of warm and cold is detected rather than the complete temperature development. The interpretation of the scattered data is difficult. Generally the deep-sea records lack information on short term climatic fluctuations due to the buffering capacity of the oceans and the mixing of the upper layer of sediment on the ocean floor. It provides, however, a well documented and consistent record of long term variations.

The patterns of climatic fluctuations obtained with different techniques and from largely different localities show a striking similarity. This suggests that we are dealing with global climatic fluctuations. It should therefore be possible to synchronize the different climate curves.

There are three independent dating methods that have provided dates for the climatic record of the last interglacial–glacial cycle.

The younger part (less than 20 000 years) of all time scales with the exception of (i) has been based on radiocarbon dates.

Time scales for the methods of continental climatic measurement (ii), (iii) and (iv) summarized above were obtained from ^{14}C dates up to the age limit of this dating method, formerly about 50 000, presently at about 75 000 years BP. A few enrichment dates obtained before 1967 were used in the 60 000 year range by Dreimanis and Karrow (1972). If a longer time scale of (ii) and (iii) is given, it is based on extrapolation and/or correlation with high palaeo sea levels reflected by dated coral terraces on Barbados (v) and with the generalized ^{18}O deep-sea record. For (iv) also interpolation between 0 and the Brunhes/Matuyama palaeomagnetic boundary (established by potassium-argon dating at about 700 000 years BP) is used.

Palaeo sea levels (v) were dated on basis of the disequilibrium activities of the decay products of ^{235}U and ^{238}U, especially ^{230}Th and ^{231}Pa, that are incorporated in corals. Based on this technique Mesolella et al. (1969) have concluded to three relatively high sea levels at Barbados about 85 000, 105 000 and 125 000 years BP. James et al. (1971) reported an additional high sea level terrace dated with $^{230}Th/^{231}Pa$ at about 60 000 years BP. On the Huon peninsula of New Guinea, Bloom et al. (1974) dated a series of 6, partly multiple, coral terraces which have originated in the same period.

The disequilibrium decay series technique has been applied also to some of the deep-sea cores (Rona and Emiliani, 1969; Broecker and Van Donk, 1970). Because generally only carbonate is available for ^{14}C dating this method cannot be used beyond about 20 000 years BP. Shackleton and Opdyke (1973) obtained a time scale by interpolation between the palaeomagnetic Brunhes/Matuyama boundary (K-Ar dated at about 700 000 years BP) and 0. For most of the cores, however, a time scale has been derived from a correlation with the dated Barbados high sea levels or with dated cores.

We will make a detailed comparison of our chronology with that obtained on the Camp Century ice core (Dansgaard et al., 1971), with the two generalized versions of the deep-sea chronology (Emiliani and Shackleton, 1974) and with the New Guinea high sea levels (Bloom et al., 1974) (fig. 6.1).

The *radiocarbon chronology* has been the subject of this thesis and needs not to be discussed here. In section 3.1 we estimated that the uncertainty of the method in the age range of 50 000 to 75 000 years BP is almost certainly less than 10% (corresponding to a factor 2 in natural ^{14}C activity).

The younger part of the *Camp Century ice core time scale* (0–12 000 years BP) was obtained by matching the periodicity of the fluctuations in the ice of δ^{18}, the relative difference in oxygen isotopic composition between a sample and the stand-

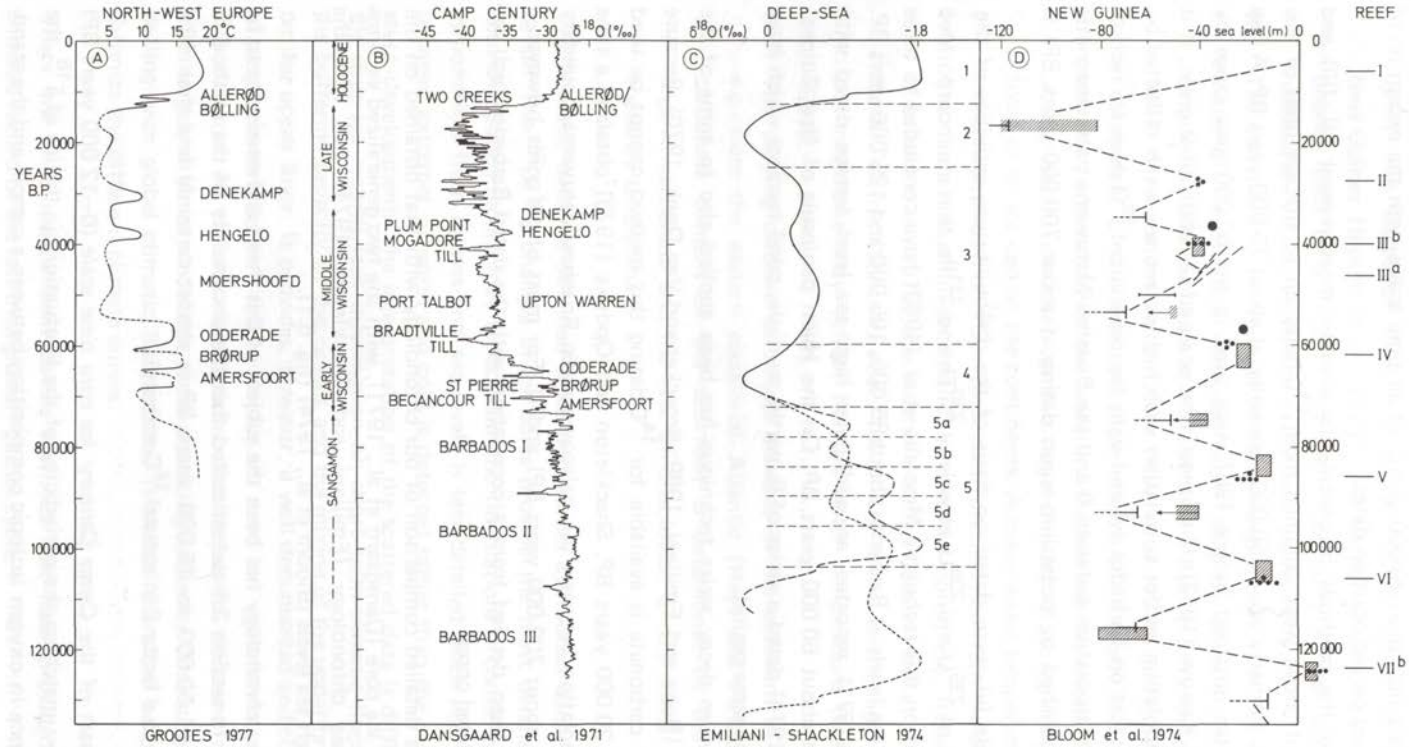

Fig 6.1. Comparison of climatic chronologies for the last interglacial–glacial cycle.
A – pollen record in North-west Europe, dated with ^{14}C,
B – δ^{18} record of the Camp Century ice core (Greenland), time scale based on constant periodicity of δ^{18} variations,
C – generalized δ^{18} deep-sea record, time scale based on $^{230}Th/^{231}Pa$ dates and interpolation between 0 and the Brunhes/Matuyama palaeomagnetic boundary at about 700 000 years BP; - - - - - Emiliani, ------ Shackleton,
D – high sea levels dated on the coast of New Guinea with ^{230}Th (and ^{14}C).

ard (c.f. sect. 2.3), with that of the variations in the atmospheric ^{14}C concentration. The latter were determined from ^{14}C measurements on dendrochronologically dated tree rings (Suess, 1970b). A good agreement was reached after a 15% change of the original Camp Century time scale, which had been based on glacier flow theory. The time scale beyond 12 000 years BP is based on the assumption that the frequency of the important climatic oscillations as reflected by δ^{18} was constant during the entire time range. The time scale is thus essentially independent of ^{14}C dating, although ^{14}C has been used in its derivation. Its accuracy is estimated to be about 10%.

The age of the climatic oscillations in the early part of the Last Glacial is approximately 8% lower on the ^{14}C scale than on the Camp Century time scale. Three percent can be attributed to the use of the conventional ^{14}C half-life of 5568 years instead of the more accurate value of 5730 years. The remaining discrepancy of 5% is within the estimated uncertainty of the time scales.

The younger part of the *deep-sea time scale* is obtained from ^{14}C ages (up to about 20 000 years BP). The older part is based on $^{230}Th/^{231}Pa$ dates on a number of Caribbean and Atlantic cores (Rosholt et al., 1961; Rona and Emiliani, 1969) and/or on a linear interpolation between 0 and 700 000 years BP (Brunhes/Matuyama boundary) for the Pacific core V28-238 (Shackleton and Opdyke, 1973). Although Emiliani and Shackleton (1974) constructed a generalized palaeotemperature time scale for the last 700 000 years, the exact position of the Last Interglacial remained undecided (c.f. fig. 6.1). An age of 100 000 years for the prominent δ^{18} peak at the beginning of stage 5 was found by Emiliani and his group. For this Shackleton obtained an age of about 120 000 years BP. This age was supported by $^{230}Th/^{231}Pa$ dates on Caribbean cores (Broecker and Ku, 1969; Broecker and Van Donk, 1970) and by a correlation with the highest palaeo sea level at Barbados also dated by $^{230}Th/^{231}Pa$ at about 125 000 years BP (Mesolella et al., 1969).

From the different results obtained on the same deep-sea core using different techniques of sample preparation (c.f. Rona and Emiliani, 1969; Broecker and Ku, 1969; Emiliani and Rona, 1969; Broecker and Van Donk, 1970) it is obvious that it is difficult to date such cores directly. In the references cited two of the problems encountered in dating deep-sea cores are discussed, viz. the admixture of continental material containing uranium and its daughters in equilibrium and the differential dissolution of uranium, thorium and protactinium when a leaching technique is used. The first effect will give ages which are too high. The effect of the latter depends on the actual fractionation.

An indication of the reliability of dates may be obtained from the $^{234}U/^{238}U$ activity ratio of the samples. This ratio, which in equilibrium is 1, is in ocean water close to 1.15 due to preferential leaching of ^{234}U from rocks.

Recently incorporated uranium shows this same ratio (Rona and Emiliani, 1969; Broecker and Ku, 1969). The observed $^{234}U/^{238}U$ ratios in the core samples, however, scatter between 0.90 and 1.09 with an average value close to 1.0. This indicates that the dates obtained on the cores may not be reliable. The analytical precision of the $^{230}Th/^{231}Pa$ dates is of the order of 5%.
The indirect dating of the deep-sea record by linear interpolation introduces considerable uncertainty. Also a correlation with the high palaeo sea levels dated on Barbados is uncertain.

The generalized curve given by Emiliani and Shackleton (1974) has lost most of the fine structure displayed by the analyses of the individual cores V28-238 and P6304-9. In the original δ^{18} curves of these cores more than three fluctuations within stage 5 can be observed (fig. 6.2), which is in contradiction with the generalized curve.

In a detailed comparison it seems reasonable to correlate the Emiliani stages 2 and 4 with the temperature minima found around 20 000 and 53 000 years BP on the radiocarbon time scale. If this is accepted stage 5 of the deep-sea record may contain both the Last Interglacial and the early interstadials of the Last Glacial as defined for North-west Europe. This conclusion is supported by the pollen record of North-west Europe and by the δ^{18} record of Camp Century, which indicate that during the early interstadials the climate was only slightly cooler than during the preceding interglacial period and distinctly warmer than during the following pleniglacial interstadials. A correlation between the Last Interglacial and the early glacial interstadials as defined in the Netherlands and Emiliani's stage 5 of the δ^{18} deep-sea curve was already suggested by Van der Hammen et al. (1967). A correlation of the Last Interglacial with the deep-sea stages 5c, 5d, 5e has been advocated by Mörner (1972). Similarly a possible correlation between the early interstadials and the younger part of stage 5 was put forward by Wijmstra and Van der Hammen (1974); the age difference between the beginning of pleniglacial conditions on the ^{14}C time scale ($\approx$ 55 000 years BP) and that of stage 4 in the deep-sea chronology ($\approx$ 70 000 years BP), however, made them suggest that all (or a part) of the early glacial interstadials would be younger than stage 4. It is questionable whether the accuracy of the time scales on the one hand and the similar shape of the curves on the other justify this suggestion.

For a proposed correlation of stage 5a in the deep-sea record with the early glacial interstadials as established by the radiocarbon time scale the difference in the age of the main early glacial cooling is about 15 000 years ($\approx$ 25%). Considering the estimated accuracy this is a significant discrepancy between the two time scales.

The age of the first high *palaeo sea level* on New Guinea (terrace I) (Bloom et al., 1974) is based on combined evidence of ^{14}C and ^{230}Th dates, that of the second on ^{14}C dates (Chappel and Polach, 1972). The remaining terraces were dated by

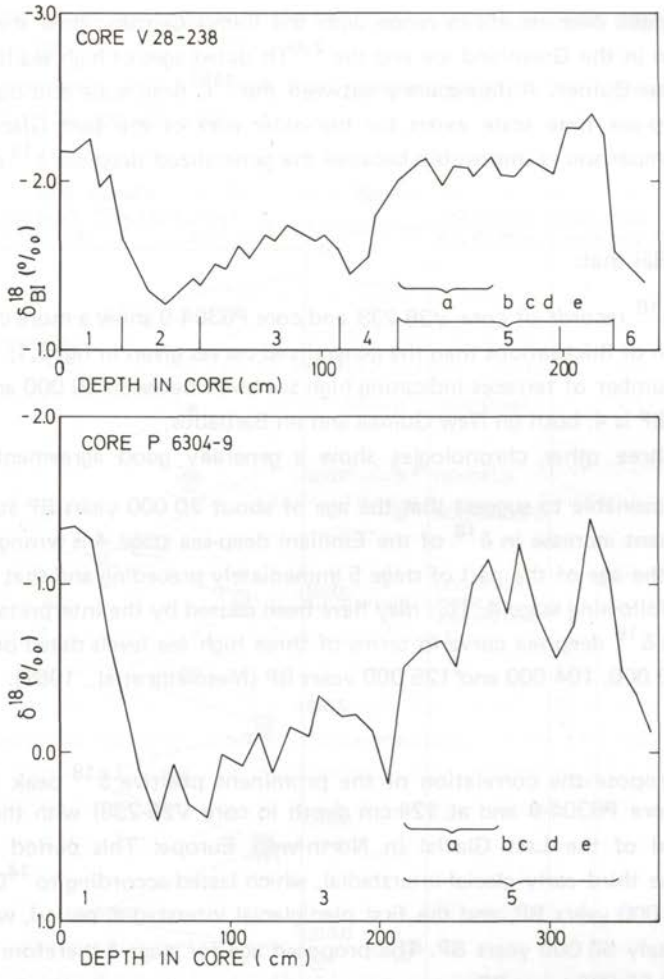

Fig. 6.2. Original δ^{18} record for core V28-238 (Shackleton and Opdyke, 1973) and core P6304-9 (Emiliani, 1966), stage 1–6 and 1, 3, 5 as given by the authors; proposed correspondence of stage 5a.

^{230}Th. For the thorium dating carefully selected corals were used. The analytical precision for each sample is 5 to 10%. The same uncertainty probably applies to the age of the dated sea levels due to age differences between samples from the same terrace.

An excellent agreement with the ^{14}C time scale is observed.

In conclusion we may say that the ^{14}C time scale for the sequence of temperate interstadial and cold stadial periods, recorded by the pollen record in North-west

Europe, agrees over its entire range with the Camp Century time scale for δ^{18} fluctuations in the Greenland ice and the ^{230}Th dated ages of high sea levels on the coast of New Guinea. A discrepancy between the ^{14}C time scale and both versions of the deep-sea time scale exists for the older part of the Last Glacial. Here a detailed comparison is impossible because the generalized deep-sea δ^{18} curve lacks detail.

If we consider that:

(i) The δ^{18} records of core V28-238 and core P6304-9 show a more complicated pattern of fluctuations than the generalized curves given in fig. 6.1;
(ii) The number of terraces indicating high sea levels between 50 000 and 130 000 years BP is 4, both on New Guinea and on Barbados;
(iii) The three other chronologies show a generally good agreement,

it seems reasonable to suggest that the age of about 70 000 years BP attributed to the prominent increase in δ^{18} of the Emiliani deep-sea stage 4 is wrong. The same applies to the age of the part of stage 5 immediately preceding and that of the part of stage 3 following stage 4. This may have been caused by the interpretation of the generalized δ^{18} deep-sea curve in terms of three high sea levels dated on Barbados at about 80 000, 104 000 and 125 000 years BP (Mesolella et al., 1969).

We here propose the correlation of the prominent positive δ^{18} peak (at 200 cm depth in core P6304-9 and at 124 cm depth in core V28-238) with the first very cold period of the Last Glacial in North-west Europe. This period is situated between the third early glacial interstadial, which lasted according to ^{14}C dating till at least 56 000 years BP, and the first pleniglacial interstadial period, which began approximately 50 000 years BP. The proposed age for stage 4 therefore is between 50 000 and 55 000 years BP.
The three early glacial interstadials found in the pollen record of North-west Europe then correlate with the moderately low δ^{18} values found near 225 cm depth in P6304-9 and around 145 cm depth in V28-238. Because indications are that the cold periods separating these interstadials were of short duration they may not be seen separately in the deep-sea δ^{18} record. The ^{14}C ages for these North-west European interstadials agree well with the high sea level dated at approximately 60 000 years BP on New Guinea and Barbados.
No finite ^{14}C ages have been obtained for climatic fluctuations preceding these early glacial interstadials.

The remaining section of P6304-9 below 235 cm shows two peaks of low δ^{18} values above the prominent peak at about 320 cm depth. Likewise V28-238 shows two low δ^{18} peaks above the prominent peak at about 204 cm depth. We propose

that these two peaks correlate with the high sea levels at about 85 000 and about 105 000 years BP.

The most prominent low δ^{18} peak then corresponds with the highest sea level dated at about 125 000 years BP.

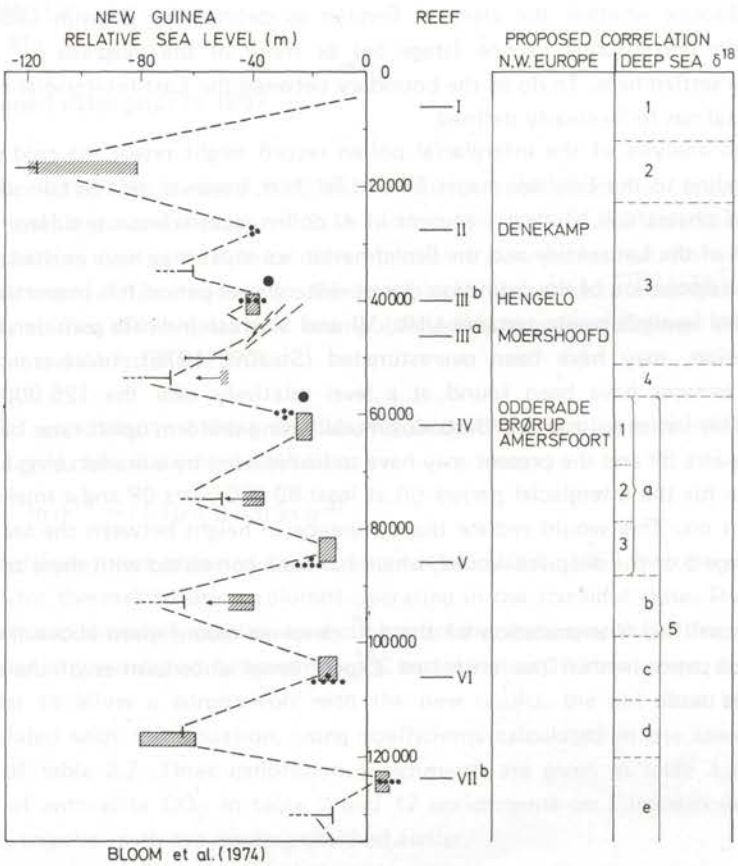

Fig. 6.3. High sea levels dated on New Guinea coral terraces; proposed correlation with the interstadials defined in the North-west European pollen record and with the stages of the generalized δ^{18} deep-sea record.

If the correlations given above are correct, the stage 5 of the generalized δ^{18} deep-sea record includes 4 high sea levels instead of three, as usually accepted ('Barbados I, II and III') (c.f. fig. 6.3). The proposed correlations support an age of about 125 000 years BP for the beginning of the Last Interglacial (the Shackleton version of the deep-sea time scale).

The plausible correlation of the deep-sea stages 5a-e is: 5e $\sim$ the 125 000 years

BP high sea level; 5c ∿ the 105 000 years BP high sea level and 5a ∿ both the 85 000 and the 60 000 years BP high sea levels. The stage 5a from this viewpoint consists of a younger phase $5a_1$ corresponding to the 60 000 years BP high sea level as well as to the three early glacial interstadials found in the North-west European pollen record and an older phase $5a_3$ corresponding to the 85 000 years BP high sea level.

The dispute whether the classical Eemian as defined by Zagwijn (1961) at Amersfoort corresponds to one (stage 5e) or more of the deep-sea δ^{18} stages cannot be settled here. To do so the boundary between the Last Interglacial and the Last Glacial has to be clearly defined.

A detailed analysis of the interglacial pollen record might reveal the cold phases corresponding to the Emiliani stages 5b and 5d. It is, however, not certain whether these cold phases will be clearly present in all pollen records because differences in behaviour of the Laurentide and the Scandinavian ice sheet may have existed.

For the discussion of the definition glacial–interglacial period it is important that the low sea levels between terraces VIIb, VI and V which indicate considerable ice accumulation, may have been overestimated (Stearns, 1976). In several places younger terraces have been found at a level relatively near the 125 000 years terrace. This indicates that the 'Barbados model' using uniform uplift rates between 125 000 years BP and the present may have to be replaced by a model using a larger uplift rate for the interglacial period till at least 80 000 years BP and a smaller one from then on. This would reduce the difference in height between the sea levels during stage 5 of the deep-sea record, which has been correlated with these terraces.

For the modified interpretation of the δ^{18} deep-sea record given above the four time scales agree within the estimated experimental uncertainties of the dating techniques used.

APPENDIX

Enrichment dates prior to 1967

From April 1957 till January 1967 the thermal diffusion enrichment apparatus has been in operation at the present F.O.M. Institute for Atomic and Molecular Physics in Amsterdam. During this period 38 enrichments were performed. We will discuss the enrichment dates obtained for European samples and make a comparison with our results. The earlier dates have been published by Vogel and Zagwijn (1967) and by Vogel and Waterbolk (1972).

The ^{14}C enrichment of those samples was calculated from the enrichment of the molecules of mass 30 using the relation

$$\ln q^{14'} = (1.10 \pm 0.03) \ln q^{30'}.$$

The coefficient was obtained by De Vries et al. (1956, 1967, written communication) for thermal diffusion columns operating in the transient state. The type of relation used, however, applies to a column in the stationary state. Therefore we developed a new relation between the ^{14}C and the mass 30 enrichments (eq. 2.19). In order to allow a comparison with the new results, the old dates have been recalculated with this equation, using coefficients calculated in the same way as those of table 2.7. Three calibration enrichments are given in table 1, 6 enrichments of anthracite CO_2 in table 2 and 17 enrichments on European samples in table 3, together with the results published earlier.

A comparison of the results of the old and the new calibration relation with the ^{14}C enrichments actually obtained (table 1) shows that both relations predict the ^{14}C enrichment with an accuracy of a few percent.

Although some of the parameters necessary for the calculation of the enrichment were unknown and had to be estimated, the enrichments of the three calibration runs calculated using eq. 2.19 differed less than 5% from the values observed. We thus conclude that eq. 2.19 can be used successfully for the samples enriched in Amsterdam.

The anthracite CO_2 samples (table 2) all showed a small but measurable radiocarbon activity. During the period in which the samples 2 and 9 were processed, no serious contamination was present. The activity found in the other samples,

Table 1. The enrichment of CO_2 mixtures of recent wood (a) and oxalic acid (b) performed in Amsterdam.

GrN	Enrichment number	Enrichment period	Enrichment		
			measured	calculated	
				from eq. 2.19	by De Vries et al.
1296[a]	1	19/4–22/5/'57	8.06 ± 0.05	8.21 ± 0.41	
2512[a]	10	3/4– 8/5/'59	9.92 ± 0.04	9.42 ± 0.47	9.85
4034[b]	21	23/1–27/3/'63	5.72 ± 0.02	5.50 ± 0.27	5.39

Table 2. The enrichment of CO_2 samples from anthracite performed in Amsterdam.

GrN	Enrich-ment number	Enrichment period	Enrichment[a]	Measured activity (pmc)	Original activity (pmc)	Apparent age (yrs BP)
1349	2	14/7–20/8/'57	10.64 ± 0.53	0.138 ± 0.034	0.013 ± 0.003	$71\,900^{+2300}_{-1800}$
1796	9	4/2–21/3/'59	10.43 ± 0.52	0.134 ± 0.036	0.013 ± 0.003	$72\,000^{+2500}_{-1900}$
3262	16	2/8–22/8/'61	9.02 ± 0.45	0.189 ± 0.044	0.021 ± 0.005	$68\,100^{+2200}_{-1700}$
4054	22	3/4–22/5/'63	10.66 ± 0.53	0.48 ± 0.15	0.045 ± 0.014	$61\,900^{+3000}_{-2200}$
4475[b]	28	25/3– 7/5/'65	11.09 ± 0.55	0.69 ± 0.10	0.062 ± 0.009	$59\,300^{+1300}_{-1100}$
4780	34	8/2–22/3/'66	13.88 ± 0.70	0.46 ± 0.09	0.033 ± 0.007	$64\,400^{+1700}_{-1400}$

a enrichment calculated from eq. 2.19
b thermal diffusion column broke during enrichment

especially in no. 28, is too large. The dates for samples measured in this period, therefore, should be seriously questioned.

Table 3 shows that the new calculation results in somewhat lower enrichments. The decrease in the measured age of the sample, however, is generally smaller than the standard deviation.

The date obtained for *Amersfoort XII* is about 5000 years younger than the new date for the Amersfoort Interstadial. Although the sample dates a somewhat later phase of the interstadial (EW IIb instead of EW Ib–EW IIa) the difference is probably caused mainly by contamination (c.f. Vogel and Zagwijn, 1967).

The *Odderade* series is internally inconsistent, which indicates the presence of contamination. The dates for Odderade 1–1 and 1–2, both taken from the *Pinus*

Table 3. European samples enriched prior to 1967 and published in Date List VI and X.

GrN	Enr. no.	Sample	Enrichment period	Enrichment[a]	Age[a] (yrs BP)	Enrich-ment[b]	Age[b] (yrs BP)	Estimated contamination[c] (pmc)
1397	3	Amersfoort XII	25/ 9– 2/ 1/'58	15.33 ± 0.70	63 500 ± 900	13.8	62 600 ± 900	≈ 0.02
1475	4	Chelford	13/ 2– 3/ 4/'58	8.12	60 800 ± 1500	7.85	60 500 ± 1500	⩽ 0.02
1470	5	Brørup Hotel Bog BP2, Zone W4	29/ 5–16/ 7/'58	9.92	59 100 ± 700	9.31	58 600 ± 700	≈ 0.03
1729	7	Brørup Hotel Bog BP1a, Zone W3c	1/10–22/11/'58	13.89	57 700 ± 700	12.78	57 000 ± 700	≈ 0.05
4157	25	Odderade 1–1	16/ 4– 8/ 7/'64	11.74	56 700 ± 800	10.15	55 500 ± 800	≈ 0.025
4671	30	Odderade 1–2	19/ 8–17/ 9/'65	12.69	58 100 ± 650	11.45	57 300 ± 650	≈ 0.02
4178	26	Odderade 1–4	3/ 9–27/10/'64	12.46	51 100 ± 400	11.47	50 400 ± 400	≈ 0.16
4698	32	Odderade 5–12	23/11–22/12/'65	11.52	54 500 ± 600	10.51	53 800 ± 600	≈ 0.12
2083	12	Lebenstedt	15/ 8– 1/10/'59	10.06	55 600 ± 900	9.25	54 900 ± 900	⩽ 0.02
4742	31	Zell am Inn 1	12/10–12/11/'65	10.43	57 000 ± 900	9.52	56 300 ± 900	≈ 0.07
4104	18	Zell am Inn 2	25/ 5– 4/ 7/'62	10.54	$65\,400\,^{+3500}_{-2600}$	9.69	$64\,700\,^{+3500}_{-2600}$	⩽ 0.01
4031	19	Grossweil 4	10/ 7–20/ 8/'62	12.91	$69\,100\,^{+2300}_{-1900}$	11.59	$68\,200\,^{+2300}_{-1900}$	≈ 0.02 ?
4001	20	Grossweil 3	26/ 9– 9/11/'62	13.46	25 160 ± 300	11.95	24 200 ± 300	≈ 5
4185	27	Grossweil 3 bis	5/ 2– 9/ 3/'65	9.29	45 800 ± 300	8.66	45 200 ± 300	≈ 0.33
2152	14	Dolní Věstonice 5	23/12– 3/ 2/'60	9.36	49 900 ± 600	8.77	49 400 ± 600	≈ 0.1
2572	11	Gnif Gnaf II	30/ 5– 6/ 7/'59	9.88	58 000 ± 500	9.47	57 700 ± 500	⩽ 0.02
5026	37	Padul VI 2, extract	29/ 9– 8/11/'66	8.00 ± 0.05[a*]	45 000 ± 330[a*]	9.13	46 100 ± 300	≈ 0.35

a enrichment and age as published in Groningen Radiocarbon Dates VI (Vogel and Zagwijn, 1967) and (a*) X (Vogel and Waterbolk, 1972)

b enrichment recalculated from mass 30 measurements using the equations obtained in this work; because some of the constants for the Amsterdam enrichment set-up are unknown, these were estimated; consequently, the enrichment is estimated to have a σ of 5%, which was not included in the standard deviation of the dates

c estimate based on the deviation from our results

phase of the Odderade Interstadial (upper peat layer), are in reasonable agreement with the new dates for the same layer, although somewhat younger. The dates for the lower peat layer are obviously wrong. Considering the results obtained for anthracite CO_2 enrichments in the same period this is not at all surprising.

The samples from *Brørup* date the first (pollen zone W3c) and the middle part (pollen zone W4) of the Brørup Interstadial. If the correlation with the second Interstadial at Amersfoort is correct (Andersen et al., 1960), the ^{14}C ages are about 7000 and 4000 years too young, respectively. These samples were enriched before the serious contamination problems started. The measurable activity of anthracite CO_2 after enrichment and the earlier problems with young humic infiltration at this site can very well account for errors in age of this size.

The result for *Chelford* agrees with the new dates obtained for the Brørup Interstadial, to which the sample was attributed.

The *Lebenstedt* sample was taken from a deposit preceding a very cold period during the early phase of the Last Glacial (De Vries, 1958). It probably dates the end of the third (Odderade) Interstadial and the transition to the Pleniglacial. If so, the date obtained fits nicely to the new time scale.

The samples *Zell am Inn 1 and 2* date the top and the base of a layer of lignite. Pollen analysis indicates an early glacial interstadial origin for this deposit and suggests a correlation with interstadial deposits in the higher part of the Grossweil lignites. The top was probably dated too young. This result was obtained in a period when serious contamination problems were encountered, as opposed to the date for the base. The latter is in good agreement with the beginning of the second Interstadial. If the lignite originates in the first Interstadial, the age is somewhat low but the standard deviation is sufficient to explain the discrepancy.

The samples from *Grossweil* provide both the highest sample age obtained prior to 1967 and the strongest evidence of contamination. The samples were taken from the deposits of the two interstadials present above the interglacial in the upper part of the Grossweil lignites. The result for Grossweil 4, dating the youngest of the two interstadials (pollen zone 13, Reich, 1953), is higher than any date hitherto obtained for the second Interstadial (perhaps with the exception of the Samerberg sample). The interpretation of the result is rather difficult, especially because in the older interstadial (pollen zone 11, Reich, 1953) a section with pollen of *Picea omorikoides* was present. If the usual correlation of the *Picea omorikoides* pollen zone with the Brørup Interstadial is made, this would suggest a correspondence between pollen zone 13 and the Odderade Interstadial. This is in strong disagreement with the age obtained for Grossweil 4. The age of Grossweil 4 rather suggests a correlation between pollen zone 13 and the Amersfoort Interstadial as dated in our work.

On basis of the pollen diagram and that of the lignites at Pfefferbichl, which shows a very similar interglacial (Reich, 1953), it cannot be excluded, however, that

the deposits are of pre-Eemian age. In that case the sample should have contained no measurable activity. The measured age would be explained by a contamination with 0.02 pmc.

The result for *Dolní Věstonice 5* must be considered a minimum age (Vogel and Zagwijn, 1967). If a correlation with the North-west European chronology is allowed and if the sample dates the top of the complex of early glacial interstadials, a date around 55 000 years BP would be expected.

The date for the *Gnif Gnaf* sample, belonging to the upper part of an early glacial deposit (c.f. Blanc et al., 1957), agrees well with the third (= youngest) Interstadial.

The ^{14}C age for the sample from *Padul* is about 9000 years too low if the supposed correlation with the end of the Odderade Interstadial is correct. The date was obtained on material extracted during the chemical pretreatment. Inconsistent conventional dates (Vogel and Waterbolk, 1972) pointed to the presence of sample contamination.

Although some of the earlier dates are in good agreement with our results (Odderade 1–1, 1–2, Chelford, Lebenstedt, Zell am Inn 2, Gnif Gnaf) they are generally younger. From our measurements of the amount of CO_2 produced during blank runs of the combustion system and its activity (c.f. sect. 4.4), we expect a laboratory contamination of the order of 0.02 pmc. Variations can result from the occasional cleaning of the combustion system and from the activity of samples combusted immediately before the sample considered. Also the increase in atmospheric ^{14}C content in 1963 should result in a slightly higher activity contributed by this source.

This combustion contamination by itself can account for the low age found at Amersfoort and for most of the deviation at Brørup. With the latter, some young humic infiltration cannot be excluded. The Dolní Věstonice sample consists of humus extracted from a soil and is therefore open to *in situ* contamination.

From the foregoing discussion it seems that, for samples enriched before September 1962, some residual sample contamination and a laboratory contamination in the combustion system of the order of 0.02 pmc satisfactorily explain the results obtained. The much higher contamination found in later samples needs a different explanation. Measurements of portions of CO_2 from Odderade 1–4 and Grossweil 3 bis before enrichment showed a lower ^{14}C activity (below the detection level) than was found after enrichment. This suggests that contamination occurred during the enrichment procedures. If contaminants are introduced into the sample, this is most likely to happen during the reduction and/or oxidation, especially the former. Here the sample is passed through a large amount of zinc powder and asbestos which is renewed for each sample. The zinc–asbestos mixture was heated to $\approx 120\,^{\circ}C$ under vacuum for several days before the reduction was started. Yet large

amounts of gas were released when the temperature was increased to ≈ 400 °C (reduction temperature), showing that the mixture still contained adsorbed gases. Even with our special cleaning procedures (c.f. sect. 4.4) some additional gas is released at 400 °C. A mass spectrum of these gases showed the peaks characteristic for the lower hydrocarbons. The zinc–asbestos can therefore easily have introduced foreign ^{14}C into the sample, particularly because in an adjacent laboratory experiments using enriched ^{14}C were carried out. The experiments with enriched ^{14}C started in August 1962 (!!) and lasted for about one year.

Other explanations such as admixture of atmospheric carbon dioxide or a memory effect of the thermal diffusion columns are less probable.

SUMMARY

The thermal diffusion enrichment apparatus in use in Amsterdam before 1967, has been rebuilt in the Groningen Radiocarbon Dating Laboratory. It has been shown to operate reliably and reproducibly. A reasonable agreement exists between the theoretical calculations and the experimental results. The ^{14}C enrichment of a CO sample is deduced from the simultaneous mass 30 enrichment, which is measured with a mass spectrometer. The relation between both enrichments follows from a series of calibration measurements. The over-all accuracy in the enrichment is a few percent, equivalent to a few hundred years in age.

The main problem in dating very old samples is their possible contamination with recent carbon. Generally, careful sample selection and rigorous pretreatment reduce sample contamination to an acceptable value.
Also, it has been established that laboratory contamination, due to a memory effect in the combustion system and to impurities in the oxygen and nitrogen gas used for combustion, can be eliminated.

A detailed analysis shows that the counter background in our set-up is almost exclusively caused by cosmic ray muons.

The measurement of 28 early glacial samples, mostly from North-west Europe, has yielded a consistent set of ages. These indicate the existence of three early glacial interstadials; using the Weichselian definitions: Amersfoort starting at 68 200 ± 1100, Brørup at 64 400 ± 800 and Odderade at 60 500 ± 600 years BP.

This ^{14}C chronology shows good agreement with the Camp Century chronology and the dated palaeo sea levels. The discrepancy in the age of the early part of the Last Glacial on the ^{14}C time scale and on that adopted for the deep-sea δ^{18} record, must probably be attributed to the use of a generalized δ^{18} curve and a wrong interpretation of this curve in terms of three Barbados terraces.

SAMENVATTING

Het doel van het in dit proefschrift beschreven onderzoek was het vergroten van het meetbereik van de ouderdomsbepaling met behulp van radio-actieve koolstof. Dit meetbereik was ongeveer 50 000 jaar. In vergelijking met een mensenleven is dit een lange periode. Geologisch is het echter heel kort. Het eerste deel van de laatste ijstijd en, wat betreft de ontwikkelingsgeschiedenis van de mens, een groot deel van de oude steentijd vallen buiten dit meetbereik. Aan de studie van de veranderingen in het klimaat in het verleden en vooral gedurende de afgelopen ijstijd wordt veel aandacht besteed. Het doel is daarbij te leren begrijpen waardoor klimaatsveranderingen bepaald worden, om met die kennis iets te kunnen zeggen over toekomstige veranderingen.

De *ouderdomsbepaling* met behulp van radio-actieve koolstof (^{14}C) berust op het voorkomen van ^{14}C in alle levende organismen (planten en dieren), maar ook in vers gevormd carbonaat en oppervlaktewater, in een vrijwel constante concentratie in evenwicht met de omgeving. Zodra geen opname van ^{14}C meer plaats vindt neemt die concentratie af door het radio-actieve verval van ^{14}C. De vervalsnelheid is bekend: deze halveert de hoeveelheid ^{14}C elke 5730 jaar. Het aantal vervallen per tijdseenheid in een bepaalde hoeveelheid materiaal noemen we de activiteit van het materiaal. Uit de gemeten ^{14}C rest-activiteit in een monster kan men de ouderdom berekenen, indien men de oorspronkelijke activiteit bekend veronderstelt (men neemt aan dat de oorspronkelijke activiteit altijd hetzelfde geweest is).

Het meten van de ^{14}C activiteit gebeurt in een *telbuis*. Het te meten monster wordt in de vorm van koolzuurgas (CO_2) in de telbuis gebracht. Het verval van een ^{14}C atoom geeft hierin een electrisch pulsje, dat geteld wordt. Het probleem bij het dateren van oude monsters is, dat de telbuis ook telt wanneer geen ^{14}C in het gas voorkomt. Dit noemen we het nuleffect van de telbuis. De rest-activiteit van een ^{14}C monster moet groter zijn dan 2 maal de grootte van toevallige schommelingen in het nuleffect om een meetbare ouderdom op te leveren.

Wij hebben het meetbereik voor ^{14}C ouderdomsbepaling vergroot door de ^{14}C concentratie in oude monsters te verhogen. Dit gebeurde door middel van *thermodiffusie isotopenscheiding* in CO. Hierbij maakt men gebruik van het feit, dat als men een mengsel van isotope moleculen (d.w.z. moleculen met dezelfde chemische eigenschappen, maar met verschillende massa, b.v. $^{12}C^{16}O$–$^{14}C^{16}O$) tussen 2 wanden van verschillende temperatuur brengt er een klein beetje ontmenging optreedt. Het zware isotoop wordt enigszins verrijkt in het gas bij de koude wand, het lichte bij de hete wand. In onze verrijkingsopstelling is de koude wand een verticale lange buis die van buiten gekoeld wordt en de hete wand een draad, gespannen langs de as van de buis. Dit heet een *thermodiffusiekolom*. Door convectie in het gas krijgen we langs de wand een stroom van gas, verrijkt in het zware isotoop, naar beneden en langs de draad komt gas, verarmd in dit isotoop, omhoog. Het resultaat is, dat onderin de kolom en in een daarmee verbonden voorraadvolume de concentratie van de zware isotope moleculen toeneemt. In een maand tijd kunnen we zo uit een groot volume gas ($\approx$ 250 l) een 10 keer verrijkt monster van 6 l maken voor ^{14}C datering. Een verrijking 10 geeft een uitbreiding van het meetbereik met 18 500 jaar.

We hebben de verrijkingsopstelling die eerst in bedrijf was in het F.O.M. Instituut voor Massascheiding in Amsterdam weer opgebouwd en getest.

Een probleem is, dat de ^{14}C verrijking van een monster meestal niet rechtstreeks gemeten kan worden. We hebben daarom een aantal verrijkingen van actief materiaal gedaan, waarbij we de verrijking van ^{14}C gemeten in de telbuis (voornamelijk $^{14}C^{16}O$) vergeleken met die van alle moleculen met massa 30 gemeten met een massaspectrometer (voornamelijk $^{12}C^{18}O$). De verrijking kwam redelijk overeen. Uit deze gegevens hebben we een verband gevonden tussen de ^{14}C en de massa 30 verrijking, zodat deze laatste gebruikt kan worden om de ^{14}C verrijking van een monster te bepalen.

We hebben reeds opgemerkt, dat het nuleffect van de telbuis mede het meetbereik bepaalt. We hebben daarom een nieuwe telbuis gebouwd van zuiver kwarts met op de binnenwand een dun laagje goud opgedampt, omdat kwarts en goud weinig radioactieve verontreinigingen bevatten en dus een laag nuleffect moeten geven. We hebben de telbuis getest en de verschillende bijdragen tot het nuleffect onderzocht. De belangrijkste bijdrage tot het nuleffect van de nieuwe telopstelling wordt geleverd door muonen in de kosmische straling. Radio-actieve verontreiniging speelt geen rol van betekenis.

Wanneer de verrijking en de telbuis het mogelijk maken om tot 75 000 jaar te meten in plaats van tot 50 000 jaar, betekent dat niet automatisch dat zinvolle dateringen verkregen worden. Een belangrijk probleem bij deze oude monsters is namelijk de verontreiniging met recente koolstof. Aangezien de te meten activiteit 1000 tot

10 000 maal zo klein is als in recente koolstof, is een bijmenging van 0,1 tot 1‰ voldoende om geheel foute dateringen te krijgen. We hebben het voorkomen van verontreinigingen onderzocht. De verontreiniging van het monster buiten het laboratorium kan klein gehouden worden door een zorgvuldige monsterkeuze. Samen met een chemische extractie levert dit meestal betrouwbare monsters. In het laboratorium treedt echter ook verontreiniging op. Dit bleek tot beneden onze meetgrens teruggebracht te worden door het gebruik van zuivere stikstof en zuurstof voor de verbranding, in combinatie met extra schoonmaken van het verbrandingssysteem en het daarin uitsluitend verbranden van oude monsters.

Wat betreft verontreinigingen kunnen monsters tot ten minste 75 000 jaar oud gedateerd worden.

We hebben een aantal monsters gedateerd afkomstig uit afzettingen van het begin van de laatste ijstijd in Noord-west Europa. De dateringen wijzen erop, dat er tussen ongeveer 68 000 en 56 000 jaar geleden drie vrij warme periodes geweest zijn, van elkaar gescheiden door vrij korte koude periodes.

Een vergelijking van onze resultaten met informatie over klimaatschommelingen, verkregen uit de verhouding van de zuurstof isotopen ($^{18}O/^{16}O$) in gletsjer ijs op Groenland, uit de $^{18}O/^{16}O$ verhouding in de kalk van schelpjes in diepzee-kernen en uit vroegere zeeniveaus afgeleid uit koraalterrassen, leert, dat een overeenkomst bestaat binnen de experimentele nauwkeurigheid van de methodes.

REFERENCES

Amdur, J. and Shuler, L. M. (1963), 'Diffusion Coefficients of the Systems CO-CO and CO-N_2'.
J. Chem. Phys. **38**, 188.

Andersen, Sv. Th., Vries, HI. de and Zagwijn, W. H. (1960), 'Climatic Change and Radiocarbon Dating in the Weichselian Glacial of Denmark and The Netherlands'.
Geologie en Mijnbouw **39**, 38.

Andersen, Sv. Th. (1961), 'Vegetation and its Environment in Denmark in the Early Weichselian Glacial (Last Glacial)'.
D.G.U. II.R. **75**, 1.

Anderson, E. C., Libby, W. F., Weinhouse, S., Reid, A. F., Kirshenbaum, A. D. and Grosse, A. V. (1947a), 'Radiocarbon from Cosmic Radiation'.
Science **105**, 576.

Anderson, E. C., Libby, W. F., Weinhouse, S., Reid, A. F., Kirshenbaum, A. D. and Grosse, A. V. (1947b), 'Natural Radiocarbon from Cosmic Radiation'.
Phys. Rev. **72**, 931.

Averdieck, F. R. (1963), 'Die Vegetationsentwicklung der Frühweichsel-Interstadiale von Odderade'.
Ber. Geobotan. Forsch. Inst. Rübel **34**, 58.

Averdieck, F. R. (1967), 'Die Vegetationsentwicklung des Eem-Interglazials und der Frühwürm-Interstadiale von Odderade/Schleswig-Holstein'.
Fundamenta R.B. **2**, 101.

Bagge, E. and Skorka, S. (1958), 'Der Übergangseffekt der Ultrastrahlungsneutronen an der Grenzfläche Luft-Wasser'.
Z. Physik **152**, 34.

Bagge, E. and Binder, Q. (1962), 'A Lunar Cosmic Ray Intensity Variation II'.
J. Phys. Soc. Japan **17** Suppl. A II, 486.

Bardeen, J. (1940), 'Concentration of Isotopes by Thermal Diffusion: Rate of Approach to Equilibrium'.
Phys. Rev. **57**, 35 and Phys. Rev. **58**, 94.

Barendsen, G. W. (1955), 'Ouderdomsbepaling met radio-actieve koolstof'.
Thesis, Groningen.

Becker, B. (1976), 'Zeitstellung und Entstehung postglazialer Baumstammlagen in Flussschottern im Bereich des Iller-schwemmkegels und des Donautals östlich von Ulm'.
I.G.C.P. excursion guide, 66.

Bigeleisen, J. (1952), 'The effects of isotopic substitutions on the rates of chemical reactions'.
J. Phys. Chem. **56**, 823.

Blanc, A. C., Vries, HI. de and Follieri, M. (1957), 'A First C14 Date for the Würm I Chronology on the Italian Coast'.
Quaternaria **4**, 1.

Bloom, A. L., Broecker, W. S., Chappel, J. M. A., Matthews, R. K. and Mesolella, K. J. (1974), 'Quaternary Sea Level Fluctuations on a Tectonic Coast: New $^{230}Th/^{234}U$ Dates from the Huon Peninsula, New Guinea'.
Quaternary Research **4**, 185.

Boersma-Klein, V. and Vries, A. E. de (1966), 'The Influence of the Distribution of Atomic Masses within the Molecule on Thermal Diffusion. I. Isotopic CO and N_2 Molecules'.
Physica **32**, 717.

Bourdier, F. (1961, 1962), 'Le bassin du Rhône au Quaternaire'.
I, II, Paris.

Brande, A. (1975), 'Vegetationsgeschichtliche und pollenstratigraphische Untersuchungen zum Paläolithikum von Mauern und Meilenhofen (Fränkische Alb)'.
Quartär **26**, 73.

Brenninkmeijer, C. A. M. and Mook, W. G. (1976), 'The Effect of Electronegative Impurities on CO_2 Proportional Counting: An On-Line Purity Test Counter'.
9th International Conf. on Radiocarbon Dating, La Jolla, California (in press).

Broecker, W. S. and Ku, T. L. (1969), 'Caribbean Cores P6304-8 and P6304-9: New Analysis of Absolute Chronology'.
Science **166**, 405.

Broecker, W. S. and Donk, J. van (1970), 'Insolation Changes, Ice Volumes, and the O^{18} Record in Deep-Sea Cores'.
Reviews of Geophysics and Space Physics **8**, 169.

Bucha, V. (1970), 'Influence of the Earth's magnetic field on radiocarbon dating'.
Proceedings of the Twelfth Nobel Symposium 'Radiocarbon Variations and Absolute Chronology', Uppsala, 501.

Cain, W. F. and Suess, H. E. (1976), 'Carbon-14 in Tree Rings'.
J. Geophys. Res. **81**, 3688.

Chapman, S. (1917), 'On the Kinetic Theory of a Gas. Part II. A composite Monatomic Gas: Diffusion, Viscosity and Thermal Conduction'.
Philos. Trans. Roy. Soc. London **A 217**, 115.

Chapman, S. and Dootson, F. W. (1917), 'A Note on Thermal Diffusion'.
Phil. Mag. **33**, 248.

Chapman, S. (1919), 'The Possibility of Separating Isotopes'.
Phil. Mag. **38**, 182.

Chappel, J. and Polach, H. A. (1972), 'Some Effects of Partial Recrystallisation on ^{14}C Dating Late Pleistocene Corals and Molluscs'.
Quaternary Research **2**, 244.

Clusius, K. and Dickel, G. (1938), 'Neues Verfahren zur Gasentmischung und Isotopentrennung'.
Naturwiss. **26**, 546.

Cocconi, G. and Cocconi Tongiorgi, V. (1951), 'Nuclear Disintegrations induced by μ-Mesons'.
Phys. Rev. **84**, 29.

Craig, H. (1954), 'Carbon 13 in plants and the relationships between carbon 13 and carbon 14 variations in nature'.
J. Geol. **62**, 115.

Craig, H. (1957), 'Isotopic Standards for Carbon and Oxygen and Correction Factors for Mass-spectrometric Analysis of Carbon Dioxide'.
Geochim. Cosmochim. Acta **12**, 133.

Curran, S. C. and Graggs, J. D. (1949), 'Counting Tubes'.
Academic Press Inc., New York.

Damon, P. E., Long, A. and Wallick, E. J. (1972), 'Dendrochronologic calibration of the carbon-14 time scale'.
8th International Conf. on Radiocarbon Dating, Lower Hutt, New Zealand, 44.

Damon, P. E., Long, A. and Wallick, E. J. (1973), 'On the magnitude of the 11-year radiocarbon cycle'.
Earth Planet. Sci. Lett. **20**, 300.

Dansgaard, W., Johnsen, S. J., Clausen, H. B. and Langway, C. C. Jr. (1971), 'Climatic record revealed by the Camp Century ice core'.
in 'The Late Cenozoic Glacial Ages' (K. K. Turekian, ed.), Yale University Press, New Haven, Conn., 37.

Depape, G. and Bourdier, F. (1952), 'Le gisement interglaciaire à Rhododendron ponticum L. de Barraux dans le Grésivaudan entre Grenoble et Chambéry'.
Trav. Laborat. Géologie de l'université de Grenoble **30**, 81.

Diethorn, W. (1956), 'A Methane Proportional Counter System for Natural Radiocarbon Measurements'.
NYO-6628, March 16.

Dreimanis, A. and Karrow, P. F. (1972), 'Glacial History of the Great Lakes–St. Lawrence Region, the Classification of the Wisconsin (an) Stage, and its Correlatives'.
International Geological Congress, 24th Session, section **12**, 5.

Duperier, A. (1949), 'The Meson Intensity at the Surface of the Earth and the Temperature at the Production Level'.
Proc. Phys. Soc. London **A 62**, 684.

Emiliani, C. (1966), 'Paleotemperature analysis of Caribbean cores P6304-8 and P6304-9 and a generalized temperature curve for the past 425 000 years'.
J. Geol. **74**, 109.

Emiliani, C. and Rona, E. (1969), 'Caribbean Cores P6304-8 and P6304-9: New Analysis of Absolute Chronology. A Reply'.
Science **166**, 1551.

Emiliani, C. and Shackleton, N. J. (1974), 'The Brunhes Epoch: Isotopic Paleotemperatures and Geochronology'.
Science **183**, 511.

Emiliani, C., Gartner, S., Lidz, B., Eldridge, K., Elvey, D. K., Ting Chang Huang, Stip, J. J. and Swanson, M. F. (1975), 'Paleoclimatological Analysis of Late Quaternary Cores from the Northeastern Gulf of Mexico'.
Science **189**, 1083.

Enskog, D. (1911a), 'Über eine Verallgemeinerung der Zweiten Maxwellschen Theorie der Gase'.
Physik. Z. **12**, 56.

Enskog, D. (1911b), 'Bemerkungen zu einer Fundamentalgleichung in der kinetischen Gastheorie'.
Physik. Z. **12**, 533.

Erlenkeuser, H. (1971a), 'Aufbau einer Thermodiffusionsanlage zur Anreicherung von Methan-Isotopen in Hinblick auf die Verwendung bei Altersbestimmungen nach der ^{14}C-Methode'.
Thesis, Kiel.

Erlenkeuser, H. (1971b), 'Predictable low enrichment of methane isotopes by Clusius-Dickel thermal-diffusion columns for use in radiocarbon dating technique'.
Z.Naturforsch. **26a**, 1365.

Erlenkeuser, H. (1976), 'A thermal diffusion plant for radiocarbon isotope enrichment from natural samples'.
9th International Conf. on Radiocarbon Dating, La Jolla, California (in press).

Felber, H. (1971), 'Altersbestimmungen nach der Radiokohlenstoffmethode an Fossilfunden aus dem Bänderton von Baumkirchen (Inntal, Tirol)'.
Z.f. Gletscherkde. u. Glazialgeol. Bd. **VII**, 25.

Felber, H. and Hernegger, F. (1971), 'Über die Anreicherung von Uran in den Fossilfunden aus dem Bänderton von Baumkirchen (Inntal, Tirol)'.
Z.f. Gletscherkde. u. Glazialgeol. Bd. **VII**, 31.

Felber, H. and Pak, E. (1972), 'Erweiterung der ^{14}C-Altersbestimmungsmethode durch quantitative Isotopenanreicherung im Trennrohr'.
Sitzber. Österr. Akad. Wiss. **180**, 299.

Felber, H. and Pak, E. (1974), 'Quantitative Isotope Enrichment in a Thermal Diffusion Arrangement'.
Appl. Phys. **5**, 147.

Ferguson, C. W. (1970), 'Dendrochronology of bristlecone pine, Pinus Aristata. Establishment of a 7484-year chronology in the White Mountains of Eastern-central California, U.S.A.'
Proceedings of the Twelfth Nobel Symposium 'Radiocarbon Variations and Absolute Chronology', Uppsala, 237.

Flint, R. F. and Deevey, E. S. (1961), 'Editorial statement'.
Radiocarbon **3**.

Florschütz, F., Menéndez Amor, J. and Wijmstra, T. A. (1971), 'Palynology of a thick Quaternary succession in southern Spain'.
Palaeogeography, Palaeoclimatol., Palaeoecol. **10**, 233.

Freundlich, J. C. and Rutloh, M. (1972), 'Radiocarbon Dating by Carbon Dioxide Method. Influence and Removal of known Impurities'.
8th International Conf. on Radiocarbon Dating, Lower Hutt, New Zealand, B 25.

Frenzel, B. (1973), 'Some Remarks on the Pleistocene Vegetation'.
Eiszeitalter u. Gegenwart **23/24**, 281.

Geel, B. van and Hammen, T. van der (1973), 'Upper Quaternary Vegetational and Climatic Sequence of the Fuquene Area (Eastern Cordillera, Colombia)'.
Palaeogeography, Palaeoclimatol., Palaeoecol. **14**, 9.

Godwin, H. (1959), 'Carbon-Dating Conference at Groningen'.
Nature **184**, 1365.

Godwin, H. (1962), 'Half-life of Radiocarbon, Decisions of the Fifth Radiocarbon Dating Conference, Cambridge 1962'.
Nature **195**, 984.

Gold, R. (1968), 'Cosmic ray neutrons near sea level'.
Phys. Rev. **165**, 1411.

Greene, E., Hoglund, R. J. and Halle, E. von (1966), A.E.C. Research and Development Report K-1469.
Union Carbide Nuclear Corp., Oak Ridge, Tennessee.

Groeneveld, D. J. (1977), 'Tritium Analysis of Environmental Waters'.
Thesis, Groningen.

Grootes, P. M., Mook, W. G., Vogel, J. C., Vries, A. E. de, Haring, A. and Kistemaker, J. (1975), 'Enrichment of Radiocarbon for Dating Samples up to 75,000 years'.
Z. Naturforsch. **30a**, 1.

Hammen, T. van der, Maarleveld, G. C., Vogel, J. C. and Zagwijn, W. H. (1967), 'Stratigraphy, Climatic Succession and Radiocarbon Dating of the Last Glacial in the Netherlands'.
Geologie en Mijnbouw **46**, 79.

Handbook of Chemistry and Physics 49th ed. (1968), C.R.C. Press, A 162 from: Fisher, R. A., 'Statistical Methods for Research Workers', 6th ed., Oliver and Boyd, Edinburgh.

Handbook of Chemistry and Physics 53rd ed. (1972), C.R.C. Press, B 245 from: Goldman, D. T., Aline, P., Sher, R. and Stehn, J. R., 'Twenty-two Hundred Meter per Second Neutron Absorption Cross Sections', Nuclear Data Section A. (1969).

Hannss, Ch., Bottema, S., Grootes, P. M., Koster, Y. M. and Münnich, M. (1976), 'Nouveaux résultats sur la stratigraphie et l'âge de la banquette de Barraux (Haut-Grésivaudan, Isère)'.
R.G.A. **64**, 495.

Haring, A., Vries, A. E. de and Vries, Hl. de (1958), 'Radiocarbon Dating up to 70 000 Years By Isotopic Enrichment'.
Science **128**, 472.

Harkness, D. D. and Burleigh, R. (1974), 'Possible carbon-14 enrichment in high altitude wood'.
Archaeometry **16**, 121.

Haubach, W. J., Eck, C. F., Rutherford, W. M. and Taylor, W. L. (1965), 'Status of stable gaseous isotope separation and purification at Mound Laboratory 1963'.
A. E. C. Report MLM-1239. TLD-4500, Oak Ridge, Tennessee.

Hays, J. D. and Peruzza, A. (1972), 'The Significance of Calcium Carbonate Oscillations in Eastern Equatorial Atlantic Deep-Sea Sediments for the End of the Holocene Warm Interval'.
Quaternary Research **2**, 355.

Hays, J. D., Imbrie, J. and Shackleton, N. J. (1976), 'Variations in the Earth's Orbit: Pacemaker of the Ice Ages'.
Science **194**, 1121.

Hellund, E. J. (1940), 'Generalized Theory of Diffusion'.
Phys. Rev. **57**, 319 and 328.

Imbrie, J. and Kipp, N. G. (1971), 'A New Micropaleontological Method for Quantitative Paleoclimatology: Application to a Late Pleistocene Caribbean Core'.
in 'The Late Cenozoic Glacial Ages' (K. K. Turekian, ed.), Yale University Press, New Haven, Conn., 71.

In Che Yang, A. and Fairhall, A. W. (1972), 'Variations of Natural Radiocarbon during the last 11 milennia and Geophysical Mechanisms for Producing them'.
8th International Conf. on Radiocarbon Dating, Lower Hutt, New Zealand, 60.

Iversen, J. O. H. S. (1975), 'The development of Denmark's nature since the Last Glacial'.
D.G.U. V.R. **7c**, 1.

James, N. P., Mountjoy, E. W. and Omura, A. (1971), 'An Early Wisconsin Reef Terrace at Barbados, West Indies, and Its Climatic Implications'.
Geol. Soc. America Bull. **82**, 2011.

Jerz, H. (1969), 'Erläuterungen zur Geologischen Karte von Bayern 1 : 25 000 Bl. Nr. 8134 Königsdorf'.
Hrsg. v. Bayer. Geol. Landesamt München.

Jessen, K. and Milthers, V. (1928), 'Stratigraphical and Paleontological Studies of Interglacial Fresh Water Deposits in Jutland and Northwest Germany'.
D.G.U. II.R. **48**, 1.

Johnsen, S. J., Dansgaard, W., Clausen, H. B. and Langway, C. C. Jr., (1972), 'Oxygen Isotope Profiles through the Antarctic and Greenland Ice Sheets'.
Nature **235**, 429.

Jones, R. C. (1941), 'On the Theory of the Thermal Diffusion Coefficient for Isotopes II'.
Phys. Rev. **59**, 109.

Jones, R. C. and Furry, W. H. (1946), 'The Separation of Isotopes by Thermal Diffusion'.
Rev. Mod. Phys. **18**, 151.

Jung, W., Beug, H.-J. and Dehm, R. (1972), 'Das Riss/Würm-Interglazial von Zeifen, Landkreis Laufen a.d. Salzach'.
Bayer. Akad. Wiss., Math.-Nat. Kl., Abhandlungen N.F. Heft **151**, 1.

Karlèn, I., Olsson, I. U., Källberg, P. and Kilicci, S. (1964), 'Absolute determination of the activity of two ^{14}C dating standards'.
Arkiv för Geofysik **4**, 465.

Katz, L. and Penfold, A. S. (1952), Revs. Modern Phys. **24**, 28, quoted in Yuan, L.C.L. and Wu, C. S., 'Methods of Experimental Physics, Nuclear Physics'.
Academic Press, New York-London (1961), 72.

Kretner, R. (1973), 'Quantitative Anreicherung von $C^{14}H_4$ mit dem Clusius-Dickelschen Trennrohr zur Anwendung in der C^{14}-Datierungsmethode'.
Thesis, Munich.

Kretner, R. and Dickel, G. (1975), 'Enrichment of $^{14}CH_4$ by Thermal Diffusion for Use in Radiocarbon Dating'.
Z.Naturforsch. **30a**, 554.

Kukla, J. (1970), 'Correlations between loesses and deep-sea sediments'.
Geologiska Föreningens i Stockholm Förhandlingar **92**, 148.

La Jolla (1976), 9th International Conf. on Radiocarbon Dating, La Jolla, California (in press).

Laranjeira, M. F. (1960), 'An Elementary Theory of Thermal and Pressure Diffusion in Gaseous Binary and Complex Mixtures'.
Physica **26**, 409.

Lerman, J. C., Mook, W. G. and Vogel, J. C. (1970), '^{14}C in tree rings from different localities'.
Proceedings of the Twelfth Nobel Symposium 'Radiocarbon Variations and Absolute Chronology', Uppsala, 275.

Libby, W. F. (1946), 'Atmospheric Helium Three and Radiocarbon from Cosmic Radiation'.
Phys. Rev. **69**, 671.

Libby, W. F. (1965), 'Radiocarbon Dating'.
University of Chicago Press, Chicago and London, 2nd ed.

Lingenfelter, R. E. and Ramaty, R. (1970), 'Astrophysical and Geophysical variations in C-14 production'.
Proceedings of the Twelfth Nobel Symposium 'Radiocarbon Variations and Absolute Chronology', Uppsala, 515.

Malota, F. (1962), 'Eine Erweiterung der Methode für Altersbestimmungen durch Anreicherung des C^{14}-Isotops im Trennrohr'.
Thesis, Munich.

Mania, D. (1967), 'Das Jungquartär aus dem ehemaligen Ascherslebener See im Nordharzvorland'.
Peterm. Mitt. **111** (Gotha), 257.

Mason, E. A. and Rice, W. E. (1954), 'The Intermolecular Potentials for Some Simple Nonpolar Molecules'.
J. Chem. Phys. **22**, 843.

Mathews, P. M. (1959), 'Atmospheric Effects on Cosmic Ray Intensity at Sea Level'.
Canadian J. Phys. **37**, 85.

McInteer, B. B. and Reisfeld, M. J. (1961), Los Alamos Scientific Laboratory, Report LAMS-2517.

Menke, B. and Behre, K.-E. (1973), 'History of Vegetation and Biostratigraphy'.
Eiszeitalter u. Gegenwart **23/24**, 251.

Meshkovskii, A. G. and Solokov, L. J. (1957).
J. Exptl. Theoret. Phys. (U.S.S.R.) **33**, 424, quoted by Nydal et al. (1975).

Mesolella, K. J., Matthews, R. K., Broecker, W. S. and Thurber, D. L. (1969), 'The astronomical theory of climatic change: Barbados Data'.
J. Geol. **77**, 250.

Michael, H. N. and Ralph, E. K. (1972), 'Discussion of Radiocarbon Dates obtained from precisely dated sequoia and Bristlecone Pine samples'.
8th International Conf. on Radiocarbon Dating, Lower Hutt, New Zealand, 28.

Mook, W. G. (1968), 'Geochemistry of the stable carbon and oxygen isotopes of natural waters in the Netherlands'.
Thesis, Groningen.

Mook, W. G. and Grootes, P. M. (1973), 'The measuring procedure and corrections for the high-precision mass-spectrometric analysis of isotopic abundance ratios, especially referring to carbon, oxygen and nitrogen'.
Int. J. Mass Spectr. and Ion Phys. **12**, 273.

Mörner, N. A. (1972), 'When Will the Present Interglacial End'.
Quaternary Research **2**, 341.

Mortillet, G. de (1850a), 'Lignites de Sonnaz'.
Bull. Soc. Hist. natur. Savoie **1**, 115 and 126.

Mortillet, G. de (1850b), 'Alluvions anciennes de la Boisse (près de Chambéry)'.
Bull. Soc. Hist. natur. Savoie **1**, 205.

Nier, A. O. (1950), 'A Redetermination of the Relative Abundances of the Isotopes of Carbon, Nitrogen, Oxygen, Argon and Potassium'.
Phys. Rev. **77**, 789.

Nydal, R., Gulliksen, S. and Lovseth, K. (1975), 'Proportional Counters and Shielding for Low Level Gas Counting'.
Proc. Conf. Low Radioactivity Measurements and Applications, High Tatras, Czechoslovakia (in press).

Olsson, I. U. (1968), 'Modern aspects of radiocarbon dating'.
Earth Sci. Rev. **4**, 203.

Oeschger, H., Houtermans, J., Loosli, H. and Wahlen, M. (1970), 'The constancy of cosmic radiation from isotope studies in meteorites and on the Earth'.
Proceedings of the Twelfth Nobel Symposium 'Radiocarbon Variations and Absolute Chronology', Uppsala, 471.

Oeschger, H. and Wahlen, M. (1975), 'Low Level Counting Techniques'.
Ann. Rev. Nucl. Sci. **25**, 423.

Pack, J. L., Voshall, R. E. and Phelps, A. V. (1962), 'Drift Velocities of Slow Electrons in Krypton, Xenon, Deuterium, Carbon Monoxide, Carbon Dioxide, Water Vapor, Nitrous Oxide and Ammonia'.
Phys. Rev. **127**, 2084.

Pak, E. (1970), 'Erweiterung der C^{14}-Altersbestimmungsmethode durch Isotopenanreicherung im Trennrohr'.
Thesis, Vienna.

Puite, K. J. (1965), 'Onderzoek van het nul-effekt bij C-14 telbuizen'.
Internal Report, Physics Laboratory, Groningen.

Raether, H. (1964), 'Electron Avalanches and Breakdown in Gases'.
Butterworths, London, 72.

Ree, J. van de (1967), 'Thermal Diffusion of asymmetric Hydrogen Molecules in Inert Gases'.
Thesis, Leiden.

Regener, V. H. (1962), 'Solar Diurnal Variation of Cosmic Rays Underground Near the Geomagnetic Equator'.
J. Phys. Soc. Japan **17** Suppl. A II, 481.

Reich, H. (1953), 'Die Vegetationsentwicklung der Interglaziale von Grossweil-Ohlstadt und Pfefferbichl im Bayerischen Alpenvorland'.
Flora **140**, 386.

Richmond, G. M. (1969), 'Development and stagnation of the last Pleistocene icecap in the Yellowstone Lake Basin, Yellowstone National Park, U.S.A.'
Eiszeitalter u. Gegenwart **20**, 196.

Richmond, G. M. (1970), 'Comparison of the Quaternary stratigraphy of the Alps and Rocky Mountains'.
Quaternary Research **1**, 3.

Richmond, G. M. and Pierce, K. L. (1972), 'Surficial geologic map of the Eagle Peak quadrangle, Yellowstone National Park and adjoining area, Wyoming'.
U.S. Geol. Survey Misc. Geol. Inv. Map I-637.

Rona, E. and Emiliani, C. (1969), 'Absolute Dating of Caribbean Cores P6304-8 and P6304-9'.
Science **163**, 66.

Rose, M. E. and Korff, S. A. (1941), 'An Investigation of the properties of Proportional Counters I'.
Phys. Rev. **59**, 850.

Rosholt, J. N., Emiliani, C., Geiss, J., Koczy, F. F. and Wangersky, P. J. (1961), 'Absolute dating of deep-sea cores by the $^{231}Pa/^{230}Th$ method'.
J. Geol. **69**, 162.

Rossi, B. B. and Staub, H. H. (1949), 'Ionization Chambers and Counters'.
McGraw-Hill Book Co. Inc., New York.

Rutherford, W. M. and Kaminski, K. J. (1967), 'Experimental Verification of the Theory of the Thermal-Diffusion Column'.
J. Chem. Phys. **47**, 5427.

Rutherford, W. M. (1970), 'Separation of Light Isotopic Gas Mixtures in the Thermal Diffusion Column'.
J. Chem. Phys. **53**, 4319.

Sancetta, C., Imbrie, J. and Kipp, N. G. (1973), 'Climatic Record of the Past 130 000 years in North Atlantic Deep-sea Core V23-82: Correlation with the Terrestrial Record'.
Quaternary Research **3**, 110.

Santamaria, C. M., Savirón, J. M., Yarza, J. C. and Carrión, J. A. (1976), 'Thermal diffusion factors for binary noble gas mixtures from column measurements, II'.
J. Chem. Phys. **64**, 1095.

Savirón, J. M., Santamaria, C. M., Carrión, J. A. and Yarza, J. C. (1975), 'Isotopic and non-isotopic thermal diffusion factors from column measurements'.
J. Chem. Phys. **63**, 5318.

Sawelski, F. S. (1968), 'A further refinement of the Radiocarbon dating method'.
Proc. Acad. Sci. USSR, geological series B **180**, 1189 (in russian).

Schirdewahn, J., Klemm, A. and Waldmann, L. (1961), 'Thermodiffusion in D_2-HT und anderen Wasserstoffgemischen'.
Z. Naturforsch. **16a**, 133.

Schneekloth, H. (1966), 'Ergebnisse weiterer Untersuchungen an den interstadialen Ablagerungen der Weichsel-Eiszeit in Oerel, Kr. Bremervörde'.
Z. Deutsch. Geol. Ges. **116**, 773.

Segrè, E. (1952), 'Spontaneous Fission'.
Phys. Rev. **86**, 21.

Selle, W. and Schneekloth, H. (1965), 'Ergebnisse einer Kernbohrung in Oerel, Kr. Bremervörde; drei Interstadiale über Ablagerungen des Eem-Interglazials'.
Z. Deutsch. Geol. Ges. **115**, 109.

Shackleton, N. J. and Opdyke, N. D. (1973), 'Oxygen Isotope and Palaeomagnetic Stratigraphy of Equatorial Pacific Core V28-238: Oxygen Isotope Temperatures and Ice Volumes on a 10^5 Year and 10^6 Year Scale'.
Quaternary Research **3**, 39.

Sonntag, Ch., Rebel, H., Ribbat, B., Thio, S. K. and Gramm, W. R. (1970), 'Experimental Evidence for the Nonstatistical Shape of the Beta Spectrum of ^{14}C'.
L. Nuovo Cimento **4**, 717.

Stearns, C. E. (1976), 'Estimates of the Position of Sea Level between 140 000 and 75 000 Years Ago'.
Quaternary Research **6**, 445.

Stephan, W. (1970), 'Frühwürmzeitliche Schieferkohlevorkommen im Bereich des östlichen Isar-Vorlandgletschers'.
Geologica Bavarica **63**, 217.

Stevens, G. A. and Vries, A. E. de (1968), 'The Influence of the Distribution of Atomic Masses within the Molecule on Thermal Diffusion. II. Isotopic Methane and Methane/Argon Mixtures'.
Physica **39**, 346.

Suess, H. E. (1970a), 'Bristlecone-pine calibration of the radiocarbon timescale 5200 B.C. to the present'.
Proceedings of the Twelfth Nobel Symposium 'Radiocarbon Variations and Absolute Chronology', Uppsala, 303.

Suess, H. E. (1970b), 'The three causes of secular carbon-14 fluctuations, their amplitudes and time constants'.
Proceedings of the Twelfth Nobel Symposium 'Radiocarbon Variations and Absolute Chronology', Uppsala, 595.

Stuiver, M. (1970), 'Long-term C-14 variations'.
Proceedings of the Twelfth Nobel Symposium 'Radiocarbon Variations and Absolute Chronology', Uppsala, 197.

Stuiver, M. and Robinson, S. W.; Göte Östlund, H. and Gorman Dorsey, H. (1974), 'Carbon-14 calibration between the University of Washington and the University of Miami Geosecs Laboratories'.
Earth Planet. Sci. Lett. **23**, 65.

Trefall, H. (1955), 'On the Barometer Effect on the Hard Component of the Cosmic Radiation'.
Proc. Phys. Soc. London **A 68**, 953.

U.S. Geological Survey (1972), 'Geologic map of Yellowstone National Park'.
U.S. Geol. Survey Misc. Geol. Inv. Map I-711.

U.S. Geological Survey (1973), 'Surficial geologic map of Yellowstone National Park'.
U.S. Geol. Survey Misc. Geol. Inv. Map I-710.

Valk, F. van der (1963), 'Thermal Diffusion In Ternary Mixtures. I. Theory'.
Physica **29**, 417.

Vasaru, G., Müller, G., Reinhold, G. and Fodor, T. (1969), 'The Thermal Diffusion Column'.
VEB Deutscher Verlag der Wissenschaften, Berlin.

Verlin, J. D., Matzen, M. K. and Hoffman, D. K. (1975a), 'Collision integrals for soft, non-spherical molecules in terms of spherical Ω^* integrals'.
J. Chem. Phys. **62**, 4146.

Verlin, J. D., Matzen, M. K. and Hoffman, D. K. (1975b), 'Temperature dependence of thermal diffusion in CO isotopic gas mixtures'.
J. Chem. Phys. **62**, 4151.

Vivien, J. (1896), 'Description des gisements ligniteux de la vallée de Chambéry'.
Bull. Soc. Hist. natur. Savoie **3**, 2^{e} série, 16.

Vogel, J. C. and Waterbolk, H. T. (1963), 'Groningen Radiocarbon Dates IV'.
Radiocarbon **5**, 163.

Vogel, J. C. and Zagwijn, W. H. (1967), 'Groningen Radiocarbon Dates VI'.
Radiocarbon **9**, 63.

Vogel, J. C. and Waterbolk, H. T. (1967), 'Groningen Radiocarbon Dates VII'.
Radiocarbon **9**, 107.

Vogel, J. C. (1969), 'The Radiocarbon Timescale'.
S. African Archeol. Bull. **24**, 83.

Vogel, J. C. and Waterbolk, H. T. (1972), 'Groningen Radiocarbon Dates X'.
Radiocarbon **14**, 6.

Vries, A. E. de (1956), 'The Enrichment of Radioactive Isotopes by Thermal Diffusion'.
Thesis, Amsterdam.

Vries, A. E. de, Haring, A. and Slots, W. (1956), 'Separation of $^{14}C^{16}O$ and $^{12}C^{18}O$ by thermal diffusion'.
Physica **XXII**, 247.

Vries, Hl. de and Barendsen, G. W. (1953), 'Radio-carbon Dating by a Proportional Counter filled with Carbondioxide'.
Physica **XIX**, 987.

Vries, Hl. de (1956a), 'Cosmic radiation during the solar flare of February 23rd and its effect on ^{14}C age measurements'.
Physica **XXII**, 357.

Vries, Hl. de (1956b), 'The contribution of neutrons to the background of counters used for ^{14}C age measurements'.
Nucl. Phys. **1**, 477.

Vries, Hl. de (1957), 'Further analysis of the neutron component of the background of counters used for ^{14}C age measurements'.
Nucl. Phys. **3**, 65.

Vries, Hl. de (1958), 'Radiocarbon Dates for upper Eem and Würminterstadial samples'.
Eiszeitalter u. Gegenwart **9**, 10.

Vries, Hl. de, Barendsen, G. W. and Waterbolk, H. T. (1958), 'Groningen Radiocarbon Dates II'.
Science **127**, 129.

Wada, M. (1962), 'Atmospheric Effects on the Cosmic-Ray Meson Intensity'.
J. Phys. Soc. Japan. **17** Suppl. A II, 508.

Wilkinson, D. H. (1959), 'Ionization Chambers and Counters'.
Cambridge University Press, Cambridge.

Wijmstra, T. A. (1969), 'Palynology of the first 30 metres of a 120 m deep section in Northern Greece'.
Acta Botan. Neerl. **18**, 511.

Wijmstra, T. A. and Hammen, T. van der (1974), 'The last interglacial–glacial cycle: State of affairs of correlation between data obtained from the land and from the ocean'.
Geologie en Mijnbouw **53**, 386.

Woillard, G. (1975), 'Recherches palynologiques sur le Pléistocène dans l'Est de la Belgique et dans les Vosges Lorraines'.
Acta Geographica Lovaniensia **14**.

Zagwijn, W. H. (1961), 'Vegetation, Climate and Radiocarbon Datings in the Late Pleistocene of the Netherlands. Part I: Eemian and Early Weichselian'.
Mem. Geol. Found. Netherlands N.S. **14**, 15.

Zagwijn, W. H. and Paepe, R. (1968), 'Die Stratigraphie der Weichselzeitliche Ablagerungen der Niederlande und Belgiens'.
Eiszeitalter u. Gegenwart **19**, 129.

Zastawny, A. (1966), 'Gas Amplification in a Proportional Counter with Carbon Dioxide'.
J. Sci. Instrum. **43**, 179.

Zeil, W. (1954), 'Geologie der Alpenrandzone bei Murnau in Oberbayern'.
Geologica Bavarica **20**, 85.

NOTES

ACKNOWLEDGEMENTS

The work described in this thesis has been made possible by the friendly cooperation of many people, among whom I mention the workers of our physics laboratory and the Dutch and German palynologists and geologists who have kindly shown me around and supplied me with the well documented samples for enrichment.

I thank John Vogel for the many things he taught me during the year I worked in his laboratory. I also wish to thank him for offering me the chance of preparing this thesis, of which he was to be the promotor. I have much appreciated the almost complete freedom. Unfortunately I have not been able to finish the work in time for him to be my promotor.

I like to thank Dick Groeneveld for the many stimulating discussions we had during the years we have been working together.

Harm-Jan Streurman showed me how routine ^{14}C dating is done and performed several of the enrichments after the system had fully entered routine operation. I have greatly appreciated his assistance.

For the construction of the elaborate glass systems of the thermal diffusion enrichment set-up, and of the combustion, reduction and oxydation stages I wish to thank Eric Kuperus. His craftsmanship finally closed all the leaks.

I also would like to thank Alja Mensink, who managed to read my hand-writing and typed the draft of this thesis, Mr. B. Kamps for preparing the figures and Roel van Zanten and Hein Leertouwer for making the photographs.

Many thanks are due to Dolf de Vries and Ton Haring for helping me on my way with the thermal diffusion system, and to Dolf especially for working through my chapter on thermal diffusion.

Last but not least I thank Grada for her patience during the many hours she spent reading through my manuscript and during the past years, when regularly we spent an evening at the laboratory. Her interest in my work has greatly encouraged me.

STELLINGEN

1

De interpretatie van de klimaatsveranderingen als een gevolg van astronomische invloeden (Milankovitch theorie) wordt niet wezenlijk beïnvloed door de nieuwe tijdschaal verkregen in dit proefschrift.

J. D. Hays, J. Imbrie, N. J. Shackleton (1976), Science **194**, 1121.

2

In de literatuur vermelde verschillen tussen thermodiffusie theorie en experiment zijn ten dele terug te voeren op het niet in de beschouwing betrekken van de massa van het zware, zeldzame molecuul.

H. Erlenkeuser (1973), Proceedings Conference 'Isotope Effects in Physical and Chemical Processes'. Cluj, Roemenië.
H. Felber, E. Pak (1973), Sitzber. Österr. Akad. Wiss. **180**, 299.

3

Het oplossen en zuiveren van collageen voor ^{14}C datering zoals voorgesteld door Longin dient te worden voorafgegaan door demineralisatie van het bot met verdund zoutzuur zoals in het Groninger ^{14}C laboratorium gebruikelijk is.

R. Longin (1970), Thesis, Lyon.

4

Het verschillend reageren van R plasmide dragende bacterie populaties op veranderingen in het antibiotica regime zou verklaard kunnen worden door het soms wel en soms niet gekoppeld voorkomen van resistentie determinanten en virulentie determinanten in één plasmide.

C. L. Hartley, M. H. Richmond (1975), British Medical Journal, 71.
B. C. Kline (1976), Mayo Clinic Proceedings **51**, 3.

5

De suggestie van Bottinga en Javoy, dat niet-ideaal gedrag van de gasfase nabij de kritische temperatuur niet van belang is voor de isotopenscheiding gas–vloeistof is onjuist.

Y. Bottinga, M. Javoy (1973), Earth Planet. Sci. Lett. **20**, 250.
P. M. Grootes, W. G. Mook, J. C. Vogel (1969), Z. Physik **221**, 257.

6

Het collageengehalte van botten, berekend op grond van een Kjeldahl stikstofbepaling, is geen juiste indicatie voor de relatieve ouderdom.

R. Berger, A. G. Horney, W. F. Libby (1964), Science **144**, 999.

7

Het gebruik van lokale criteria voor het definiëren van interglaciale en interstadiale periodes bemoeilijkt de correlatie van klimaatsveranderingen in verschillende gebieden.

8

Het verdient aanbeveling om de tijdsduur tussen twee ^{14}C activiteitsmetingen van hetzelfde monster niet overeen te laten komen met één van de periodes van fluctuaties in de kosmische straling.

A. Fréon (1962), J. Phys. Soc. Japan **17** suppl. A-II, 418.

9

Dit proefschrift is gebaseerd op het 'niet isotoop' zijn van isotopen.

10

Het verdient aanbeveling om het wonen op het platteland door stedelingen afhankelijk te stellen van een 'hinderwet vergunning'.

11

Bij emancipatie bewegingen lijken dikwijls de begrippen gelijkheid en gelijkwaardigheid verward te worden.

12

Het zijn de kleine dingen die het doen.

Stellingen, behorende bij het proefschrift van P. M. Grootes, getiteld *Thermal diffusion isotopic enrichment and radiocarbon dating beyond 50 000 years BP.*
April 1977.